# Smart polymer platforms for in vitro drug screening assays based on drug-loaded nanoparticles

**Faralli, Adele; Larsen, Niels Bent**

*Publication date:*
2015

*Document Version*
Publisher's PDF, also known as Version of record

# Smart Polymer Platforms For *In Vitro* Drug Screening Assays Based on Drug-loaded Nanoparticles

Adele Faralli
PhD Thesis July 2015

DTU Nanotech
Department of Micro- and Nanotechnology

# Smart Polymer Platforms For *In Vitro* Drug Screening Assays Based On Drug-Loaded Nanoparticles

**Adele Faralli, PhD Thesis**

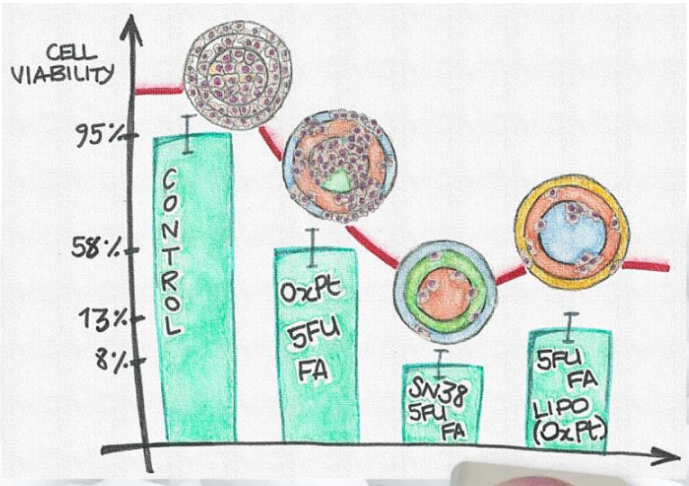





DTU Nanotech
Department of Micro- and Nanotechnology

PhD Thesis – Adele Faralli
Supervisor – Niels B. Larsen
DTU Nanotech, Department of Micro- and Nanotechnology
Technical University of Denmark
July 2015

# Abstract

The present PhD thesis represents a contribution to the *IndiTreat* project which started on January 1st 2011 supported by the Danish Council for Strategic Research. The main goal of the project is to improve chemotherapeutic treatment of patients suffering from colorectal cancer (CRC). In this thesis we investigate the use of polymers for drug screening assays. The aim of this study is the development of a polymer platform that enables to overcome some of the limitations that characterize the existing screening methods, by requiring very small amounts of tissues and permitting a fast and low-cost screening of individual drugs as well as combined drugs. Human colorectal adenocarcinoma cell line (HT-29) has been selected as cell culture model because easy to handle and phenotypically stable. The responsiveness of HT-29 cells to the individual and combined drug regimens normally selected for colorectal cancer therapy is finally evaluated using our technologies. Two main platforms are proposed: one is based on the use of poly(ethylene glycol) diacrylate (PEGDA) hydrogels for controlled drug release, and the second one consists on the use of poly(3,4-(1-azidomethylene)-dioxythiophene) (PEDOT-$N_3$) micro-electrodes for co-localization of drug-loaded nanoparticles (liposomes) and cancer cells.

PEGDA hydrogels are widely used in different fields including tissue engineering and *in vivo* drug delivery. A home-made setup for the fabrication of PEGDA hydrogels through visible-light photo-polymerization is described in detail. The method is utilized to create gels in which various clinically relevant drugs are embedded within the polymer network. The release profile of these molecules is determined and the anti-proliferative effect of passively released drugs is evaluated on HT-29 cultures. Individual drugs and combinations of chemotherapeutics are embedded within PEGDA gels as free molecules or loaded into nanoparticles (liposomes). The release of molecule from liposomes is temporally controlled through heat treatment and stable nanoparticles embedded within polymer networks are achieved. With the developed technology, various hydrogel architectures and sizes are produced allowing the confinement of targeted molecules within defined volumes of gel. From our described findings, the PEGDA-based hydrogel platform can ideally be applied for the screening of different compounds and to explore *in vitro*, various pathological cell lines.

In this thesis is presented also an alternative methodology for drug screening purposes, consisting on the fabrication of a micro- and nano-platform for drug-loaded liposomes immobilization and cell capture. PEDOT-$N_3$ micro-electrodes are fabricated through printed dissolution that, contrarily to the traditional lithography processes, preserves the biochemical properties of the exposed substrates. Cyclic olefin copolymers (COC) supports are used for PEDOT-$N_3$ deposition and *in situ* polymerization. Various chemical modifications to create a coating onto the support surface are also explored. A variety of highly hydrophilic poly(ethylene glycol) (PEG)-based molecules are photo-chemically grafted onto COC supports to form protein repellent surfaces. Post-fabrication covalent modifications of polymer

micro-electrodes are investigated and the use of “click-chemistry reaction” permits to modify free available azide groups presented at the surface of micro-electrodes. By covalently attaching appropriate bi-functional molecules onto a thin PEDOT-$N_3$ film, chemical reactive liposomes (~100nm in diameter) are immobilized onto electrodes.

In addition to these findings, an extensive optimization of electrodes fabrication, liposomes stability and chemical engineering of the support areas between the electrodes for cell capture purposes, is necessary. We find that it would be highly relevant for future studies to explore the mechanisms involved on co-localization of liposomes, that are triggered for drugs release, and specific cell lines.

# Dansk resumé

Denne ph.d. afhandling er et bidrag til *IndiTreat* projektet, der startede 1. januar 2011 støttet af Det strategiske Forskningsråd. Projektets hovedmål er at forbedre kemoterapi af patienter med kolorektal cancer. I denne afhandling har vi udforsket anvendelse af polymerer i systemer til at måle effekten af forskellige typer medicin ("screening"). Formålet med dette studie er at udvikle en polymer-baseret teknologi, der undgår begrænsninger i eksisterende screening-systemer ved at muliggøre analyse på meget små vævsmængder og analyse af både individuelle aktive stoffer og kombinationer af stoffer. En human kolorektal adenocarcinoma cellelinie (HT-29) blev valgt som cellemodel da den er let at arbejde med og fænotypisk stabil. Den udviklede teknologi er blevet anvendt til at eksponere HT-29 celler til individuelle stoffer eller kombinationer af stoffer, der normalt anvendes ved behandling af kolorektal cancer, hvorefter stoffernes indvirkning på cellerne er evalueret. To forskellige teknologiplatforme bliver foreslået. Den ene platform gør brug af poly(ethylenglykol)-diakrylat (PEGDA) hydrogeler til styret frigivelse af aktive stoffer. Den anden platform er baseret på poly(3,4-(1-azidomethylen)-dioxythiophen) (PEDOT-$N_3$) mikroelektroder til at samlokalisere stof-fyldte nanopartikler (liposomer) og cancerceller.

PEGDA hydrogeler anvendes i mange arbejdsområder inklusive vævs regenerering og medicinfrigivelse i kroppen (*in vivo*). En instrumentel opstilling og eksperimental procedure til fremstilling af PEGDA hydrogeler ved fotopolymerisering med synligt lys er detaljeret beskrevet. Metoden er blevet anvendt til at fremstille geler med klinisk relevante stoffer indlejret i polymernetværket. Den tidslige profil for frigivelse af disse molekyler samt den vækshæmmende effekt af passivt frigivne stoffer på HT-29 cellekulturer er blevet analyseret. Individuelle stoffer såvel som kombinationer af kemoterapeutiske stoffer blev indlejret i PEGDA geler som frie molekyler eller indkapslet i nanopartikler (liposomer). Frigivelsen af molekyler fra liposomer kan tidsligt styret ved en varmebehandling, og stabile nanopartikler indlejret i polymere netværk blev fremstillet. Den udviklede teknologi blev anvendt til at producere en række forskellige hydrogel-former og -størrelser, hvilket tillod afgrænsning af de ønskede aktive stoffer til veldefinerede gel-volumener. Vores resultater muliggør anvendelse af den PEGDA-hydrogel baserede teknologiplatform til screening af forskellige stoffer og til at udføre laboratorieforsøg (*in vitro*) på forskelllige cellelinier.

Denne afhandling præsenterer også en alternativ metode til medicin-screening baseret på fremstilling af en mikro- og nano-platform til at immobilisere medicin-fyldte liposomer og indfangne celler. PEDOT-$N_3$ mikro-elektroder blev fremstillet med metoden "opløsning ved stempling", der, til forskel fra traditionelle litografiske processer, bevarer de biokemiske egenskaber af det eksponerede underlag. Underlag fremstillet i cyklisk olefin copolymer (COC) blev anvendt til deponering og *in situ* polymerisering af PEDOT-$N_3$, og forskellige typer af kemiske modificeringer af overfladen blev udført

og karakteriseret. En række meget hydrofile poly(ethylen glykol)-baserede molekyler blev fotokemisk bundet til COC underlagene for at skabe proteinafvisende overflader. Kovalent modificering af de fremstillede polymer mikro-elektroder blev undersøgt, hvor "klik-kemi" blev anvendt til modificering af de tilgængelige azid-grupper på overfladen af mikro-elektroderne. Kovalent binding af udvalgte bi-funktionelle molekyler på en tynd PEDOT-$N_3$ film gjorde det muligt at immobilisere kemisk reaktive liposomer (~100 nm i diameter) på elektroderne.

I tillæg til de opnåede resultater vil det være nødvendigt at udføre en omfattende optimering af elektrodefremstilling, liposomstabilitet, og kemisk styring af områderne af underlag mellem elektroderne for indfangning af celler. Vi mener at det vil være meget relevant i fremtidige studier at undersøge de underliggende mekanismer bag samlokalisering af specifikke cellelinier og liposomer der er blevet stimuleret til stoffrigivelse.

# Table of Contents

# List of abbreviations and IUPAC nomenclature

| | |
|---|---|
| Bz | 4-benzoyl benzylamine hydrochloride or benzophenone |
| CAFs | Cancer-associated fibroblasts |
| Carboplatin | cis-diammine(cyclobutane-1,1-dicarboxylate-O,O')platinum(II) |
| Cisplatin | (SP-4-2)-diamminedichloroplatinum(II) |
| COC | Cyclic olefin copolymers |
| CRC | ColoRectal Cancer |
| CuAAC | Copper(I)-catalyzed azide-alkyne Huisgen 1,3-dipolar cycloaddition |
| DACH | Diaminocyclohexane |
| DLS | Dynamic Light Scattering |
| DMEM | Dulbecco´s Modified Eagle Medium |
| DSPC | [(2R)-2,3-di(octadecanoyloxy)propyl]2-(trimethylazaniumyl)ethylphosphate or Distearoyl phosphatidylcholine |
| DTCs | Disseminated tumor cells |
| dTMP | Deoxythymidine monophosphate |
| dUMP | Deoxyuridine monophosphate |
| ECM | Extracellular matrix |
| EDOT | 3,4-ethylenedioxythiophene |
| EDOT-$N_3$ | 3,4-(1-azidomethylethylene)-dioxythiophene |
| FBS | Fetal bovine serum |
| FDA | Food and Drug Administration |
| FdUMP | Fluorodeoxyuridine monophosphate |
| FITC | Fluorescein isothiocyanate |
| FOLFIRI | FOL: folinic acid; F: 5-fluorouracil; IRI: irinotecan |
| FOLFOX | FOL: folinic acid; F: 5-fluorouracil; OX: oxaliplatin |
| FOLFOXIRI | FOL: folinic acid; F: 5-fluorouracil; OX: oxaliplatin; IRI: irinotecan |

| | |
|---|---|
| Folinic Acid, FA | (2S)-2-{[4-[(2-amino-5-formyl-4-oxo-5,6,7,8-tetrahydro-1H-pteridin-6-yl)methylamino]benzoyl]amino}pentanedioic acid or Leucovorin |
| HCT | Human colorectal carcinoma cells |
| HT-29 | Human colorectal adenocarcinoma cell line |
| I2959 | 1-[4-(2-Hydroxyethoxy)-phenyl]-2-hydroxy-2-methyl-1-propane-1-one or IrgaCure 2959 |
| ICP-MS | Inductively coupled plasma mass spectrometry |
| Irinotecan, CPT-11 | (S)-4,11-diethyl-3,4,12,14-tetrahydro-4-hydroxy-3,14-dioxo1H-pyrano[3',4':6,7]-indolizino[1,2-b]quinolin-9-yl-[1,4'bipiperidine]-1'-carboxylate |
| LAP | Lithium phenyl-2,4,6-trimethyl-benzoylphosphinate |
| Lurtotecan, GW211 | (S)-8-ethyl-8-hydroxy-15-((4-methylpiperazin-1-yl)methyl)-11,14-dihydro-2H-[1,4]dioxino[2,3-g]pyrano[3',4':6,7]indolizino[1,2-b]quinolone-9,12(3H,8H)-dione |
| LUVs | Large unilamellar vesicles |
| MDSCs | Myeloid-derived suppressor cells |
| MLVs | Multilamellar vesicles |
| MMPs | Matrix metallopeptidases |
| MTS | [3-(4,5-dimethylthiazol-2-yl)-5-(3-carboxymethoxyphenyl)-2-(4-sulfophenyl)-2H-tetrazolium] |
| NCF | Normal human colonic fibroblasts |
| NCM | Normal human colonic mucosa cells |
| NHS | N-Hydroxysuccinimide group |
| Oxaliplatin, OxPt | [(1R,2R)-cyclohexane-1,2-diamine](ethanedioato-O,O')platinum(II) |
| PBS | Phosphate buffer solution |
| PC | [(2R)-3-hexadecanoyloxy-2-[(Z)-octadec-9-enoyl]oxypropyl]2-(trimethylazaniumyl)ethyl phosphate or Phosphatidylcholine |
| PE | [(2R)-1-[2-aminoethoxy(hydroxy)phosphoryl]oxy-3-pentadecanoyloxypropan-2-yl] icosanoate or Phosphatidylethanolamine |
| PEDOT | Poly(3,4-ethylenedioxythiophene) |
| PEDOT-$N_3$ | Poly(3,4-(1-azidomethylethylene)-dioxythiophene) |
| PEDOT-$N_3$:TsO | *p*-doped PEDOT-$N_3$ containing tosylate anions |
| PEG | Poly Ethylene Glycol |

| | |
|---|---|
| PEGDA | Poly Ethylene Glycol Diacrylate |
| POC | Point-of-care |
| PS-$N_3$ | Poly(4-(azidomethyl)styrene) |
| PSS | Poly(styrene sulfonic acid) |
| rpm | Revolutions per minute |
| SN-38 | 7-Ethyl-10-hydroxy-camptothecin |
| SUVs | Small unilamellar vesicles |
| TAMs | Tumor associated macrophages |
| $T_m$ | Phase transition temperature of liposomes |
| TME | Tumor microenvironment |
| TNM | T, N, M are the categories of the universal staging system used to classify tumors |
| Topo I | Topoisomerase I |
| TS I | Thymidylate synthase |
| TsO | Tosylate group Fe(III)TsO |
| Vitamin B9, folic acid | (2S)-2-[[4-[(2-amino-4-oxo-1H-pteridin-6-yl)methylamino]benzoyl]amino] pentanedioic acid |
| WHO | World Health Organization |
| XPS | X-ray photoelectron spectroscopy |
| 5-fluorouracil, 5-FU | 5-Fluoro-1H,3H-pyrimidine-2,4-dione |
| 9-AC | 9-aminocamptothecin |
| 9-NC | 9-nitrocamptothecin |

# 1 Introduction

## The *IndiTreat* project: from prevention to personalized medicine

The present PhD thesis represents a contribution to the *IndiTreat* project. This project, which started on January 1st 2011 supported by the Danish Council for Strategic Research, aims at improving chemotherapeutic treatment of patients suffering from colorectal cancer (CRC). The main purpose is to develop a micro- and nano-platform able to test different combinations of available chemotherapeutic compounds on each malignant tissue collected from individual patient and thereby enable a personalized medical treatment. To fulfill the project´s goals, nanotechnology researchers, medical doctors, cell biologists, and a private company collaborate to develop the system and establish its efficiency for treatment of colorectal cancer.[1]

At the moment, colorectal cancer is the second leading cause of cancer-related death in Denmark and it is the most diagnosed cancer in European countries. CRC is a highly heterogeneous disease with multiple interconnected extra- and intra-cellular pathways implicated on the cancer onset.[2] The complexity of processes involved on colorectal malignancy is reflected on patients with a diverse responsiveness to standard chemotherapeutic treatments. Nowadays, various chemotherapeutical treatments (FDA approved) are daily used together with surgery to cure CRC. Some examples are the application of antibodies against the epidermal growth factor receptor, EGFR such as cetuximab and panitumumab. It has been shown that these antibodies are effective only when the related protein KRAS involved in the intracellular signaling pathway is un-mutated.[3] Therefore, in patients where KRAS protein is mutated, different chemotherapeutic treatments are needed. Currently, 47 new drug candidates are under evaluation in CRC trials and 42 of them are administrated in combination regimens.[3] Thus, *in vitro* screening assays to predict individual patient responsiveness to drugs or combinations of drugs are required and their demand is gradually increasing. Recently, various cell-handling techniques prove a great correlation of *in vitro* results with the *in vivo* physiological condition of patients.[4–9] Such correlation between *in vitro* and *in vivo* data has led the US Government social insurance program, Medicare, to evaluate the *in vitro* efficiency of adjuvant medical treatment for individual cancer patient. Normally, patients presenting primary tumor are subjected to surgery and adjuvant chemo- or radio-therapy, whereas patients with primary metastasis or recurrent malignancy are offered combination chemotherapies as palliative treatment and to prolong survival. The aim of *IndiTreat* is to improve the responsiveness to chemo-treatment and decrease the risk of resistance to the selected treatment raising the clinical response rates.

In the light of that, the overall objective is to develop a micro- and nano-technology platform that enables fast, reliable and inexpensive efficacy and resistance test of the colorectal drug combination therapies used clinically in small tissue volumes from individual patients. The nano-technological

platform should identify the optimum drug combinations for the treatment of colorectal cancer and introduce the established technology for the *in vitro* study of various pathological diseases.

## 1.1 Multi-drug screening *in vitro* and *in vivo*

One of the major challenges encounters on chemosensitivity screening is the evaluation of *in vitro* and *in vivo* correlation. To determine the cytotoxic or apoptotic effect induced by anticancer drugs, *in vitro* evaluation in cell culturing systems is required, and a subsequent chemosensitivity assessment in animal models is essential. Many studies have shown the substantial evidence that *in vitro* chemosensitivity is associated with *in vivo* drug response.[10,11] As a consequence, the understanding of drug sensitivity of a specific tumor for a certain drug can help doctors to choose and plan chemotherapy treatment for each patient. There are many fundamental questions at which scientists should answer when evaluating *in vitro* drug screening assay: i) are the *in vitro* results obtained with tumors of a specific histological cell line similar to those clinically observed for the same tumor type? ii) can the selected chemotherapy improve the patient survival after a prolonged time of drug exposure? iii) are the *in vitro* results comparable to those *in vivo*? When malignant cells deriving from tumor biopsy are cultured for drug screening purposes, they are subjected to an extensive manipulation that could alter their drug response. Moreover, the *in vitro* growth rate of tumor cells may be much faster than *in vivo* and false-positive results may be obtained.[7] Another concern is whether the tumoral cells selected for *in vitro* assays are representative of the cancer cells in patient´s tumors. In fact, primary tumors and metastasis are highly heterogeneous in terms of cell populations and it could be that the cell line used *in vitro* is predictive for only a small portion of the patient´s tumor.[7] Although the *in vitro* chemosensitivity study is a simplified approach for the investigation of *in vivo* cell responsiveness on tumor, it is necessary to predict the sensitivity, accuracy and specificity of chemotherapeutics. Among the existing *in vitro* assays, one should select the one which better satisfy the following requirements: the results should correlate with clinical response and survival; the outcome of the assay must be related to the effect of drugs on a certain cell line; the assay information must be easy to interpret and apply; and the test should be inexpensive. The most common *in vitro* assays used to evaluate drug-induced cell proliferation are various: clonogenic,[12] cell suspension,[13] differential staining cytotoxicity,[14] Kern,[15] and collagen gel droplet drug sensitivity[16] tests are usually employed to evaluate the dose-response curves. Another class of drug screening assays is based on the measurement of the cell metabolic activity in response to therapy, such as the ATP bioluminescence,[17] the coloration with sulfo-rhodamine, the fluorescence generated from cellular hydrolysis of fluorescein diacetate,[18] the coloration with reduction of MTS or MTT,[19] the measurement of extra-cellular acidification rate[20] or quantification of cellular protein content. An alternative technique to evaluate the effect of drugs on a cell line is to measure the DNA damage at the chromosome level, for instance rearrangement, loss, breakage of chromosomes, cell division inhibition,

cell apoptosis and necrosis.[21] No matter which *in vitro* assay is chosen, all the listed methods must provide a drug sensitivity index in order to compare outcomes obtained using different approaches. Moreover, when multi-drug regimens are adopted for curative therapy, the *in vitro* assay must also assess the drug interactions providing eventual synergism, additivity or antagonism behavior.[7]

In general, the study of *in vivo* chemosensitivity in preclinical tumor-bearing animal models must be also evaluated. In fact, *in vitro* assays do not take into account many relevant concerns: the distribution of drug to tumor is poor or absent due to a missing vascularization system, the need for drug activation, difference in tumor growth rate *in vitro* and *in vivo*, pharmacological barriers.[7] In conclusion, *in vitro* results obtained from one site of solid tumor may not be representative of other sites in the same patient, thus new approaches able to correlate drug treatment to tumor cell sensitivity are required.

## 1.2 Fabrication of miniaturized platforms for drug-screening in colorectal cancer therapy

The existing point-of-care (POC) devices have a proven role in diagnosis and assessment of colorectal cancer. Although many of the screening tests previously described are well established and validated in diverse commercially available POC devices, their accuracy remains an important drawback.[22] The POC diagnostic industry is gradually expanding with an estimated 35% share of the *in vitro* diagnostic market within United States and was valued at $15.1 billion in 2011.[23] Despite the increasing number of screening strategies and the emerging technologies in molecular marker application, not all methods satisfy the criteria required for screening tests in population programs.[24] Another issue that must be considered is the current discovery of new FDA-approved drugs. Only few novel drugs for colorectal cancer therapy have been developed and anyhow, the traditional drugs for colorectal cancer treatment remain the favorited and mostly used (Figure 1.1) due to the observed survival rate. On the other hand, because of the large heterogeneity of colorectal cancer and patient´s responsiveness to drug therapy, a personalized chemotherapeutical treatment for individual patients is required. Nanotechnology is an emerging discipline in the fields of drug delivery and drug screening. Micro- and nano-systems are widely used in cell culture based studies due to their unique physico-chemical and biological properties, small sizes (ranging between 10-100nm in at least

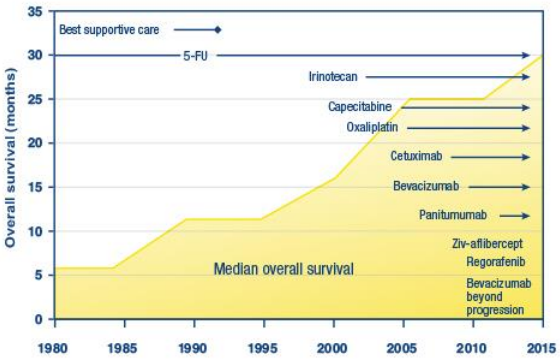


**Figure 1.1** Overall survival of patients with colorectal cancer diagnosed after prolonged chemotherapeutic treatment (data reported from 1980 to 2015).[200]

one dimension), and their ability to protect encapsulated molecules susceptible to the environment (pH, enzymatic degradation, ionic strength) and enhancing drug biodistribution when involved in *in vivo* applications.[25] However, to achieve these goals offered by nanodelivery systems, many issues which include the development of toxic-free system, improved biocompatibility, effective drug loading, and release process, must be assessed.[25,26] In particular, biocompatibility and biodistribution are crucial key points in achieving *in vitro* and *in vivo* successful outcome for drug development. The properties of these delivery systems are strictly influenced by the synthetic process by which they are produced, the coating materials, the particles size, the route of administration and the method used to induce drug release.[27,28] Over the last six decades, more than 85000 compounds were screened against cancers using cancer nanotechnology because of its emerging interdisciplinary research and great potential in diagnosis and treating cancers.[29] *In vitro* models are characterized by the absence of immune effect, blood proteins, and endocrine systems, thus limiting the use of cell culture-based results obtained with nanotechnology to animal models.[30] However, animal systems are extremely complicated with unique bio-distribution, clearance mechanism, immune response and metabolism; therefore, *in vitro* studies can complement animal studies in assessing nanodelivery systems.[26]

The *IndiTreat* project provides a distinct technology that selects specific drug treatment based on cellular responsiveness of tissues from individual patient. The micro- and nano-technologies proposed here may overcome some of the limitations that characterize the existing screening methods, by requiring very small amounts of tissue and permitting a fast and low-cost drug screening of individual drugs and combinations of them. In this thesis, human colorectal adenocarcinoma cell line (HT-29) have been selected as cell culture model because ease to handle (cells can be passaged many times, up to 200 passages) and they are phenotypically stable. The responsiveness of HT-29 cells to the individual and combined drug regimens normally selected for colorectal cancer therapy is finally determined using the developed nanotechnologies.

### 1.2.1 Development of PEG-based hydrogel for multi-drug release

Hydrogels are a large class of biomaterials with numerous advantages and widely applied for simultaneous encapsulation of cells and biomolecules. Poly(ethylene glycol) (PEG)-based hydrogels have been extensively used as matrices for controlling drug delivery, as well as cell delivery vehicles for promoting tissue regeneration. Particularly interesting is the use of poly (ethylene glycol) di-acrylate (PEGDA) hydrogels in many biomedical applications due to their cytocompatibility, poor cell adhesion and ease to handle.[31,32] Some of the PEGDA applications include hydrogel development for drug delivery, tissue engineering, wound healing and electrospinning processes.[33–35] In this thesis, PEGDA hydrogels have been fabricated through visible-light photo-polymerization for drug release purposes, in particular creating three-dimensional (3D) hydrogel structures in which different drugs are embedded. The release of each anti-colorectal cancer drug (5-FU, oxaliplatin, SN-38 and folinic acid

described in detail in the following sections) is characterized and tuned to guarantee a release for three days. Moreover, drug-loaded nanoparticles (liposomes) are employed and embedded within hydrogels to protect and control the release of oxaliplatin, otherwise rapidly lost during washing process (Figure 1.2).

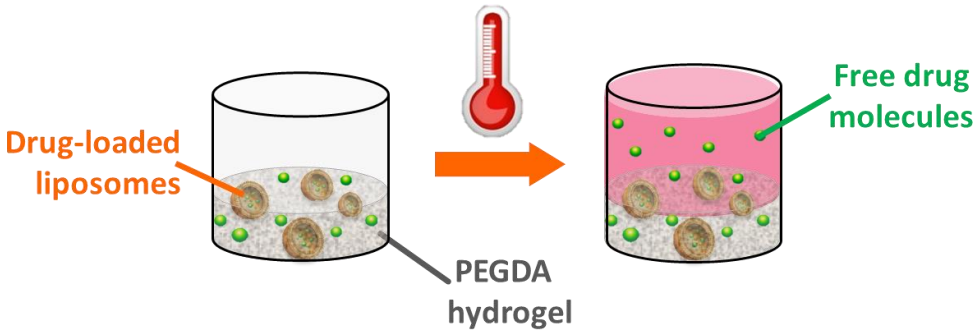


**Figure 1.2** Schematic of the nanotechnology presented in this thesis. The system involves three-dimensional (3D)-hydrogel structures composed of PEGDA and anti-colorectal cancer drugs embedded within polymeric network. Human colorectal adenocarcinoma cells (HT-29) are cultured onto the hydrogel surface and the effect of released compound doses on cell proliferation is evaluated. Drugs are embedded within the network as free drugs or loaded into nanoparticles (liposomes) which are thermally triggered. The passively released molecules are collected into the supernatant and quantified.

The effect of individual embedded drug and combinations of embedded compounds is evaluated by culturing human colorectal adenocarcinoma cells onto the hydrogel surface, and the response of cells exposed to different drug doses is determined (cell proliferation or cell cytotoxicity). Among the existing drug releasing systems, the proposed nanotechnology has a number of advantages:

a) PEGDA hydrogels are easily fabricated through photo-polymerization (the process takes 1 minute to completely crosslink a solution of polymer and photo-initiator);
b) the material is biocompatible due to the choice of light source, photo-initiator and reactants concentration;
c) multiple solutions can be polymerized at the same time (12 wells are crosslinked in 1 minute);
d) traditional disposable may be employed for hydrogel curing and drug release study (96 well-microtiter plates);
e) drugs with a determined concentration are directly embedded within polymeric network during photo-polymerization;
f) after a washing step, the drug-hydrogel system is utilized for cell culture purposes and because of the miniaturized technology, various parameters may be tested in the same experiment (for instance drug dose and cell concentration);

g) the release of drugs can be tuned by changing the physico-chemical properties of hydrogel (small and hydrophilic compounds are quickly released from hydrogel);
h) the use of drug-loaded nanoparticles embedded within hydrogel ensures a protection of molecules from the environment and controls drug release through the application of a proper trigger (thermo-sensitive liposomes are sensitive to temperature changes, so their content is released only when a certain temperature is reached);
i) a direct dose-cytotoxicity outcome is obtained using conventional proliferation assays (for example metabolic activity assays) with a high reproducibility.

Besides the specific employment of PEGDA hydrogels for drug screening in colorectal cancer therapy, the described nanotechnology may be transferred to other types of solid cancers and can be further developed for large-scale production and perhaps at a smaller scale. A detailed description of the PEG-based hydrogel nanotechnology is found in Chapter II.

### 1.2.2 Fabrication of inter-digitated PEDOT-$N_3$ electrodes for co-localization of nanoparticles and colorectal cancer cells

In this thesis, a micro- and nano-technology platform has been also explored with the aim of co-immobilizing drug-loaded nanoparticles (liposomes) on functionalized polymer micro-electrodes and human colorectal adenocarcinoma cells (HT-29) on the surrounding electrodes areas. More specifically, we wanted to capture cell subpopulations, in particular cancer stem cells.
Conductive and semi-conductive polymers are an extensive class of materials largely used for bio-medical devices due to their ability to replace expensive metals and semiconductors. Conductive polymers have the capability to act as conductors and bio-molecules may be embedded within the polymer during polymerization process or attached by post-polymerization coupling chemistry. The release of certain molecules may be induced as an example, upon an electrical trigger without altering the physico-chemical properties of the targeted compound.[36,37] Specifically, poly(3,4-(1-azidoymethylethylene)-dioxythiophene) (PEDOT-$N_3$) has been used for the fabrication of such system due to its ease of handling, chemical stability, cellular compatibility and post-fabrication chemical functionalization. Briefly, PEDOT-$N_3$ electrodes are fabricated using printed dissolution technique on a PEG-coated support which is used to discourage protein and cell adsorption (Figure 1.3).

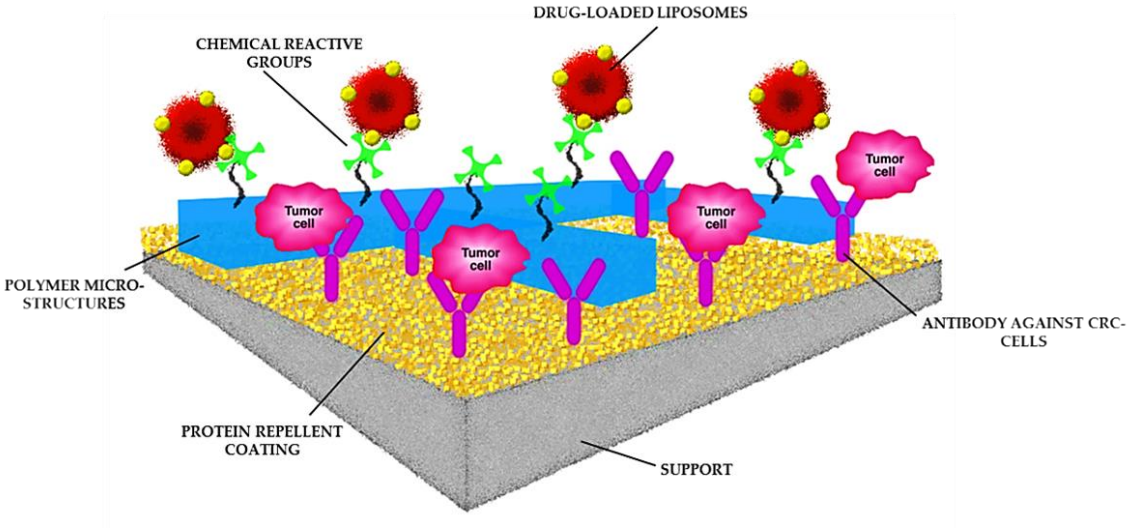


**Figure 1.3** Schematic of the micro- and nano-technology platform. Polymer micro-structures (width around 100μm) are fabricated through printed dissolution method and subsequently functionalized via "click chemistry" to ensure drug-loaded liposomes immobilization. A specific antibody against cell-membrane antigen expressed by colorectal cancer cell line (HT-29) is stabilized onto the areas surrounding the electrodes. The application of a certain current through the polymer electrodes enhances a thermal leakage of nanoparticles and the effect of released drugs is evaluated.

The printed dissolution technology, previously investigated in our group, is based on the use of agarose stamps presenting micro-structures on their surface; the contact of such stamps with polymer films allows the removal of polymer only from the areas which were in contact with the stamp. After fabrication, drug-loaded liposomes are immobilized on the electrodes surface through "click chemistry" (Copper(I)-catalyzed azide-alkyne Huisgen 1,3-dipolar cycloaddition or CuAAC) and biotin-avidin conjugation.

Such micro- and nano-technology presents many benefits:

a) No need for cleanroom facilities for the micro-electrodes fabrication;
b) the miniaturization of the drug screening system (the polymer electrodes have a width of 100μm and liposomes have an average diameter of 100nm);
c) a spatially-controlled liposomes immobilization;
d) the overall electrodes area may be increased by maximizing the number of micro-electrodes in order to augment the concentration of immobilized drug-loaded liposomes and potentiate the cytotoxic effect of released drugs.

However, the fabrication method used to produce micro-electrodes was challenging and an extensive optimization of the process was required. The lack of a technique able to create reproducible and defined polymer electrodes led us to explore other fabrication methods. A deeper explanation of the described micro- and nano-technology is reported in Chapter III.

In future, the integration of nanofabricated PEDOT-$N_3$ electrodes with the already established electrode functionalization will be explored in more detail. Ideally, once the liposomes are immobilized onto PEDOT-$N_3$, a certain current may be applied on the conductive electrodes. The electrical current through the electrodes will lead to resistive heating and consequently drug molecules loaded into liposomes may be released from the aqueous interior compartment due to temperature changes.

## 1.3 ColoRectal Cancer (CRC)

Colorectal cancer (CRC) is a pathology in which malignant cells form a tumor in the tissues of colon and rectum. The colon is part of the digestive system in which nutrients are processed and removed from the body. The digestive system is composed of the esophagus, stomach, small and large intestines. The colon, also defined as large bowel, is the first tract of the large intestine and is about 1.5 meters long, and the rectum represents the final part of the large intestine (circa 20 centimeters long) (Figure 1.4A). The large intestine is a muscular tube and its wall is formed by several and different layers (Figure 1.4B), from the lumen to the outer: the mucosa which is composed by many layers including a thin muscle layer, the submucosa (mainly fibrous tissue), the muscularis propria (a thick layer of muscle that contracts to force the nutrients of the intestines along), the subserosa (a thin stratum of connective tissue) and the serosa, the second and outer layer of connective tissue.

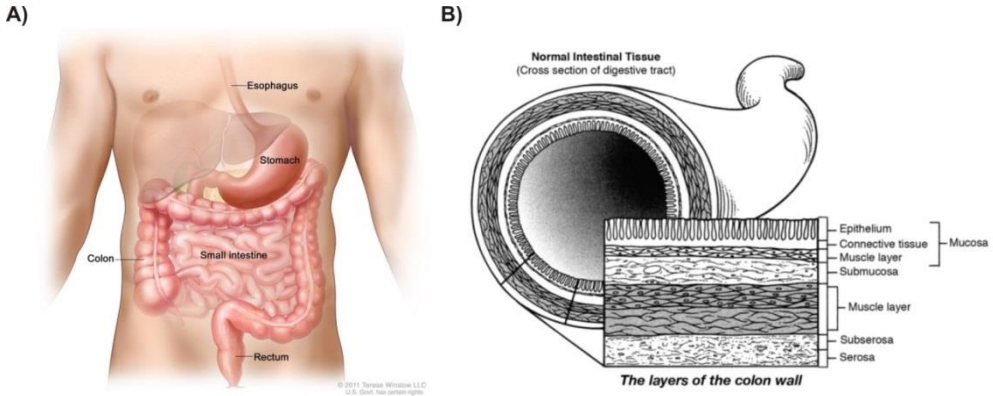


**Figure 1.4** (**A**) Anatomy of the lower digestive system showing the colon and other organs.[23] (**B**) Layers composing the colon wall.[38]

### 1.3.1 Tumor cell properties

The development of cancer occurs when an imbalance of cell homeostasis and unregulated proliferation of cells are found. Cancer cells grow and divide in an uncontrolled manner and are represented by highly heterogeneous neoplastic cell populations. This heterogeneity is dynamic, changing continuously over time and in certain cases, it can turn to irreversible state with an increased

biological aggressiveness of tumor in terms of spreading in normal tissues and organs, and metastatic features.[39] The generalized loss of growth control showed by cancer cells derives from an increased number of abnormalities in cell regulatory systems and it is recognizable in several aspects of cell behavior that discern cancer cells from their normal counterparts.[40] The tumoral cells possess defined characteristics: accelerated cell cycle, genomic alterations, invasive growth, enhancement of cell mobility, changes in the cellular surface and morphology, and a variation of the secreted molecules pool.[41] At the cellular level, cancer cells present large nucleus, irregular size and morphology, increased number of nucleoli and a poor density of cytoplasm. Further, changes on the organization of the genetic material and proliferation are displayed: a scarce content of heterochromatin, a higher number of nuclear membrane pores, and atypical structures formed during mitosis process are discovered on multinucleate cells. The cell membrane of cancer cells plays also a crucial role in the tumor progression: proteins and surface receptors undergo important modifications, thus losing their normal sensitivity towards natural ligands; rather, new molecules are exposed on the surface where mainly act as antigens favoring the recruitment of immune system response.

### 1.3.2 Colorectal cancer staging

Staging of the disease and a complete visualization of colon regions are required once colorectal cancer is diagnosed.[42] There are two main questions that patients ask to doctors in order to learn how survive to a disease: firstly, what is the prognosis to be followed in order to achieve the greatest recovery and survival; and secondly, what treatment should be applied. A possible answer to these questions is given by the knowledge of the type of cancer and how advanced it is.[38] The staging of cancer is one of the crucial parameters to take into account because it defines the growth and the location of cancer. Once the stage is known, then the doctor may be able to predict the course of tumor and the best suitable treatment for each individual patient. The TNM staging system is a universal and standardized method for doctors to classify the spreading degree of cancers. Except for leukemia and brain cancer, it is applicable to any kind of disease:

- T category: it is used for primary tumors where tumors are localized in a specific region and/or a specific cell line;
- N category: it is referred to regional metastasis (or primary metastasis) in which the malignant cells have spread to the nearby tissues, for instance lymph nodes;
- M category: it is used to indicate distant metastasis (or secondary metastasis); this class includes all the malignant cells which have invaded organs or distant areas of the body.

Once the patient´s tumor has been recognized within a T, N, M class, the illness degree is evaluated, normally after surgery in order to define the progression and the severity of the tumor (expressed in

Roman numerals from stage 0 to stage IV) (Figure 1.5). Despite surgery is the first treatment for many people with colorectal cancer, some of them may receive radiation and/or chemotherapy before surgery. Thus, the stage of cancer after treatment is an important information for doctors to evaluate the prognosis and treatment choice for each patient.

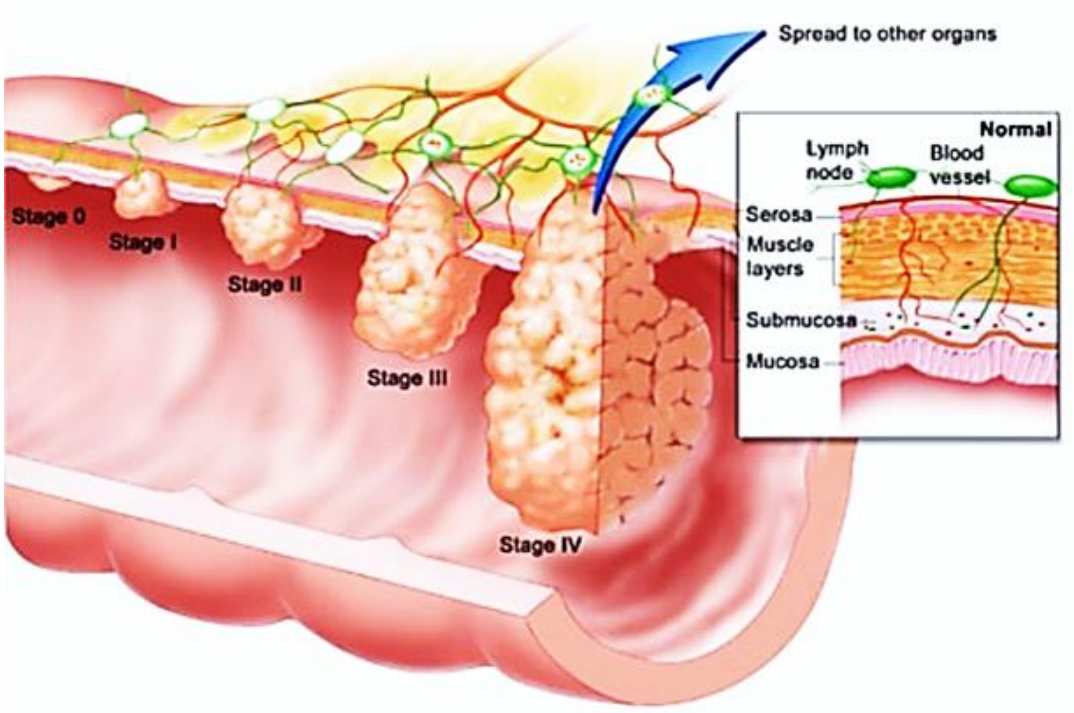


**Figure 1.5** Schematic of the invasiveness of tumors in different stages.[43]

### 1.3.3 Pathogenesis

Colorectal cancer is a very heterogeneous disease that, as many other cancers, is caused by the interaction of genetic alterations and environmental factors. Most of the CRCs arise at a certain age (usually after 40 years) and only a small proportion of these cancers (20-25%) are connected to hereditary component, such as familial adenomatous polyposis.[44] Generally, colorectal cancer is provoked by a gradual accumulation of genetic and epigenetic changes, leading normal colonic mucosa cells to phenotypically transform into malignant and invasive cells. The majority of CRC cancers develop from adenomas which are able to become neoplastic cells within 10-15 years.[24]

Once colorectal cancer is diagnosed, the following treatment consists on the surgical removal of primary tumor combined with a pre- and post-surgical therapy which may be radiotherapy, chemotherapy or adjuvant chemo-radiotherapy. Often adjuvant chemo-radiotherapy is applied for loco-regional cancer treatment because of great improvements on the eradication of malignant

metastasis.[45] As reported in literature, important progresses have been done on the research of new drugs or new combinations of individual drugs. As widely demonstrated by MOSAIC project,[46] increased survival rates are obtained when FDA-approved chemotherapies (FOLFOX and FOLFIRI) are administrated to patients with primary colorectal tumor. In light of the fact that approximately half of the patients diagnosed with CRC develop metastasis, especially in the liver, specific treatments are needed. Surgical removal of small and large metastasis is still necessary and other techniques (radiofrequency ablation,[47] hepatic arterial chemotherapy[48] and radioembolization with yttrium-90 microspheres[49]) have been incorporated as a complement to surgery to achieve resectability.[24] For neo-adjuvant treatments of resectable liver metastasis, FOLFOX, FOLFIRI and FOLFOXIRI have shown high response rates with similar survival outcomes of 30% for FOLFOX and FOLFIRI[50] and 66% for FOLFOXIRI treatment,[51] respectively.

## 1.4 Chemotherapeutics approved for CRC treatment

Colorectal cancer refers to cancer of the colon (bowel) and rectum. When cancer is diagnosed, screening tests are used to characterize the type of colorectal cancer, the stage (meaning how far the cancer has progressed), the localization and the grade of tumor. These characteristics are then used to determine the most suitable treatment for each individual patient. Nowadays, the drugs approved by Food and Drug Administration (FDA) for colorectal cancer are commonly used as combinations of individual drugs (FDA-approved), while drug combinations themselves are not approved (Table 1.1).[52] In this thesis, four drugs against colorectal cancer have been selected and studied: SN-38 (the active metabolite of Irinotecan), 5-fluorouracil, oxaliplatin and leucovorin hydrochloride (also known as folinic acid). These drugs were used as individual treatment and as well as combinations of drugs; further, their anti-proliferative effect was evaluated on human colorectal adenocarcinoma (HT-29) cell line. The cellular function and molecular characteristics will briefly be discussed in the following subsections.

**Table 1.1** Individual drugs and drugs combinations approved by FDA for the treatment of ColoRectal Cancer.[52]

| Individual drugs for ColoRectal cancer (FDA-approved) | Drug combinations for ColoRectal cancer (FDA-approved) |
|---|---|
| Adrucil (Fluorouracil)<br>Avastin (Bevacizumab)<br>Bevacizumab<br>Camptostar (Irinotecan Hydrochloride)<br>Capecitabine<br>Cetuximab<br>Efudex (Fluorouracil)<br>Eloxatin (Oxaliplatin)<br>Erbitux (Cetuximab)<br>Fluoroplex (Fluorouracil)<br>Fluorouracil<br>Irinotecan Hydrochloride<br>Leucovorin Calcium<br>Oxaliplatin<br>Panitumumab<br>Regorafenib<br>Stivarga (Regorafenib)<br>Vectibix (Panitumumab)<br>Wellcovorin (Leucovorin Calcium)<br>Xeloda (Capecitabine)<br>Zaltrap (Ziv-Aflibercept)<br>Ziv-Aflibercept | CAPOX<br>FOLFIRI<br>FOLFIRI-BEVACIZUMAB<br>FOLFIRI-CETUXIMAB<br>FOLFOX<br>FU-LV<br>XELIRI<br>XELOX |

### 1.4.1 Camptothecin and its chemical analogues

Irinotecan and SN-38 are derivatives of camptothecin, a water-insoluble natural alkaloid produced by *Camptotheca acuminate*[53] and *Mappia foetida*[54] Asian trees. This compound demonstrated excellent anti-cancer activity in early clinical trials for gastric cancer treatment, but also important side effects such as hemorrhagic cystitis, gastrointestinal toxicities and myelosuppression.[55,56] The main mechanism of antitumor activity of camptothecin was assessed as inhibitor of topoisomerase I (Topo I) enzyme.[57] Due to poor water-solubility and severe side effects of camptothecin, researchers began to synthesize analogue compounds of it, and currently the most clinical used analogues are Topotecan and Irinotecan. Topotecan, commercialized as Hycamtin® is used for the treatment of patients with metastatic ovarian cancer, while Irinotecan (Campto®) is widely applied in several European countries as second-line treatment of recurrent metastatic colorectal cancer. Even though Irinotecan induces remissions in 11-23% of the 5-fluorouracil (5FU)-resistant tumors,[58] the combination of Irinotecan

with 5FU and Leucovorin (also known as Folinic Acid, FA) has been approved as first-line chemotherapy for patients with metastatic colorectal cancer.[59] As depicted in Figure 1.6, all camptothecin analogues have a common chemical structure composed of a planar five-ring system with a lactone group. Further substitutions at positions 7, 9 and 10 are usually responsible for an enhanced Topo I inhibitory activity,[60,61] whereas substitutions at carbons C-12 and C-11 result on a activity neutralization.[60]

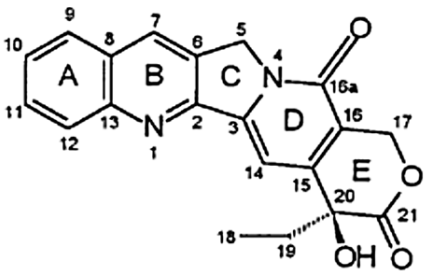


*Substituent Group*

| *Compound* | C-11 | C-10 | C-9 | C-7 |
|---|---|---|---|---|
| Camptothecin | H | H | H | H |
| Irinotecan | H | 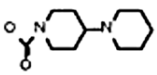 | H | $CH_2CH_3$ |
| SN-38 | H | OH | H | $CH_2CH_3$ |
| Topotecan | H | OH | 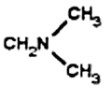 | H |
| Lurtotecan |  | | H | 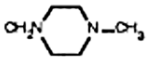 |
| 9-aminocamptothecin | H | H | $NH_2$ | H |
| 9-nitrocamptothecin | H | H | $NO_2$ | H |
| DX-8951 | F | $CH_3$ | $CH_2$ | $CH\text{-}NH_2$ |

**Figure 1.6** Structures of camptothecin and analogues: Topotecan, Irinotecan (CPT-11), Lurtotecan (GW211), 9-aminocamptothecin (9-AC), 9-nitrocamptothecin (9-NC) and DX-8951.[62]

The biological function of the nuclear enzyme topoisomerase I is to remove torsional stress generated during DNA replication and transcription preserving the three-dimensional DNA conformation. As reported by Takimoto *et al.*,[63] topoisomerase I interacts with supercoiled double strands DNA forming a transient catalytic intermediate (cleavable complex), in which the enzyme is covalently bound to DNA and torsionally relaxed single-stranded DNA are produced. With a rapid re-ligation mechanism,

original double-strands of DNA are reformed. Camptothecins inhibit the re-ligation process by non-covalently association to the Topo I-DNA cleavable complex, and single strand DNA breaks are therefore accumulated within the cell (Figure 1.7).

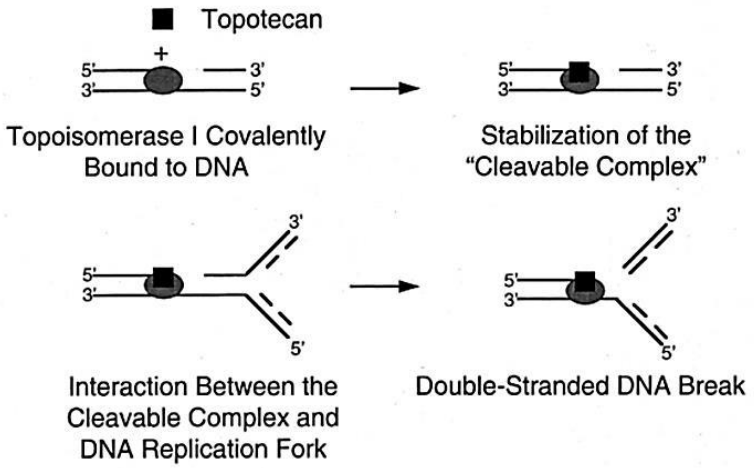


**Figure 1.7** Mechanism of Topotecan action: the stabilization of DNA-topoisomerase I cleavable complex in presence of ongoing DNA replication generates cytotoxic DNA damage.[63]

Cytotoxicity of camptothecins can be attributed to the arrest of the replication fork and finally cessation of RNA synthesis.[64] Since the activity of Topo I is often higher in colorectal tumors than in normal colonic tissues, it may confer tumor specificity of the Irinotecan-mediated effects.[65] This cytotoxic DNA damage in some cancer cell lines leads to programmed cell death or apoptosis,[66] and because of the need of ongoing DNA synthesis, camptothecin is mostly active during S-phase of the cell cycle. The cytotoxic potency of camptothecin analogues against human colorectal adenocarcinoma (HT-29) cells differs widely with the following order of anti-proliferative activity: SN-38 (the active metabolite of irinotecan) > camptothecin > 9-AC > topotecan >> irinotecan.[67] The effect of irinotecan itself is minimal, whereas when a rapid hydrolysis of irinotecan to SN-38 occurs a higher anti-proliferative effect is observed. All camptothecin derivatives commonly used in clinical trials possess a lactone ring which is chemically unstable; however the need of an intact lactone group is essential for the interaction of drug with DNA-enzyme complex. Under acidic conditions (pH<4), the lactone moiety prevails whereas under basic conditions (pH>10), an open-ring state is mostly present.[68] As depicted in Figure 1.8, at physiological pH all camptothecins are converted to the carboxylate form except for SN-38.

*In vitro* studies have shown that the treatment of HT-29 cell line with SN-38 is 100-1000 fold more potent than the water-soluble irinotecan.[67] It has been also reported that irinotecan (also known as CPT-11) induces a dose-dependent apoptosis or premature senescence in a large variety of cell lines.[69] Rudolf *et al.* evaluated irinotecan cytotoxicity in normal human colonic fibroblasts (NCF),

normal human colonic mucosa cells (NCM) and human colorectal carcinoma cells (HCT).[70] The treated HCT and NCM cell lines showed typical apoptotic morphologies (cell rounding, shrinkage and blebbing), while these phenomena were significantly reduced in NCF cells which displayed alternative morphologies, enlargement of cell bodies and a reduced cellular density. When HT-29 carcinoma cell line is subjected to SN-38 treatment, a dose- and exposure duration-dependent anti-proliferative activity of drug is established.[71]

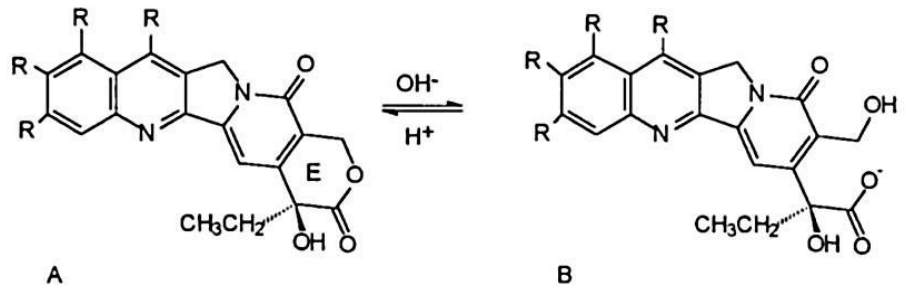


**Figure 1.8** Schematic representation of the reversible pH-dependent hydrolysis of the lactone ring (**A**) into the carboxylate form (**B**) of camptothecin analogues.[62]

SN-38 is considered an S-phase cytotoxic compound and it has a very small effect on apoptosis and percentage survival in HT-29 during the first 48h for concentrations lower than 5ng $mL^{-1}$. Conversely, when higher SN-38 doses are used (100 ng $mL^{-1}$), an immediate arrest in the S-phase is achieved.[71] At the moment, irinotecan is used as an effective chemotherapeutic agent for advanced colorectal cancer as first- and second-line treatment. Irinotecan has been reported to be active also in gastric cancer, non-small lung cancer and small-cell lung cancer, as individual therapy or in combination with other cytotoxic agents.[72]

### 1.4.2 5-fluorouracil (5-FU)

5-fluorouracil (5-FU) is a fluoro-pyrimidine compound largely used in the treatment of a broad range of cancers, such as colorectal and breast cancers and tumors of the aerodigestive tract. Although 5-FU in combination with other chemotherapeutics improves the response and survival rates in breast, neck and head cancers, it is in colorectal cancer that 5-FU explicates the greatest anti-tumor activity.[73] 5-FU has a dual anti-tumor mechanism: it inhibits essential biosynthetic processes and is directly incorporated into nucleic acid molecules (RNA and DNA) impairing their normal function. 5-fluorouracil is an analogue of uracil and presents a fluorine atom at the carbon C-5 (Figure 1.9A). When cells are treated with this drug, it rapidly enters the cell using the same transport mechanism of uracil,

and once located into cytoplasm, 5-FU is converted intracellularly to various active metabolites.[74] These active metabolites are responsible for the interruption of RNA synthesis and the enzymatic activity of thymidylate synthase (TS). Briefly, this enzyme catalyzes the reductive methylation of deoxyuridine monophosphate (dUMP) to deoxythymidine monophosphate (dTMP), normally used as essential component for DNA replication and repair. The metabolite of 5-FU (fluorodeoxyuridine monophosphate, FdUMP) covalently occupies the substrate-binding site of TS forming a stable ternary complex, and thus inhibiting the DNA replication[75,76] (Figure 1.9B).

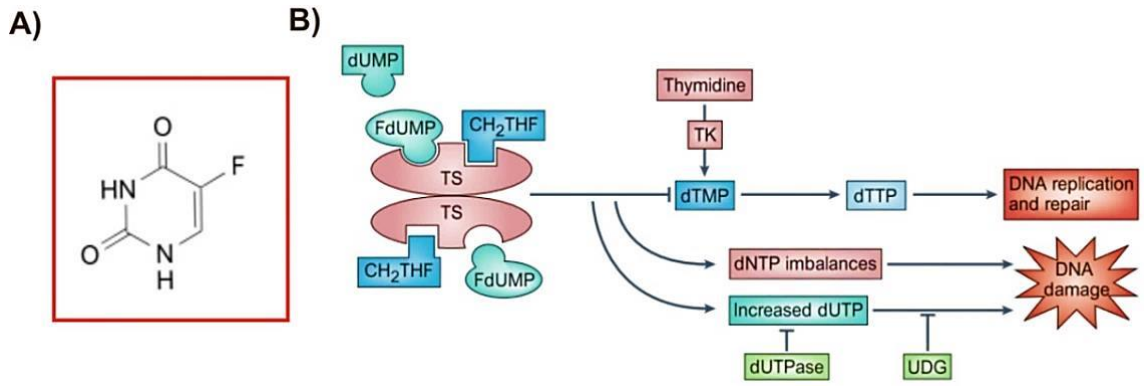


**Figure 1.9** Structure of fluoropyrimidine 5-FU (**A**) and mechanism of thymidylate synthase inhibition by 5-FU (**B**). The active metabolite FdUMP (fluorodeoxyuridine monophosphate) blocks the binding site of TS normally occupied by the natural substrate dUMP (deoxyuridine monophosphate). A consequent deoxynucleotide (dNTP) pool imbalances cause the inhibition of DNA synthesis and DNA damage.[73]

5-FU-based chemotherapy improves overall survival of patients with resected stage III colorectal cancer.[77] Despite that, the response rates for the 5-FU treatment as first-line therapy for advanced colorectal cancer are only 10-15%.[78] Consequently, the combination of 5-FU with other chemotherapies such as Irinotecan or oxaliplatin has enhanced the response rates for advanced colorectal cancer to 40-50%.[79,80]

### 1.4.3 Oxaliplatin and platinum-based chemotherapeutics

Although for more than four decades 5-FU has been the most commonly used drug for the treatment of colorectal cancer, the development of new active drugs for CRC treatment, such as oxaliplatin, has improved clinical outcome and has offered alternative therapeutic options.[81] In particular, platinum-based drugs including cisplatin, carboplatin and oxaliplatin, have been widely studied and used for the treatment of lung, colorectal, ovarian, breast, head, neck and testicular cancers.[82] Cisplatin was approved as anti-cancer drug in 1978 and within a decade, a second-generation platinum drug

(carboplatin) replaced cisplatin due to higher stability. Nowadays, oxaliplatin (OxPt), the third-generation platinum drug, is the standard compound used for the treatment of advanced and metastatic colorectal cancers in combination with 5-fluorouracil and leucovorin. An improved survival among stage III-patients when OxPt/5-FU/leucovorin poly-chemotherapy is observed compare to 5-FU/leucovorin therapy showed an inferior response.[83] Cisplatin, carboplatin and oxaliplatin chemically differ in solubility, reactivity, structure, pharmacokinetics, and toxicology (Figure 1.10A).[84] Each compound has a different chemical structure and oxaliplatin contains a diaminocyclohexane (DACH) group which is more reactive with nucleophiles than the other drugs.

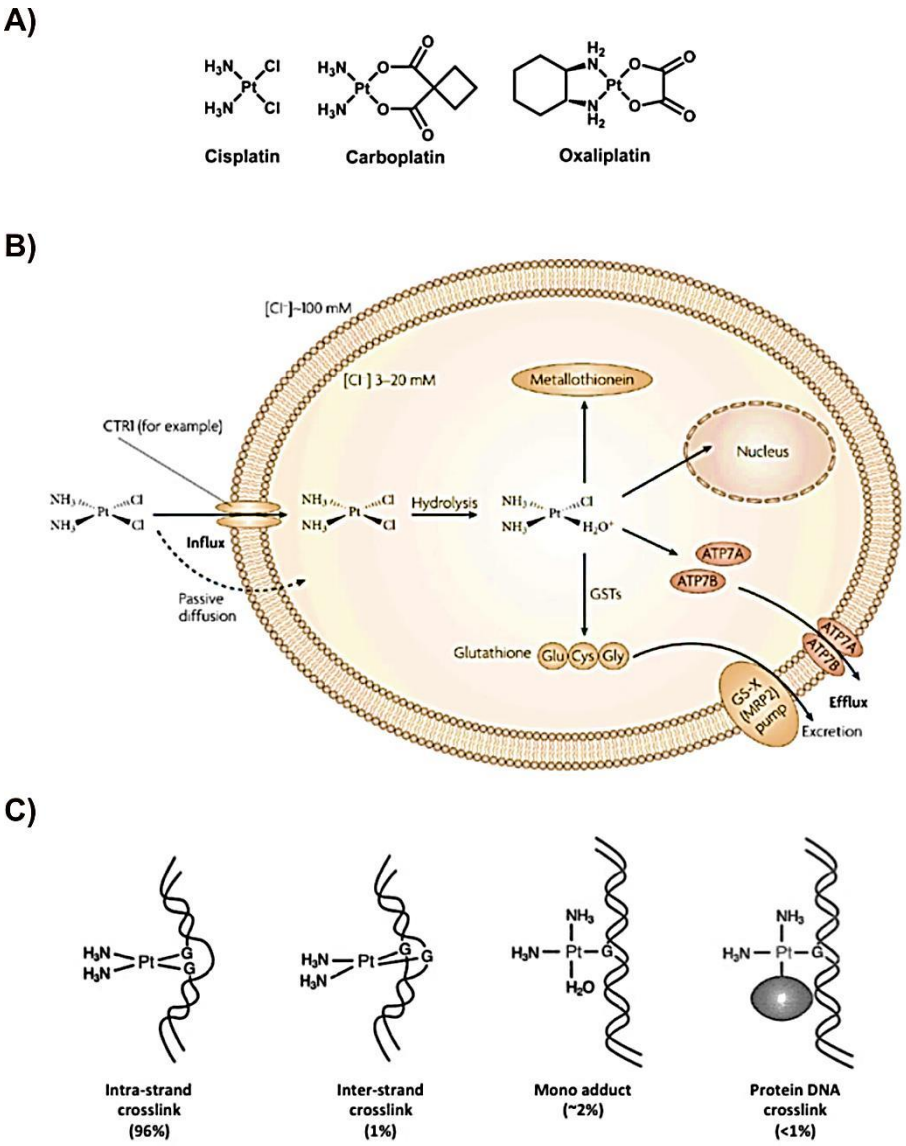


**Figure 1.10** (**A**) Chemical structure of platinum-based drugs: cisplatin, carboplatin, oxaliplatin. (**B**) Schematic of cisplatin uptake inside cell and consequent aquation into the cytoplasm. The compound is then translocated into the nucleus where it explicates its toxicity.[85] (**C**) Schematic of different complexes formed by the interaction of platinum-based molecules and double-stranded DNA and nuclear proteins.

Platinum-based drugs undergo hydrolysis reaction by which one or both oxygenated groups are replaced by molecules of water, thus resulting in positively charged molecules (Figure 1.10B). The aquation reaction represents the crucial step by which drugs manifest their toxicity: only when the drugs are in the charged state are able to form covalently stable adducts with double-stranded DNA.[86] The cross-linking of platinum-drug molecules to DNA leads to the inhibition of synthesis and repair of DNA and finally to apoptosis (Figure 1.10C).[87,88] Even though the cellular damage is thought to be induced by the formation of these DNA adducts, additional complexes of platinum-DNA-protein have been demonstrated as potentiating mechanism of cytotoxicity.[89] Nevertheless, these platinum agents have also shown a significant neurotoxicity (cisplatin > oxaliplatin >> carboplatin). Therefore, the efficacy of platinum-based drugs is often impaired because the substantial risk for severe toxicities.[82] Indeed, the FDA reported that more than 70% of the patients receiving oxaliplatin as main chemotherapy are affected by some degree of sensory neuropathy.[90]

### 1.4.4 Leucovorin

Leucovorin is also called folinic acid (FA) or 5-formyltetrahydrofolate and is generally administered as calcium or sodium folinate. Commonly, FA is an adjuvant used in cancer chemotherapy in combination with methotrexate,[91] or with 5-fluorouracil in treating colorectal, head and neck, esophageal cancers, and other cancers of the gastrointestinal tract. FA should be distinguished from folic acid which is a necessary vitamin (B9), even though FA is an analogue of folic acid and has the full vitamin activity of vitamin B9. FA is not a drug itself and has almost no side effects but when used in combination with methotrexate it acts as chemo-protectant because it preserves the bone marrow and gastrointestinal mucosa cells from methotrexate side effects. Contrarily, the effect of folinic acid in combination with 5-FU is to enhance the cytotoxic effect of 5-FU by further inhibition of thymidylate synthase enzyme and by prolonging the availability of 5-FU in cancer cells. FA is a 5-formyl derivative of tetrahydrofolic acid (Figure 1.11) and when administered, it is rapidly converted to other folinic acid analogues (tetrahydrofolate).

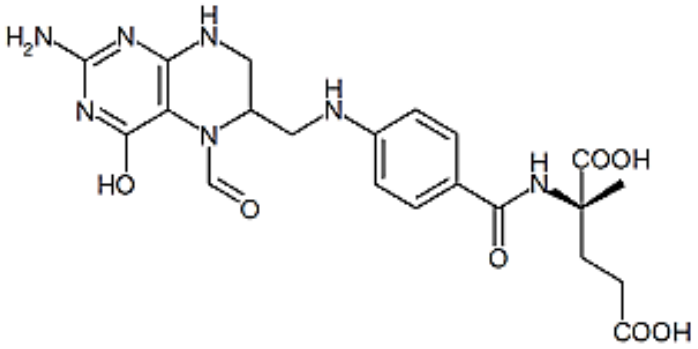

**Figure 1.11** Chemical structure of Leucovorin (folinic acid, FA).

Therefore, FA has a vitamin activity comparable to folic acid and because it does not require the action of enzymes for its conversion, FA biological function as vitamin is always guaranteed. Leucovorin is also used by itself for the treatment of anemia defects when folic acid deficiency is present.

## 1.5 Effect of drugs combinations on the treatment of CRC

Although the approved chemotherapeutics (Irinotecan, oxaliplatin, 5-FU and Leucovorin) have proved to be active for the treatment of colorectal cancer when used as single agents, combinations of these drugs have reported great results and an increased survival rate.[92] Nowadays, the significant reduction in the risk of death even in patients having earlier-stage colorectal cancer, is attributed to the use of combination regimens such as FOLFOX and FOLFIRI. FOLFOX corresponds to the chemotherapy combination FOLinic acid/Fluorouracil/OXaliplatin, and FOLFIRI is the common name used to indicate the combined drugs FOLinic acid/Fluorouracil/IRInotecan. To the extent that 5-FU and irinotecan each have a substantial single agent activity and they appear to be relatively non-cross-resistant, researchers have started to explore modes in which both drugs may be used simultaneously as front-line systemic therapy for the treatment of advanced colorectal cancers.[93] Preclinical studies have demonstrated that the simultaneous administration of Irinotecan and 5-FU resulted in a reduced cytotoxicity of the active metabolite SN-38, suggesting that 5-FU may interfere with the metabolic conversion of irinotecan to SN-38.[94] Indeed, the addition of leucovorin to irinotecan and 5-FU combination enhances the overall cytotoxicity of therapy.[95] Moreover, Mullany *et al.*[96] have proposed a sequence-dependent synergy between SN-38 and 5-FU/FA and provided a possible mechanistic model for this observation. Briefly, the *in vitro* cytotoxicity obtained after the simultaneous or sequential drugs treatment (SN-38 followed by 5-FU/FA or 5-FU/FA followed by SN-38) were found to be different. As described for FOLFIRI therapy, also the FOLFOX treatment has shown successful results: despite oxaliplatin-based therapy has been used for many decades as powerful treatment against colorectal cancers as single agent, when combined with 5-FU/FA, the response rate and overall

survival are improved more than double.[79] FOLFOX and FOLFIRI are therefore widely used as first-line and second-line chemotherapy for metastatic colorectal cancer. However, in some cases, especially those with metastatic lesions, solid tumors may acquire chemo-resistance to therapy. Most solid tumors present a central area which is characterized by a poor vascularization, intratumoral perfusion and a hypoxic environment.[94] It is well-known that tumor cells under hypoxic conditions are more resistant to ionizing radiation and chemotherapy.[97] The effect of hypoxic environment on the chemo-sensitivity of human colorectal adenocarcinoma (HT-29) cells exposed to FOLFOX and FOLFIRI treatments has been evaluated.[94] The addition of FOLFOX at different doses to HT-29 cells under normoxia conditions strongly affected their proliferative activity; contrariwise, the effect of FOLFOX therapy was completely abrogated when cells were cultured under hypoxia. Unexpectedly, the cytotoxicity of FOLFIRI chemotherapy was still maintained even under hypoxic conditions, overcoming the chemoresistance developed by intra-tumoral cells.

In conclusion, the success of FOLFOX and FOLFIRI regimens has been demonstrated to provide clinical benefit in the treatment of colorectal cancer which are not reported only in an advanced stages, but also earlier-stages of tumor. In particular, FOLFOX has been approved by FDA as adjuvant therapy for resected stage III colon cancer.[46]

# 2 PEGDA hydrogels for drug screening assays

In this chapter, a technology based on the use of poly(ethylene glycol) diacrylate (PEGDA) hydrogels for drug screening purposes is described in detail. Hydrogels are widely applied in many fields, for instance in tissue engineering, for *in vivo* drug delivery and for the fabrication of micro- and nano-structures. Here, we want to focus on the application of hydrogels for *in vitro* molecules embedding and their consequent release through passive diffusion or stimulated by the application of a proper trigger. Hydrogels are polymeric 3D networks which are formed via chemical or physical crosslinking and they are characterized by a high water content. Different methods are generally used to create gels and *in situ* radical photo-polymerization has been selected to embed compounds within PEGDA hydrogel. An extensive study of the fabrication conditions (photo-initiator compound, source light, PEGDA and photo-initiator concentrations, PEG length chain and exposure time) are explored. Furthermore, a technology able to create 3D shaped PEGDA hydrogels has been adopted in order to entrap molecules within certain volumes of gel. The passive release of different molecules in terms of size and chemical properties from hydrogels is also determined. On the basis of the observed release profiles, the properties of PEGDA gels are tuned to enhance the diffusion of molecules which are slowly released and to prevent a rapid diffusion of released compounds. In this case, molecule-loaded liposomes are employed to control the release of such molecules applying a thermal-trigger which destabilize the lipid bilayer. The developed system is then used to embed multiple drugs (which are selected as relevant candidates for the treatment of human colorectal adenocarcinoma cell line, HT29) within the gel. Finally, the cytotoxic effect of individual and combined drugs is evaluated culturing HT29 cells onto the surface of 3D shaped hydrogels.
The drug screening technology presented here is characterized by different properties:

a) the developed technology is fast since the polymerization process takes place within 30-60 seconds to create a completely crosslinked polymer network;
b) the equipment adopted to produce the gels has a low cost because composed of a modified projector which has an emitting intensity at 410nm, a stage where the support used to contain pre-polymer solutions can be located, and a computer mainly utilized to illuminate the samples with a desired digital mask;
c) multiple hydrogels may be produced simultaneously reducing the fabrication time;
d) different 3D architectures can be obtained according to the final application of the gels in aqueous media;
e) multiple molecules can be embedded within defined volumes of hydrogel and afterwards release them into a reservoir; on the basis of the chemical nature and size of targeted molecules, nanoparticles can be included within the matrix to prevent rapid diffusions;

f) once the drugs are embedded within the hydrogel the system can be stored at 5 ˚C in a humidified atmosphere and on demand, the cytotoxic effect of releasing drugs on the proliferation of a specific cell line can be studied;
g) ideally this technology can be applied for any type of pathological condition once the release kinetics of drugs is optimized and the PEGDA hydrogel features are tuned.

In this chapter, an overview of the applications of hydrogels in bio-medicine and drug delivery fields is given, with a particular focus on the mechanisms involved on the encapsulation and release of bio-active molecules when embedded within PEGDA hydrogels. Moreover, the use of liposomes as potential drug carrier for controlled release is also discussed. A detailed description of the photo-polymerization of PEGDA gels and the optimization of the parameters affecting the process (light source, photo-initiator and equipment) is provided. A new technology recently developed in our group for the crosslinking of PEGDA hydrogels is reported and applied for controlled *in situ* embedding of relevant drugs used for the treatment of ColoRectal Cancer (CRC) cells. The release kinetics of these compounds is characterized and controlled by tuning the hydrogel physical and chemical properties or introducing drug-loaded nanoparticles within the polymer network. Further, an extensive study of the cytotoxic effect induced by drug releasing hydrogel systems is evaluated using the human colorectal adenocarcinoma cell line (HT29). Finally, a short conclusion summarizes the key points encountered on the fabrication of hydrogel systems used for drug screening purposes, and what are the benefits and the future improvements of our developed technology. An experimental section at the end of the Chapter II is also included and all the materials, equipment and protocols adopted for our experimental results are described.

## 2.1 Hydrogels and liposomes as drug carrier

During the last few decades, hydrogels have reached increasing interest with more than 2000 papers published up to now. A widely range of definitions exists for terming 'hydrogel' and the most referred definition is the one given by Peppas.[98] Hydrogels are water-swollen cross-linked polymeric structures which either present covalent bonds deriving from the reaction of one or more co-monomers, or are physically cross-linked due to polymer chains entanglements or hydrogen bonds and van der Walls interactions between chains.[99] In general hydrogels are hydrophilic polymer networks able to absorb from 10%-20% up to thousands times their dry weight in water. They may be chemically stable or may degrade and eventually disintegrate and dissolve. Hydrogels in a cross-linked state reach an equilibrium swelling in aqueous solutions which depends on the polymer cross-linking density. In fact, when a dry hydrogel starts to absorb water from the environment the first water molecules entering the matrix, also called primary bound water, hydrate the polar and hydrophilic

chemical groups of the network. As soon as these groups are hydrated, the overall matrix swells meaning that also the hydrophobic groups are exposed to water molecules and new hydrophobically-bound water molecules are included within the structure (secondary bound water). The additional swelling water that is imbibed after ionic, polar and hydrophobic groups become saturated is called free water and it is assumed to fill the space between network chains. In case of degradable polymer, the matrix will begin to disintegrate and dissolve with a certain rate depending on its composition and cross-linking degree.[100] The volume fraction of water contained within the polymeric matrix influences the absorption and diffusion of solutes through the gel. Indeed, the release of molecules from a hydrogel is mainly controlled by the pore size, pore volume fraction, pore interconnections, molecule dimension, and strength of interaction between the embedded compound and polymer chains. The space available between macromolecular chains is responsible for molecule diffusion; moreover, highly cross-linked hydrogels have a tighter structure in which the overall chains mobility is hindered and a lower swelling is observed. Therefore, the application of hydrogels for drug release purposes is strictly dependent on these concerns and when designing a 3D-network for controlled drug release, the polymer composition and the cross-linking density should be tuned according to the molecules size and physical-chemical properties.[100] Moreover, other parameters like the processing conditions, the method of polymerization, and the incorporation of various polymers to achieve a biomaterial with determined characteristics are extremely important.[101]

Hydrogels are classified on the basis of different parameters such as the preparation method used to cross-link them, the overall monomer or macromer charge and the mechanical and structural features. For instance, according to the preparation method, hydrogels can be defined as homo- or co-polymer hydrogels and they may have a neutral, anionic, or cationic charge depending on the building blocks charges. Further, hydrogels can exist as amorphous, semi-crystalline, hydrogen-bonded, supramolecular or hydro-colloidal physical state. The reason for the extensive study and application of hydrogels is their great retain of large amount of water and excellent biocompatibility, so they are mostly applied in the medical field because mimicking a favorable environment for cell proliferation. Moreover, hydrogels have a poor tendency to adsorb proteins from body fluids due to a low interfacial tension, whereas natural polymers (such as collagen or gelatin) are prone to protein adsorption.[102] Many studies have demonstrated the need of extra-cellular matrix proteins deposition onto the hydrogel surface to achieve cell adhesion. Other applications concern the use of hydrogels as drug releasing system where different release profiles are obtained by tuning hydrogel properties.[103] The applicability of hydrogels as biomedical materials depends mainly on their bulk structure. Some of the most relevant parameters characterizing the network structure are the molecular weight of polymer chains, the corresponding mesh size, and the network density which are measurable through equilibrium-swelling theory and the rubber-elasticity theory.[99]

### 2.1.1 Loading and release mechanisms of biomedical relevant molecules

The delivery and release study of various biomedical relevant molecules has been the subject of intensive research. The compounds which are embedded within polymer networks are different in terms of size (low and high molecular weight molecules), nature (proteins, peptides, DNA, RNA and drugs) and physical-chemical properties. Hydrogels are a class of materials greatly suitable for delivery and molecules release applications because of their ability to encapsulate biomolecules and tailor the gel´s physical and chemical structure.[104] Many improvement have been reported in drug delivery hydrogel-based systems, and over the numerous polymers applied for that purpose, poly(ethylene glycol) (PEG)-based hydrogels are extraordinarily promising biomaterials.[104] Over the past few decades, PEG hydrogels have been extensively used as matrices for controlling drug release, as well as cell delivery vehicles for promoting tissue regeneration.[105–108] PEG polymer is water soluble and resists recognition by the immune system.[108] It also exhibits a rapid clearance from the body and has been approved for many applications. The versatility of PEG macromer chemistry[109] together with its excellent biocompatibility resulted on the development of many smart-designed hydrogel systems for regenerative medicine applications.[104] Further, PEG hydrogels provide a unique niche for cell encapsulation because of high biocompatibility to cells under proper polymerization conditions,[32] and the coupling of biological molecules to PEG usually contributes to its biological activity.[108] In the context of drug delivery, one of the most relevant requirement is the capacity of the hydrogel to provide an extended release of the embedded therapeutics, prevent unfavorable reactions and maintain the bioactivity of compounds. Consequently, several considerations must be assessed: the gelation and loading/release mechanisms, the molecular characteristics of the drug to be delivered, the possible interaction with polymeric chains and the method used to cross-link the hydrogel. For example, PEG-hydrogels are usually cell-repellent materials meaning that the adhesion of cells onto their surface is discouraged; thus the introduction of moieties like RGD-peptide (an Arg-Gly-Asp tripeptide) within the network promotes the adhesion and survival of encapsulated cells such as osteoblasts.[110] Targeted molecules may be embedded within polymeric networks using two different approaches: one consists on *in situ* polymerize the compound and polymer chains at the same time, and the second one in based on the embedding after hydrogel polymerization (Figure 2.1A). The *in situ* polymerization has important advantages due to the simultaneous molecule loading and hydrogel network cross-linking; thus, multiple and highly concentrated compounds may be entrapped in a rapid manner within the matrix.

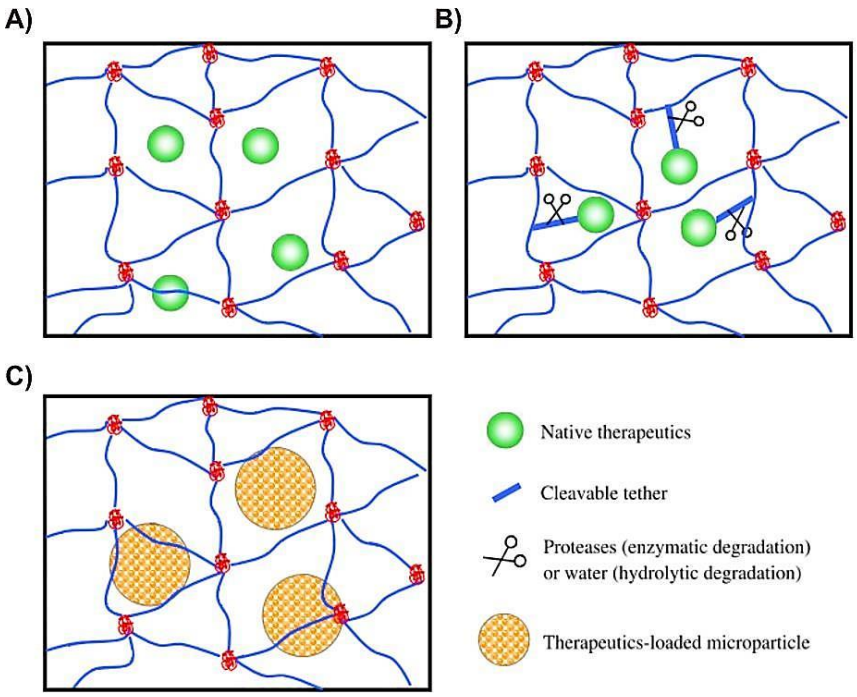


**Figure 2.1** Schematic of loading strategies used to embed therapeutics within hydrogels. (**A**) Compounds can be entrapped through *in situ* polymerization or after hydrogel fabrication; (**B**) drugs are bound to degradable linkers included in the polymer structure and molecules release is induced by enzymatic degradation of the linkers; (**C**) drug-loaded micro- or nano-particles are directly embedded within the hydrogel during polymerization .Figure reproduced from [104].

On the other hand, depending on the polymerization method adopted to cross-link the mixture, potential reactions between molecules and polymer may occur with the risk of affecting the final compound bioactivity. The embedding of drugs after polymerization consists on the incubation of pre-formed hydrogels with highly concentrated molecule solutions which are entrapped within the matrix through osmotic driving force until solute equilibrium is reached. Despite this approach preserves drug bioactivity, it does not permit accurate control over the amount of drug loading because of partitioning limitations.[104] Moreover, it appears difficult to fabricate hydrogels with multiple drugs at defined concentration for sophisticated bio-medicine applications. Although the loading method used to embed compounds within hydrogel is extremely important, release mechanisms are likewise relevant for the design of controlled release systems. Because of the diversity in the chemistry and size of released molecules, the criteria for controlled release from hydrogels may widely differ from one application to another. In general, for drug release purposes two major concerns must be considered: the availability and the stability of released therapeutics. In fact, to achieve a desired therapeutic effect *in vitro* or *in vivo*, the drugs should be delivered at a right dosage (availability) and with preserved molecular structure and bioactivity (stability). The commonly used mechanisms of molecular release from hydrogels include diffusion-, swelling-, and chemically-controlled delivery.[104] When the releasing compounds are small in terms of size and molecular weight such as drugs, peptides or small

proteins, the high permeability of hydrogels towards small molecules does not permit to control their release kinetics.

At the moment, different methods suitable to control the release profile and to tune the gel permeability are normally used. One of these approaches is based on modulating the cross-linking density, thus by increasing the cross-linking density, the number of network chains per unit volume also increases and a smaller network mesh size limits rapid molecule diffusion. However, this method relies on size-exclusion concept, so the release of small compounds like drugs is not controlled in any case; further, an increase on the cross-linking density results on a reduced hydrophilicity of hydrogel which corresponds to a poor cytocompatibility.[104] Another strategy primarily used for drug encapsulation is the use of pro-drug molecules: in this approach drugs can be covalently immobilized within hydrogel network via functional groups. The introduction of degradable linkers between drug and tether allows the liberation and release of molecules when enzymatic degradation of linkers occurs (Figure 2.1B).[111,112] The pro-drug strategy is effective on controlling drug release but has an important drawback: the covalent association of drugs to degradable linkers may impair the bioactivity of molecules especially when fragile peptides and proteins are the target therapeutics.[104] Furthermore, the chemistry adopted to include linkers into polymer structure must be biocompatible and designed in such way that completely degradation of linkers occurs.[113] However, the use of pro-drug molecules requires the synthesis of a new compound which is a modified version of an already existing drug, thus a consequent approval of the new pro-drug is needed. A third strategy to entrap drugs within hydrogel consists on the incorporation of drug-loaded micro- or nano-particles into the network prior to polymerization (Figure 2.1C). In particular, drug-loaded liposomes have been extensively studied and applied for different purposes. According to the chemical properties of the molecule loaded into liposomes and the lipid composition of these nanoparticles, a controlled release can be achieved. In conclusion, the maintenance of drug stability is of critical importance not only for drug release purposes but also for biocompatibility issues; in fact it has been shown that the entrapment of proteins and peptides into hydrogel induces their denaturation and their consequent *in vivo* immunogenic effect.[114]

### 2.1.2 Diffusion of drugs from hydrogels and liposomes

The diffusion of drugs from hydrogels or other drug carriers depends on various parameters. A slow release of drug from network corresponds to a therapeutic but non-toxic concentration and a prolonged release profile, meaning that less frequent administrations of drug are needed since the therapeutic concentration is not reached.[115] On the other hand, when drug compounds diffuse rapidly from a matrix, a toxic concentration may be obtained; a controlled drug releasing system is therefore necessary to achieve the right therapeutic dose. Mathematical models are normally used to predict the

temporal release of encapsulated cargo molecules as well as to describe the release mechanisms supported by experimental verification.[116] Since diffusion of drugs strictly depends on the structure through which the diffusion takes place, models that assess polymer morphology and properties are needed.[116,117] The mechanism of drug release from hydrogels can be i) diffusion-controlled; ii) chemically controlled; iii) osmotically controlled; and iv) swelling- and/or dissolution-controlled.[117] Drug release from different carriers consists on the movement of molecules through the bulk of polymer, a process that can be described by Fick´s laws of diffusion for transport in one dimension (Equation 2.1 and Equation 2.2):

$$j_i = -D_{ip}\frac{dc_i}{dx} \qquad \textbf{Eq. 2.1}$$

$$\frac{\partial c_i}{\partial t} = D_{ip}\frac{\partial^2 c_i}{\partial x^2} \qquad \textbf{Eq. 2.2}$$

Here, the concentration and mass flux of species *i* are designated as $c_i$ and $j_i$, respectively; $D_{ip}$ is the diffusion coefficient of species *i* in the polymer matrix and *x* and *t* are position and time, respectively.[98] A semi-empirical power law equation (Higuchi kinetic equation)[118] widely used to describe diffusion- controlled drug release from semi-solid polymeric systems is stated in Equation 2.3:

$$\frac{M_t}{M_\infty} = \mathrm{k}t^n \qquad \textbf{Eq. 2.3}$$

Here, $M_t$ and $M_\infty$ are the cumulative amounts of drug released at time *t* and at the equilibrium point, respectively; *k* represents structural and geometrical information regarding the device and *n* is indicative of the drug release mechanism. The presented equation is the result of a detailed mechanistic process that includes diffusional process (Fickian) and additional relaxational or convection mechanisms. Further, the mathematical solutions of Equation 2.1 for Fickian drug diffusion result in release kinetics with n = 0.5, whereas when the release is zero-order, n = 1.[117] Therefore, the diffusion of drug from polymeric systems can be obtained directly from the slope of the linear part of plots $M_t/M_\infty$ versus $t^{1/2}$, as shown in Figure 2.2.[119]

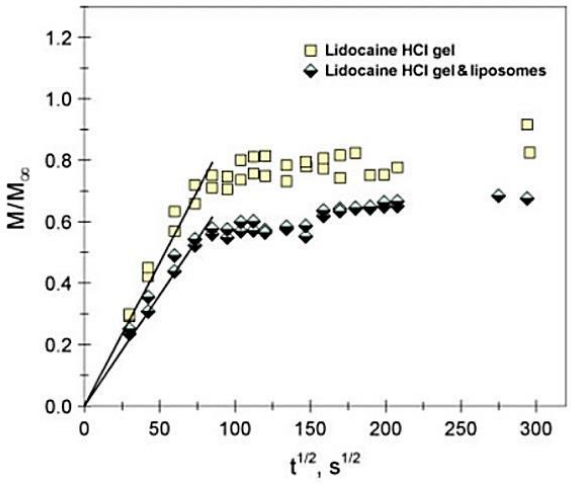


**Figure 2.2** Release of Lidocaine Hydrochloride from gel (open squares) and from liposomes embedded within the gel (half-filled diamonds).Figure reproduced from [119].

The linear part of curves corresponds to pure diffusion according to Eq.2.3 and Figure 2.2. A later stage of drug release up to equilibrium point is characterized by a non-linear behavior until approaching steady state where the driving force for mass transfer of drug diffusion gradually slows. In Figure 2.2 should be also noted that, as expected, the diffusion of lidocaine hydrochloride from a gel is faster than the diffusion of the same compound when loaded into liposomes and mixed to the gel.

### 2.1.3 Liposomes for controlled drug release

Over the last 30 years, the application of liposomes as drug carriers in pharmaceutical and medical fields is considerably increased.[120,121] Liposomes are self-assembled spherical soft-matter particles consisting of a central aqueous compartment surrounded by one or more concentric phospholipids layers, also called lamellas (Figure 2.3).[122,123] Liposomes, as analog of natural membranes, are formed by auto assembling of natural or synthetic lipids. The application of liposomes for drug and gene delivery purposes is extensively studied because of liposomes amphiphilic nature; in fact, liposomal particles are used as vehicle for both lipophilic and hydrophilic compounds. Hence, hydrophilic molecules are loaded in the interior aqueous compartment while lipophilic compounds are entrapped within the lipid bilayers. Liposomes constitute a physical barrier and can protect the loaded substances from the surrounding environment and degradation processes (induced for example by pH changes). Due to the variable nature of lipids, liposomes are classified in terms of composition, size, number of bilayers forming the vesicle and according to the mechanism of release/delivery.[122]

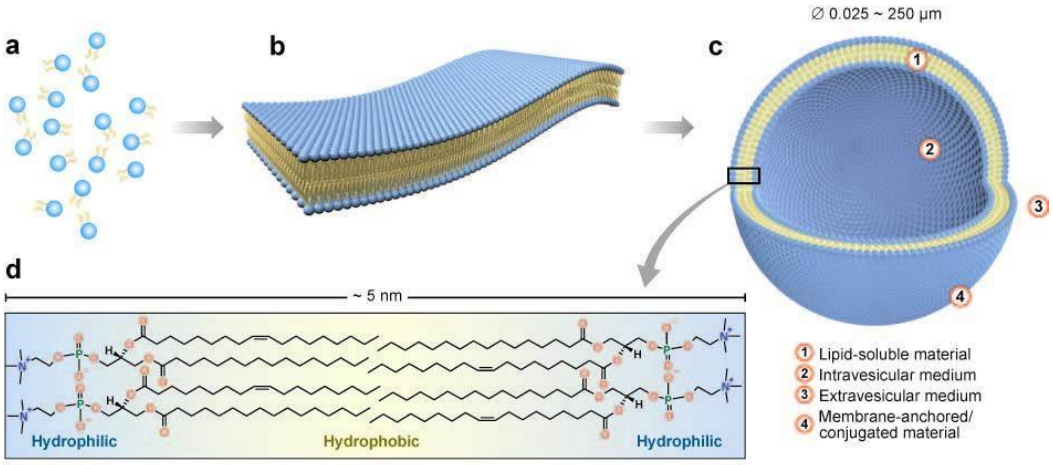


**Figure 2.3** Schematic illustration of self-assembly process involved on the liposomes formation from individual phospholipid molecules (**a**) to a bilayer membrane (**b**), followed by organization into liposomes (**c**). Normally, a single bilayer has a thickness around 5nm which consists of arranged single lipid molecules with their hydrophobic tails facing each other and their hydrophilic headgroups facing toward the internal and external aqueous compartment (**d**). Figure reproduced from [123].

Among the variety of available phospholipids involved in the process of liposome production, phosphatidylcholine (PC) and phosphatidylethanolamine (PE) are the main structural components of biological membranes. Further, liposome membrane may also contain other constituents, for instance cholesterol, largely used to improve the membrane fluidity and stability, and hydrophilic polymer-conjugated lipids such as PEG-based lipids. Nowadays, the methods available for liposomes synthesis are various and they can be applied singularly or as combination of processes. A suitable method for liposome manufacture must ensure a high degree of structural homogeneity in order to achieve the optimal performance of vesicle as molecule-carrier.[124] The method mostly used for liposome synthesis is the classical hydration technique (also called Bangham method).[125] This approach consists on the dispersion of lipids in an organic solvent which is removed after solubilization through evaporation; a thin dried lipidic film is obtained. Then the film is hydrated in aqueous buffer solution under stirring at a temperature above the lipid transition temperature. The dispersed phospholipid populations form a suspension of multilamellar liposomes (MLVs) which are characterized by a high heterogeneity in terms of size and shape (usually ranging from 1 to 5µm in diameter). The synthesis of small unilamellar vesicles (SUVs) or large unilamellar vesicles (LUVs) is achieved by extruding the lipid suspension through a polycarbonate filter which has the appropriate pore size in diameter to obtain the final desired size of liposomes (for example 100 or 200µm). Among the traditional multi-step film hydration technique, an alternative method can be adopted and it is called DELOS approach. In this case, advanced equipment composed of a system for the compression of fluid ($CO_2$) and pressurized chambers are needed. The depressurization of an expanded liquid organic solution has proved to provide crystalline solids having a high purity.[126] Elizondo *et al.*[127] have demonstrated by Cryo-TEM

microscopy that liposomes prepared with traditional film hydration method are a mixture of multilamellar, unilamellar and multivesicular particles, whereas homogeneous populations of unilamellar liposomes are achieved with DELOS procedure. Independently from which technique is used for liposomes synthesis, the chemical and physical properties of vesicles must be assessed in order to guarantee their stability as drug nanocarrier. The main parameters affecting liposome features are: i) the size, expressed as average mean diameter; ii) the polydispersity index which provides the degree of suspension homogeneity; iii) the surface charge, or zeta potential; iv) the lamellarity; v) the encapsulation efficiency; vi) the *in vitro* drug release and mostly important vii) the liposomes stability. One of the major concerns for liposomes use as drug carrier is their stability, meaning that stable vesicles must maintain their physical integrity over time and they should not influence the chemical integrity of the encapsulated cargo. However, liposomes naturally tend to be unstable because of aggregation and leakage processes when they are kept upon long term storage; further, the interaction of lipids with the loaded cargo may interfere with drug availability and stability. Normally, liposomes are characterized through dynamic light scattering (DLS) to evaluate the average mean size and polydispersity index; moreover, the overall charge of liposomes surface is established via zeta potential which is a good index to predict the stability of colloidal suspension.

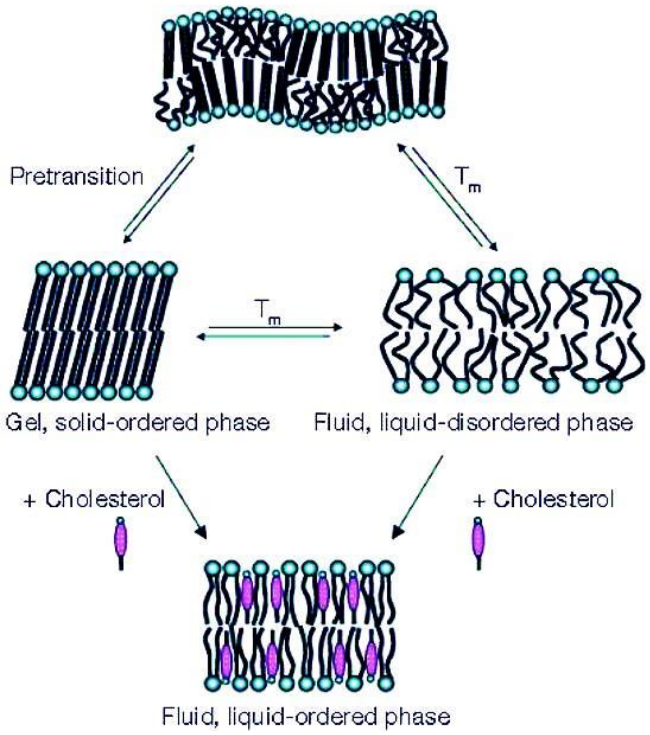


**Figure 2.4** Illustration of three different physical states adopted by a lipid bilayer in aqueous medium. $T_m$ stays for phase transition temperature. Figure reproduced from [128].

Two issues become immediately relevant when trying to encapsulate drugs into liposomes: firstly, the encapsulation of molecules is more difficult and inefficient as the size of compound increases, and secondly, the encapsulation efficiency strictly depends on the method adopted to load drugs into the bilayer. Therefore, a liposomal drug carrier must be stable whilst circulating (drug retention) and render the drug bioavailable when it reaches the targeted site (drug release). These parameters are strictly dependent on the bilayer permeability properties: the liposome bilayer is a selective barrier and membrane permeability varies for different types of solutes, such as water, electrolytes and non-electrolytes. Moreover, the membrane features can be regulated by changing the lipid composition, for instance the saturation number of lipids, length of fatty acid chains and charge of headgroup, or by introducing cholesterol molecules which are responsible for liposome stabilization. Phospholipids have a phase transition temperature ($T_m$) which defines their physical state (Figure 2.4): when heated, phospholipids undergo a shift from a well-ordered and tightly packed gel phase to a fluid and disordered liquid-crystalline state.[128,129]

In this thesis and in other numerous published applications, heat is employed to induce drug release from liposomal vesicles through temperature changes. Thermo-sensitive liposomes containing drug molecules into the aqueous cavity are studied; the effect of temperature and lipid composition is evaluated in order to achieve the maximum released drug amount. When a certain heat treatment is applied above the transition temperature, the lipid membrane of thermo-sensitive liposomes undergoes a gel-to-liquid-crystalline conformation transition which results on an increased permeability towards water and solutes due to an augmented phospholipids mobility.[130]

## 2.2 Development of PEGDA hydrogels for digital drug dosing

Poly(ethylene glycol) diacrylate (PEGDA) hydrogels are largely used in many biomedical applications and their study is gradually increasing due to favorable properties: excellent biocompatibility, poor cell attachment, ease of use and PEG-chemistry versatility. These hydrogels are employed for various purposes including tissue engineering, wound healing, electrospinning processes and drug delivery.[33–35] In this thesis, PEGDA hydrogels are fabricated through visible-light photo-polymerization for drug release purposes: different drugs commonly used for the treatment of colorectal cancer are embedded within PEGDA hydrogels via *in situ* polymerization. Further, the release kinetics of chemotherapeutics and their cytotoxic effect on human colorectal adenocarcinoma cell line (HT-29) are evaluated. For this purpose, various issues are considered:

a) the cross-linking method used to polymerize PEGDA monomers and consequent embedding of various molecules (drugs and proteins);

b) the release study of embedded compound and tuning of chemical and physical hydrogel properties;
c) the use of drug-loaded nanoparticles (liposomes) embedded within PEGDA hydrogels and study of controlled drug release;
d) fabrication of 3D hydrogel structures for drug confinement in a small scale;
e) multi-drug dosing within PEGDA hydrogel for drug screening purposes;
f) evaluation of cytotoxic effect of different drug releasing systems.

### 2.2.1 Photo-polymerization of PEGDA gels

Among various method of gelation (physical, ionic or through covalent interactions), chemical- or covalent-crosslinking leads to relatively stable hydrogel with tunable physiochemical features. Nowadays, photopolymerization is one of the preferable way to fabricate hydrogels because is a rapid process (quite often the polymerization is completed within few seconds) and is suitable for encapsulation of cells and fragile molecules.

In this thesis, PEGDA hydrogels are fabricated through *in situ* photopolymerization which is a process that requires photoinitiator species and a light source. This approach provides a spatial and temporal control over the formation of the material. When a solution of PEGDA monomer and photoinitiator is exposed to a specific wavelength, gelation will occur. During the reaction the photoinitiator species are decomposed into reactive radicals which are responsible for polymerization initiation. Photoinitiators are normally classified into two classes: type I (or cleavage type) includes photoinitiators that are split into two radical species after photon absorption, and type II comprises photo-initiating systems that after photon absorption are in an excited state and a second co-initiator species extract from them a hydrogen atom.[131] When selecting the photoinitiator to use for a certain application, it is important to consider a variety of parameters. Most of the photoinitiators commonly used for polymerization process are water-insoluble and they must be dissolved in organic solvents which are cytotoxic; thus, the use of these initiators precludes the possibility to photo-encapsulate fragile molecules and living cells. Moreover, the majority of photoinitiators require UV light to initiate the polymerization with the risk of generating damages on the encapsulated molecules, such as double-strand DNA breaks in encapsulated cells.[132] Eosin Y for example is a widely used photoinitiator because of its great cytocompatibility, water solubility and photon absorption in the visible range.[133] However, eosin Y suffers from many drawbacks: first it requires a co-initiator and accelerant species to produce enough radicals for initiating the process; secondly, the eosin Y absorption and emission spectra overlap with many fluorophores commonly used in cellular imaging.

#### 2.2.1.1 Fabrication of PEGDA hydrogel using IrgaCure 2959 photoinitiator

For the fabrication of photopolymerized three-dimensional PEGDA hydrogels, the commercially available compound IrgaCure™ 2959 (I2959) is selected as photoinitiator candidate. This initiator is the most commonly used compound for cellular encapsulation within hydrogels, despite its low solubility (less than 2%wt). I2959 is a type I photoinitiator meaning that when these molecules are irradiated in the UV light range, they are decomposed into two radical forms (Figure 2.5A). Then, in presence of PEGDA monomeric molecules, these free radicals propagate through double bonds of PEGDA chemical structure and chain polymerization occurs (Figure 2.5B).

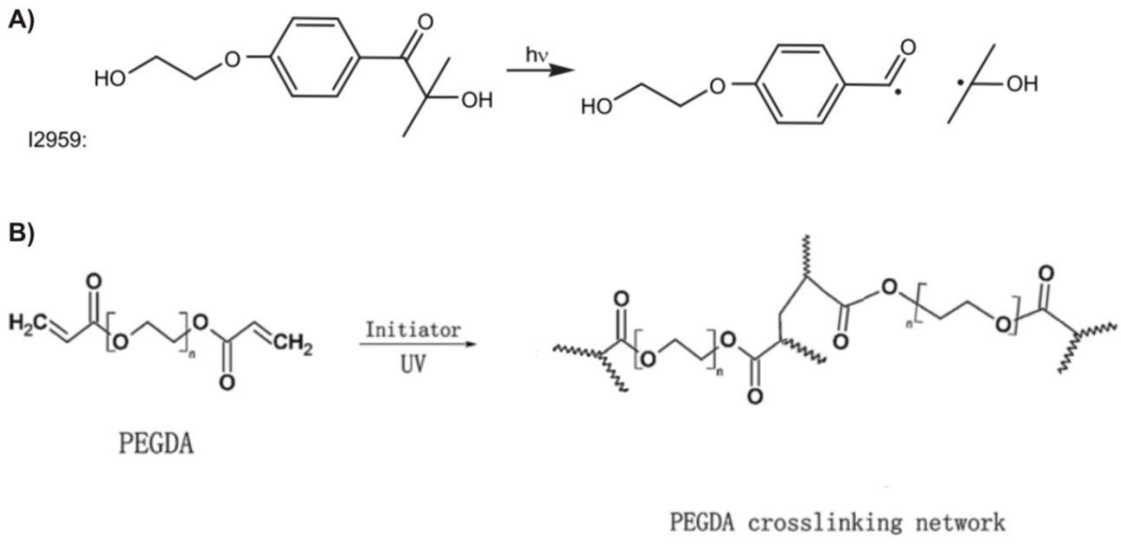


**Figure 2.5** UV-photopolymerization of PEGDA and IrgaCure 2959 solutions. (**A**) Mechanism of radicals formation from I2959 UV-light exposure; (**B**) Polymerization of PEGDA monomers together with free I2959 radicals to form a three-dimensional hydrogel.

A preliminary study is conducted to evaluate optimal concentrations of PEGDA (MW 700Da) and I2959 needed to obtain homogeneous and transparent hydrogels. As depicted in Figure 2.6A, different concentrations of PEGDA (700Da) dissolved in MilliQ water and IrgaCure 2959 dissolved in acetone/milliQ water (1:1) are tested. In a 24 well-microtiter plate these pre-polymer solutions are exposed to UV-light in a photo-reactor for 1 hour. From the photo of the obtained gels, it is notable that partially formed hydrogels are found (red circles on the first plate column), suggesting that the initiator concentration may be too low to ensure a complete crosslinking of the solutions. On the other hand, PEGDA hydrogels are formed when IrgaCure amount is equal or higher than 0.5%w/v. However, the fabricated hydrogels are extremely heterogeneous and colored even though the entire solutions

are crosslinked. Further, some particles are found on the bottom of the wells which can indicate a low solubility of the initiator when diluted in the polymer solution. Since the efficiency of photopolymerization depends on how many photons are absorbed by the initiator molecules and on the amount of radicals produced after photon absorption, the UV-vis spectra of different concentrations of I2959 dissolved in acetone/water (1:1) not exposed to UV-light are reported (Figure 2.6B). It should be noted that as the initiator concentration increases, a linearly proportional UV-vis absorption is measured. In fact, for low concentration of IrgaCure the absorption at 365nm is negligible, whereas it starts to absorb at this wavelength for concentrations higher than 0.5%w/v. These results obtained from the UV-vis analysis are in agreement with what is observed from the polymerization of gels after exposure. In fact, the fabrication of completely crosslinked solutions is achieved for concentration of IrgaCure 2959 higher than 0.5%w/v, as shown in the photo of the well plate (Figure 2.6A). Therefore, to fabricate PEGDA hydrogels using I2959 as photoinitiator, a suitable concentration is needed (at least 0.5%w/v). Despite hydrogels can be produced when a certain concentration of initiator is used, there still an issue that should be clarified or at least optimized: the color of gels suggests a low solubility of I2959 when added to polymer solution due to its low water solubility (less than 2%w/v).

To further improve the quality of hydrogels, a different polymer composition is used to evaluate how the physical and chemical properties of PEGDA affect the hydrogel fabrication. Thus, PEGDA having different PEG chain lengths (1kDa, 5kDa and 6kDa) and concentrations are mixed with PEGDA (700Da) and a constant amount of IrgaCure 2959 (1%w/v) is used. In a 24-well microtiter plate, the solutions are UV-exposed for 1 hour in the photo-reactor (Figure 2.7). The resulting hydrogels are less colored than those obtained from the mixtures of PEGDA (700Da) and I2959, but they are still imperfect because of high heterogeneity and extremely soft materials. These characteristics are important to accomplish the desired drug releasing platform, meaning that hydrogels must be ease to reproduce, colorless, homogenous in terms of composition and thickness, and it should be possible to polymerize gels within a shorter exposure time (less than 1 hour) and eventually create desired 3D-structured hydrogels. In light of these considerations, a preliminary test for the fabrication of 3D-shaped PEGDA hydrogels is conducted by mixing different amounts of $PEGDA_{700Da}$ with IrgaCure 2959 as photoinitiator and UV-irradiated through a traditional photolithography aligner (Figure 2.8A).

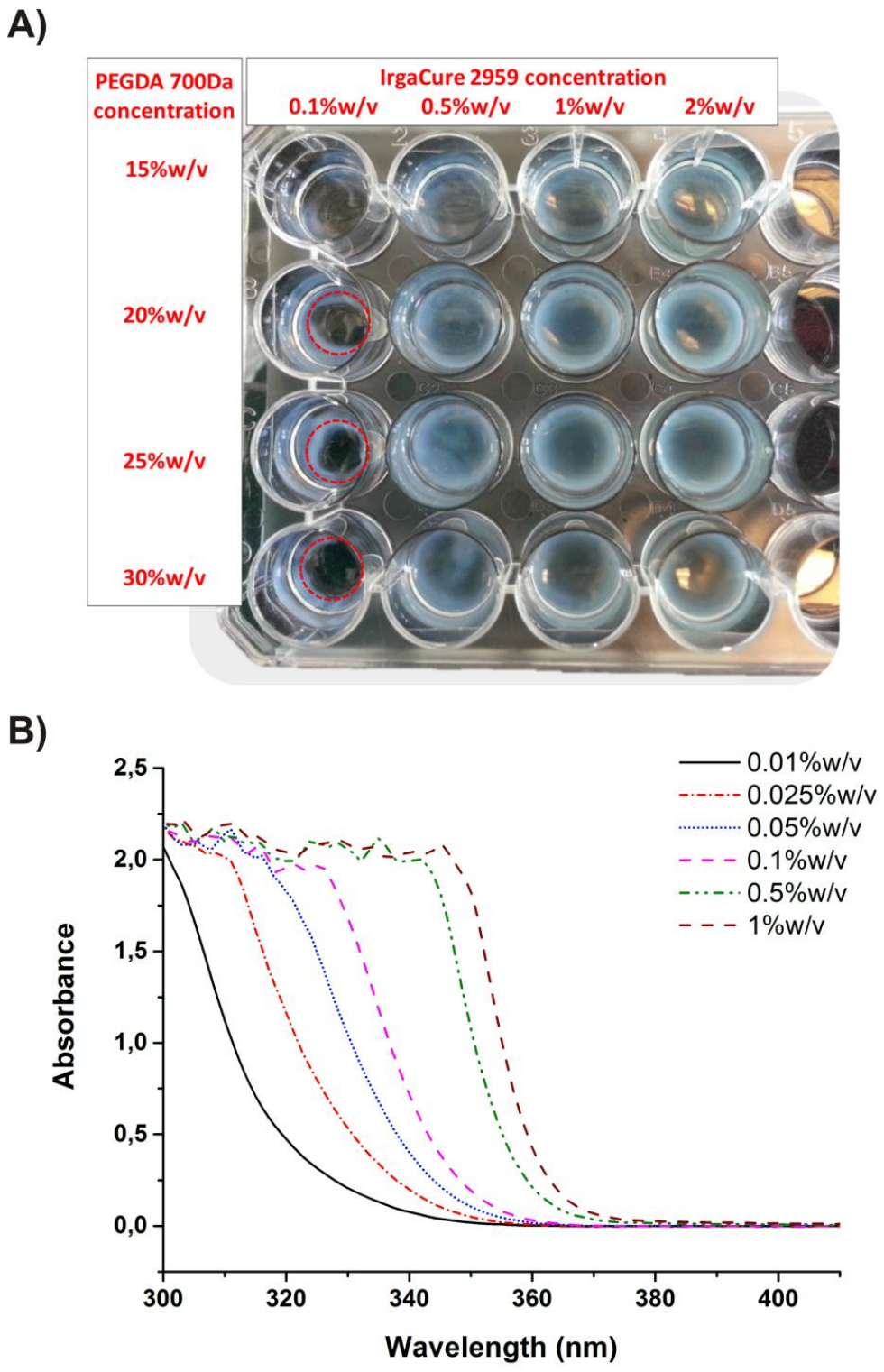


**Figure 2.6** PEGDA hydrogel fabrication via UV-light photo-polymerization. (**A**) Photo of a 24 well-microtiter plate of various concentrations of PEGDA (700Da) and IrgaCure 2959 after exposure to UV-light (emitting range 330-380nm) for 1h. In the first column of the plate it is notable the incomplete polymerization of pre-polymer solutions and the presence of holes in the center of well (red circles) (**B**) UV-vis spectra of different concentrations of I2959 dissolved in acetone/water (1:1) not UV-exposed.


**Figure 2.7** Hydrogel fabrication using 1%w/v IrgaCure 2959 dissolved in acetone/water (1:1). PEGDA (700Da) solutions are mixed with various concentrations of different PEGDA chain lengths (1kDa, 5kDa and 6kDa). Photo of a 24 well-microtiter plate where the mixed PEGDA compounds are exposed to UV-light for 1 h in presence of photoinitiator. Less colored and softer hydrogels are obtained when PEGDA 700Da is mixed with different PEG chain lengths, and all the tested amounts generate a crosslinked solution even though with some inhomogeneity.

Different solutions composed of PEGDA (700Da), photoinitiator and fluorescein are poured inside a GeneFrame® and sealed with a coverslip. For the polymerization of 3D-structured hydrogels, two different chrome masks are employed: one of them consists of square grids of different diameters (Figure 2.8B); the other mask is made up of dual sets of interdigitated electrodes 200µm wide and 3.5mm long and with 200µm spacing (Figure 2.8C). The gene frame is exposed for 10min to UV-light (365nm) using one of these photomasks and the obtained structures are washed several times with MQ water to remove un-exposed compounds. In Figure 2.9, some examples of 3D structures are reported: well-defined structures are obtained when a square grid with diameter of 25µm, a center-to-center interspace of 66µm and 5 x 5 structures is applied (Figure 2.9A and D). Conversely, when a larger square grid with the same diameter (25µm) and interspace (66µm) but 20 x 20 total structures is applied, a hydrogel with not defined squares, rather with circle-like morphology with a central cavity is obtained (Figure 2.9B and E).

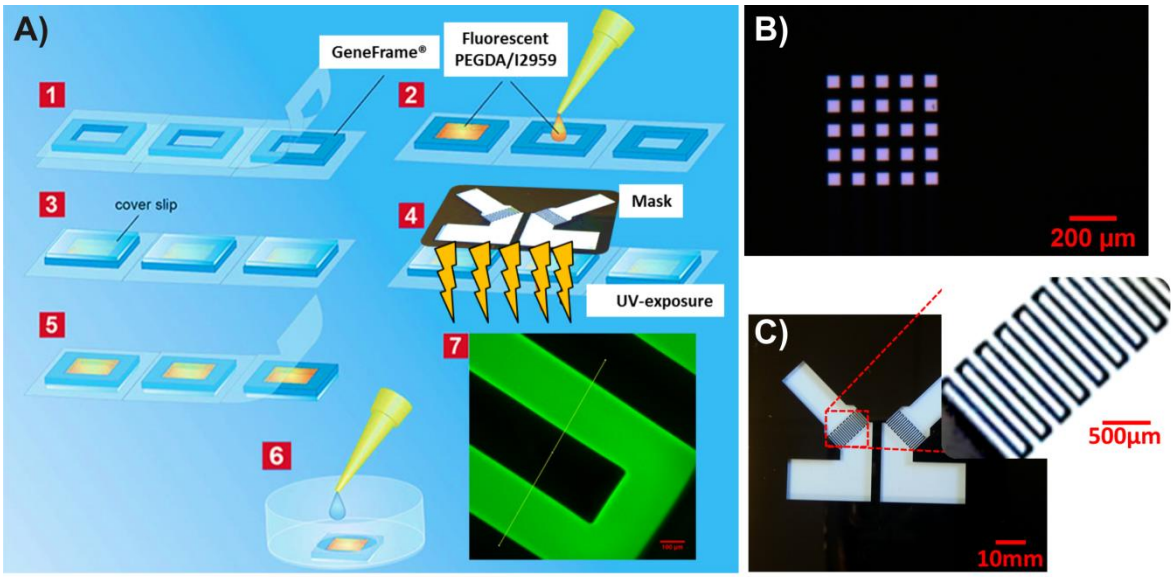


**Figure 2.8** Schematic of the process used to photo-polymerize 3D-structured PEGDA hydrogels. (**A**) The steps involved on the hydrogel structures fabrication are: a gene frame of the dimension of 1.5 x 1.5cm is used to contain the pre-polymer solution (1); a solution of PEGDA 700Da, IrgaCure 2959 and fluorescein is poured into the gene frame (2); the solution is covered with a cover slip and protected from light (3); a chrome mask is used to create 3D hydrogel structures by illuminating the solution to UV-light for 10min using the UV-aligner (4); the cover slip is removed (5) and the obtained shaped hydrogel is washed with water to remove un-reacted compounds (6). The produced hydrogels are observed through confocal microscope using an excitation light at 488nm and collecting the fluorescence for wavelengths longer than 505nm (7). (**B**) and (**C**) represent the chrome mask designs employed to create the structures within the gene frame. In Figure 2.8A, the confocal picture of the obtained hydrogel structures (step 7) is produced by exposing the solution to UV-light using the mask reported in Figure 2.8C which is composed of interdigitated electrodes having a width of 200µm and a spacing of 200µm. The mask reported in Figure 2.8B includes a pattern of squares having a dimension of 60µm and spacing 60µm.

Defined 3D-electrode shaped hydrogels are achieved when the fluorescent PEGDA/photoinitiator solution is exposed to UV-light through the second mask (Figure 2.9C and F); as depicted in Figure 2.9F, the fluorescence profile across the electrodes reveals a width of each structure approximately of 230µm, not far from the line width on the photo-mask (200µm).

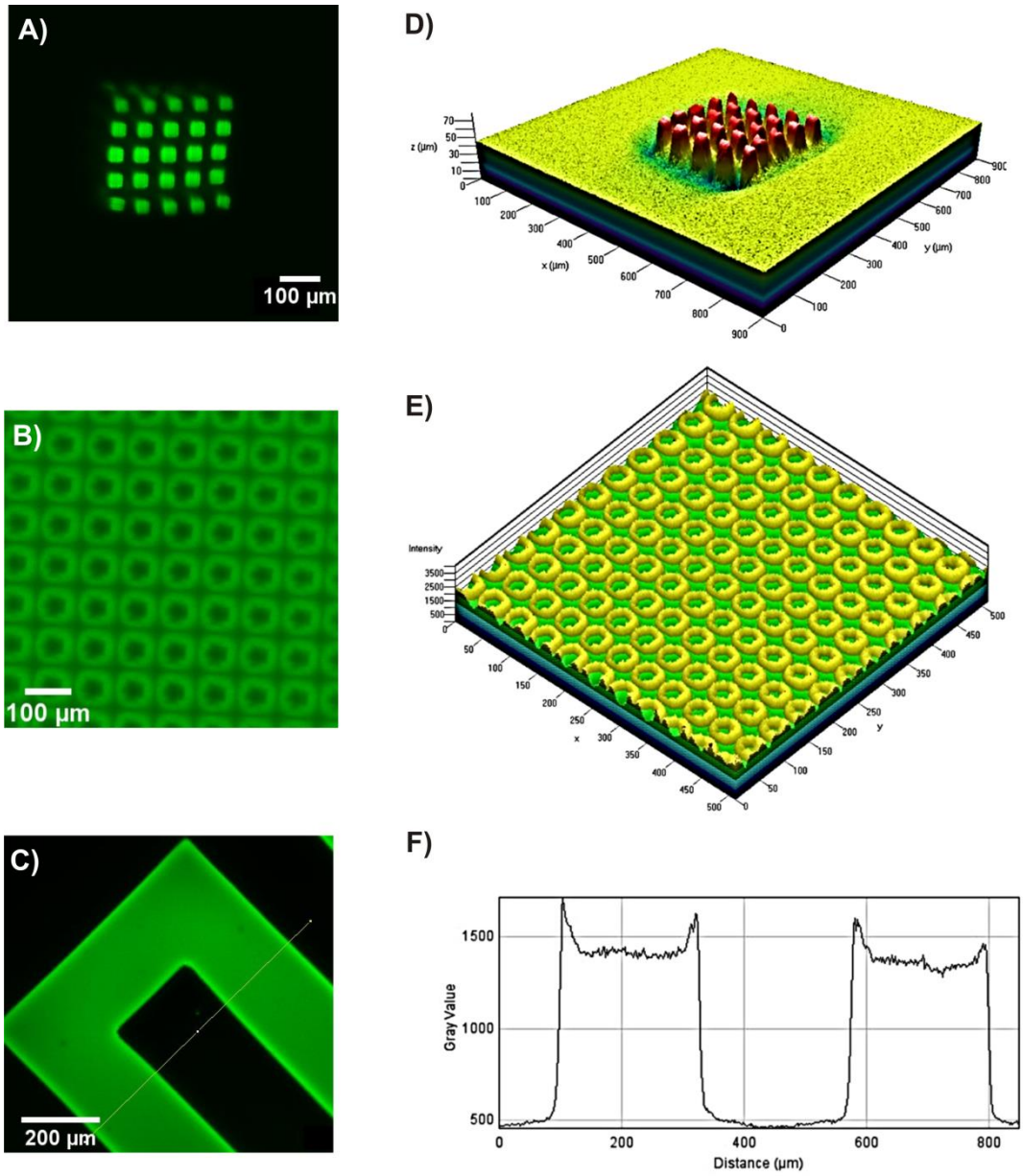


**Figure 2.9** Confocal microscope images of the 3D-structured PEGDA hydrogels obtained after curing. (**A**) and (**D**): square design with a diameter of 25µm, interspacing of 66µm and the pattern is composed of 5 x 5 squares; (**B**) and (**E**): square design with a diameter of 25µm, interspacing of 66µm and the pattern is formed of 20 x 20 squares; (**C**) and (**F**): inter-digitated electrodes design characterized by an electrode width of 200µm, 3.5mm long and 200µm spacing. In F), the fluorescence profile of fluorescein across the electrodes is shown.

The method proposed here to fabricate hydrogels should be then applied for drug molecules embedding and consequent release study. As described in the introduction, different suitable ways for molecule entrapment may be used: inclusion of compounds within the network during polymerization, or chemical bonding of molecules to a pre-formed matrix, or the embedding of molecule-loaded micro- or nano-particles within the gel. A preliminary study for drug encapsulation within PEGDA hydrogels is

conducted. The approach which is intended to use for that purpose consists on the *in situ* photo-polymerization of pre-polymer solution together with drug molecules. Ideally using this technique, the initial concentration of the targeted compound should be entirely confined within a certain volume of gel. Further, the release kinetics can be determined by quantifying the number of molecules diffused into the supernatant. For that purpose, the drug SN-38 commonly used for the treatment of colorectal cancer (CRC) is chosen as model molecule. SN-38 is a small molecule (MW = 392.4 g/mol), hydrophobic, poorly soluble in water and has a major UV-vis absorption peak at 374nm. Therefore, for the fabrication of SN38 embedded molecules within PEGDA hydrogels, different concentrations of PEGDA (700Da) and IrgaCure2959 with a constant amount of SN-38 are cured for 1 hour through UV-light exposure in a photo-reactor. After polymerization, milliQ water is added into the well and the released drug molecules are quantified via UV-vis spectrophotometry. From the analysis of collected supernatants, no peaks are detected, especially the characteristic doublet peak of SN-38 (365-385nm, as shown in Figure 2.10A). Furthermore, when a PEGDA and SN-38 mixture is exposed to UV-light for 1 hour without gelling due the absence of the photoinitiator, the corresponding visible spectra are totally comparable to the one observed without UV-exposure. Indeed, in Figure 2.10B is reported the spectrum of a PEGDA solution (green line) and the spectrum of PEGDA-SN38 solution (red line) after exposure. Contrarily to that, a solution of I2959-SN38 irradiated to UV-light for 1 hour presents a spectrum with a single peak, which is the result of two overlapped peaks (Figure 2.10C). The impossibility to quantify the concentration of released SN38 due to a problematic overlapping of IrgaCure absorption with the compound spectrum, limits the use of UV-vis spectrophotometry as detection tool. Other methods to measure the released SN38 may be applied, for instance chromatography techniques or mass spectrometry; on the other hand, an analytical method as simple as possible should be recommended for a fast measurement. Also notable is the available volume of supernatant in which compounds are released; in fact, the polymerization of gels may be adapted to smaller support including 96-well microtiter plates or even tinier.

The need of a different quantification method to identify the released drug is not the only issue: in fact, the presence of I2959 into the supernatants even after an extensive washing of hydrogels is detected, indicating a possible accumulation of the photoinitiator molecules within the network as unmodified compound or as radical species. Moreover, after curing, the hydrogels with embedded SN-38 appear more colored than those fabricated in absence of drug which is also confirmed by the UV-vis spectra of I2959-SN38 after exposure. A long tail of their spectrum is observed when drug and initiator spectra are overlapped even for wavelengths longer than 400nm that may confer to gels a stronger color in comparison to those without drug.

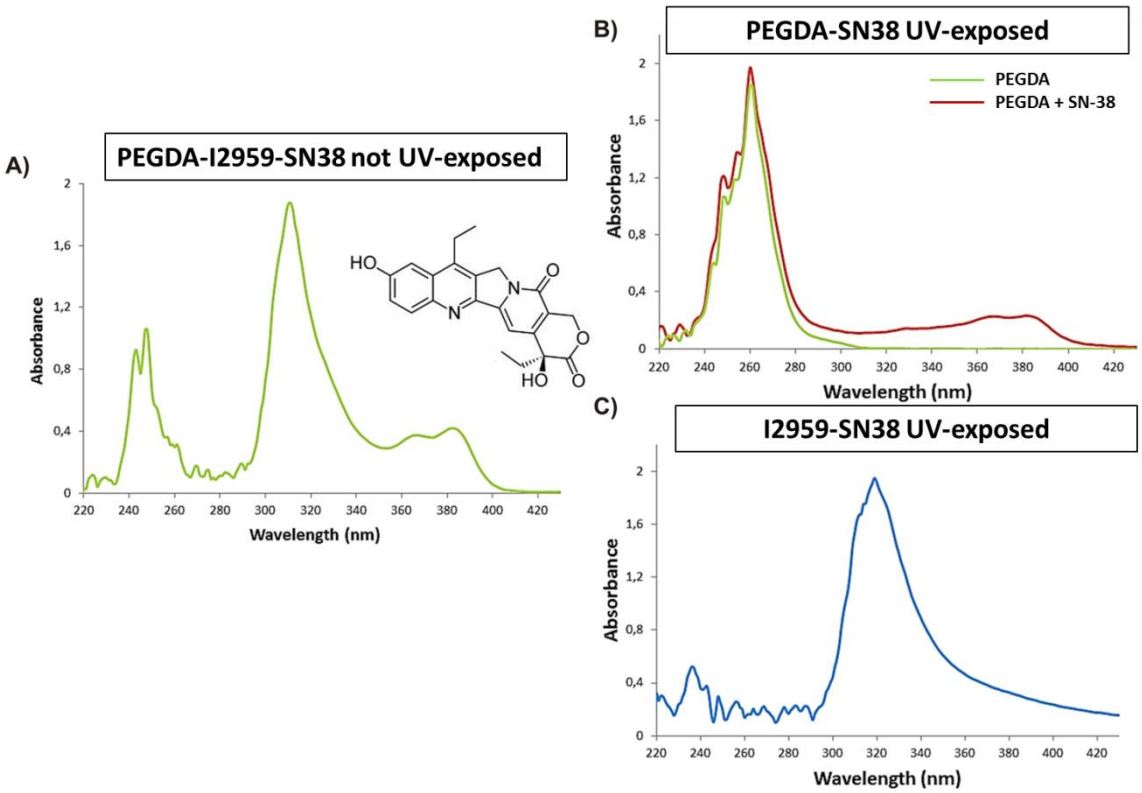


**Figure 2.10** UV-vis spectrophotometric characterization of PEGDA, I2959 and SN-38 solutions. (**A**) UV-vis spectrum of a solution composed of 30%w/v PEGDA (700Da), 0.5%w/v I2959 and 100µM SN-38 not exposed to UV-light. The relevant absorption peaks of the drug at 365nm and 385nm are marked. (**B**) UV-vis spectra of 30%w/v PEGDA (700Da) in green and 30%w/v PEGDA (700Da) with 100µM SN-38 in red after 1h UV-exposure. (**C**) UV-vis spectrum of a solution composed of 0.5%w/v I2959 with 100µM SN-38 after 1h irradiation to UV-light.

Taking into account all these considerations, the use of IrgaCure 2959 as photoinitiator to photopolymerize PEGDA hydrogels is not particularly satisfying for many reasons: firstly the photoinitiator is poorly soluble in water, thus fresh solution of I2959 dissolved in acetone/water (1:1) need to be prepared all time to avoid acetone evaporation during handling; secondly, to achieve a complete crosslinking of PEGDA solutions, a high concentration of photoinitiator has to be used (≥ 0.5%w/v) and a long UV-exposure time (1 hour for hydrogels with a thickness of 1.5 mm or more and 10min for thickness of 200µm). Moreover, when trying to produce 3D-structured hydrogels only large sized patterns can be fabricated since smaller features are obtained with a low resolution precluding the possibility to create miniaturized gels (as described in Figure 2.9B and E). Regarding the embedding process of desired molecules, a rapid and ease method to evaluate the released molecule amount even at smaller volume scale is fundamental. An efficient and reliable polymerization may be achieved using an initiator that greatly absorbs on the range of the emitting light source. The molar extinction coefficient of I2959 at 365nm is very low ($\varepsilon_{365}$ = 4 $M^{-1}$ $cm^{-1}$ in acetone) and trails off almost entirely before 370nm, thus limiting the polymerization kinetics at or near these wavelengths.

Polymerization at longer wavelengths such as in the visible or violet light may be also possible but for I2959 is completely precluded because of negligible absorption of light in that range. As widely reported in literature, although IrgaCure 2959 is relatively cytocompatible for many cell lines at concentration between 0.03-0.1%, it has been demonstrated that various cell types show differential toxicity towards both photoinitiator and UV-light.[32,134] It has been also reported that the UV photo-encapsulation of proteins or nucleic acids causes important damages like protein degradation or DNA breaks.[132]

Therefore, according to all these issues, the photopolymerization of PEGDA hydrogel with an alternative photoinitiator which may satisfy some of the described features is explored.

#### 2.2.1.2 Fabrication of PEGDA hydrogels using LAP photoinitiator

In the light of the discussed limitations on using IrgaCure 2959 as photoinitiator, another compound is evaluated for PEGDA hydrogel polymerization. This compound is a lithium acylphosphinate salt, shortly called LAP, which has been synthesized according to the protocol published by Majima *et al.*[135] The detailed synthesis of LAP photoinitiator is reported in the Experimental section of the manuscript in Appendix 1.

LAP is a type-I photoinitiator, water soluble, cytocompatible and largely used for the encapsulation of cells within photopolymerized PEGDA hydrogels.[136] Contrarily to IrgaCure 2959, LAP is highly water soluble and has a significant absorbance at 365nm (molar extinction coefficient at 365nm, $\varepsilon$ = 218 $M^{-1}$ $cm^{-1}$).[136] Additionally, as reported in Figure 2.11A, the photoinitiator absorbs, albeit weakly, also in the visible range between 400-420nm (molar extinction coefficient, $\varepsilon$ = 51 $M^{-1}$ $cm^{-1}$) which corresponds to purple light. When the LAP is exposed to UV-light, a change of its absorption is observed: in fact the molecule is photo-cleaved into two reactive radical species (Figure 2.11C). As the acylphosphinate is cleaved, the chromophore responsible for LAP absorption is lost (black line, Figure 2.11B). Therefore, after UV-exposure a much lower absorption is detected between 365-420nm (red line, Figure 2.11B) due to the chromophore loss. The features of LAP photoinitiator are particularly interesting for our application since it has a good solubility in water, eventually it is possible to polymerize hydrogels with visible light (from 400nm to longer wavelengths), is cytocompatible[136] and has a higher absorption than IrgaCure 2959. Moreover, the absence of LAP absorption after UV-exposure for wavelengths longer than 365nm may be useful for the spectrophotometry detection of molecules released from gels which absorb in this range. Hence, the conditions involved on the polymerization process with PEGDA polymer and LAP photo-initiator are studied and optimized in order to obtain successful drug releasing hydrogels.

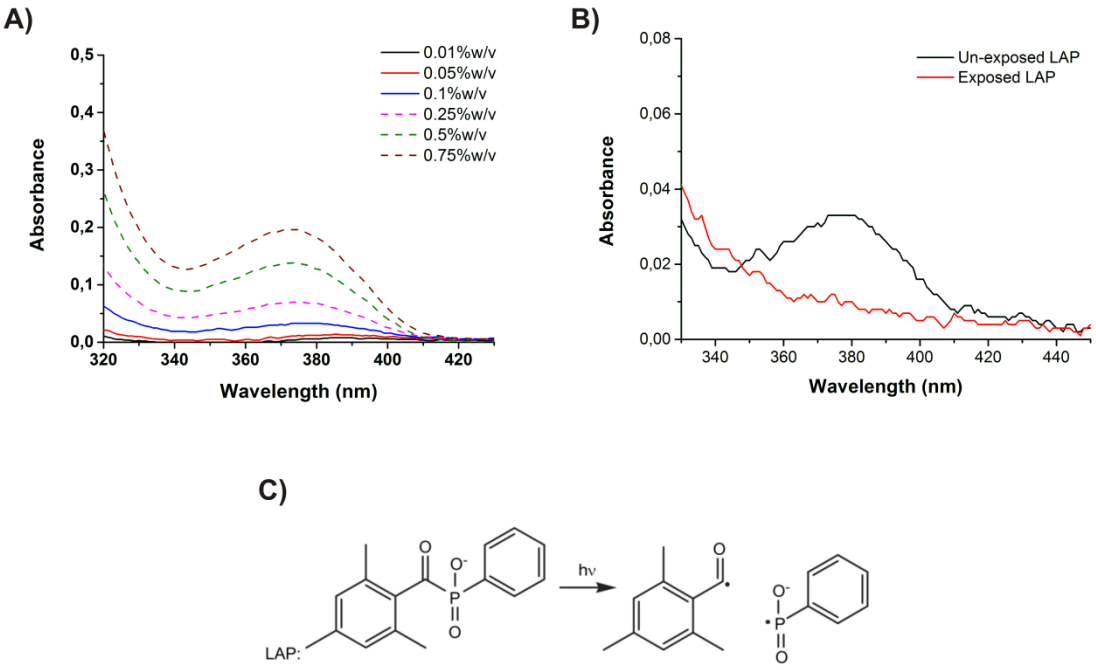


**Figure 2.11** UV-vis spectrophotometric characterization of LAP photoinitiator. (**A**) Spectra of different concentrations of LAP dissolved in MilliQ water. (**B**) Spectra of a solution 0.1%w/v LAP before (black line) and after (red line) 10min exposure. (**C**) Mechanism of photo-cleavage of LAP molecule induced by UV-light exposure.

In order to determine the optimal photopolymerization conditions for PEGDA hydrogels fabrication, various experimental parameters are considered. In a 24well-microtiter plate, different concentrations of $PEGDA_{700Da}$ and LAP, both dissolved in MQ water are mixed and exposed to UV-light in a photo-reactor for 10min. Already after 2min of exposure a complete gelation of all tested solutions occurs. As shown in Figure 2.12A, when a solution of highly concentrated LAP (1%w/v) without polymer is exposed to UV-light, a whitish solution is produced. On the other hand, when a constant concentration of LAP is mixed with various amounts of PEGDA, the color disappears as the PEGDA concentration increases until colorless, homogeneous and completely photo-crosslinked hydrogels are achieved. The Figure 2.12B shows the UV-vis characterization of formed hydrogels which are prepared by mixing a large excess of LAP (1%w/v) and increasing concentrations of PEGDA (between 0.1-1-5%w/v). A strong absorbance in the visible range (from 400 to 500nm) is observed and its magnitude decreases as the concentration of PEGDA increases. This behavior is probably due to an abundant amount of photoinitiator which produces a large number of radical species that, in presence of low PEGDA molecules, crosslink all the PEGDA monomers and confer to the final gel a whitish coloration due to light scattering by particulates.

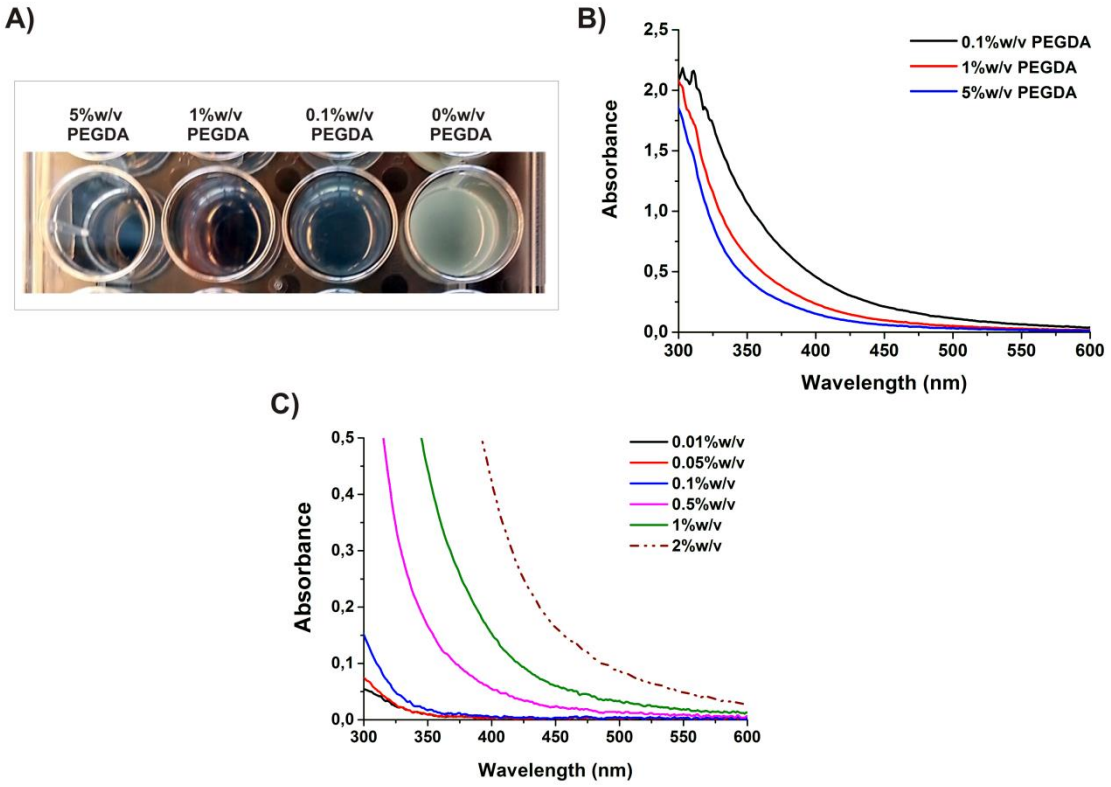


**Figure 2.12** Fabrication of PEGDA hydrogel in presence of the LAP photoinitiator. (**A**) Photo of a 24 well-microtiter plate where various concentrations of PEGDA are crosslinked in presence of 1%w/v LAP dissolved in MQ water upon UV-exposure in a photo-reactor for 10min. As the concentration of PEGDA added to the pre-polymer solution increases, the whitish color of exposed LAP solution disappears. (**B**) UV-vis characterization of hydrogels showed in Figure 2.12A. (**C**) UV-vis spectra of gels composed of a constant PEGDA concentration (5%w/v) and variable amounts of photoinitiator after 10min of curing.

As the concentration of polymer molecules increases, the overflow of radicals still crosslinks completely the polymer and the hydrogels look less colored. A similar behavior is observed when a constant concentration of polymer is used (5%w/v) and excess amounts of LAP are used (Figure 2.12C): the addition of 0.01%w/v of LAP to 5%w/v of PEGDA already results on a completely cured hydrogel after 2min of exposure. Although PEGDA hydrogels are formed in all the tested conditions, the gels have varying appearances: as described above, some of the gels are strongly colored because of an excess amount of LAP compared to that of the monomer, whereas others are completely colorless but extremely soft due to a low content of polymeric molecules. According to these considerations, a PEGDA (700Da) concentration of 20%w/v and 0.5%w/v of LAP are chosen as optimal concentrations for the fabrication of reproducible, un-colored, completely crosslinked and homogeneous gels in terms of thickness and shape.

The use of LAP as candidate photoinitiator results in improved polymerization rate since the time required for a complete crosslinking of PEGDA solutions is one order of magnitude lower for LAP than for I2959 with 365nm illumination at the same intensity and initiator concentration. Further, when

LAP is used as initiator the polymerization takes place also for longer wavelength light (between 400-420nm), contrarily to IrgaCure 2959. In general, the polymerization rate is proportional to the square root of the initiation rate, $R_i$[137] which is given by:

$$R_i = \frac{2\phi\varepsilon f I C_i}{N_A\, h\upsilon} \qquad \textbf{Eq. 2.4}$$

Here, $I$ is the incident light intensity (units of power per area) and $C_i$ is the initiator concentration. The initiator properties that influence the photo-initiated polymerization rate are $\varepsilon$, the molar extinction coefficient; $\phi$, the quantum yield or cleavage events that occur per photon absorbed; $f$, the photoinitiator efficiency or the ratio between initiation events and total radicals generated by photolysis. The Avogadro´s number, $N_A$ ; the Planck´s constant, $h$ and the frequency of initiating light, $\upsilon$ are included for unit conversion. From this equation it is clear that the utility and performance of a photoinitiator are affected by various parameters. Usually, to increase the polymerization rate, $I$ or $C_i$ are increased, but high light intensity and initiator concentration can induce important cytotoxic effect. In the case of I2959 is not possible to increase its concentration because of poor water solubility which limits its utility. Furthermore, as the initiation rate strictly depends on the photons absorbed by the initiator, the weak absorbance profile of I2959 restricts its usefulness for polymerization in a narrow UV-vis region centered at 365nm; in contrast, LAP absorbs also in the visible range (400-420nm). The main benefits on using LAP instead I2959 are not only due to a higher extinction coefficient of LAP, but also higher quantum yield and initiation efficiency ($\phi$ and $f$ respectively in the equation).[136]

#### 2.2.1.3 Photo-polymerization of PEGDA hydrogel through projector light

According to the reported considerations about LAP properties and its utility on photo-polymerization process, one should also consider the light source that mostly satisfies the requirements for hydrogel fabrication. As previously reported, the curing of PEGDA gels is UV-light-assisted and simple equipment is used for their processing. Solutions of polymer and photoinitiator are dispensed into well plates and protected from light until intended crosslinking.

The entire well plate is located inside a photo-reactor which is mainly composed of a series of UV-lamps on the top and bottom of the chamber (Figure 2.13A). Therefore, the curing process takes place on both interfaces of each well. For hydrogel crosslinking, a traditional UV-aligner may be also employed: this machine is normally used for microlithography purposes and its functioning consists in positioning the sample in the stage, align and put it in contact with a mask which presents desired features, and expose the sample to UV-light at 365nm (Figure 2.13B). Both techniques are relatively

simple, ease to handle and they do not require specific sample manipulation. However, these two approaches are not suitable for the fabrication of our intended PEGDA hydrogels, as they should be able to create 3D-structured hydrogels without damaging gel properties. The use of a photo-reactor is consistently limited to a complete crosslinking of the poured solution and 3D-structures are impossible to form with this technique due to the diffused UV-light all over the chamber. Contrariwise, the use of a UV-aligner permits to selectively crosslink certain areas within the solution according to the pattern designed on the mask.

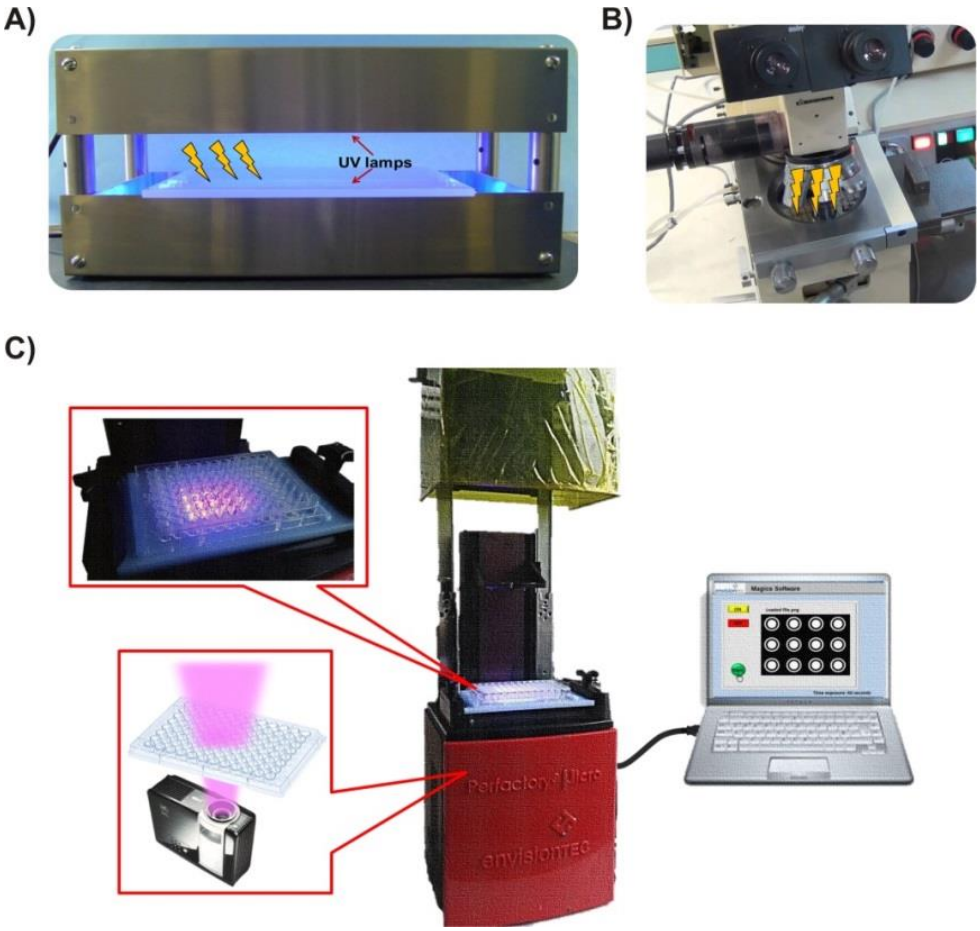


**Figure 2.13** Schematic illustration of the equipment used for photo-polymerization process. (**A**) A photo-reactor based on a series of UV-lamps is used to polymerize multiple solutions without particular 3D-structures; (**B**) a traditional UV-aligner is employed to create 3D-structured PEGDA hydrogels on glass slides, and (**C**) a micro 3D-printer machine is utilized to simultaneously polymerize multiple pre-polymer solutions illuminating them with visible light generated by a modified projector with a maximum emitting light at 410nm. On the enlargements are reported a home-made support which permits to exactly fit a 96 well-microtiter plate on the printer stage (on top), and the tools required for visible-photopolymerization, a projector and a support where pre-polymer solutions are contained (on bottom).

To achieve this goal, the sample has to be in contact with the mask, thus thick supports like well-microtiter plates or Petri dishes cannot be used for this purpose. The main advantage on using well plates is the ability to crosslink multiple solutions at the same time in a rapid step; therefore, when using an aligner, a proper support needs to be used, such as glass slides, wafers and any kind of flat and thin surface. Moreover, when the sample is in contact with the mask an appropriate confinement of the solution on the support should be adopted since when in contact mode, the solution will tend to be squeezed out and its final thickness will be difficult to control. It is clearly needed to use a different method for the simultaneous crosslinking of multiple polymer/photoinitiator solutions having desired 3D-structures. Since the LAP photoinitiator absorbs not only in the UV range (maximum peak absorption at 375nm) but also in the visible region (between 400-420nm), a visible light source can be considered. As illustrated in Figure 2.13C, the EnvisionTEC Perfactory® Micro 3D-printer is utilized for *in situ* visible-light photopolymerization. The equipment is composed of a projector on the bottom of the instrument which is modified to have a maximum emitting light at 410nm based on a LED light source, a stage where the sample is located, a light-protected box which is moved during the polymerization process to protect the sample from external light, and a computer connected to the machine (Magics Desktop Software). A home-made support to exactly locate 96 well-microtiter plates on the stage is used to polymerize simultaneously 12 wells in a single step, as depicted on the enlargement (top, Figure 2.13C). When the sample is placed on the support, the polymerization starts as the projector light coming from the bottom of the sample is turned on. In addition, any desired 3D-structure may be produced in each well: digital masks, based on a grayscale graphic file (with a final resolution of 650dpi), are designed and directly projected onto the sample. Hence, through a simple and cheap light source like a projector, multiple hydrogels can be fabricated in a single step and with desired 3D-structures. Further, many types of support may be used: well-microtiter plates with various shapes and sizes, Petri dishes, glass slides, coverslips, etc.; the only requirement for a successful process is the need of completely transparent supports to permit projected light to pass through it.

#### 2.2.1.4 Characterization of PEGDA hydrogels

When solutions of PEGDA and photoinitiator are mixed and poured into a certain support and exposed to projected light, the entire volume of the solution is crosslinked. According to the initial volume of mixture, a certain exposure time is needed to achieve a complete cured gel. Besides that, the final morphology of the hydrogel is basically controlled by the shape of the support in which the volume is poured, meaning that desired shapes of gel maybe be obtained by changing the support. However, by varying the morphology of the solution support one can control only the appearance of the edges of the gel, for instance square, circle, needle-like shapes may be produced. The exposure to digital masks presenting characteristic features permits to create multiple 3D-structures having various

morphologies within the gel with a great resolution. A preliminary study for the fabrication of PEGDA hydrogels through visible-light photo-polymerization is conducted using the micro-3D printing technology. In a 96 well-microtiter plate, pre-polymer solutions with the same total volume composed of $PEGDA_{700Da}$ and LAP are poured in each well. In order to evaluate the patternability of gels with desired structures, two simple digital masks are designed: one consists of a semi-circle (half in white and half in black), and the second is a completely white circle.

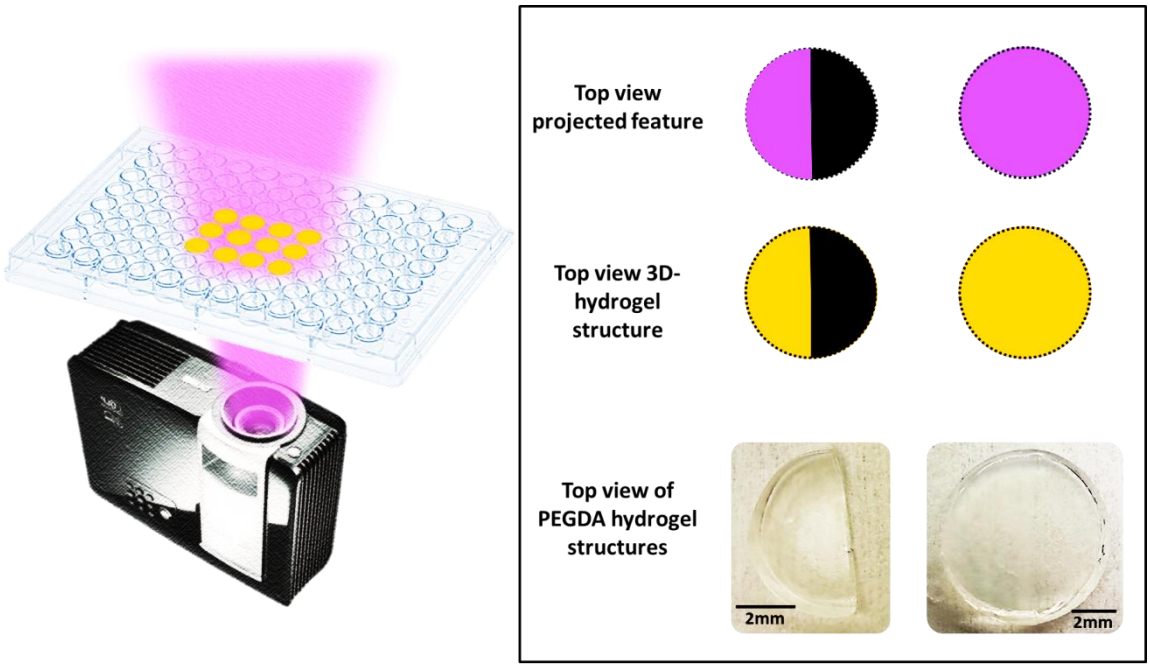


**Figure 2.14** Illustration of visible-light projection technology: in a 96 well-microtiter plate the pre-polymer solutions are poured and a modified LED-light projector that has a maximum emitting light at 410nm, is used to cure the solution (on the left). Two digital masks are designed to create 3D structures on the gels: a semi-circle and circle structures are tested (in the panel on the right). A schematic of the top view of projected mask, exposed solutions and the obtained hydrogel 3D-structures having a thickness of 1.5mm are reported.

These two masks are then projected onto the bottom surface of the well plate; so, the corresponding white areas of digital masks are projected while black areas not (top view of projected feature in Figure 2.14). The solutions are exposed for 1min to visible light through digital masks. The final 3D-structures of hydrogel correspond to a semi-circle and an entire circle as also confirmed by the obtained shaped PEGDA hydrogels in Figure 2.14 (top view 3D-hydrogel structure and PEGDA hydrogel structure). The entire volume of solution is completely crosslinked in the case of circle design, while only half solution volume is cured when a semi-circle pattern is applied.

An important parameter that should be also evaluated is the thickness of the final structured hydrogels, and how it changes when different times of exposure and solution volumes are employed.

To investigate that, in a 24 well-microtiter plate different volumes of the mixture 20%w/v PEGDA and 0.5%w/v LAP are poured in each well; then the solutions are exposed to a semi-circle shaped digital mask for increasing exposure time (15, 30, 60 and 120 seconds). The fabricated hydrogel thicknesses are measured through a caliber and they are plotted as function of the exposed solution volume (in microliter) and exposure time (in second) (Figure 2.15A). As reported in the graph, when the volumes are illuminated for 60seconds, a linear increase of hydrogel thickness is found suggesting that a complete crosslinking of the exposed area is occurred. However, when solutions are exposed to visible-light for more than 60s for example 120seconds, a substantial decrease of hydrogel thickness is observed. In Figure 2.15B a possible explanation to this behavior is suggested. In fact, a prolonged exposure of PEGDA/photoinitiator solutions through the semi-circle digital mask results on an over-crosslinking; in other words, in the solution not only the exposed areas are crosslinked but also those which should not be cured (since corresponding to black regions on the digital mask).

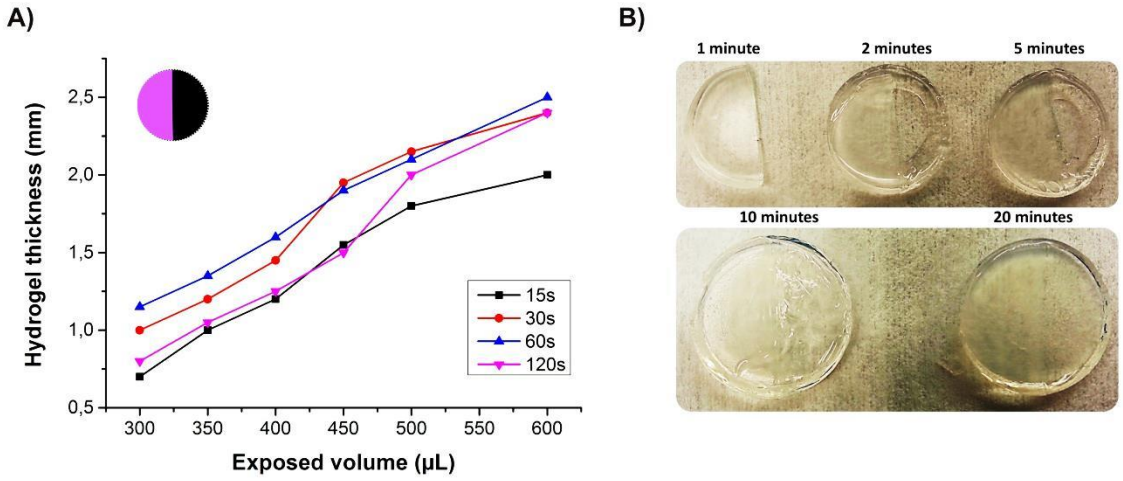


**Figure 2.15** (**A**) Hydrogels thickness plotted as function of the exposed volume of 20%w/v PEGDA and 0.5%w/v LAP solutions and as function of exposure time. Each 24-well is illuminated through a semi-circle shaped digital mask for different period of curing. (**B**) Hydrogels obtained after prolonged exposure times using the semi-circle shaped mask. An over-crosslinking is observed when pre-polymer solutions are cured for more than 60s and the desired shape (semi-circle) is lost when the exposure time rises up to 10 or 20min.

Indeed, as the exposure time increases a larger area of the well is photopolymerized indicating that a short curing time may be optimal for 3D-patterning. Since during light-exposure the molecules of photoinitiator absorb photons, a diffusion of radicals from the crosslinked areas may cause a polymerization of the non-illuminated regions. Moreover, the emitted light may be scattered on the already crosslinked gel and thereby is also directed into the nominally dark areas.

The wettability of PEGDA hydrogels formed by visible-light photo-polymerization is also evaluated. De-hydration (loss of water content) and hydration (uptake of water content) processes are sequentially conducted on hydrogels formed by different PEGDA and LAP amounts in order to evaluate whether the

gels can be maintained in a humidified environment once the drugs are embedded within the matrix. A total volume of 2mL of PEGDA/LAP mixture is crosslinked for 1minute without any particular 3D-structure in a Petri dish and the formed gels have a final thickness of 2.2mm. The weights of empty Petri dish, solution-Petri dish, and hydrogel-Petri dish are measured to evaluate the water loss and uptake. The water exchange through the gels is determined studying the de-hydration and hydration processes. The crosslinked hydrogels in the Petri dishes are incubated in the oven in dehumidified atmosphere at 60° C over time, and every certain interval their weight is measured. As shown in Figure 2.16D, once the evaporation of water from hydrogels takes place, a delamination and shrinkage is observed. After 19hours, a box containing water is located inside the oven which is always maintained at 60° C and gels hydration is estimated again by measuring their weight. Three different compositions of PEGDA and three different amounts of LAP are tested: 0.05 – 0.1 - 0.5%w/v of LAP and 10 – 20 – 30%w/v of $PEGDA_{700Da}$.

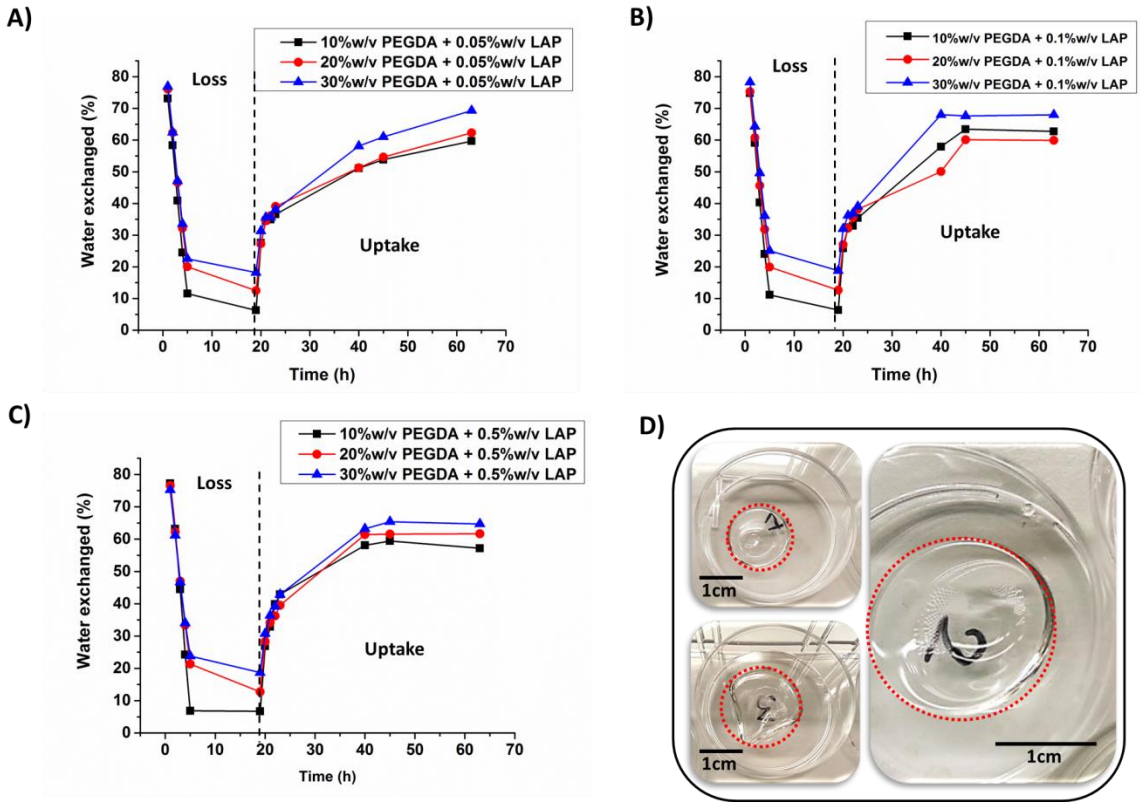


**Figure 2.16** Graphical description of water exchange from visible-photopolymerized hydrogels cured for 1minute. (**A, B** and **C**) Three different concentrations of PEGDA (10-20-30%w/v) and three variable amounts of LAP (0.05-0.1-0.5%w/v) are tested. The loss of water is induced by evaporation in an oven at 60° C over time in a de-humidified atmosphere, and the water uptake is ensured by introducing a bath of water inside the oven. To evaluate the content of loss and uptake of water content, the weights of samples are measured before and after polymerization and during the de-hydration and hydration processes. (**D**) Photos of hydrogels after 19h of de-hydration: the evaporation of water induces a shrinkage of hydrogels on their support.

In Figure 2.16A, B and C, the plots of water exchanged over time are reported including two physical phases pointed out: an initial phase in which water is lost from polymeric networks and a second stage where gels uptake water from the environment. Within the first 19hours, the networks show a rapid loss of water and the water evaporation content is inversely proportional to the PEGDA concentration composing the gels. This behavior is mainly due to a different amount of water in the initial solution prior crosslinking, thus on gels where the polymer concentration is 10%w/v a higher volume of water is included in the matrix. The evaporation process is followed by the uptake of water from the environment which is rapid within the first 4hours and slower during the remaining period. At the end of the hydration process, almost all the prepared hydrogels reach an equilibrium state meaning that the amount of water up-taken from gels is in equilibrium with that present in the environment and no more water can enter the matrices. However, from the plot in Figure 2.16A it is notable that when hydrogels are crosslinked with a concentration of 0.05%w/v LAP after 70hours they do not reach an equilibrium state, rather a liner increasing amount of water up-taken from the environment is detected. These hydrogels are particularly soft and maybe the presence of a low concentration of photo-initiator results on a diminished crosslinking degree of gels. The entire process of water loss and uptake depends on the experimental conditions inside the oven (for instance temperature and humidity). Therefore, once the gels are loaded with various drugs, they can be stored in humidified atmosphere to keep them in a wet state.

#### 2.2.1.5 3D-structured PEGDA hydrogels

One of the important issues for the final goal of fabricating hydrogels for drug release purposes is the patternability of PEGDA material in 3D hydrogel structures. The main parameters that need to be considered are the shape of these 3D-structures according to the intended use and the support that will be employed for hydrogel fabrication. The hydrogel platform for drug screening applications must be fabricated in a cytocompatible support because cell culture experiments will be conducted onto the hydrogel surface, and it should be as small as possible in term of size in order to maximize the number of hydrogel structures on the same support. The shape and size of hydrogels are directly defined by the designed digital mask, the volume of PEGDA/photoinitiator solution and the time of visible-light exposure. Various shapes, sizes and supports are tested in order to have an idea of which combination of these parameters is mostly suitable for our purpose. In Figure 2.17 some examples are reported: all the obtained structures are prepared through visible-light photopolymerization of solutions composed of 20%w/v PEGDA (700Da) and 0.5%w/v LAP illuminated for 1min using a specific digital masks.

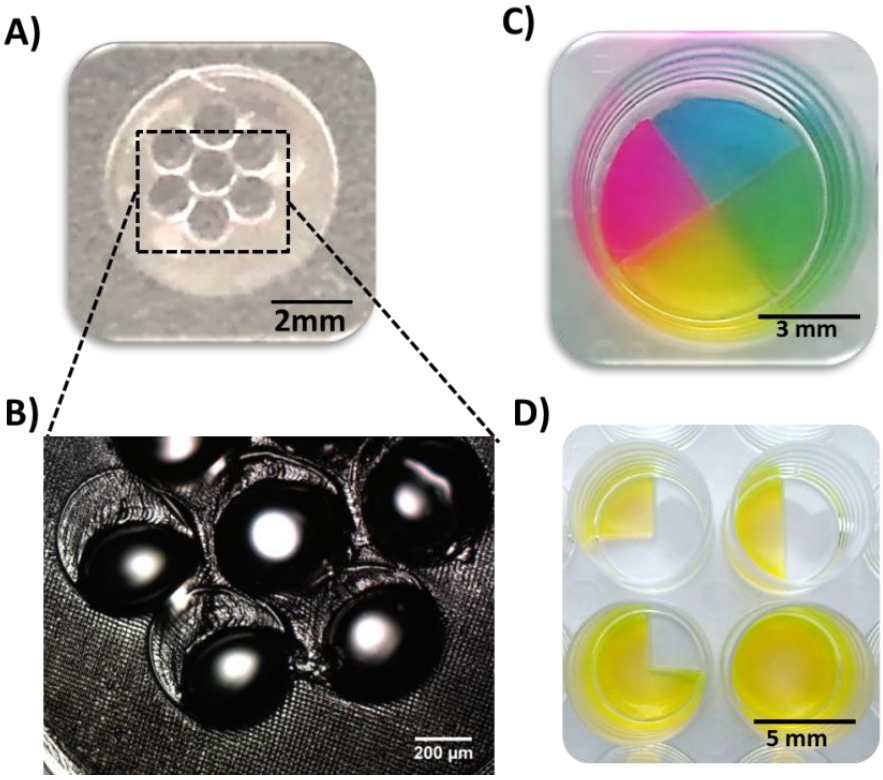


**Figure 2.17** Pictures of some examples of PEGDA hydrogels obtained by visible-light photopolymerization with different digital mask designs. All the 3D structures are obtained exposing for 1min a solution of 20%w/v PEGDA and 0.5%w/v LAP. (**A**) A photo of a circle shaped hydrogel 6.2mm in diameter with (**B**) holes of 500µm in diameter. (**C**) A photo of a circle shaped hydrogel composed of four segments loaded with four food colors, and (**D**) a photo of different volumes of hydrogel (25-50-75 and 100% of the total well area) loaded with calcein.

Rectangular, circle, segments and holes may be fabricated of different sizes; further, they can be prepared in Petri dishes, or glass slides or well plates of various dimensions. Figure 2.18 shows a hydrogel composed of 20%w/v PEGDA and 0.5% LAP exposed for 1min with a digital mask. The design is a bit more complicated than those showed in Figure 2.17 because in this case the gel is formed by multiple concentric circles (where the larger measures 6.2mm) and with a central hole (Ø = 600µm) . The particularity of this structure is that on the digital mask (Figure 2.18C) each circle has a different greyscale value; therefore less or more light intensity will pass through each concentric circle. The application of this design results on a rounded hydrogel with a hole in the center and a gradual slope along the structure (3D-plot of hydrogel in Figure 2.18D). This construct is particularly useful when culturing cells, like spheroids; due to the poor cell attachment properties of PEGDA hydrogel, spheroids may be seeded into the central hole facilitating their handling and characterization since cultured on a confined area.

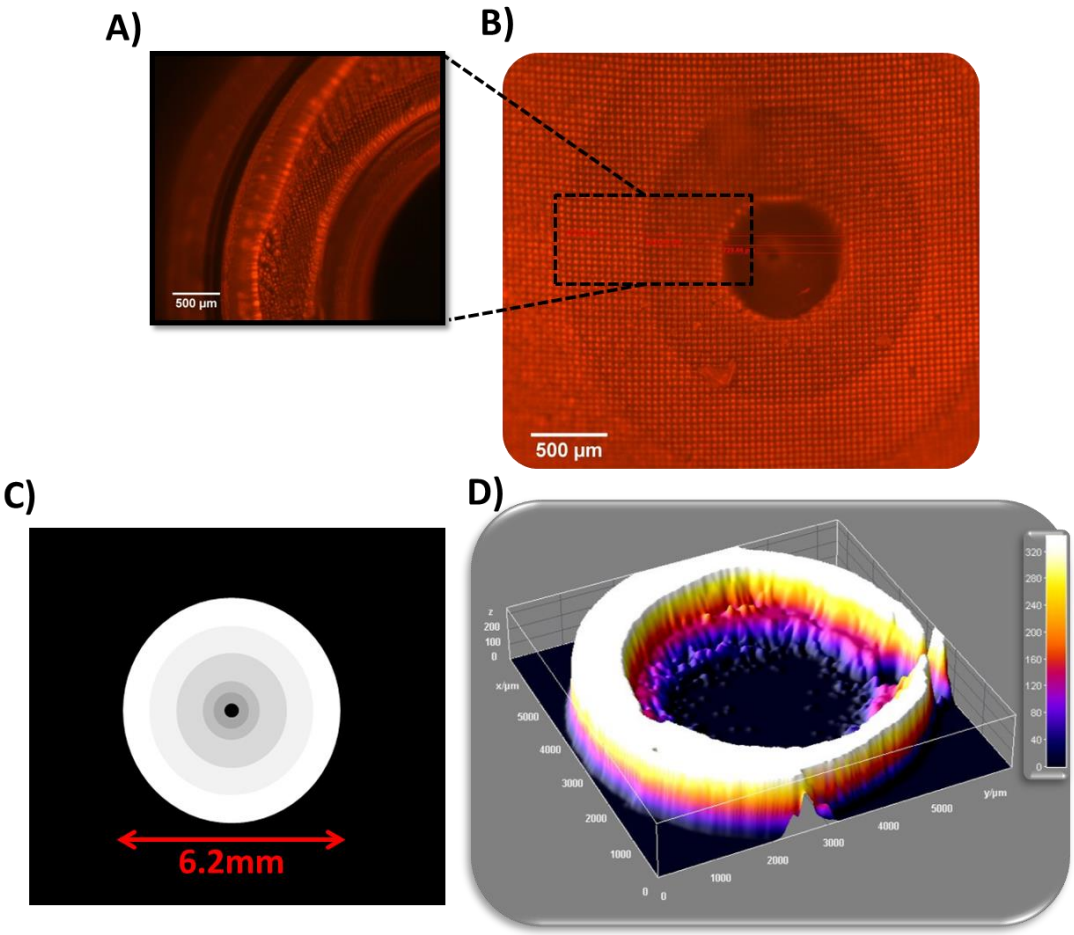


**Figure 2.18** (**A**) and (**B**) fluorescence micrographs of a PEGDA hydrogel obtained by visible-light photopolymerization using a particular digital mask design. The 3D structure is obtained exposing for 1min a solution of 20%w/v PEGDA and 0.5%w/v LAP. (**C**) The mask is made of multiple concentric circles which have different grayscale values. In that way, the sample will be exposed to different light intensities and (**D**) a final 3D structure with a slope will be obtained.

A digital mask with three concentric circles which completely cover the entire well area may be also used (Figure 2.19A) and it could be useful to confine multiple compounds within various hydrogel volumes. Contrarily to the design showed above (Figure 2.18), the three circles are fabricated in three steps: an external ring is exposed for 1min to visible-light, a second ring with smaller diameter than the previous one is also formed, and the remaining volume is crosslinked by a third circle with an even smaller diameter. The resulting 3D hydrogel is shown in Figure 2.19B and for a better visualization of the three structures the pre-polymer solutions are mixed with dyes: the external circle is labeled with Rhodamine-labeled albumin, the circle in the middle is composed of un-labeled hydrogel and the last central circle is visualized through embedding of FITC-labeled albumin. The final hydrogel is the result of three constructs which cover the entire well area and have a constant thickness of 1mm.

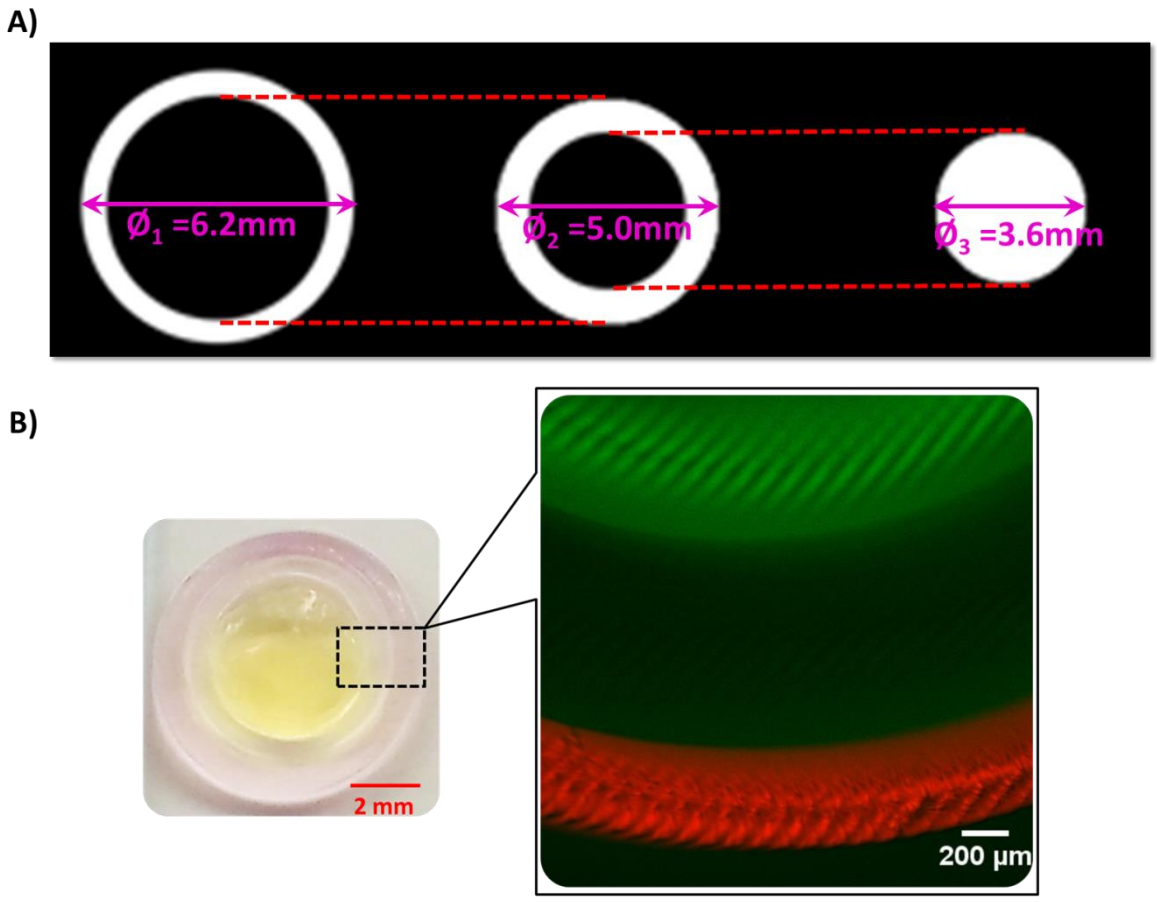


**Figure 2.19** Fabrication and visualization of three-circle shaped PEGDA hydrogel loaded with two different dyes and fabricated through a multi-step process. An external ring structure (radius$_1$ =3.1mm; area ring$_1$ =10mm$^2$; thickness =1mm) is produced by illuminating a solution of 20%w/v PEGDA (700Da), 1%w/v PEGDA (5kDa), 0.5%w/v LAP and 5µM Rho-labeled albumin for 1min. A second circle-shaped hydrogel is formed by illuminating a solution of 20%w/v PEGDA (700Da), 1%w/v PEGDA (5kDa) and 0.5%w/v LAP using a smaller ring structure (external radius$_2$ =2.5mm; internal radius$_2$ =1.8mm; area ring$_2$ =10mm$^2$; thickness =1mm). A third circle is produced by illuminating a solution of 20%w/v PEGDA (700Da), 1%w/v PEGDA (5kDa), 0.5%w/v LAP and 5µM FITC-labeled albumin (radius$_3$ =1.8mm; area ring$_3$ =10mm$^2$; thickness =1mm). (**A**) Digital masks used for the multi-step hydrogel fabrication. (**B**) Photo of the produced hydrogel and corresponding enlargement obtained through confocal microscope. The dimensions of structures are defined by the digital masks (**A**) while the thickness of each gel is controlled by the pre-polymer solution volume.

The network is visualized through confocal laser scanning microscope to detect the fluorescent dyes embedded within the external and internal circles. Rhodamine-labeled albumin is detected using an excitation light at 543nm and collecting the fluorescence at wavelengths longer than 560nm, whereas for FITC-labeled albumin detection, an excitation light at 488nm is used and emitted light is collected for wavelengths longer than 505nm. As shown in the two panels on the bottom of Figure 2.19, the 3D-fluorescence profile of FITC-albumin embedded within the internal circle is reported (on the left), and the 3D-fluorescence profile of Rho-labeled albumin embedded within the external ring structure is

described on the right panel. No fluorescence is detected corresponding to the circle structure in the middle.

### 2.2.2 Molecule and drug release study from PEGDA hydrogels

In general, the diffusion of molecules embedded within hydrogels depends on several parameters including the physical-chemical properties of the molecule and polymeric network and the crosslinking degree of the matrix, thus on the network pore size. Considering these factors, according to the mesh size of gel, small molecules will diffuse faster than larger ones, such as proteins or nucleic acid. Moreover, the photoinitiator concentration, exposure time, or hydrogel thickness are parameters that affect the release rate of targeted compounds. To evaluate whether PEGDA hydrogels are suitable as releasing systems, different model compounds are considered; these molecules are chosen in such way that various molecular weights and physical-chemical properties are investigated. A preliminary study is conducted by encapsulating a concentration of 50μM calcein within 20%w/v PEGDA (700Da) and 0.5%w/v LAP photo-crosslinked for 1min. Calcein is a small and hydrophilic molecule (MW 666.50 g/mol) usually employed as fluorescent dye because of its excitation at 495nm and emission at 515nm. The hydrogels are formed without a digital mask, thus all the area is exposed to projected light. Moreover, cylindrical gels are produced in various well plates (12, 24, 48 and 96-well microtiter plate) using pre-polymer solution volumes which are of the same height but different area (corresponding to the well area). After polymerization, homogeneous and colored gels are produced demonstrating the presence of calcein entrapped within the matrix. The gels are then washed with MQ water and a certain volume of buffer is added to each well promoting calcein release into the supernatant. The release of calcein from PEGDA hydrogels is measured over time through UV-vis spectrophotometric characterization of the collected supernatants until complete release. As reported in Figure 2.20A, a rapid release of calcein is found within the first 90minutes of release experiment, while almost no increase of released molecules is observed during the following 18h. In fact, as depicted in the panel, the hydrogels lose their coloration already after 90min due to calcein release. Moreover, it is possible to observe that the maximum cumulative release reachable corresponds to 50% of the total embedded calcein. Since the hydrogels have clearly lost their coloration after 90min of release study, it is highly probable that most of the compound is wasted during the prior washing steps because of the rapid diffusion of calcein. Figure 2.20B also shows the UV-vis spectra of supernatants obtained from the measurement of calcein absorption at 495nm; the spectrum related to the released calcein after 90min confirms a decreasing amount of compound into the supernatant.

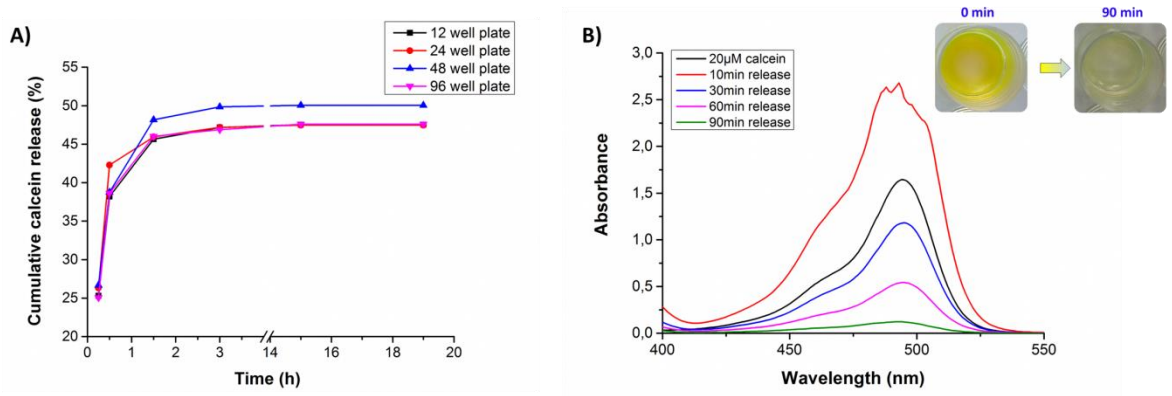


**Figure 2.20** (**A**) Cumulative release profile of calcein from PEGDA hydrogels. The gel is composed of 20%w/v PEGDA (700Da), 0.5%w/v LAP and 50μM calcein solution which is crosslinked for 1min without using digital mask to form a cylindrical gel. Different well sizes are used to produce gels of same thickness but various areas (which corresponds to the well area). The pictures of a calcein-embedded gel at time zero and at time 90min of release study are also reported. (**B**) After washing, a certain volume of supernatant is added to each well (1000μl in 12 wells, 580μL in 24 wells, 326μL in 48 wells and 110μL in 96 well). At different intervals the supernatants are collected and replaced with fresh solutions. The UV-vis spectra of calcein content released into supernatants collected over time is measured at 495nm.

Therefore, small and hydrophilic molecules such as calcein embedded within this specific hydrogel composition are rapidly released because they are smaller than the gel pore size and their diffusion through the gel rapidly occurs. In the light of these considerations, the behavior of small but hydrophobic compounds is also explored: in particular, SN-38 is chosen as model molecule. SN-38 is one of the drugs used for the treatment of colorectal cancer (CRC); it is a small molecule (MW =392.4g/mol), hydrophobic and poorly water-soluble. In a 96 well-microtiter plate, a solution of 20%w/v PEGDA (700Da), 0.5%w/v LAP and 200μM SN-38 is cured for 1min without any digital mask. The hydrogels are extensively washed with MQ water and the release of drug is collected over time into the supernatants. The released SN-38 molecules are quantified through UV-vis measurement recording the absorption at 374nm (Figure 2.21B). The cumulative profile (Figure 2.21A, black line) shows that the drug is slowly released and the 90% of total embedded molecules is obtained after a week of release study (data not shown). Because of that, the composition of PEGDA hydrogel is modified by introducing longer PEG chains: different concentrations of PEGDA 5kDa (0.1-0.5-1-1.5%w/v) are added to the main precursor solution (20%w/v PEGDA 700Da and 0.5%w/v LAP). In Figure 2.21A, an enhancement of drug release is achieved as the concentration of PEGDA 5kDa increases. Although no difference is observed between the release profile of SN-38 in presence of 0.1%w/v or 0.5%w/v PEGDA 5kDa, or when it is used a concentration of 1%w/v or 1.5%w/v PEGDA5kDa, a remarkable difference is shown between 0%w/v and 0.1%w/v PEGDA 5kDa. A further enhancement of drug release results when 1%w/v PEGDA 5kDa is used. The presence of longer PEG chains induces an increase of the pore size on the polymeric network,[138] thus promoting the diffusion of hydrophobic molecules such as SN-38. A complete release of drug is then achieved in a shorter time

compared to the partial release obtained from PEGDA hydrogel free of PEGDA 5kDa which requires up to a week.

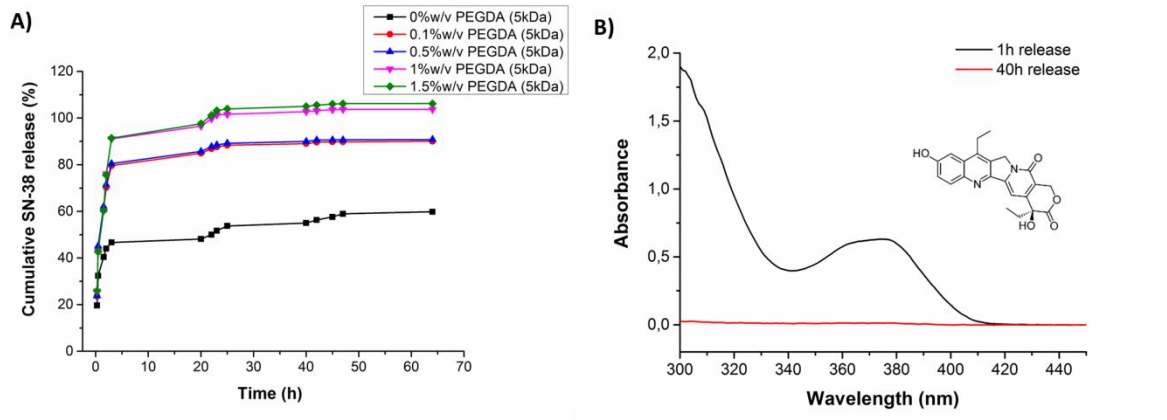


**Figure 2.21** (**A**) Cumulative release profiles of SN-38 embedded within PEGDA hydrogels in 96 well plate. Different gel compositions are tested: 20%w/v PEGDA (700Da), 0.5%w/v LAP, 200μM SN-38 plus 0-0.1-0.5-1-1.5%w/v PEGDA (5kDa). (**B**) After washing, a specific volume of supernatant (110μL) is added to each well and at different intervals the supernatants are collected and replaced with a fresh solution. The UV-vis spectra of supernatants collected after 1h release (black line) and after 40h release (red line) from a gel composed of 20%w/v PEGDA (700Da), 1%w/v PEGDA (5kDa), 0.5%w/v LAP and 200μM SN-38 are measured. SN-38 has a maximum absorption peak at 374nm. The experiment is replicated three times (n=3).

The embedding of larger molecules in terms of high molecular weight is studied by entrapping a concentration of 5μM FITC-albumin within PEGDA hydrogel. The labeled-protein has a molecular weight of ~ 66kDa and an amphiphilic behavior. Because of the protein dimensions, the molecule is photopolymerized within hydrogels composed of 20%w/v PEGDA (700Da), 0.5%w/v LAP and 1%w/v PEGDA (5kDa) based on the results obtained without including PEGDA (5kDa) in which no release is observed (data not shown). The release profile of FITC-albumin is reported in Figure 2.22: the protein content is collected into the supernatants which are measured through UV-vis spectrophotometry and the amount of dye molecules is quantified at 495nm. Although the protein is bigger than the compounds previously tested (calcein and SN-38), within a period of circa 5 days an almost complete release of the protein is obtained. An increase of PEGDA 5kDa concentration may facilitate further molecules diffusion, thus reducing the time needed for a complete release. From these preliminary studies it emerges that the release of a certain compound from PEGDA hydrogels can be easily optimized by tuning gel composition. In that way, even bigger molecules like proteins may be released in a reasonable time without their damage, since the spectra of released molecules are identical to those of free compounds.

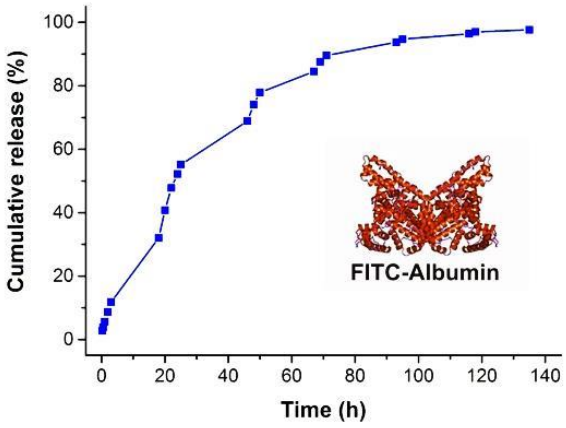


**Figure 2.22** Release profile of 5μM FITC-albumin embedded within a hydrogel composed of 20%w/v PEGDA (700Da), 0.5%w/v LAP and 1%w/v PEGDA (5kDa). The content of released protein is characterized by UV-vis spectrophotometry recording its absorbance at 495nm.

The application of this hydrogel is intended for drug release purposes and in specific, on the release of relevant chemotherapeutics commonly used for the treatment of colorectal cancer (CRC). Since, as already discussed in the introduction, the application of such hydrogels is intended for drug release purposes, the release profile of various drugs is characterized: SN-38, already described above, Oxaliplatin, 5-FU and Folinic acid (FA). Oxaliplatin (MW =397.3g/mol), 5-FU (MW =130.1g/mol) and FA (MW =511.5g/mol) are relatively small and hydrophilic drugs. Hence, each individual drug is entrapped within gel composed of 20%w/v PEGDA (700Da) and 0.5%w/v LAP, except for SN-38 which is embedded in a hydrogel made of 20%w/v PEGDA (700Da), 0.5%w/v LAP and 1%w/v PEGDA (5kDa). The precursor solutions are crosslinked for 1min in a 96 well-microtiter plate without the use of digital mask, thus all the liquid is cured to form cylindrical gels with dimension of 6.2mm in diameter and thickness of 1mm. After photopolymerization, the gels are washed and the released molecules are collected into the supernatants. The contents are then evaluated through UV-vis spectrophotometry for SN-38 (at 374nm), 5-FU (at 288nm) and FA (at 300nm), whereas oxaliplatin is quantified via inductively coupled plasma mass spectrometry (ICP-MS).

As shown in Figure 2.23, 90% of 5-FU is released within 30 h, circa 90% of FA already after 5 h is diffused into the supernatant and SN-38 is completely released after 1 day. Contrariwise, oxaliplatin reaches a value around 65% after 2 days releasing. All the experiments are terminated when no molecule signal is detected into supernatant; in fact, even if the maximum release reachable by OxPt is around 65%, no drug is detected after 2 days. This behavior may be due to a loss of drug during the washing step which cannot be prevented with the tested PEGDA composition. An eligible approach to prevent loss of compounds during washing step is the use of drug-loaded nanoparticles, such as

liposomes which can be used to encapsulate oxaliplatin into their aqueous cavity, embed them within polymeric network and on demand, release drug molecules by applying a proper trigger.

In the next paragraphs, the release of oxaliplatin when loaded into liposomes is characterized. In particular, the effect of thermal triggering of OxPt-loaded liposomes is investigated.

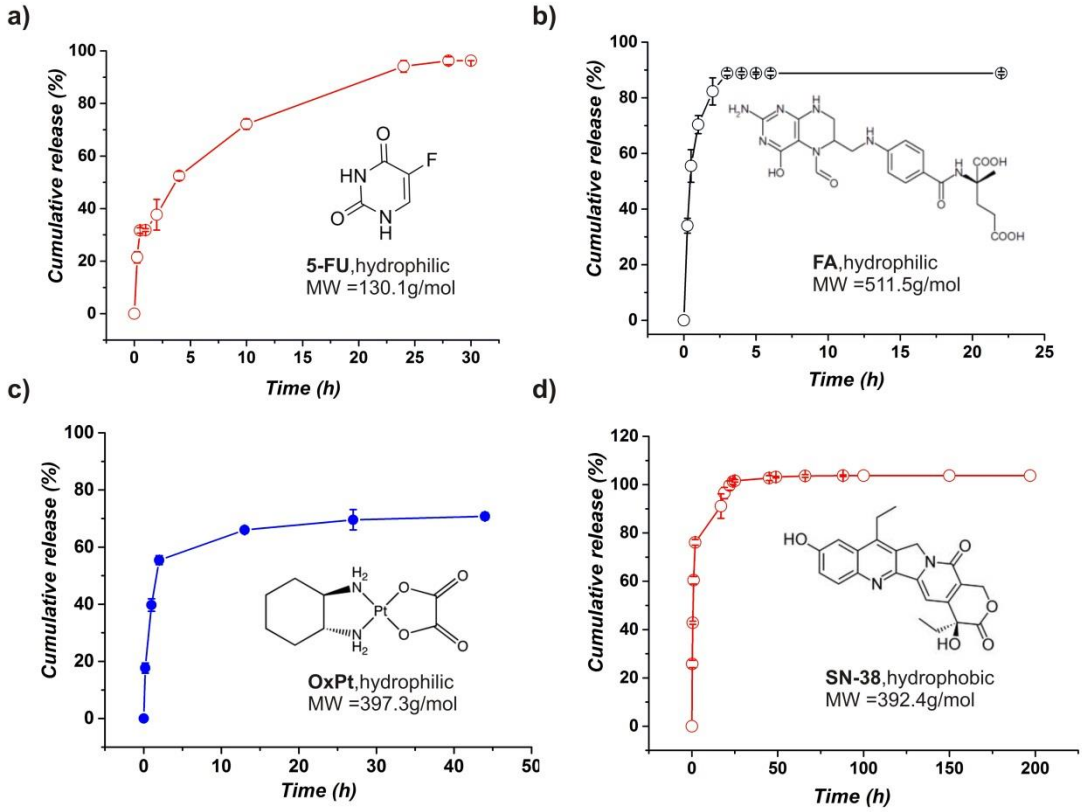


**Figure 2.23** Release profiles of various chemotherapeutics from PEGDA hydrogels. 1mM 5-FU (**a**), 200µM FA (**b**), and 200µM oxaliplatin (**c**) are embedded within hydrogels composed of 20%w/v PEGDA (700Da) and 0.5%w/v LAP; 200µM SN-38 (**d**) is entrapped in a gel made of 20%w/v PEGDA (700Da), 0.5%w/v LAP and 1%w/v PEGDA (5kDa). All the solutions are crosslinked for 1min by visible-light exposure. The released molecules are collected into the supernatant and quantified through UV-vis spectrophotometry (374nm for SN-38, 300nm for FA, and 288nm for 5-FU), and ICP-MS for oxaliplatin. All the experiments are repeated three times (n=3).

### 2.2.3 Drug-loaded liposomes and their embedding within PEGDA hydrogels

After a molecule is embedded within a polymeric network an extensive washing step is crucial. In fact, after polymerization, even though the entire solution is crosslinked to form homogeneous gels, radical species and un-reacted compounds must be removed to avoid interference with the encapsulated molecules which may affect the release. These reasons lead us to consider the use of nanoparticles as drug carrier; the main advantages on using drug-loaded nanoparticles are due to the ability of nano-

carriers to protect compounds from the chemical and physical environment, control their release by applying a certain trigger and the possibility to load a high concentration of molecules into small vesicles (around 100nm in diameter). In this work, liposomes are used as oxaliplatin carrier. Two different stocks of oxaliplatin-loaded liposomes are synthesized according to the protocol described in the Experimental section of the manuscript in Appendix 1. One liposomal formulation is composed of DPPC/HSPC/cholesterol/DSPE-PEG2kDa components (thermo-sensitive liposomes which have an average diameter of 112.7nm with a polydispersity of 0.022), while the other composed of DSPC/cholesterol/DSPE-PEG2kDa (stealth liposomes which are characterized by an average diameter of 132.5nm and polydispersity of 0.016). The main difference between these two suspensions is their response to heat treatment: thermo-sensitive liposomes become leakier when heated up at a certain temperature and their cargo can diffuse outside from the interior aqueous compartment. Stealth liposomes are much more stable in terms of bilayer mobility because of the presence of DSPC lipids which have a higher phospholipids phase transition temperature. The phase transition temperature ($T_m$) of thermo-sensitive liposomes is determine by embedding in a 96 well-microtiter plate a concentration of 100μM OxPt-loaded liposomes is embedded within a hydrogel composed of 20%w/v PEGDA (700Da) and 0.5%w/v LAP both dissolved in phosphate buffer solution (PBS) which is photopolymerized for 1min and extensively washed with PBS (30min). Figure 2.24A shows a schematic illustration of the nano-system used to evaluate the phase transition temperature of thermo-sensitive OxPt-loaded liposomes. After entrapment of vesicles within the gel, the hydrogels are heated at different temperatures for 1h in a thermo-block hotplate. The released OxPt is thus collected into the supernatant and the aliquots are measured through ICP-MS.

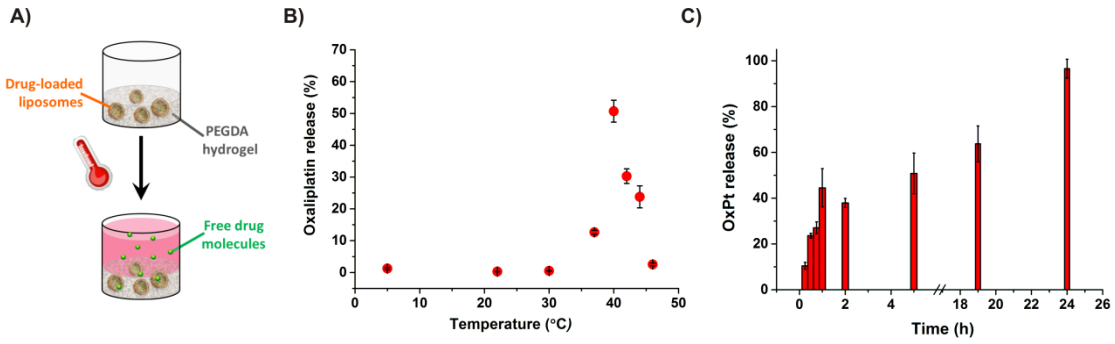


**Figure 2.24** (**A**) Schematic illustration of thermo-sensitive OxPt-loaded liposomes embedded within PEGDA hydrogel; a following heat treatment of the nano-platform induces a liposomes leakage and consequent drug release. (**B**) The phase transition temperature of thermo-sensitive liposomes is characterized by heat treatment for 1h at different temperatures when vesicles are embedded within gel. (**C**) The OxPt release induced at 40° C at different times of heat exposure is also measured; the nanoparticles are always entrapped within PEGDA hydrogels. The concentration of OxPt is collected into supernatants and determined by ICP-MS.

In Figure 2.24B, the amount of drug leaked from liposomes and diffused from the gel into supernatant is plotted against the applied temperature. When the system is heated for 1h the maximum release of OxPt is obtained at 40° C of heat treatment while almost no leakage is shown between 5° C and 30° C. As the phase transition temperature is passed, a decrease of molecules release is observed: in fact, already at 46° C the amount of drug leaking out approaches zero. A further investigation consists of establishing the heating time required to reach the maximum release. Hence, 100μM of OxPt-loaded thermo-sensitive liposomes are entrapped within 20%w/v PEGDA (700Da) and 0.5%w/v LAP dissolved in PBS, cured for 1min and subjected to a 30min washing step. The hydrogels are then heated up at 40° C for different heat exposure times; as before, the amount which leaks out into the supernatant is detected by ICP-MS and plotted against the time of heat exposure (Figure 2.24C). As previously found, after 1h heat treatment the concentration of OxPt released is almost 50% of the total embedded drug whereas the highest leaked amount is achieved after 24h of heating. Also notable is that after 30min already more than 20% of the embedded drug is released, suggesting a rapid phase transition of lipids within the bilayer. Heat triggering is one of the most interesting strategies for active release of content from nano-carriers; indeed, these liposomes are largely used for hyperthermia medical applications which are based on lipid formulations having a narrow phase transition temperature just above body temperature.

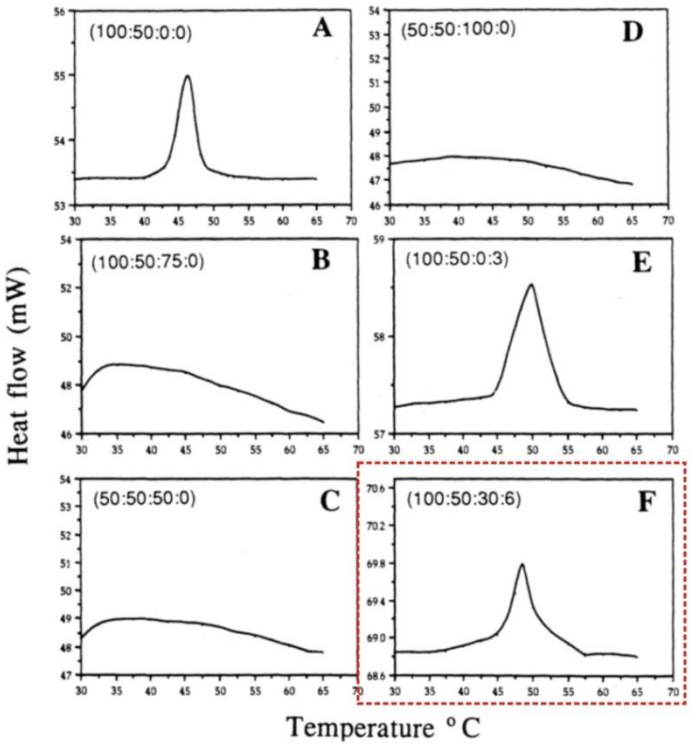


**Figure 2.25** Differential scanning calorimetry thermos-grams for different liposomes compositions. Liposomes are composed of DPPC/HSPC/cholesterol/DSPE-PEG at the indicated molar ratios. Figure reproduced from [139].

When close to the $T_m$, heterogeneity in the membrane will occur and the cargo leakage from interfacial membrane regions is induced. The thermo-sensitive liposomes used for drug release purposes are composed of DPPC/HSPC/cholesterol/DSPE-PEG2kDa at molar ratios of 100/50/30/6. A similar lipid composition has been explored by Gaber *et al.*[139]: the thermotropic transitions for different liposome compositions were detected by differential scanning calorimetry (DSC). As shown in Figure 2.25, they found that when the molar ratio of cholesterol to phospholipids is higher than 2 or more, there is no clear phase transition (Figure 2.25B, C and D), and that the composition which seems to be optimal for drug release has a phase transition at 48° C (Figure 2.25A, E and F). Moreover, the presence of DSPE-PEG causes a small increase in the phase transition temperature, 2° C higher than the same composition in absence of PEG-grafted lipid (Figure 2.24A and E). It is generally recognized that the presence of cholesterol decreases the permeability of liposomes and protects them from destabilizing environments, while PEG-grafted lipids provide a hydrophilic surface coating (steric stabilization) onto liposomes membrane. Gaber *et al.*[139] also showed the release of doxorubicin from these described lipid compositions at three different temperatures (Figure 2.26). The release of doxorubicin in the panels from A to D is very low and it poorly increases by raising the temperature from 37° C to 42° C and 45° C, indicating that the presence of cholesterol reduces the drug release compare to liposomes without cholesterol. In fact, when vesicles are made of only phospholipids (DPPC and HSPC), a high release is detected at 45° C which corresponds to the phase transition temperature (panel A). As stated before, the optimal lipid composition is observed in the panel F that is similar to the thermo-sensitive liposomes synthetized for our purposes. Indeed, these liposomes when heated for 30min at 42° C or 45° C leak out almost 50% of the loaded doxorubicin. Therefore, in order to have liposomes that are stable at 37° C but release their content at 42-45° C, the phospholipid composition should be prepared in such way to undergo a phase transition around 45° C.

Hence, the OxPt release from thermo-sensitive liposomes when embedded within PEGDA hydrogels is in agreement with the findings reported in literature. Stealth liposomes instead are composed of DSPC/cholesterol/DSPE-PEG2kDa with molar ratios of 55/40/5. These liposomes are more stable than thermo-sensitive liposomes simply because formed by an abundant amount of DSPC which has a phase transition temperature at 58° C. Contrarily, DPPC, the main component of thermo-sensitive liposomes, presents a main transition temperature at 41° C and a pre-transition temperature at 34° C as described in Figure 2.27.[140]

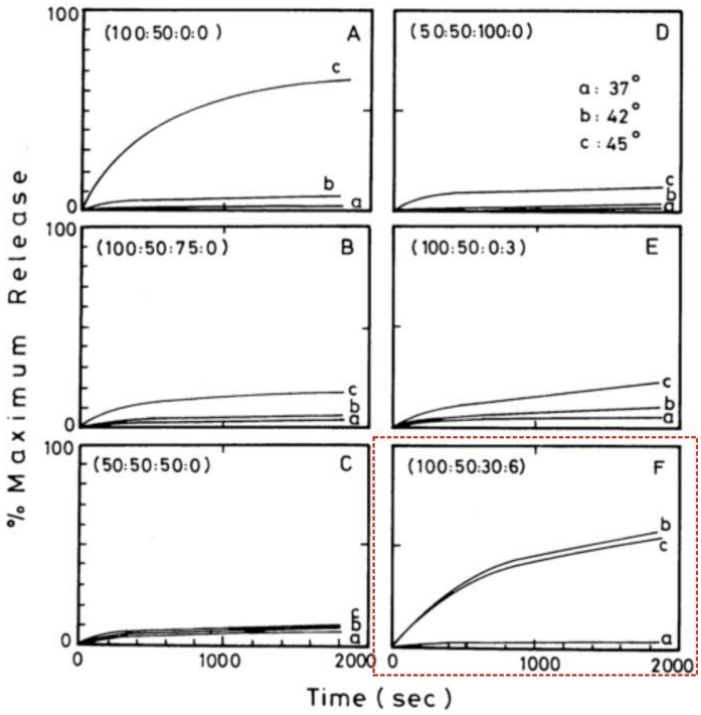


**Figure 2.26** Release kinetics in buffer of doxorubicin-loaded liposomes with different molar ratios of liposome components. Temperatures at 37° C, 42° C and 45° C are tested for release study. Figure reproduced from [139].

TABLE III: Phospholipid Transition Temperatures and Enthalpy Changes Determined by Hinz and Sturtevant (1972).

| | Lower Transition | | Main Transition | |
|---|---|---|---|---|
| Phospholipid | $T_{m1}$ (°C) | $\Delta H_{m1}$ (kcal/mol) | $T_{m2}$ (°C) | $\Delta H_{m2}$ (kcal/mol) |
| DMPC | 13.5 ± 0.2 | 1.1 ± 0.2 | 23.70 ± 0.09 | 6.26 ± 0.18 |
| DPPC | 34.0 ± 0.2 | 2.3 ± 0.2 | 41.75 ± 0.06 | 9.69 ± 0.21 |
| DSPC | 49.1 ± 0.2 | 1.4 ± 0.2 | 58.24 ± 0.03 | 10.84 ± 0.17 |

**Figure 2.27** Table reported by Yelling *et al*[140] representing some phospholipids transition temperatures and enthalpy changes.

Thus, the heat treatment of stealth liposomes at 40° C, that corresponds to the temperature at which thermo-sensitive liposomes release the highest concentration of drug, results on a stable state and a weak leakage (according to transition temperature of DPPC and DSPC in Figure 2.27). The lipid composition of liposomes affects also the stability of vesicles suspension since after their synthesis, liposomes naturally tend to aggregate and precipitate. The presence of cholesterol and PEG-grafted lipids together enhance liposome stability for a prolonged time. However, when drug-loaded liposomes are stored for extended periods a possible leakage may occur even without heat treatment. Therefore, the stability of both OxPt-loaded liposomes (thermo-sensitive and stealth) is evaluated over a period of 100 days; in specific, 100μM OxPt-loaded liposomes are embedded within a hydrogel composed of

20%w/v PEGDA (700Da) and 0.5%w/v LAP cured for 1min. The entrapped liposomes are kept for 100 days at 5° C and 22° C (room temperature) in a wet state (supernatant); aliquots are taken at different intervals and the amount of OxPt into supernatant is measured through ICP-MS. As expected, the leakage of thermo-sensitive and stealth liposomes embedded within PEGDA hydrogels at 5° C over a period of 100 days is very low (circa 10% of the total encapsulated drug). No relevant difference is observed for the two liposome stock suspensions (Figure 2.28A), meaning that liposomes are very stable for prolonged time when stored at 5° C. A diverse scenario is found when both liposome suspensions entrapped within gels are maintained at room temperature (22° C): the OxPt leakage is above 60% and this value seems to increase over time, while a lower but still large leakage is measured also from stealth liposomes (Figure 2.28B). The collected supernatants are also analyzed through dynamic light scattering (DLS) to evaluate the possible presence of liposomes into the supernatants by measuring the average diameter of aliquots. An average diameter of 4.6nm (polydispersity index =0.017) for thermo-sensitive liposomes and 4.14nm (polydispersity index = 0.035) are detected when the system is stored at 22° C. These values indicate that no liposomal vesicles are escaped from hydrogel network and that the oxaliplatin detected into supernatants is mainly due to leakage process. Taking into account all the obtained results, a given instability of vesicles over prolonged storage is observed; however, the suspensions can be kept in a stable state for long periods at 5° C with a loss of loaded compound of around 10%.

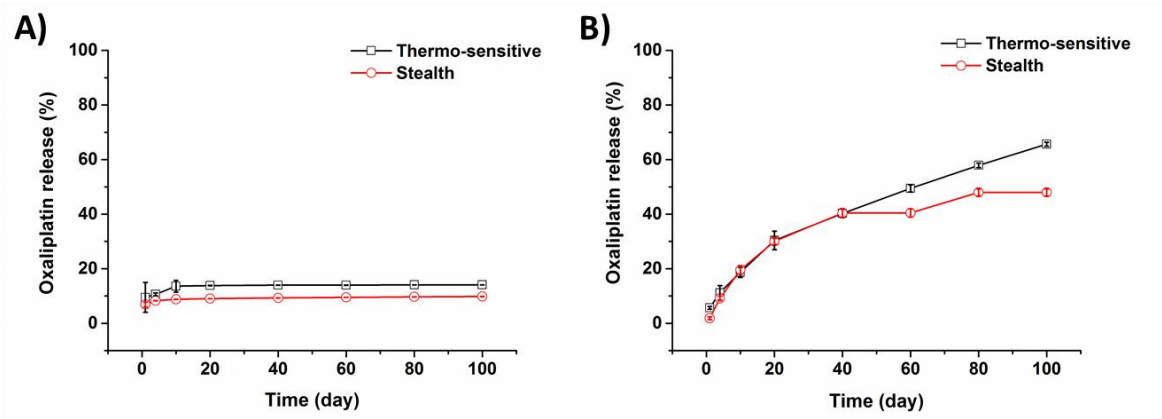


**Figure 2.28** Oxaliplatin leakage from stealth and thermo-sensitive liposomes embedded within 20%w/v PEGDA (700Da) and 0.5%w/v LAP after 1min curing; the liposomes embedded within hydrogels are kept at 5° C (**A**) and 22° C (**B**) over a period of 100 days. The content of released drug into supernatant is characterized by ICP-MS.

### 2.2.4 Digital drug dosing

The release profiles of chemotherapeutics (SN-38, 5-FU, Oxaliplatin and Folinic acid) from PEGDA hydrogels (reported in Section 2.2.2) demonstrate the possibility to entrap within certain volumes of gel, specific concentration of compounds and completely release them into an aqueous compartment over a certain period (maximum in 24h). A rapid diffusion of oxaliplatin from the polymeric network is prevented by including OxPt-loaded nanoparticles into the gel and promoting drug release by applying heat treatment. As stated in the introduction of this thesis, the colorectal cancer chemotherapy is based on a combination of multiple drugs: FOLFOX (5-FU, Folinic acid and oxaliplatin) and FOLFIRI (5-FU, Folinic acid and Irinotecan). These drug combinations are thus embedded within hydrogels and their release and cytotoxicity are evaluated. A relevant question that could be interesting to answer is whether these drugs when entrapped together into the matrix are still stable and efficient. Further, how the concentration of embedded compounds can be controlled in order to reach the therapeutic doses after release? The simplest approach when the release profile of a certain compound is known consists of encapsulating a certain concentration of drug within the gel to release the desired therapeutical dose into the supernatant. In general this approach is the easiest way to proceed when the release profile of a certain compound is known. However, here a smart and reproducible method based on digital photo-polymerization and drug dosing processes is proposed. To give an idea of how the process works, two model molecules are considered: FITC-labeled albumin and Rhodamine-labeled albumin. As reported before, albumin is a medium size protein and its diffusion through PEGDA hydrogel has been optimized to guarantee a sustained release. Indeed, gels composed of 20%w/v PEGDA (700Da), 1%w/v PEGDA (5kDa) and 0.5%w/v LAP are employed for protein encapsulation. In a 96 well-microtiter plate, hydrogels of 6.2mm in diameter and 1mm in height are polymerized by visible-light exposure using a digital mask with a design made of three concentric circles (the same that has been adopted to create 3D-circle shaped hydrogels in the paragraph 2.2.1.5, Figure 2.19). These circles are prepared in such way that different combinations of hydrogel areas are produced and in each circle a different compound is embedded: FITC-albumin within the external circle, bare hydrogel in the middle, and Rhodamine-albumin within the internal circle. Figure 2.29A shows a schematic of the three concentric circles produced on the hydrogel and the molecules embedded: in orange the FITC-albumin gel, in light blue the bare hydrogel, and in magenta the Rho-albumin gel.

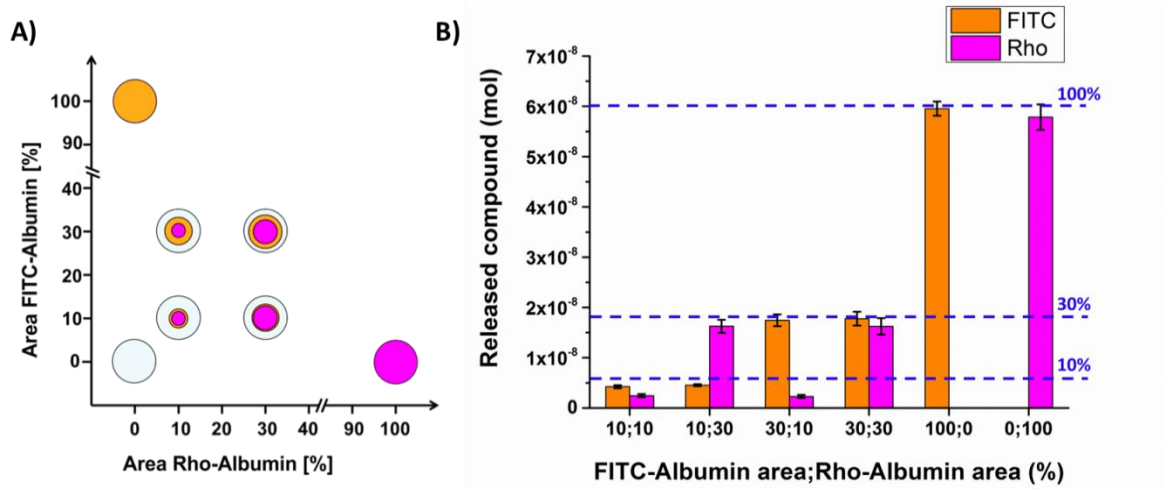


**Figure 2.29** (**A**) Schematic of digital molecule dosing method. Three-circle shaped PEGDA hydrogels are used to embed two labeled compounds: 200µg/mL of FITC-albumin and Rhodamine-albumin both dissolved in PBS. Combinations of different areas of embedded FITC-albumin (in orange), Rhodamine-albumin (in magenta) and bare hydrogel (in light blue) are fabricated to determine the resulting molecules release. (**B**) The cumulative amounts of FITC-albumin and Rho-albumin into the supernatants after 48h of release are plotted as function of the area in which they were originally entrapped. The experiment is triplicated (mean ± SD, n=3).

The final 3D circle shaped hydrogel is obtained through a multi-step process: first, a solution of FITC-albumin, PEGDA (700Da and 5kDa) and LAP is cured for 1min using the corresponding digital mask (external circle, Ø =6.2mm); then the formed structure is washed and the second circle is fabricated polymerizing a PEGDA and LAP solution, and a Rho-albumin, PEGDA and LAP solution is cured to create a third structure. Since the thickness of these three structures is constant (1mm), only their area will change; the chosen hydrogel areas, as reported in the *x* and *y* axis of Figure 2.29A, correspond to 10 – 30 – 100% of the total well area. The release of compounds entrapped within various areas is evaluated by collecting the supernatants over a period of 48h and measuring the UV-vis absorption of FITC and Rhodamine at 490nm and 540nm, respectively through a microplate reader (Figure 2.29B). As already mentioned earlier, normally when considering drug releasing systems one should increase the initial compound concentration to obtain a desired released amount on the basis of known release kinetic. With this method, the released concentration is controlled mainly by changing the area of hydrogel in which the compound is embedded; in other words, the number of molecules that are released into a supernatant is directly proportional to the area in which molecules are confined. Another benefit from this technology is that multiple compounds may be embedded in a hydrogel produced in a single well through a multi-step process, where each specimen is confined in a certain area. In order to test the cytotoxic effect of combinations of chemotherapeutics, the hydrogels are produced by entrapping multiple drugs within 3D-structured circles of the same area (10mm$^2$) and thickness (1mm). In the following paragraph, these three-circle shaped hydrogels are used to test the

cytotoxicity effect of combined drugs that are released in cell culture media when human colorectal adenocarcinoma cells (HT29) are cultured onto the shaped gels.

## 2.3 Drug screening of individual and combined free chemotherapeutics

A preliminary study of the cytotoxic effect of SN-38, 5-FU, Oxaliplatin and Folinic acid (FA) as individual and combined treatment is conducted. Different concentrations of each drug are explored in order to test the inhibition degree on proliferation of human colorectal adenocarcinoma cell line (HT29) as function of drug doses. A simple illustration of the method used to evaluate drug cytotoxicity on HT29 is shown in Figure 2.30.

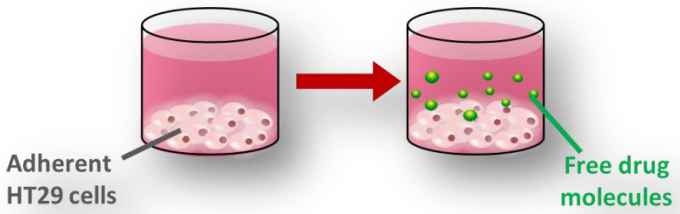


**Figure 2.30** Illustration of the approach adopted to evaluate free drug cytotoxicity on HT29 cell line. Cells are initially cultured at a concentration of 100 000 cells/mL on a 96 well-microtiter plate and after 24h growth, a certain concentration of drug is added to the medium. The drug dose effect is evaluated by measuring the cell viability after 48h from drug treatment.

The protocol consists on culturing the HT29 cells in Dulbecco´s Modified Eagle Medium (DMEM) in a 96 well-microtiter plate. A concentration of 100 000 cells/mL and kept in the incubator for 24h in order to allow cell adhesion on the well surface. Cells are then exposed to different concentrations of individual drugs (SN-38, 5-FU, Oxaliplatin and FA). These drugs are dissolved in dimethyl sulfoxide (DMSO) except for FA which is solubilized in water. It is well-known that organic solvents such as DMSO are cytotoxic (as also reported in Figure 2.31). Therefore, concentrated stock solutions of drugs are prepared in order to add the minimum volume of DMSO-solubilized drug and limit the solvent toxicity. In particular, 1µL of each concentrated drug solution is added to the adherent cells and 1µL of DMSO is used as control. The 96 well-microtiter plate is maintained in the incubator for 48h. To determine the cell viability after drug exposure, the commonly used [3-(4,5-dimethylthiazol-2-yl)-5-(3-carboxymethoxyphenyl)-2-(4-sulfophenyl)-2H-tetrazolium] (MTS) assay is performed.

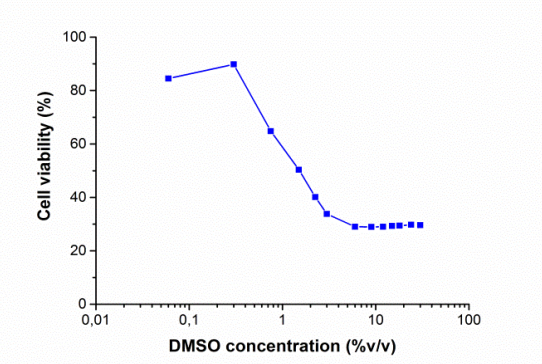


**Figure 2.31** Cytotoxic effect on HT29 proliferation of different concentrations (logarithmic scale) of dimethyl sulfoxide (DMSO) which is used to solubilize drugs. An increasing volume of solvent is added to 100 000 cells/mL and incubated for 48h. Cell viability is evaluated through MTS bioassay.

The MTS substrate is bio-reduced into a colored and soluble formazan product only when metabolically active cells are present (Figure 2.32A).

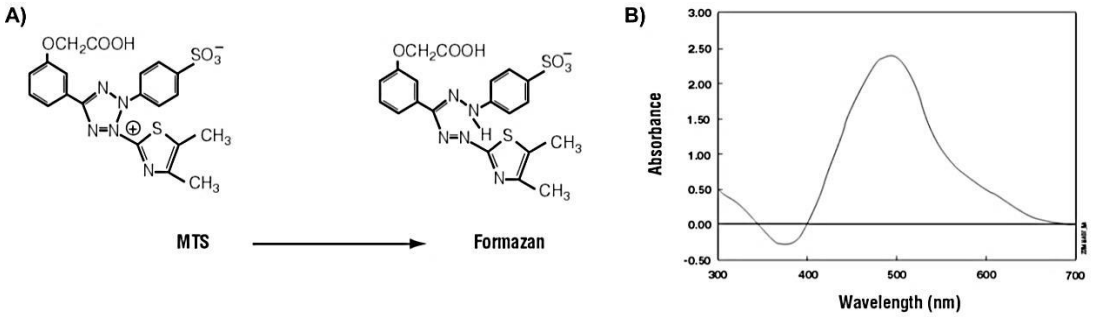


**Figure 2.32** (**A**) Chemical reduction of MTS substrate into a formazan product; this conversion is achieved only when metabolically active cells are present and is therefore proportional to viable cells concentration. (**B**) Absorption spectra of a formazan solution which has a maximum absorption at 490nm, while the negative absorption at 382nm corresponds to the disappeared MTS compound. Figures reproduced from Promega CellTiter 96® AQueous Assay protocol.

The absorbance spectrum of the formazan product resulting from reduction of the MTS tetrazolium compound shows a maximum absorbance at 490nm. The negative absorbance values correspond to the disappearance of MTS due to its conversion to formazan (Figure 2.32B). A microplate reader is used to measure the absorbance of each well at 490nm and the resulting coloration of the well will be proportional to the number of viable cells. Figure 2.33 shows the effect of different drug doses (logarithmic scale). In panel **A,** the SN-38 cytotoxicity is shown and a clear anti-proliferative effect is detected; already at a concentration of 0.5μM of SN-38 almost half of cell population is dead. A

different scenario is observed when folinic acid is added, since an increased cell viability results when FA doses in the range between 0.5-7.5μM are used (panel **B**).

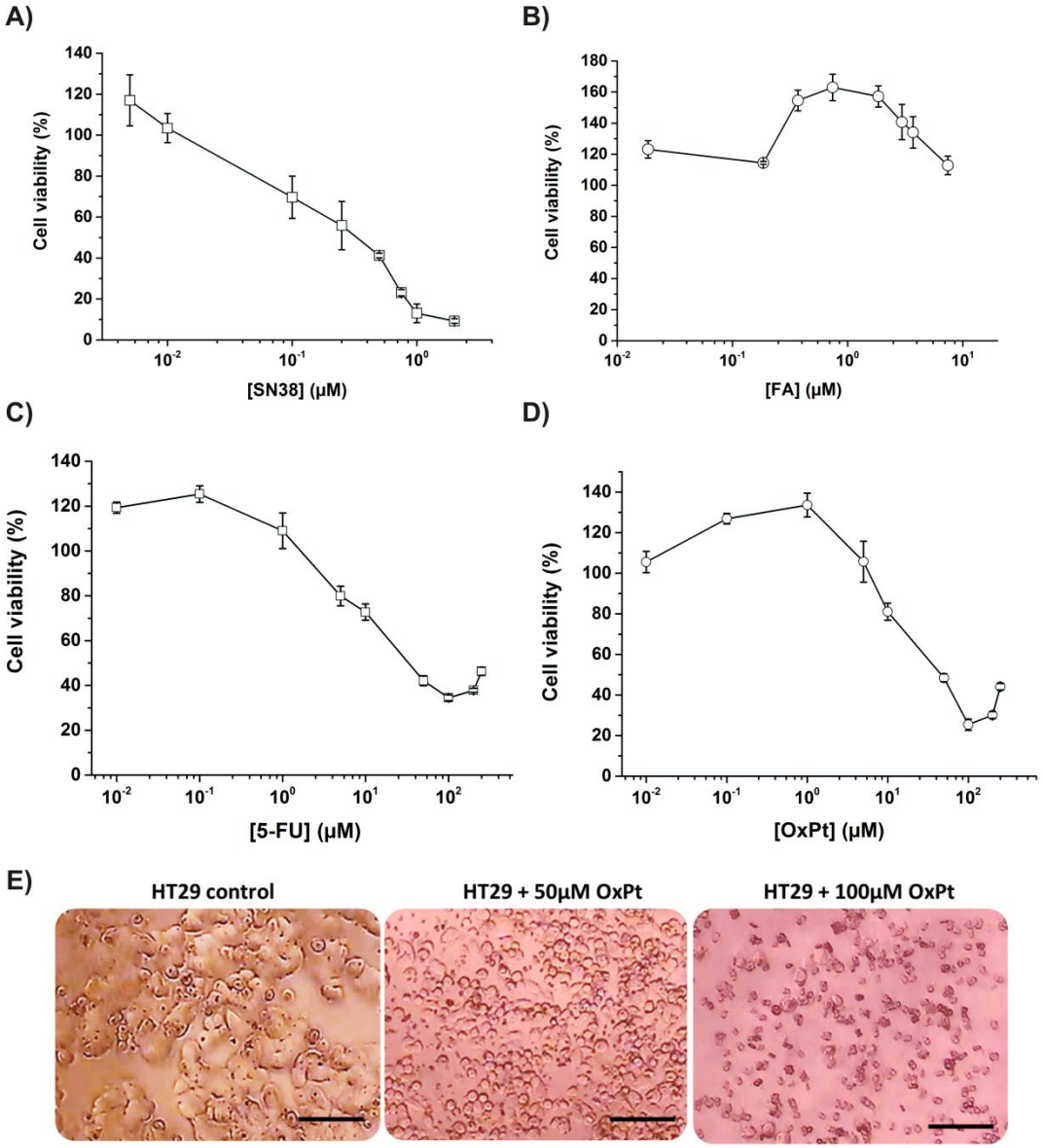


**Figure 2.33** Cytotoxic effect induced by different doses of (**A**) SN-38, (**B**) folinic acid, (**C**) 5-FU and (**D**) oxaliplatin on proliferation of human colorectal adenocarcinoma cell line (HT29). In a 96 well-microtiter plate, 24h after seeding, different drug doses are added to adherent cells (100 000 cells/mL) and incubated for 48h. The MTS assay is used to evaluate cell viability. All the experiments are run three times and values are represented by mean and SD (n =3). On the bottom panel, phase contrast microscope pictures of HT29 cells incubated for 48h with free oxaliplatin are reported (**E**). The scale bar value corresponds to 50μm.

The addition of 5-FU or Oxaliplatin to the seeded cells causes a detrimental cell death (panel **C** and **D**, respectively) comparable to that induced by SN-38 doses (panel **A**). However, the cytotoxic effect provoked by SN-38 is two orders of magnitude more efficient than 5-FU or Oxaliplatin because a two-

fold lower concentration produces a similar effect. In Figure 2.33E, phase contrast microscope images of HT29 cells incubated for 48h with 50µM and 100µM oxaliplatin are reported: when cells are exposed to the drug a morphology change is observed, including cell rounding, shrinkage, blebbing, lower cell density, an enlargement of cell bodies and abnormal cell morphologies. All these cell features suggest an apoptotic state of cells after drug exposure.

Although the *in vitro* cytotoxicity of individual therapy on cell viability is significant, except for folinic acid that seems to have a pro-proliferative effect, many studies reported in literature and from FDA approvals demonstrate a higher anti-proliferative effect when these drugs are used in a combined therapy. Thus, the cytotoxic effect of combined therapeutics is also measured on HT29 cell line.

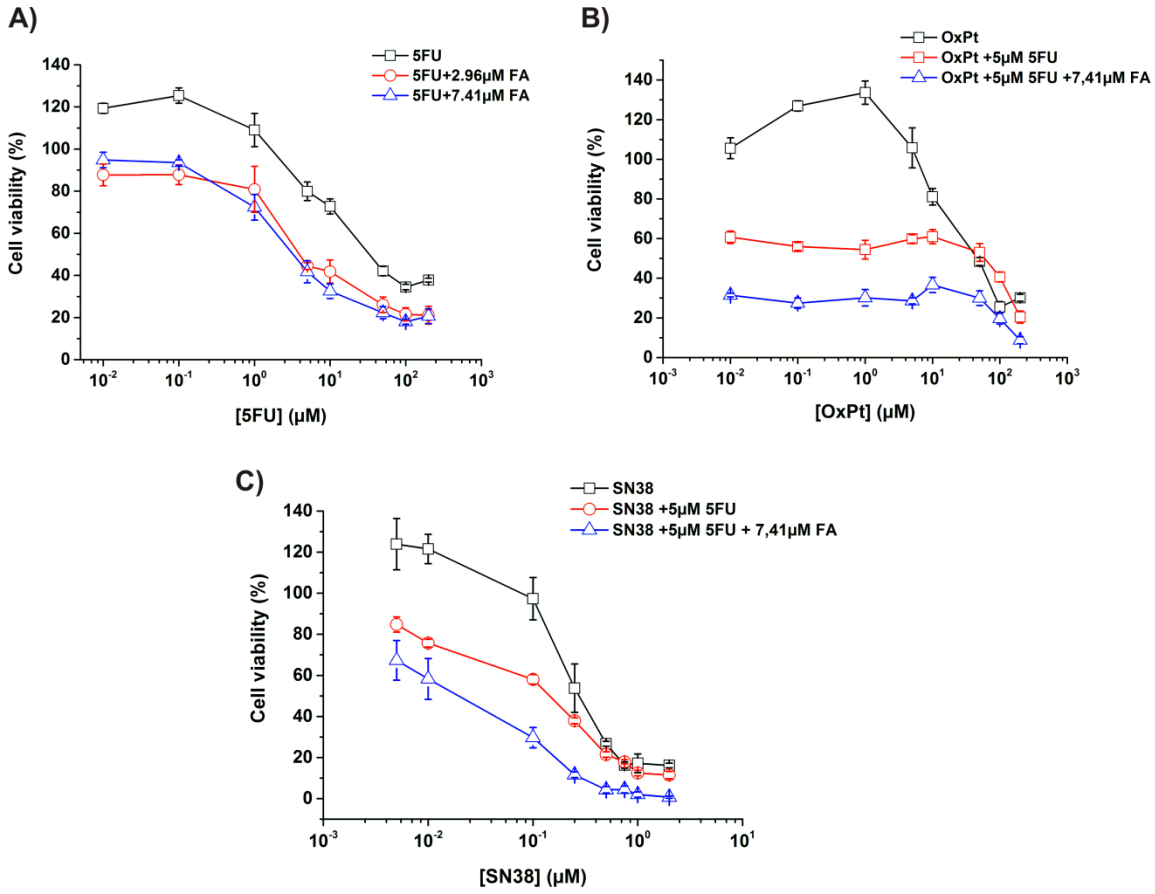


**Figure 2.34** Cytotoxic effect of drug combination therapy on proliferation of human colorectal adenocarcinoma cell line (HT29). Cells (100 000 cells/mL) cultured for 24h in a 96 well-microtiter plate, are exposed to chemotherapeutics for 48h. (**A**) 5-FU therapy potentiated by the addition of FA at two different concentrations (2.96µM and 7.41µM); (**B**) OxPt therapy in association with 5-FU (5µM) and FA(7.41µM); (**C**) the SN-38 cytotoxicity is further augmented by the addition of 5-FU (5µM) and FA (7.41µM). Cell viability is evaluated through MTS assay measuring the absorbance at 490nm. Values are represented by mean and SD (n =3).

In Figure 2.34, all combined drug treatments are reported: in panel **A**, the 5-FU toxicity (black line) is enhanced when FA is added (red line, 2.96μM and blue line, 7.41μM, respectively) by decreasing cell viability down to 20%; in panel **B**, the combination of oxaliplatin and 5-FU demonstrates a strong anti-proliferative effect (red line). In fact, when 5μM 5-FU is combined together with oxaliplatin, a decrease of 40% viability is caused already at 0.01μM oxaliplatin dose. This cytotoxic behavior is additionally potentiated when FA is combined to OxPt and 5-FU (blue line). A similar outcome is observed for SN-38 therapy (panel **C**) where doses in the range of nano-molarity induce a further reduction of cell viability. As expected, all combined treatments have a detrimental effect on cell viability and the role of folinic acid is relevant only when associated to the other drugs. Due to its vitamin activity, the folinic acid itself does not induce toxicity because it possesses a vitamin activity;[141] whereas when used as adjuvant in chemotherapy against colorectal cancer it prolongs the bioavailability of 5-FU and enhance thymidylate synthase inhibition (more details about FA and 5-FU interaction can be found in Chapter I).

The effect of FOLFOX and FOLFIRI chemotherapy (blue lines in Figure 2.34b and c, respectively) has been validated for the selected cell line (HT29) and the results are totally in agreement with those found for the same and other colorectal cancer cell lines.[92] The main challenge is to evaluate whether these drug combinations are able to induce a similar cytotoxic effect when embedded within PEGDA hydrogels. In particular, the FOLFOX and FOLFIRI compounds are entrapped within three-circle shaped hydrogel 3D-structures and the toxic effect of released drugs on HT29 cells cultured onto the hydrogel surface will be determined.

## 2.4 Cytotoxic effect of triggered OxPt-loaded liposomes

So far, the release profile of oxaliplatin from PEGDA hydrogel has shown a rapid diffusion of OxPt through the matrix and a waste of drug during the washing process. Hence, the cytotoxicity induced by embedded oxaliplatin will be lower than that expected because of drug loss. This issue, as previously reported, can be circumvented using oxaliplatin-loaded liposomes which protect the drug during the manipulation of hydrogels and discourage OxPt waste. The cytotoxicity of OxPt-loaded thermo-sensitive and stealth liposomes must be also assessed. In particular, stealth liposomes are used as negative control, meaning that from their heat treatment at 40 ° C no release of oxaliplatin should be induced, thus no effect on cell viability is expected. In Figure 2.35, the characterization of liposomes effect on proliferating HT29 cells is described: in panel **A**, a schematic illustration of the procedure adopted to test liposomes toxicity is shown. Briefly, different concentrations of OxPt-loaded liposomes are added to the medium and heated up at 40° C for 1h in a thermo-block in sterile conditions.

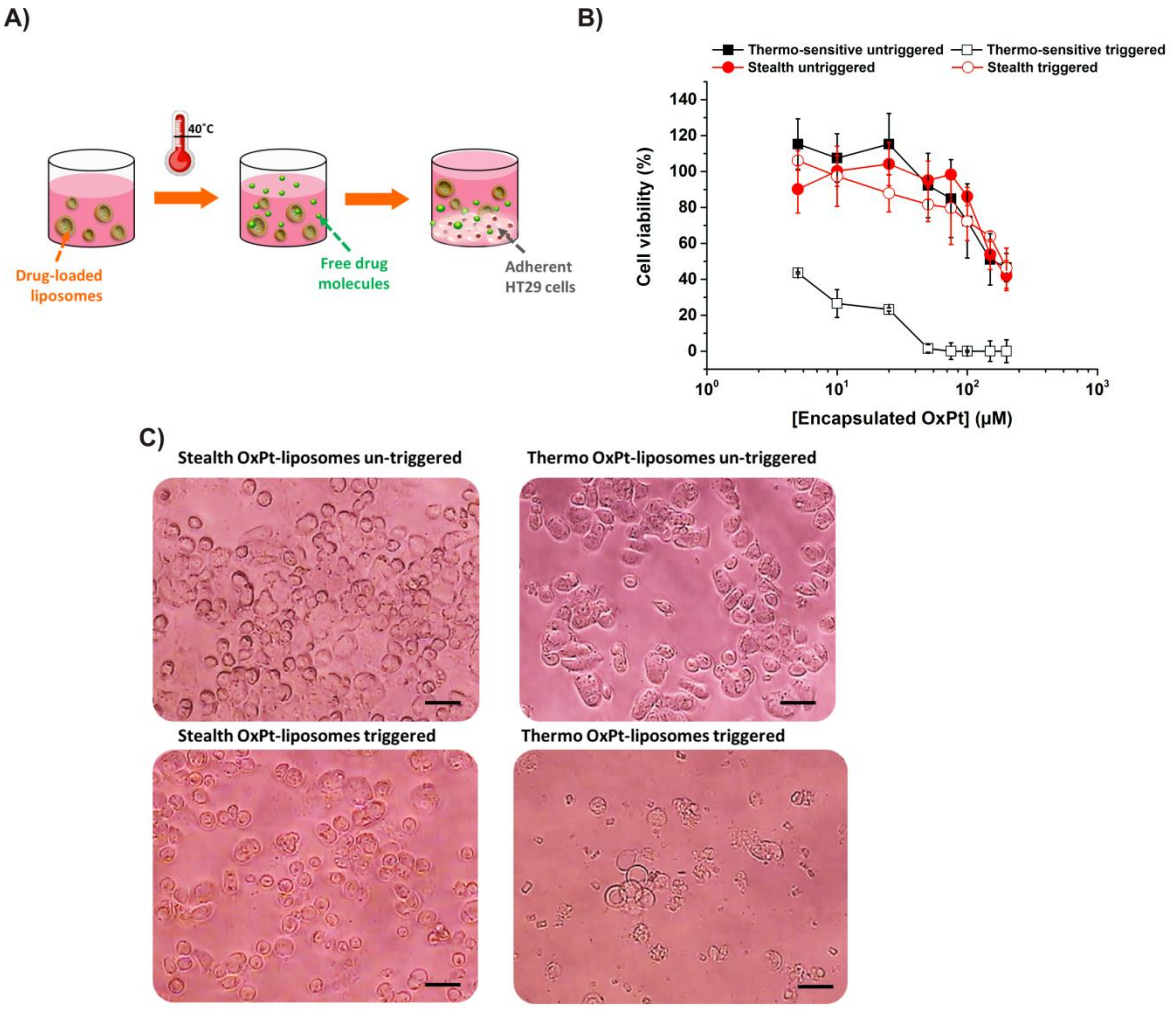


**Figure 2.35** Cytotoxic effect induced by thermal triggering of thermo-sensitive and stealth OxPt-loaded liposomes. (**A**) Illustration of the procedure adopted to evaluate liposomes effect on proliferating HT29 cell line. (**B**) Cytotoxicity induced by different doses of stealth OxPt-loaded liposomes (negative control) and thermo-sensitive OxPt-loaded liposomes with and without heat exposure prior cells seeding. A concentration of 100 000 cells/mL is incubated in each 96-well and cells are exposed to liposomes for 48h under culture conditions. The MTS assay is used to evaluate cell viability. Values are represented by mean and SD (n =3). (**C**) Phase contrast microscope images of cells exposed for 48h to various liposomes suspensions at the same OxPt dose (50μM) (the scale bars correspond to 20μm).

For negative control, the same concentrations of liposomes in the medium are incubated at 37° C for 1h in order to evaluate also the effect of leakage when cells and liposomes are maintained under culture conditions. After heat treatment of stealth and thermo-sensitive liposomes, they are cool down at room temperature and a concentration of 100 000 cells/mL is seeded in each 96-well. HT29 cells are exposed to thermal un-triggered and triggered stealth and thermo-sensitive liposomes for 48h, and cell viability is evaluated through MTS assay. In Figure 2.35B, the cytotoxic effect of different doses of OxPt-loaded liposomes is reported: stealth liposomes (negative control) show a similar cytotoxicity when triggered and un-triggered (in Figure 2.35B, open red circles and filled red circles, respectively),

meaning that the lipid composition of stealth liposomes prevents oxaliplatin leakage even upon heat treatment. However, as the concentration of liposomes increases a significant cell death is observed. A different scenario appears when various doses of thermo-sensitive liposomes are added to cells: un-triggered OxPt-loaded thermo-sensitive liposomes induce a toxic effect similar to that caused by stealth nanoparticles (filled black squares), while triggered thermo-sensitive liposomes produce a significant cytotoxicity with about 100% cell death when 75μM of OxPt-loaded liposomes are used (open black squares).

These results are also confirmed by the phase contrast microscopy in panel **C** where a clear apoptotic effect is induced by thermo-sensitive OxPt-loaded liposomes after their heat triggering.

The heat treatment of drug-loaded liposomes successfully induces the release of oxaliplatin. The toxic effect caused by un-triggered liposomes is mainly ascribed to partial lipid toxicity; an improvement may be made by synthetizing liposomes with a higher concentration of loaded drug. In that way, the same anti-proliferative effect due to the drug can be achieved by using a lower volume of vesicles suspension, therefore a smaller number of nanoparticles.

## 2.5 Three-circle shaped PEGDA hydrogels for combined-drug release

In the light of the results showed above, the toxicity of FOLFOX and FOLFIRI is also determined when drug combinations are embedded within three-circle shaped PEGDA hydrogels. Firstly, the effect of bare PEGDA hydrogels resulting from visible-light polymerization of various concentrations of PEGDA (700Da) and LAP is tested. In a 96 well-microtiter plate, different mixtures of PEGDA (700Da) and LAP are crosslinked for 1min without digital mask in order to obtain cylindrical gels of 6.2mm in diameter and 1mm in thickness. The gels are washed extensively to remove un-reacted precursors and a concentration of 100 000 cells/mL is seeded onto the surface of each gel. HT29 cells are incubated for 48h onto polymeric networks and their viability is evaluated by MTS bio-assay.

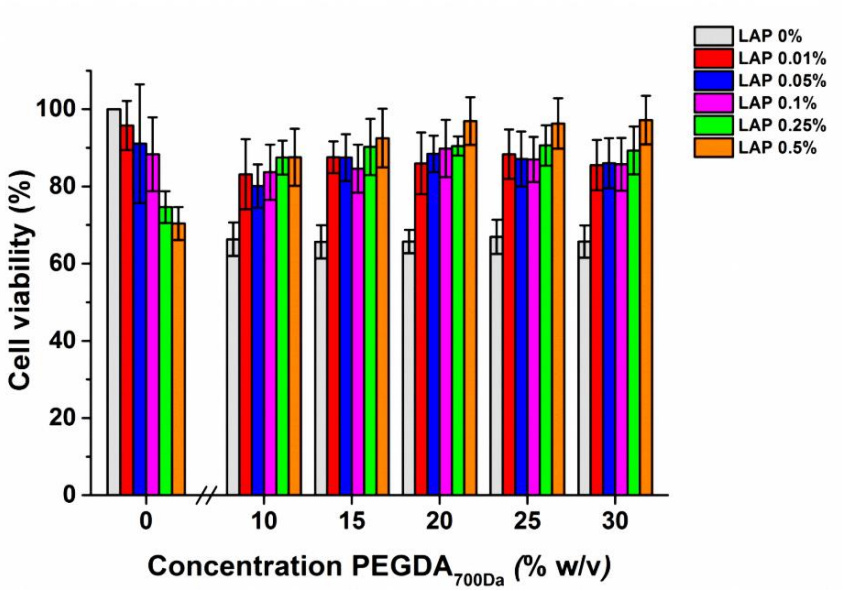


**Figure 2.36** Cell bio-compatibility of PEGDA hydrogels on HT29 proliferation. Gels are produced by exposing the precursor solutions to visible-light for 1min without digital mask, thus cylindrical networks are formed (Ø =6.2mm; thickness =1mm). All the solutions are illuminated to visible light even though one of the reagents, LAP or PEGDA, is missing. After hydrogel fabrication, a concentration of 100 000cells/mL is seeded onto gel surface and incubated for 48h; cell viability is evaluated through MTS bio-assay. The experiment is repeated three times and the values are represented by mean and SD (n =3).

As reported in Figure 2.36, different concentrations of PEGDA (700Da) without photoinitiator solution are illuminated with visible-light, and they induce equal toxicities due to the acrylate groups which are known to be cytotoxic.[32] Solutions of LAP exposed to visible-light in absence of polymeric monomers cause a decrease of cell viability proportional to photoinitiator concentration. When PEGDA and LAP solutions are mixed and exposed for 1min to projector light, cell viabilities are found to be in the range between 80%-95% suggesting a good bio-compatibility of PEGDA and LAP when in a hydrogel state. Also notable is that when the concentration of LAP is increasing while PEGDA concentration is constant, a higher cell viability is measured. As the photoinitiator amount increases, the number of un-reacted acrylate groups is reduced whereas more covalent monomer interactions are formed. On the basis of these results and the characterized drug release kinetics, the concentrations that are selected for the fabrication of three-circle shaped gels are 20%w/v PEGDA (700Da) and 0.5%w/v LAP with the addition of 1%w/v PEGDA (5kDa) for the entrapment of SN-38. In the light of that, the toxicity induced by free drugs in the medium is compared to the anti-proliferative effect caused by combinations of drugs embedded within shaped hydrogels. FOLFOX and FOLFIRI therapeutics are therefore embedded within PEGDA hydrogels using three-circle shaped structures which are fabricated through a multi-step process, as previously described. In Figure 2.37A, the combination and dose of drugs, the area and radius of each circle, and the hydrogel composition for each formed circle are reported. These values are chosen in agreement with our previously described findings, in particular considering the release

profiles of drugs from un-structured PEGDA hydrogels and the HT29 cells response when exposed to individual and combined drugs. The final gel structure is thus composed of three hydrogel circles containing each of them a drug. The gels are produced in a 96 well-microtiter plate and during the fabrication for every polymerization step, an extensive washing is conducted. The 3D drug-embedded hydrogel has a total diameter of 6.2mm and a thickness of 1mm. HT29 are then seeded onto the surface of each polymeric system at a concentration of 100 000cells/mL, and cells are exposed to the releasing platforms for 48h (illustration in Figure 2.37B). The viability of HT29 is then determined though MTS assay (Figure 2.37C). As expected, the empty structured hydrogel has a cytotoxic effect comparable to that observed from un-structured gel (Figure 2.36), while the cytotoxic effect induced by embedded OxPt/5-FU/FA (FOLFOX) is less pronounced than the toxicity caused by the free drugs (Figure 2.34b). On the contrary, the cell death resulting from the treatment of embedded SN-38/5-FU/FA (FOLFIRI) is remarkable and similar to that induced by free drugs (Figure 2.34c). The poor potency of embedded OxPt/5-FU/FA is mainly determined by the loss of oxaliplatin during the washing step, thereby a partial effect of its toxicity is measured together with 5-FU/FA. According to the release profiles showed in Figure 2.23, a complete passive release of SN-38, 5-FU and FA is obtained after 24h; cells are therefore exposed to drugs for the entire period of incubation. The embedding of drugs (SN-38, 5-FU and FA) and OxPt-loaded liposomes is also conducted by using three-circle shaped PEGDA hydrogels in which combinations of drugs and liposomes are employed. In Figure 2.37A, the parameters considered for the embedding process are reported. Each drug or liposome formulations is entrapped within a certain circle structure, washing each structure after gel polymerization, and then the platform is heated up at 40˚ C for 1h in sterile conditions. OxPt and the other drugs will diffuse in the medium and HT29 cells are seeded onto hydrogel surface at a concentration of 100 000cells/mL just after cooling down the sample from 40˚ C to room temperature. The system is incubated for 48h and cell viability is measured.

A)

| Drug combination | OxPt embedded [μM] | SN38 embedded [μM] | 5FU embedded [μM] | FA embedded [μM] | Circle 1 (radius=3.1mm; Area= 10mm$^2$) | Circle 2 (radius=2.5mm; Area= 10mm$^2$) | Circle 3 (radius=1.8mm; Area= 10mm$^2$) |
|---|---|---|---|---|---|---|---|
| **OxPt/5FU/FA** | 10 | - | 5 | 7.41 | **OxPt** within 20%w/v PEGDA(700Da) + 0.5%w/v LAP | **5FU** within 20%w/v PEGDA(700Da) + + 0.5%w/v LAP | **FA** within 20%w/v PEGDA(700Da) + 0.5%w/v LAP |
| **SN38/5FU/FA** | - | 0.5 | 5 | 7.41 | **SN38** within 20%w/v PEGDA(700Da) + 1%w/v PEGDA(5kDa) + 0.5%w/v LAP | **5FU** within 20%w/v PEGDA(700Da) + + 0.5%w/v LAP | **FA** within 20%w/v PEGDA(700Da) + 0.5%w/v LAP |
| **OxPt-loaded Thermo-sensitive liposomes/5FU/FA** | 10 | - | 5 | 7.41 | **OxPt-liposomes** within 20%w/v PEGDA(700Da) + 0.5%w/v LAP | **5FU** within 20%w/v PEGDA(700Da) + + 0.5%w/v LAP | **FA** within 20%w/v PEGDA(700Da) + 0.5%w/v LAP |
| **OxPt-loaded Stealth liposomes/5FU/FA** | 10 | - | 5 | 7.41 | **OxPt-liposomes** within 20%w/v PEGDA(700Da) + 0.5%w/v LAP | **5FU** within 20%w/v PEGDA(700Da) + + 0.5%w/v LAP | **FA** within 20%w/v PEGDA(700Da) + 0.5%w/v LAP |

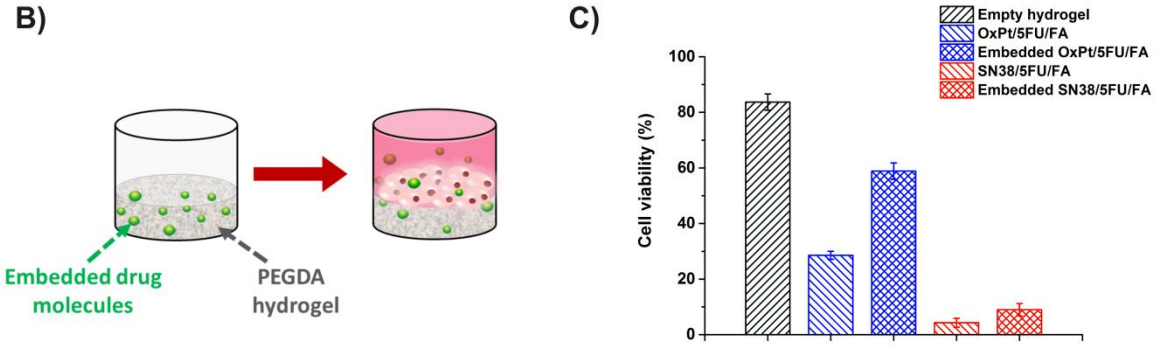


**Figure 2.37** Cytotoxicity induced by passive release of combinations of drugs embedded within three-circle shaped PEGDA hydrogels produced in a 96 well-microtiter plate with a multi-step fabrication process. (**A**) The table summarizes the drug combinations, drug concentrations, area and radius of each circle structure and hydrogel composition that are employed to evaluate multi-drug release system toxicity. (**B**) Schematic of the procedure adopted to test HT29 viability onto hydrogel surfaces. 3D circle shaped PEGDA hydrogels are fabricated, washed and a concentration of 100 000cells/mL is seeded onto the surface of the gel. After 48h of incubation, cell viability is evaluated through MTS assay. (**C**) Comparison of cell anti-proliferative activity induced by combinations of free drugs (dispersed in the medium) and embedded compounds; the growth of cells onto the surface of empty hydrogel is also presented (mean ± SD, n=3).

The combinations of OxPt-loaded liposomes with 5-FU and FA are tested for both stealth and thermo-sensitive liposomes when exposed and not exposed to a thermal trigger (Figure 2.38B). The toxicity induced by un-triggered liposomes/5-FU/FA is around 50% for thermo-sensitive liposomes and 60%

for un-triggered stealth liposomes; here a cell viability decrease results from the effect of 5-FU and FA. When liposomes are heated at 40° C, a different situation is observed: stealth liposomes/5-FU/FA cause a comparable cell death when in triggered and un-triggered state, while thermo-sensitive liposomes/5-FU/FA heated up produce a consistent reduction of cell proliferation that is higher than that induced by combined free drugs.

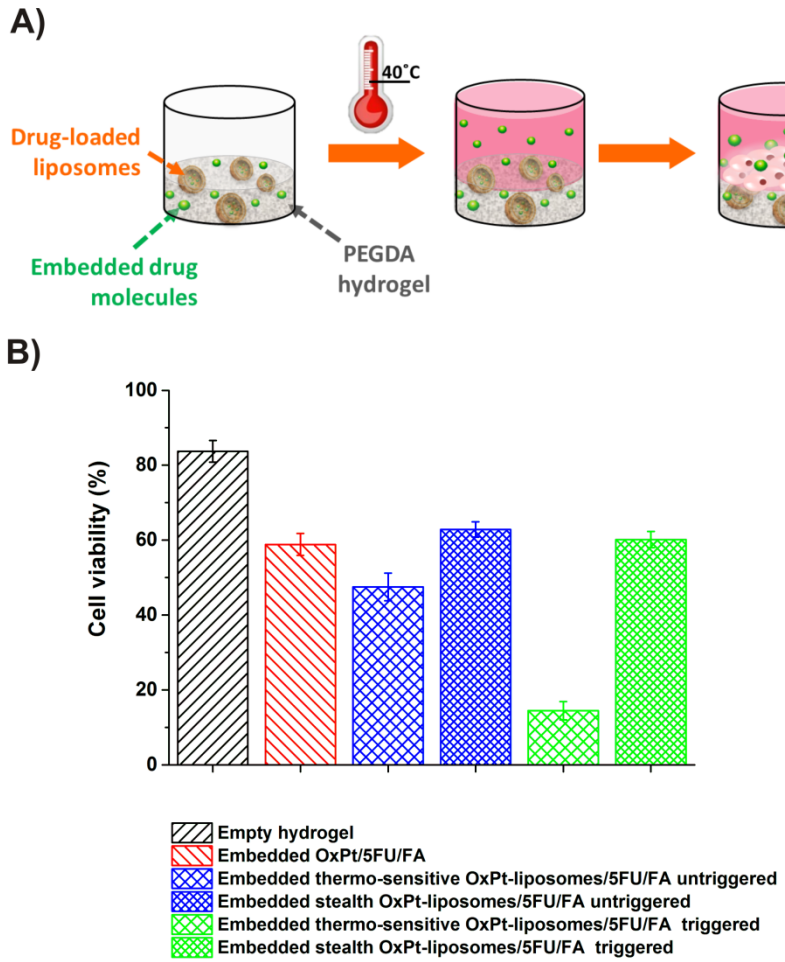


**Figure 2.38** Cytotoxicity induced by the combinations of embedded free drugs and liposomes (OxPt-loaded liposomes/5-FU/FA). (**A**) Illustration of the procedure utilized for liposomes leakage and cell drug exposure. (**B**) The HT29 anti-proliferative activity induced by passively released drugs upon heat treatment and without triggering is measured.

The use of drug-loaded liposomes is a great tool to prevent the fast diffusion of oxaliplatin from the polymeric matrix, and the combined effect of drugs can be detected when HT29 cells are cultured together with the hydrogel releasing systems. These results are important not only because a cytotoxic effect is reached after passive release, but especially because the drug releases are temporally controlled and tuned according to the hydrogel and drug properties.

## 2.6 Conclusion

The nano-technology platform presented here offers the possibility to overcome some of the limitations characterizing the existing drug screening approaches. Usually, the application of drug screening assays requires high doses of drugs and small volumes of tumor tissues. Moreover, the need of new drugs for the treatment of many pathological diseases is gradually increasing. The major benefits of using this technology is the possibility to modulate the desired concentration of released compounds by varying the volume of the hydrogel in which they are embedded, and to study the combined cytotoxic effect of multiple FDA-approved drugs.

The use of PEGDA as biomaterial for the evaluation of individual and combined drug treatment on cancer cell lines is very useful. A smart method for PEGDA hydrogel fabrication has been explored and optimized in order to match the features necessary for drug screening purposes and to create a miniaturized platform. The choice of an appropriate photoinitiator compound, light source and polymerization conditions are crucial parameters to ensure a spatial and temporal control of releasing molecules. The visible-light photopolymerization of hydrogels ensures the fabrication of homogeneous, reproducible and structured gels at a small scale with a low-cost and rapid process. The use of projector light as photo-crosslinking source with an emitting light centered at 410nm together with an initiator absorbing in this wavelength range (LAP), allow the encapsulation of molecules within hydrogels reducing the fabrication time and controlling the initial embedded concentration of molecules. Moreover, digital masks which consist of graphics files are designed to selectively polymerize certain volumes of precursor solution in a short time (from few seconds to few minutes depending on the solution height). The release kinetics of several molecule types has been explored: compounds having various molecular weights and chemical-physical properties have been studied. Thereby, the chemical and physical features of PEGDA hydrogels were tuned to control the compounds release profile. Two main approaches were explored to limit or augment molecules passive release: the introduction of long PEG chains within PEGDA network resulted on an accelerated SN-38 release, otherwise slowly diffusing due to its hydrophobicity. On the other hand, a rapid passive diffusion of oxaliplatin was avoided by encapsulating the drug into nanoparticles (liposomes). These nano-vesicles not only protect drug from the environment and from its elimination through washing step, but also permitted to temporally control the oxaliplatin release. In particular, thermo-sensitive OxPt-loaded liposomes have been used for this purpose, thus the application of a thermal trigger provokes drug release from vesicles. Finally, the cytotoxicity on human colorectal adenocarcinoma cell line (HT29) caused by the release of combined drugs entrapped within PEGDA hydrogels was evaluated.

Ideally, once the compounds of interest are embedded within desired polymer structures, the entire platform (such as a 96 well-microtiter plate) may be stored in a humidified environment until needed and a specific cell line may be seeded onto pre-fabricated drug-loaded hydrogels to evaluate

chemotherapeutic effect. The use of PEGDA hydrogels to passively release different and multiple molecules represents a smart designed platform for drug screening purposes.

## 2.7 Experimental section

*Fabrication of PEGDA hydrogels using IrgaCure 2959 photoinitiator*

The fabrication of PEGDA hydrogels performed through photopolymerization was optimized by evaluating different parameters: polymer concentration, I2959 concentration, exposure time to UV-light and volume of pre-polymer solution. Poly(ethylene glycol) diacrylate (PEGDA) with an average $M_n$ 700Da and IrgaCure 2959 (1-[4-(2-Hydroxyethoxy)-phenyl]-2-hydroxy-2-methyl-1-propane-1-one) MW=224.25g/mol were purchased from Sigma Aldrich (Brøndby, Denmark). For light exposure of pre-polymer solutions, a custom built photo reactor with a broad illumination maximum from 330–380 nm (Philips Cleo S-R fluorescent tubes) was utilized: it is composed of a large chamber presenting UV-lamps on the top and bottom sides, and a transparent support where the sample is located. In that way, the crosslinking process should be homogeneous on both solution interfaces. A stock solution of 80%w/v $PEGDA_{700Da}$ was dissolved in milliQ water and a stock solution of 10%w/v I2959 was prepared by dissolving it in acetone/milliQ water (volume ratio 1:1). In a 24-well microtiter plate (Nunc, Thermo Scientific, Roskilde, Denmark) different combinations of PEGDA and I2959 concentrations were tested: 15 – 20 – 25 – 30%w/v PEGDA and 0.1 – 0.5 – 1 – 2%w/v I2959 for a total volume of 300µL. The well plate was exposed to UV-light in the photo-reactor for 60min (32 J/cm$^2$) including a reservoir of water to limit evaporation, and the formed hydrogels were washed extensively (30min) with milliQ water. The UV-vis absorption of different concentrations of IrgaCure2959 dissolved in acetone/milliQ water (1:1) was measured using a Nanodrop spectrophotometer (model 2000c, Thermo Scientific) without exposing the solutions to UV-light. A quartz cuvette (Fisher Scientific, Thermo Fisher Scientific, Germany) was used to collect the UV-vis spectra of I2959 in the range of 300-500nm.

*Fabrication of PEGDA hydrogels with different PEG chain lengths using IrgaCure 2959 photoinitiator*

PEGDA hydrogels were produced also by adding longer PEG chain lengths to the main component $PEGDA_{700Da}$: stock solutions of 40%w/v PEGDA $M_n$=1kDa, 5%w/v PEGDA $M_n$=5kDa and 10%w/v PEGDA $M_n$=6kDa (all obtained from Iris Biotech) were dissolved in milliQ water. In a 24 well-microtiter plate, various combinations of PEGDA concentrations were mixed to a 1%w/v IrgaCure 2959 dissolved in acetone/milliQ water (1:1). The tested amounts of each PEGDA solution were: 15, 20, 25, 30%w/v of $PEGDA_{700Da}$, 1 – 5%w/v of $PEGDA_{1kDa}$, 0.5 – 1%w/v of $PEGDA_{5kDa}$ and 1 – 2%w/v of $PEGDA_{6kDa}$. A total volume of 300µL of polymer-photoinitiator mixture was poured in each well and exposed to UV-light for 1 hour in a photo-reactor. Then hydrogels were washed for 30min with milliQ water.

*Fabrication of 3D-structured PEGDA hydrogels defined by static mask motifs*

The patternability of PEGDA hydrogels was evaluated creating 3D structures on solutions made of $PEGDA_{700Da}$, I2959 and a fluorescent dye, fluorescein. Stock solutions of 80%w/v $PEGDA_{700Da}$ dissolved in milliQ water, 10%w/v I2959 dissolved in acetone/milliQ water (1:1) and a solution of 100µM fluorescein sodium salt dissolved in milliQ water (MW= 376.27 g/mol, obtained from Sigma Aldrich, Brøndby, Denmark) were prepared. Different concentrations of PEGDA and I2959 were tested: 20, 25, 30%w/v PEGDA and 0.5, 1, 2%w/v IrgaCure 2959. For polymerization process, a GeneFrame® with a dimension of 1.5 x 1.5 cm (obtained from Thermo Scientific, Waltham, Massachusetts), was stuck in a glass slide. Then 200µL of PEGDA/I2959/10µM fluorescein mixture was poured within the frame and a coverslip was placed onto the gene frame to squeeze the solution within the cavity. Exposure proceeded using 365nm light at ~6mW/cm$^2$ in a mask aligner (Karl Süss MA4, Munich, Germany) used together with a chrome-on-glass photo-mask. Two different chrome masks were employed: one of them consisted of square grids of different dimensions and spacing, and the other mask was made up of dual sets of interdigitated electrodes 200µm wide, 3.5mm long and with 200µm spacing. The gene frame was exposed for 10min to UV-light in the aligner to reach a dose of 4 J/cm and using a photomask; the obtained structures were washed several times with MQ water to remove un-exposed compounds. To visualize the structures, the samples were rinsed with water and sealed with a glass cover slip; then, confocal laser scanning microscopy (LSM700, Zeiss, Germany) was used to analyze the 3D structures resolution (excitation light at 488nm and collecting the fluorescence at wavelengths longer than 505nm).

*Embedding of SN38 drug within PEGDA gels*

To evaluate the release kinetics of small molecules from PEGDA hydrogels, SN38 (obtained from Sigma Aldrich, Brøndby, Denmark) was chosen as model molecule. In a 24-well microtiter plate, a constant concentration of SN38 dissolved in DMSO (100µM) was mixed with various amounts of $PEGDA_{700Da}$ dissolved in milliQ water (at a concentration of 15, 20, 25, 30%w/v) and I2959 dissolved in acetone/milliQ water (1:1) (at a concentration of 0.4, 0.6, 0.8, 1%w/v) for a total volume of 300µL. The well plate was exposed to UV-light in the photo-reactor for 1 hour to obtain gels with a thickness of 1.5mm and they were extensively washed with milliQ water. Then, 600µL of milliQ water was added to each well as supernatant volume in which the molecules of drug were passively released and collected over a period of 24 hours. The supernatants were characterized by UV-vis spectrophotometry (Nanodrop 2000c, Thermo Scientific) using a quartz cuvette and acquiring the spectra between 300-500nm.

*Photo-polymerization of PEGDA solutions with LAP initiator*

According to the discussed features of I2959 in Chapter II, an alternative photo-initiator (lithium acylphosphinate salt, LAP kindly provided by Dr. Esben Larsen and Dr. Sergey Chernyy) was tested for the fabrication of PEGDA hydrogels. Stock solutions of 80%w/v $PEGDA_{700Da}$ and 2%w/v LAP both dissolved in MQ water were prepared and in a 24 well-microtiter plate various amounts of them were tested: 0.1, 1, 5, 10, 20, 30%w/v $PEGDA_{700Da}$ and 0.01, 0.05, 0.1, 0.5, 1, 2%w/v of LAP. A total volume of 300µL of pre-polymer solutions were exposed to UV-light using the photo-reactor for 10min. Already after 2min completely cured gels were formed. The obtained gels were washed in water and analyzed through spectrophotometry. Gels were transferred into a cuvette in such way that they were adhering to the cuvette wall and their spectra were acquired between 300-500nm in water.

*Apparatus used for visible-light photo-polymerization*

Among the available methods described in Chapter II to photo-polymerize hydrogels (photo-reactor or a conventional aligner), the gels were crosslinked with the photo-initiator LAP using a visible-light emitting system. In detail, an EnvisionTEC Perfactory® Micro 3D-printer (Gladbeck, Germany) was utilized for *in situ* visible-light photopolymerization. The equipment is composed of a projector modified to have a maximum emitting light centered at 410nm (Direct Light Projection technology from Texas Instruments®, based on a LED light source); a stage where the sample is located; a light-protected box which is moved during the polymerization process to protect the sample from external light; and a computer connected to the machine. A home-made support to exactly locate 96 well-microtiter plates on the stage was used to simultaneously polymerize 12 wells in a single step. When the sample was placed on the support, the polymerization started as the projector light coming from the bottom of the sample was turned on and all the exposed volume of pre-polymer solution was cured within 30-60s to form a homogeneous gel. In addition, any desired structure was easily produced in each well: digital masks were designed and directly projected onto the sample. These digital masks consisted of a graphical picture (.png file) with a dimension of 1024 x 768 pixels drawn in a greyscale. When the desired picture was projected on the bottom of the sample, it was crosslinked on the basis of the mask greyscale. In other words, the resulting thickness of the gel was higher in the areas corresponding to a white mask and it decreased according to the grayscale of the mask, until completely black mask corresponded to no cured solutions. Therefore, by simply designing such digital masks was possible to tune the light intensity across the pre-polymer solution and define the final thickness of the gel.

*Characterization of hydrogel morphology and thickness*

To evaluate the efficiency of light projection to create 3D structures on pre-polymer solutions, different digital masks were designed according to the final application of the hydrogel. A preliminary test to determine the final morphology and thickness of gels was conducted. In a 96-well microtiter plate, 200µL of 20%w/v PEGDA (700Da) and 0.5%w/v LAP both dissolved in MQ water were exposed for 1min to two different digital masks: one consisted of a semi-circle (half white and half black, Figure 2.39A), and the other was a white circle (Figure 2.39B). The dimension of each picture was 1024 x 768 pixels, and the diameter of the circles was drawn to completely cover the area of a 96 well- microtiter plate (Ø = 6.2mm).

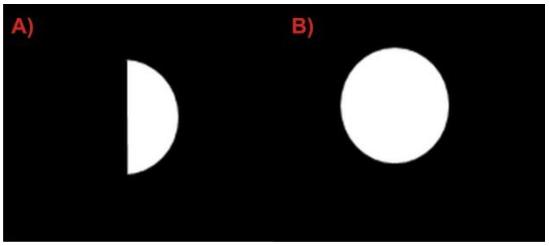


**Figure 2.39** Two examples of digital masks drawn with CorelDraw X3 (.png files). (**A**) A semi-circle structure in which only half of the circle was projected, thus the corresponding pre-polymer solution was crosslinked only in correspondence of the white area. (**B**) A white circle was used to polymerize the entire volume of PEGDA/LAP since the diameter corresponds to the 96-well area.

When the solutions were exposed to visible-light for 1min, a corresponding hydrogel structure was obtained and its thickness was evaluated. Solutions of 20%w/v $PEGDA_{700Da}$ and 0.5%w/v LAP dissolved in MQ water were exposed to projected light through the semi-circle shaped digital mask to determine their thickness. In a 24 well-microtiter plate, different volumes of mixture (300, 350, 400, 450, 500, 600µL) were exposed to the half circle digital mask for various exposure times (15s, 30s, 60s, 2min, 5min, 10min and 20min). The thickness of the obtained gels was then analyzed and plotted as function of initial volume of pre-polymer solution and exposure time.

*Hydrogel de-hydration and hydration processes*

Swelling of the polymer network influences the ability of a hydrogel to release molecules embedded within its matrix. A study of the de-hydration (loss of water content) and hydration (uptake of water content) processes was conducted by using different amounts of $PEGDA_{700Da}$ and LAP. Stock solutions of 80%w/v $PEGDA_{700Da}$ and 2%w/v LAP both dissolved in MQ water were prepared. In a Petri dish with diameter of 3.4cm, 2mL of various PEGDA/LAP concentrations were poured and crosslinked for 1min with projected light without using any digital mask; thus, the entire solution volume was cured

obtaining a final thickness of 2.2mm. The weights of empty Petri dish, pre-polymer solution-Petri dish, and hydrogel-Petri dish were measured. The water exchange through the gels was determined studying the de-hydration and hydration processes. For the de-hydration mechanism, the crosslinked hydrogels in the Petri dishes free of lid were incubated in the oven in dehumidified atmosphere at 60° C over time, and every certain interval their weight was measured. After 19 hours of water loss from films, a box containing water was located inside the oven which was always maintained at 60 °C over time, and the gels hydration was estimated again by measuring the weight of samples.

*Embedding of various compounds within PEGDA hydrogels*

The release kinetics of different molecules in terms of size and chemical properties from PEGDA hydrogel were characterized. The hydrogels were all produced in a 96 well-microtiter plate by pouring a volume of 60 µL of pre-polymer solution together with a certain concentration of targeted molecule; the volumes were crosslinked for 1 min by visible-light exposure without using any digital mask and gels with a final diameter of 6.2 mm and thickness of 1mm were obtained. The hydrogels were washed with MQ water for 30 min and 240 µL of supernatant were added into the well. Stock solutions of 80%w/v $PEGDA_{700Da}$, 40%w/v $PEGDA_{5kDa}$, 2%w/v LAP all dissolved in MQ water were prepared. In specific, the pre-polymer mixtures for releasing studies were prepared as follows:

- ✓ Embedding of calcein within hydrogels: calcein disodium salt (MW =666.50g/mol) was purchased from Sigma Aldrich (Brøndby, Denmark). A solution of $PEGDA_{700Da}$, LAP and calcein was prepared to have a final concentration of 20%w/v, 0.5%w/v and 50µM, respectively. In a 12 well plate, 500µL of this mixture were poured; in a 24 well plate, 290µL; in a 48 well plate, 165µL; and in a 96 well plate, 60µL. The volumes of pre-polymer solution in various well plates had the same height but different area. The calcein absorbance was recorded through Nanodrop by measuring the supernatants at 495nm.
- ✓ Embedding of SN-38 within hydrogels: 60µL of a solution composed of 20%w/v $PEGDA_{700Da}$, (0.1, or 0.5, or 1, or 1.5%w/v) $PEGDA_{5kDa}$, 0.5%w/v LAP and 200µM SN-38 were poured into a 96 well-microtiter plate and after a washing step, 240µL of supernatant were added onto the hydrogel surface. For UV-vis detection of SN-38, the absorbance of collected supernatants was measured at 374nm.
- ✓ Embedding of FITC-albumin within hydrogels: albumin from bovine serum (BSA) conjugated to FITC (MW~66kDa, dissolved in PBS) was obtained from Life Technologies, Thermo Fisher Scientific, Naerum, Denmark. A solution of $PEGDA_{700Da}$, $PEGDA_{5kDa}$, LAP and FITC-albumin was prepared to have a final concentration of 20%w/v, 1%w/v, 0.5%w/v and 5µM, respectively. In a 96 well-plate, 60µL of the mixture were crosslinked to form the gel and after washing, 240µL

of supernatant (PBS) were added to collect the released molecules into it. For the UV-vis detection of molecules into collected supernatants, the absorbance was measured at 495nm.

- ✓ Embedding of 5-fluorouracil (5-FU) within PEGDA hydrogels: 5-fluorouracil (MW =130.1g/mol, dissolved in DMSO) was obtained from Sigma Aldrich, Brøndby, Denmark. A solution of $PEGDA_{700Da}$, LAP and 5-FU was prepared to obtain a final concentration of 20%w/v, 0.5%w/v and 1mM, respectively. 60µL of the mixture were cured and after washing a supernatant was added (240µL). For UV-vis detection of 5-FU into collected supernatants, the absorbance was measured at 288nm.
- ✓ Embedding of Folinic acid (FA) within PEGDA hydrogels: folinic acid calcium salt hydrate (MW =511.5g/mol, dissolved in DMSO) was obtained from Sigma Aldrich, Brøndby, Denmark. Solutions of $PEGDA_{700Da}$, LAP and FA were mixed to obtain a final concentration of 20%w/v, 0.5%w/v and 200µM, respectively. 60µL of the mixture were cured and after washing a supernatant was added (240µL). For UV-vis detection of FA into collected supernatants, the absorbance was measured at 300nm.
- ✓ Embedding of Oxaliplatin (OxPt) within PEGDA hydrogels: oxaliplatin (MW =397.3g/mol, dissolved in DMSO) was obtained from Lianyungang Guiyuan Chempharm Co. LTD, Jiangsu, China. A solution of $PEGDA_{700Da}$, LAP and OxPt was prepared to obtain a final concentration of 20%w/v, 0.5%w/v and 200µM, respectively. 60µL of the mixture were cured and after washing a supernatant was added (240µL). For quantification of oxaliplatin into collected supernatants, the UV-vis characterization was not used since the compound does not absorb in the UV-vis range. Therefore, mass spectrometry ICP-MS, ICAOq, Thermo Scientific, Hvidovre, Denmark, was used to evaluate the concentration of OxPt released. 25µL of supernatant was added to 2.5mL of a solution of Iridium in phosphate buffer as internal standard.

*Characterization of thermo-sensitive OxPt-loaded liposomes and their embedding within PEGDA hydrogels*

Two different compositions of Oxaliplatin-loaded liposomes were synthesized by Dr. Fredrik Melander (the detailed procedure is reported in the Experimental section of the manuscript in Appendix 1) and characterized through ICP-MS and DLS (Thermo Scientific and Brookhaven Instruments Corporation, respectively). The ability of thermo-sensitive liposomes to release their content, oxaliplatin, after thermal trigger was evaluated by entrapping 100µM OxPt-loaded liposomes (thermo-sensitive) within gels composed of 20%w/v $PEGDA_{700Da}$ and 0.5%w/v LAP both dissolved in PBS. The hydrogels were formed in a 96 well-microtiter plate by visible-light exposure (1 min) of 60µL mixture. Then gels were extensively washed with PBS and a supernatant of 240µL was added to each gel. The samples were

heated up at different temperatures for 1h in a thermo-block hotplate keeping the plate sealed during the process. The supernatants were then collected and analyzed through ICP-MS to evaluate the content of OxPt released during thermal triggering. The same procedure was adopted to determine the period of heat exposure needed to obtain the maximum amount released of OxPt; therefore, the hydrogels were heated up at different times for a maximum of 24h at which it corresponded the highest drug release (almost 100%). The stability of liposomes when embedded within gels for prolonged periods was also characterized. 100μM of OxPt-loaded liposomes were embedded within 20%w/v $PEGDA_{700Da}$ and 0.5%w/v LAP, both dissolved in PBS, by exposing 200μL of mixture to visible-light for 1min in a 24 well-microtiter plate. The gels were then washed with PBS and 400μL of PBS were added to each sample as supernatant. Both OxPt-loaded liposomes stock suspensions were tested: thermo-sensitive and stealth. Four different 24-well plates were prepared: two containing stealth liposomes within the hydrogels, and the other two presenting thermo-sensitive liposomes within gels. Then, one plate of each type of liposome suspension was kept at 5° C and at 22° C. The supernatants were collected at different intervals for a total of 100 days by replacing the supernatant with equal volumes of fresh PBS. The amount of OxPt released into supernatants was evaluated through ICP-MS using an Iridium solution as internal standard (2.5mL of Iridium solution + 25μL supernatant), and via DLS (1.5mL PBS + 15μL supernatant).

*Digital molecule dosing*

The use of visible-light photopolymerization technology was applied for the confinement of multiple compounds within different hydrogel areas. With this method we wanted to prove that to achieve a desired concentration of released compound, it was possible to vary the area of the hydrogel in which it was embedded, rather than increase the initial molecule concentration. For that reason, a solution of FITC-albumin (200μg/mL) and Rhodamine-albumin (200μg/mL, obtained from Life Technologies, Thermo Fisher Scientific, Naerum, Denmark) both dissolved in PBS buffer were prepared and embedded within gels. For the fabrication of hydrogels a digital mask composed of three circles was employed: an external ring structure ($radius_1$ =3.1mm; area $ring_1$ =10$mm^2$; thickness =1mm) was produced illuminating for 1min a solution of 20%w/v PEGDA (700Da), 1%w/v PEGDA (5kDa), 0.5%w/v LAP and 200μg/mL Rho-labeled albumin (60μL total volume). A second circle-shaped hydrogel was formed crosslinking a solution of 20%w/v PEGDA (700Da), 1%w/v PEGDA (5kDa) and 0.5%w/v LAP (60μL total volume) using a smaller ring structure (external $radius_2$ =2.5mm; internal $radius_2$ =1.8mm; area $ring_2$ =10$mm^2$; thickness =1mm). A third circle was produced photo-crosslinking a solution of 20%w/v PEGDA (700Da), 1%w/v PEGDA (5kDa), 0.5%w/v LAP and 200μg/mL FITC-labeled albumin (60μL total volume) using a digital mask with specific dimensions ($radius_3$ =1.8mm; area $ring_3$ =10$mm^2$; thickness =1mm).

By using these digital masks, three equal areas of hydrogel with different embedded molecules were obtained. The same procedure was adopted to produce hydrogels composed of three circle structures of different areas (10 – 30 – 100% of the total well area). Therefore, the molecules were embedded within various areas and their release was reported as function of embedded gel area. After washing, 240μL of PBS were added to each gel and the release of multiple compounds into the same supernatant was collected over a period of 48h. The absorbance of FITC-albumin and Rhodamine-albumin released into supernatants were measured using a microplate reader (Victor3, PerkinElmer, Denmark) by measuring the absorbance of FITC at 490nm and Rhodamine absorbance at 540nm. The moles of compounds released were then plotted as function of the hydrogel area in which the initial moles were embedded.

*Effect of free drugs and combinations of free drugs on HT29 proliferation activity*

The cytotoxic effect of different doses of drugs (SN-38, 5-FU, OxPt and FA) used as free compounds was evaluated on human colorectal adenocarcinoma cell line (HT29, ATCC, Rockville, USA). Different stock solutions of drugs were prepared by dissolving them in DMSO solvent, except for FA that was solubilized in MQ water. Due to solvent toxicity induced on HT29 proliferation, highly concentrated solutions of drugs were made. For drug screening on HT29 cells, an experimental protocol was established: HT29 cells suspended in Dulbecco´s Modified Eagle Medium (DMEM obtained from Sigma Aldrich) with 100μg/mL penicillin, 100μg/mL streptomycin and 10%v/v heat-inactivated fetal bovine serum (FBS) (all purchased from Sigma Aldrich) were seeded in a cultivation flask. Cells were maintained in the incubator at 37° C in a humidified atmosphere with 5%$CO_2$, and their passaging took place upon approximately 90% confluence. For drug treatment, cells grown in a cultivation flask were washed twice with PBS and harvested with 0.1% trypsin-EDTA (from Sigma Aldrich) for 5min kept in the incubator. Then, fresh medium was added to the detached cells and centrifuged at 1000rpm for 5min. After removal of supernatant, the pellet was re-suspended in fresh medium and cells concentration was evaluated by automated cell counter (ORFLO Technologies, USA). In a sterile 96 well-microtiter plate, a concentration of 100000cells/mL was seeded into each well and kept in the incubator for 24h in order to reach cell adhesion. Cells were then exposed to different concentrations of single drugs (SN-38, 5-FU, OxPt and FA) by adding 1μL of different drug stock solutions which were dissolved in DMSO. Cells were incubated in presence of chemotherapeutics for 48h. The cytotoxic effect of compounds was evaluated by using the MTS bio-assay (CellTiter 96® Aqueous One Solution Cell Proliferation Assay, from Promega Biotech, Sweden), by adding 20%v/v of MTS substrate ([3-(4,5-dimethylthiazol-2-yl)-5-(3-carboxymethoxyphenyl)-2-(4-sulfophenyl)-2H-tetrazolium]) to each well. After 1h incubation of cells with MTS, the absorbance of wells was measured at 490nm using the microplate reader. At this wavelength (490nm) the bio-reduced product resulted from the metabolically activity of living cells converting MTS substrate into a colored compound, was detected.

The higher the value recorded at 490nm and the higher was the concentration of viable cells after 48h drug treatment. A well containing only cells (100 000cells/mL) and another with cells exposed to DMSO (1µL) without drug were used as controls. The percentage of cell viability was then plotted as function of drug doses in logarithmic scale.

The same protocol was adopted to evaluate the cytotoxicity induced by combinations of drugs, where a maximum of three drugs were simultaneously added to adherent cells (HT29). Briefly, cells were seeded into a 96 well-microtiter plate and after 24h incubation a volume of 1µL of each drug was added to the medium as free compound. As control, an equal volume of DMSO was introduced with cells to test the effect of solvent on cell viability.

*Effect of thermal trigger on OxPt-loaded liposomes when cultured with HT29 cells*

The cytotoxic effect of OxPt-loaded liposomes, both stealth and thermo-sensitive, was evaluated by suspending different doses of liposomes in a 96 well-plate containing medium (DMEM + 1%v/v penicillin/streptomycin + 10%v/v FBS). Then the samples (thermo-sensitive and stealth liposomes) were heated up at 40° C for 1h in sterile conditions to induce oxaliplatin leakage from vesicles. The same procedure was adopted for thermo-sensitive and stealth liposomes without exposing them to thermal trigger, rather their plates were kept at room temperature until cell seeding. After cooling down the plates that were heated up, a concentration of 100 000cells/mL was seeded in each well and incubated for 48h. The viability of HT29 cells was evaluated by using the MTS bio-assay.

*Effect of multi drugs release from 3D-shaped hydrogels on HT29 proliferation*

3D-circle shaped hydrogels were produced according to the procedure used for digital drug dosing experiments. In specific, different drugs were embedded within various hydrogel structures having the same area (10mm$^2$) and same thickness (1mm). As reported in Figure 2.37A, each circle structure was loaded with a certain compound concentration or OxPt-liposomes. After hydrogels were fabricated, HT29 cells were incubated onto their surface at a concentration of 100 000cells/mL in DMEM + 1%v/v penicillin/streptomycin + 10%v/v FBS for 48h. The combined cytotoxic effect of drugs was detected by measuring the absorbance of MTS at 490nm. A slightly different procedure was followed when drugs and liposomes were embedded within gels: before cell seeding, the hydrogels were kept in a wetted state (medium) and heated up at 40° C for 1h in sterile conditions. Then, the samples were cooled down at room temperature and the same concentration of cells (100000 cells/mL) was incubated with the releasing system. Also in this case, after 48h of drugs exposure the cell viability was measured by adding 20%v/v MTS to each well and recording the absorbance at 490nm.

# 3 PEDOT-$N_3$ micro-electrodes for drug-loaded liposomes and cells immobilization

This chapter describes another micro-/nano-technological platform which consists of micro-fabricated PEDOT-$N_3$ electrodes on a PEG-coated support that are post-fabrication functionalized via covalent coupling with various molecules to ensure the immobilization of drug-loaded liposomes onto the electrodes surface (Figure 3.1). The liposomes intended to use for this scope are similar to those applied for drug embedding and release within PEGDA hydrogels, and in addition they contain functional groups in their bilayer which permit the chemical bonding to the fabricated polymer surface. Ideally, once the nano-particles are immobilized onto the electrodes, a certain current may be applied to induce local resistive heating that will release the encapsulated drugs. During the development of such platform many challenges were encountered and some of them were essential for the final achievements success. Alternative methods for the optimization and future development of the intended technology will also be discussed. Therefore, in this chapter it will be described the method that we have used to create micro-electrodes of PEDOT-$N_3$ and the approach involved on liposomes immobilization onto polymer electrodes. Further, a detailed description of the materials, equipment, and procedures adopted for the fabrication of the micro- and nano-platform are found at the end of the chapter in the Experimental section.

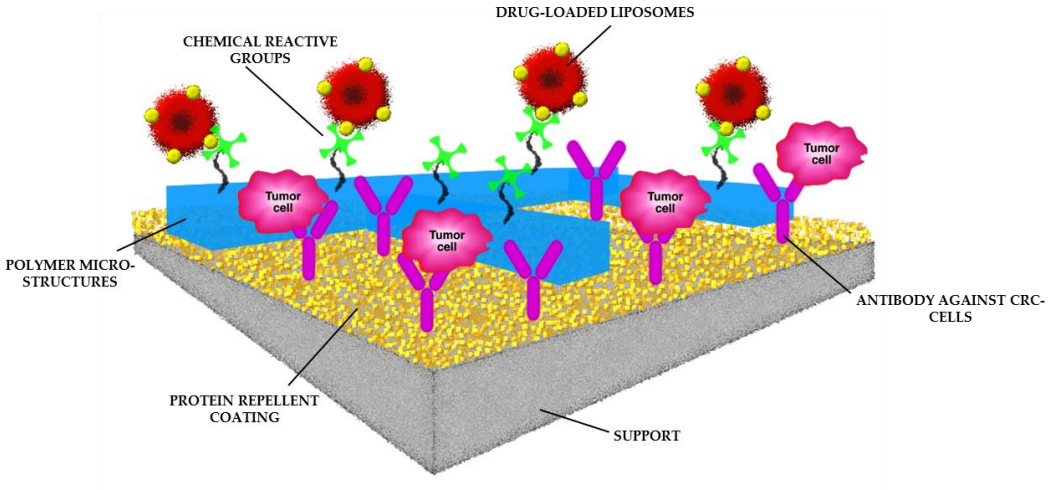


**Figure 3.1** Schematic of the polymer-based platform designed for drug screening purposes. PEDOT-$N_3$ electrodes are fabricated in a protein repellent coating deposited on a support. These electrodes (100µm in width, 3.5mm long and 100-150nm thick) are functionalized through ´click-chemistry` reaction in order to immobilize drug-loaded liposomes onto their surface. A second chemistry may be utilized to immobilized antibody molecules in the neighboring regions between the electrodes. The incubation of human colorectal adenocarcinoma cell line (HT29) with the described platform could result on cells capture onto the surface due to antigen-antibody complexation. Ideally, the application of a specific potential to the electrodes may induce a local thermal increase which represents the trigger for inducing drug release from drug-loaded liposomes. (The image is not to scale).

With the development of such platform we should be able to immobilize drug-loaded liposomes and specific cell populations onto the same surface. The application of a proper trigger will then enhance the release of drugs from immobilized particles and the captured cells will be exposed to these compounds. For the realization of such platform, various issues have been considered and we selected the main components to build our platform. First, conductive polymer wires can be fabricated to immobilize drug-loaded nanoparticles onto their surface. A proper chemical functionalization of polymer wires for enhancing a stable attachment of liposomes is needed; moreover, a second chemical modification allows the functionalization of the areas between wires to introduce cell-capture molecules (for instance antibodies). Multiple processes for platform functionalization are involved, therefore a proper chemical modification of the support must be adopted in order to avoid non-specific binding of drugs or cells onto the support surface.

## 3.1 Conductive polymers

Conductive polymers have been extensively studied during the last few decades because of their great suitability in chemical and biological applications used as sensors,[142] organic solar cells,[143] or organic light-emitting diodes.[144] In general, polymers have very poor electrical conductivity and most of them find applications as electrical insulator, such as polytetrafluoroethylene which has a conductivity of $10^{-18}$ S $cm^{-1}$.[145] As an example, natural rubber is an excellent insulator and its conductivity could be significantly increased by adding carbon black or acetylene black which is used as antistatic device in hospitals. On the other hand, polymers able to transport electrons have conductivity in the range of 10-$10^6$ S $cm^{-1}$ like polysulfurnitride that has a conductivity of $\sim 10^3$ S $cm^{-1}$. Conductive polymers in the neutral state (uncharged) show almost no conductivity, whereas their intrinsic conductivity results from the formation of charge carriers upon oxidizing (*p*-doping) or reducing (*n*-doping) their conjugated backbone.[142] Some examples of doped polymers are poly(*p*-phenylene), polypyrrole, polythiophene, polyaniline, and polyacetylene which is usually doped with electron donor (alkali-metal ion) or electron acceptor leading its conductivity to values comparable to that of conductive metals like copper ($10^4$ S $cm^{-1}$).[145]

A key property that makes conductive polymers suitable for electron transport is the presence of conjugated double bonds along the backbone of polymer, as shown with some examples in Figure 3.2A. The conjugation of localized σ-bonds that form strong chemical bonds and π-bonds which are weaker than single bonds, constitutes the chemical structure of conductive polymer. However, the conjugation of such bonds is not enough to guarantee conductivity to the material. The doping process induces an electron imbalance along the polymer structure and the extended π-conjugated bond system allows the new electron population to migrate a long distance along the backbone when an electric potential is applied (Figure 3.2B). In general, metals have a high density of electronic states meaning that

electrons can easily move from an atom to another one under an applied electric field. Since the electrical properties of a material are ascribed to its electronic structure, in metals the orbitals of a certain atom are overlapped with those of neighboring atoms. Typically, the energy spacing between the highest occupied (valence band) and the lowest unoccupied (conduction band) electronic states is called the band gap. Therefore, the conductivity of metals is due either to a partially filled valence or conduction bands, or to a band gap that is near to zero; so, even for weak electric field the electrons easily redistribute along the orbitals (Figure 3.3B).[146] Hence, the conductivity increases with decreasing band gap which is the energy required to promote an electron to move from the highest occupied energy level to an empty level immediately above it (conductive band). While metals have almost zero band gaps, insulators such as many polymers have large band gaps in the 1.5 – 4eV range which impairs electron flow. By a proper charge injection (doping) it may be possible to reduce this band gap value to 0.5 – 1eV.[142] The doping of conductive polymers leads to interesting phenomena which can be useful in various applications. For instance, the change of the electronic band structure is accompanied by a change of physical features like the optical properties in the UV-vis and NIR-regions which are exploited in electrochromic displays and optical sensors. Furthermore, the electroluminescence of some conductive polymers is used for OLEDs, while photoluminescence is applied for the fabrication of fluorescence-based biosensors.[142]

The doping process of conductive polymers can be achieved either chemically or electro-chemically. In chemical charge injection the polymer is exposed to oxidizing vapors, like iodine. Chemical doping is an effective method but it is poorly reproducible because it is difficult to quantitatively control the polymer oxidation. Another approach is the electro-chemical doping that provides fine tuning of the doping level through electrical potential adjustment.[142]

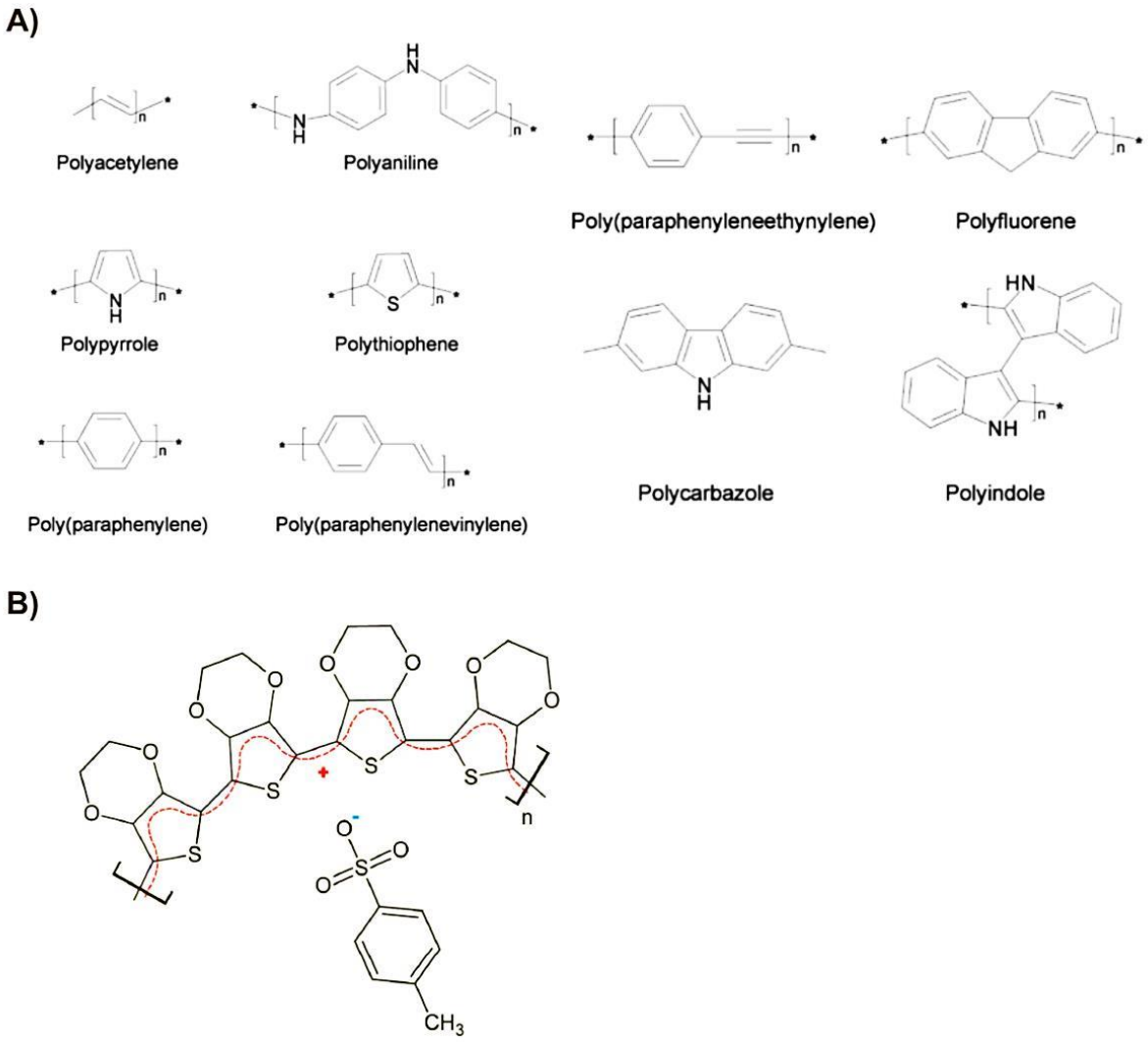


**Figure 3.2 (A)** Chemical structures of main classes of conductive polymers,[142] and (**B**) p-doped PEDOT (poly(3,4-ethylenedioxythiophene)) containing tosylate anions (TsO). A ratio of one tosylate per 3-4 PEDOT monomers is typically found; the electron acceptor tosylate is negatively charged while a dislocated positive charge results in the conjugated system of polymer (shown in red).

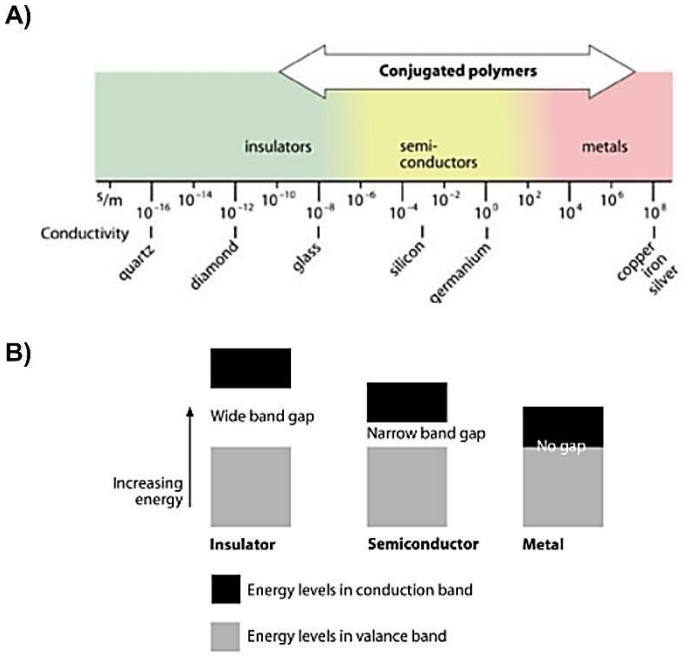


**Figure 3.3** (**A**) Some examples of conductivity values (S/m), and (**B**) the band gaps characterizing insulator, semi-conductive and conductive materials. When the gap between the lowest occupied conduction band and the highest occupied valence band is closed to zero, metal-like features are achieved. Reproduced from [146].

The fields in which conductive polymers find a great applicability are many and with various purposes. Polypyrrole for example is used as pH sensor due to its pH and potential dependencies; in fact, the protonation of polymer enhances its conductivity, whereas deprotonation leads to a lower conductivity.[147] Otherwise, some conductive polymers show an intrinsic affinity for a variety of metal ions, as polycarbazol that provides a selective potentiometric response to Cu(II) ions,[148] or PEDOT that has a great affinity for $Ag^{+}$-ions due to the coordination of ions to the sulfur atom of polymeric monomer.[149] Conductive polymers may be used as receptors for detection of organic molecules like dopamine,[150] saccharides[151] or ATP.[152] Conductive polymers are widely studied also as transducers or as components of transducers because of their ability to change electrical and optical properties upon oxidation/reduction, protonation/deprotonation and conformational changes induced by the binding of different analytes.[142]

One of the more attractive challenges on using conductive polymers is the possibility to modify and immobilize molecules onto or within the polymer matrix.[153] Nowadays, the immobilization procedures commonly used are based on non-covalent interactions (physical adsorption, electrostatic assembly, hydrophobic interactions), or covalent binding of molecules to the conductive polymer. The physical adsorption is rarely adopted because generate weak bonding that consequently leads to a loss of molecules, despite its practical easiness.[154] Another approach is based on the Langmuir-Blodgett technique that is a relatively simple technology used to obtain highly ordered films functionalized with desired molecules. However, the resulting system may be unstable and the film may contain a lot of defects; thus, this technique has been replaced by technologies of self-assembly based on layer-by-layer deposition, or modification by silanization and covalent immobilization. The layer-by-layer deposition method requires an alternate electrostatic adsorption of molecules and opposite charged polymer layers onto a solid support. This method is governed by multiple effects such as shielding, hydrogen bonding, dispersion forces that determine film thickness and morphology.[155] Due to the complexity of the process, the multilayers are extremely sensitive to variations of ionic strength and

drying processes may occur destabilizing the assembled layers. Mechanical embedding also represents a good candidate for non-covalent immobilization: thereby molecules are in the vicinity of electrode and consequent electro-polymerization leads to the entrapment of molecules into the growing polymer layer. The success of this method depends on the concentration of molecules that should be high and the electrodeposition should occur at mild conditions. Nevertheless, the content of molecules finally embedded into the film is insufficient and often surfactants need to be added to enhance monomer solubility.[156] Among the existing non-covalent immobilization processes, the covalent reaction of functional groups of molecules and polymer provides the strongest interaction (Figure 3.4). The easiest way is to polymerize monomer derivative bearing receptor molecules (panel 1) or any functionality (panel 2) in order to obtain polymers presenting the desired moiety in each monomer or with a high functionalization yield. These methods are limited by the availability of synthetic pathways to create certain polymeric derivatives; further, the low solubility of modified monomers and low conductivity of the resulting polymer can be crucial for biomolecules immobilization.[157]

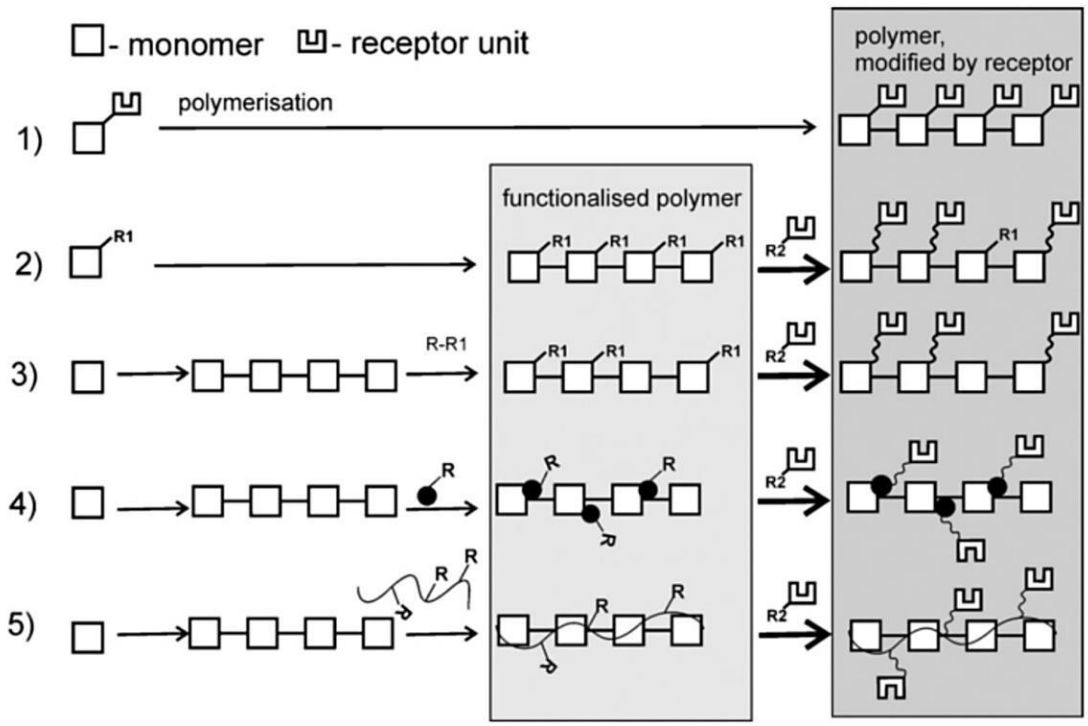


**Figure 3.4** Various methods commonly used to chemically immobilize a receptor unit to a polymer. These mechanisms include: polymerization of a monomer already bearing receptor unit (path 1); polymerization of functionalized derivatives and following chemical receptor immobilization (path 2); post-modification of polymer through functional groups: grafting (path 3), incorporation of modified nanoparticles (path 4), and polyelectrolytes (path 5). Reproduced from [142].

To overcome the problem of poor derivative solubility, two general approaches for covalent immobilization can be used: one is the post-polymerization grafting (panel 3) that is achieved through thermal grafting, wet chemical, organosilanization, UV irradiation, or ionized gas treatment;[158] an alternative approach is based on co-polymerization or polymer deposition in presence of modified nanoparticles bearing functional groups of interest (panel 4)[159] or polyelectrolytes (panel 5).[160] All the presented methods are useful for polymer modification; sometimes the poor compatibility of optimal polymerization conditions and the limited stability of biomolecules onto polymer surface can be overcome by post-modification based on affinity interactions. The known biotin-avidin conjugate is the mostly used system because of high complexation constant;[161] otherwise his-tag moiety,[162] or complementary nucleotides sequences may be adopted.

An important parameter that must be considered when synthesizing polymeric films is their adhesion to a certain solid support. The adhesion of polymer depends on many parameters including the chemical nature of the polymer and support (for instance the hydrophobicity), the procedure of synthesis, solvent and counter-ions. Usually polymer adhesion may be improved by modification of either physical (surface area, hydrophobicity/hydrophilicity) or chemical (including chemical anchor groups) features of solid surface.[142] For example, a simple chemical modification is based on the use of organosiloxanes to promote specific adhesion of polypyrrole and enhance its lateral growth on solid insulating support.[163] Otherwise, mono-molecular self-assembled layers for covalent binding of synthesized polymers can be adopted; for example, thiol derivatives of monomers form monolayers on metallic surfaces (Au, Pd, Ni, Cu, Ag and others) achieving a strong binding of polymers.[164]

A central aim of this thesis is the fabrication and post-polymerization covalent modification of thin films of PEDOT-$N_3$, poly(3,4-(1-azidomethylethylene)-dioxythiophene). One of the major challenges is the production of polymer micro-electrodes and consequent functionalization to immobilize drug-loaded nanoparticles. The need of a fabrication process which has a good biocompatibility and guarantees the biological activity of functional moieties is crucial. In the following paragraphs, a detailed description of polymerization, covalent modification and liposomes presentation at the electrodes surface is found.

## 3.2 PEDOT-$N_3$: properties and applicability

Conducting polymers are characterized by a lower conductivity compare to that of metals and semiconductors, and also a lower long-term stability which renders metals favorable for many applications.[165] Nonetheless, conducting polymers are widely applied in various fields because of their low cost, ease to handle and fabricate, and moreover their electronic, optical, chemical and

biological features can be tuned according to the application requirements. Chemically polymerized PEDOT was discovered in 1988,[166] and its first commercial application was its use as an antistatic layer in photographic films due to its ability to form transparent and conductive films.[167] Within the last two decades, the commercialization of PEDOT have been expanded to many other applications including solid electrolyte capacitors, printed wiring boards, packaging films, touch screens, organic light-emitting diodes (OLEDs) and organic photovoltaics (OPV).[168] Regarding the biological applicability of conductive polymers, including PEDOT, have been found to have a great cell-cytocompatibility and their conductance can be exploited for electric or electric-mechanical stimulation of cells,[169] or electroporation devices.[170] PEDOT as conducting polymer is considered to be a semiconductor since native PEDOT has a band gap of ~1.5eV;[165] however, conducting polymers can be doped to increase conductivity through partial oxidation of polymer. A net charge is introduced in the polymer backbone and counterions will ensure charge neutrality to the material reaching conductivity values in the order of $10^1$-$10^3$ S $cm^{-1}$.[165] The choice of counterions influences the properties of the material and can thus be used to tune the conductive features of the polymer.

PEDOT can be prepared by oxidative polymerization of the monomer 3,4-ethylenedioxythiophene (EDOT).[171] As illustrated in Figure 3.5, each EDOT monomer loses two electrons and a conjugated polythiophene chain is formed.

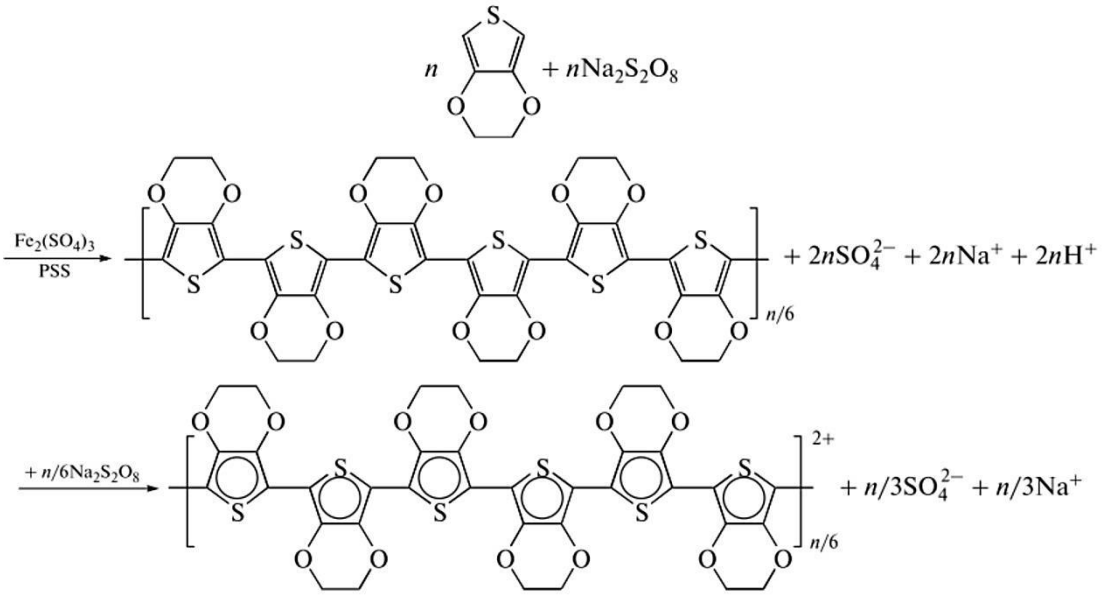


**Figure 3.5** Chemical oxidative polymerization of the monomer 3,4-ethylenedioxythiophene (EDOT) through the oxidation agent persulfate and poly(styrene sulfonic acid) (PSS) to form a water-soluble polyelectrolyte complex (PEDOT:PSS). Reproduced from [166].

Under traditional oxidation conditions, PEDOT is not in a neutral form, instead it appears positively charged. Hence, these charges need to be stabilized by the presence of suitable counterions. It has been reported that sulfonic acids like the one reported in Figure 3.5 are the best choice to achieve a stable PEDOT/counterions complex.[165] In this chemical process should be noted that the oxidation of polymer is not accomplished by the counterions, rather by the oxidation agent. Further, the polymerization of PEDOT is normally performed on the surface of a support through the so called *in-situ* polymerization where a solution of EDOT monomers and an oxidation agent, such as Fe(III)tosylate (TsO), are mixed to form a polymeric film.[172] Alternatively, the evaporation of EDOT monomers onto a support surface may be adopted to enhance polymer synthesis; this process can be conducted by simultaneously adding the oxidation agent as $FeCl_3$ or through deposition of Fe(III)TsO (also an oxidation agent) prior polymerization.[173] The oxidative polymerization may be also conducted by involving sulfonic acid in the reaction, such as poly(styrene sulfonic acid) (PSS); a polyelectrolyte complex is formed and it appears like a water-soluble stable dispersion.[174] This dispersion is characterized by gel particles of PEDOT/PSS polyelectrolyte which have typically a dimension of 20-500nm;[168] despite their stability, these dispersions have a really low pH, in the range of 1-2 and a base needs to be used to neutralize the acid pH (Figure 3.5). Unfortunately, during the neutralization process the PEDOT component is not stable and the complexes result in a changed color and films lose their conductivity.[166] Depending on the final application in which PEDOT films want to be used, a certain polymerization reaction and counterions should be evaluated; for instance, the biological application of PEDOT polymer requires mild reaction conditions. For many chemical reactions, specific solvents and elevated temperatures are often needed resulting therefore to be incompatible with biomolecules and bio-applications.

We chose to use 3,4-(1-azidomethylethylene)-dioxythiophene (EDOT-$N_3$) monomer that was studied in our group prior the work presented in this thesis. It was found the EDOT-$N_3$ could be chemically oxidized to yield p-doped PEDOT-$N_3$ films containing tosylate (TsO) anions as stabilizing counterions.[175] These films resulted to be stable, insoluble and chemically modifiable with a wide range of alkyne reactants,[175] and their conductivity was found to be $\sim 6 \cdot 10^1$ S $cm^{-1}$, a lower value compared to the native PEDOT film which has a conductivity of $\sim 7 \cdot 10^2$ S $cm^{-1}$.[165,175] Here the PEDOT-$N_3$ substrates are intended to be used as micro-platform for the immobilization of drug-loaded nanoparticles (liposomes) and consequent study of molecules release. In order to achieve this goal, PEDOT-$N_3$ micro-electrodes (100µm in width) are fabricated on a protein repellent support (PEG-coated COC discs) in order to discourage passively adsorption of molecules during electrodes modification. Through a selective chemical functionalization of PEDOT-$N_3$ electrodes, based on the known "click-chemistry reaction", drug-loaded liposomes are immobilized onto the polymer surface. According to the original idea on developing such system, the employment of an additive modification chemistry may be applied to functionalize the areas between the electrodes (also 100µm in width) with other molecules such as antibodies that can be used for the recognition of specific cell types. Thus,

two main components may be co-immobilized onto the micro-platform (antibodies and drug-loaded liposomes). Ideally, the conductive properties of polymeric electrodes may be utilized to induce a local thermal increase when a certain voltage is applied onto electrodes surface. Because of the thermal sensitivity of our synthesized liposomes, a consequent drug leakage may be induced. Such technology should allow the capture of desired cell type from a mixture of different cell lines according to the specific antibody molecules immobilized onto the platform surface, and control the drugs release for drug screening purposes. As stated in the introduction of this chapter, many issues were encountered and some of them were solved while others still need to be optimized. The main obstacle during the development of this platform was the fabrication of micro-electrodes. Even though in our group and more in general in our department (DTU Nanotech) clean room facilities for micro- and nano-fabrication are available, the process required for the production of PEDOT-$N_3$ electrodes should be cheap and more importantly should be able to maintain the biological properties of the PEG-coating produced onto the solid support prior electrode fabrication.
The feasibility of such micro- and nano-platform depends on many parameters due to the challenging fabrication and modification processes:

a) a stable and efficient protein repellent coating of the support is needed in order to avoid passively adsorption of chemicals and molecules during the functionalization processes; in particular, this step has to be conducted prior electrodes fabrication;

b) a suitable technology for electrodes fabrication that preserves the chemical and physical properties of the support and its coating is required;

c) stable and selective chemical reactions conducted upon mild conditions that permit to anchor drug-loaded liposomes to the electrodes surface and antibody molecules onto the coated support surface, respectively are required;

d) a proper liposomes trigger should be applied without altering the physical-chemical properties of the platform and of captured cells;

e) the overall micro- and nano-platform must be cytocompatible.

All these issues will be considered in the following sections, with a particular focus on the chemistries adopted for the specific binding of nanoparticles and the fabrication methods used to create 3D-microelectrodes.

## 3.3 Deposition and fabrication of thin PEDOT-$N_3$ electrodes

### 3.3.1 Thin film deposition of PEDOT-$N_3$

A thin film can be described as a uniform layer of material ranging from a nanometer to few micrometers in thickness. The applications of these films include telecommunications, micro electro mechanical systems (MEMS), bio-MEMS, flat screen displays such as LCDs, flexible OLEDs, laser diodes and magnetic read/write heads.[176] Currently, the deposition techniques available for thin films fabrication are based on vacuum and non-vacuum methods. Vacuum techniques include physical vapor deposition and chemical vapor deposition technologies which permit to fabricate films and coatings with a thickness in the range of 10nm-1μm.[177] Non-vacuum methods are normally adopted for low-cost processes especially when larger thicknesses are required (more than 1μm). Further, non-vacuum techniques like polymer spray coating, spin coating, metal electroplating, roll-to-roll deposition or liquid flame spray nano-coating are more convenient for large scale production. In any case whatever technique is adopted, the deposited film must possess some specific characteristics that are essential for the final purpose.[177] Firstly, the uniformity of a film is required to meet both electrical and mechanical specifications; for instance, the deposited thin film must be continuous, free of pin holes, flat and smooth in order to minimize cracking and its adhesion to the support surface should be optimized. The presence of cracks into the film generates a surface roughness and allows contamination of polymer.[178]

In this thesis, PEDOT-$N_3$ films are produced by using spin-coating technology which is one of the most commonly used techniques for deposition of thin film onto supports. At present, the use of spin-coating is widespread in organic electronics and nanotechnology fields because of the easiness and fast process and its ability to produce very uniform films from few nanometers to few micrometers in thickness. Moreover, a simultaneous deposition and polymerization of polymer in self-assembled layers occurs during the casting process.[179] The spin coating process involves the deposition of a certain polymer dissolved in a solvent (ink) onto the support surface while it is rotating (Figure 3.6A, panel 1). The support is rotated at high speeds and the majority of the ink solution is flung off the edges of the support (panel 2); most of the solvent is then dried by airflow (panel 3) and after a while a complete evaporation of solvent occurs and a dry film remains attached onto the surface (panel 4). The rotation of substrate at high speed, normally higher than 600rpm (revolutions per minute), pulls the liquid out due to a centripetal force combined with the surface tension of the solution. Therefore, the thickness of a spin coated film is proportional to the inverse of the square root of the spin speed, as shown in Figure 3.6B and as expressed by Equation 3.1, where $t$ is the film thickness and $\omega$ is the angular velocity.

$$t \propto \frac{1}{\sqrt{\omega}} \qquad \textbf{Eq. 3.1}$$

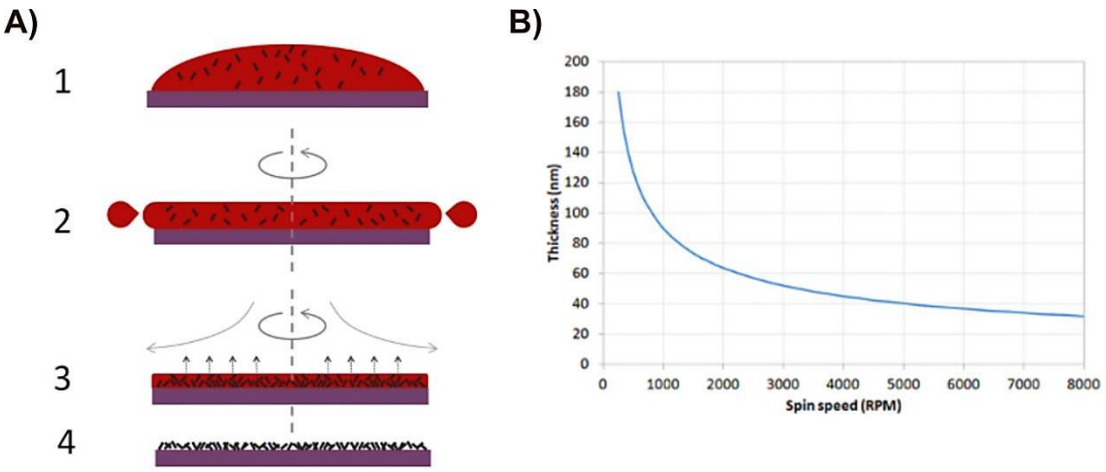


**Figure 3.6** Spin-coating of thin films. (**A**) Schematic illustration of the spin coating process: the ink solution (in red) is subjected to a high speed through horizontal rotation (minimum 600rpm) of the support and after evaporation of the solvent a thin film is obtained. (**B**) Graphical relation between the spin coating speed (rpm, revolutions per minute) and resulting film thickness (nm).

The PEDOT-$N_3$ films are produced through spin-coating technique on cyclic olefin copolymers (COC) supports. Topas® is the trade name for advanced polymers´ cyclic olefin copolymers (COC)[180] which consists of amorphous, transparent copolymers based on cyclic olefins and linear olefins (Figure 3.7A). Cyclic olefin copolymers are a new class of FDA-approved polymeric materials with a unique combination of features that can be varied by changing the chemical structure of the copolymer. Topas resins are suitable for the fabrication of transparent moldings in the field of optical data storage, optics, and industrial products. Currently, different COC grades are commercially available and they mainly differ on their heat deflection temperature, which is determined by the ratio of co-monomers, and on their flowability that decreases with increasing viscosity number. In fact, the various grades of COC are normally indicated by 4 digit number, where the first two indicate the viscosity and the last two digits describe the heat deflection temperature. The COC resin is a clear thermoplastic material with high strength, rigidity and according to the grade, heat deflection temperature (in the range of 75° C - 170° C); moreover, the high transparency of the material remains unaffected by temperature changes. Further, COCs are very good electrical insulating material with a dielectric constant of 2.35 and a surface resistivity > $10^{14}$ Ω. The high transparency of Topas in the visible and near ultraviolet regions coupled with a refractive index of 1.53 makes these polymers attractive for high-quality optical components.

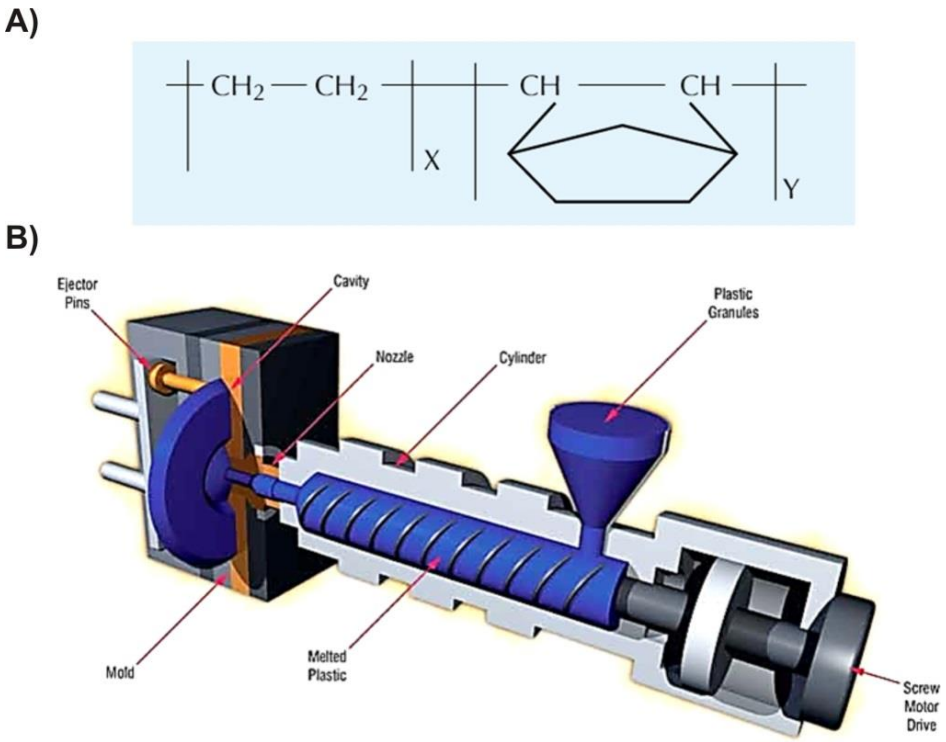


**Figure 3.7** Topas® cyclic olefin copolymers (COC). (**A**) Chemical structure of co-monomers used to synthesize cyclic olefin copolymers. The ethylene and norbornene monomers form the COC copolymer through chain co-polymerization. (**B**) Illustration of a standard injection molder used for the fabrication of macro-scale objects but also different micro- and nano-structures. The main components of the machine are reported: to produce COC 5013 discs of 5 cm in diameter and 2mm in thickness, shims with completely flat surfaces are employed.

Regarding COC chemical properties, it is a water-repellent (hydrophobic) material and thus exhibits only negligible swelling when immersed in water; COCs are also resistant to hydrolysis, acids and alkalis, as well as to polar solvents such as methanol. However, Topas is attacked by non-polar solvents like toluene. The specific grade of COC that is employed for spin-coating of PEDOT-$N_3$ films is the COC (5013) which has a glass transition temperature at 130° C and it is particularly suitable for accurate molding replication. The injection molding process is used to fabricate COC discs with a diameter of 5 cm and thickness of 2mm; in this fabrication process the nozzle-cylinder components are heated up at a temperature above the glass transition temperature of polymer granulates (between 240° C and 280° C). Then the polymer is melted until it reaches the nozzle exit and fills the cavity between the two mold shims which are also at a temperature above the glass transition temperature. The system is cooled down and an external pressure is applied to balance the shrinkage or expansion of polymer during the cooling. Since the melted polymer fills completely the micro- and nano-voids on the shims, high fidelity replica can be obtained. For our purpose a completely flat shim is used to fabricate multiple COC (5013) discs in a short time.[181,182]

Hence, PEDOT-$N_3$ films are obtained by spin-coating onto COC support a polymer mixture composed of: monomer solution (EDOT-$N_3$), Fe(III)TsO shortly tosylate which is the oxidation agent, and the solvent (butanol). The solution volume is spin-coated at a spin speed of 1000rpm for 30 seconds in order to obtain a final film thickness around 150nm. After spin-coating, the coated supports are heated up at 70° C to enhance homogeneous solvent evaporation and already after 2 min a completely polymerized PEDOT-$N_3$ is obtained (Figure 3.8). Therefore with these processes, spin-coating and baking, an *in situ* polymerization of thin PEDOT-$N_3$ films is allowed.

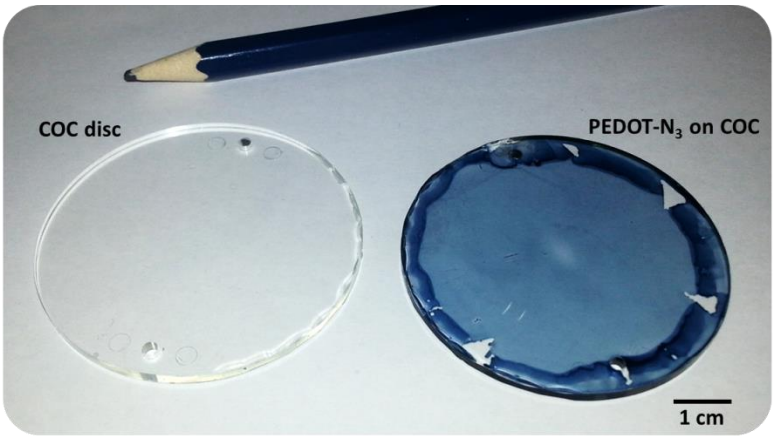


**Figure 3.8** Photo of a Topas COC 5013 disc (on the left) and a spin-coated PEDOT-$N_3$ film on COC support after polymerization (on the right). Both discs have a diameter of 5cm and a thickness of 2mm. The final polymer thickness is around 150nm. A pencil is introduced to compare object sizes.

### 3.3.2 Fabrication of micro-electrodes on PEDOT-$N_3$ thin films

The technologies available for micro- and nano-fabrication of structures are many and presenting different benefits and drawbacks. Some of them, such as nanolithography, electron beam lithography or reactive ion etching (RIE), are particularly useful for the fabrication of small feature sizes and high aspect ratio structures; however, the use of such methods requires expensive clean room facilities and materials. Further, since PEDOT-$N_3$ is a polymer and thus sensitive to moisture and chemicals, micro-fabrication techniques used for patterning metals are most of the times unusable for PEDOT-$N_3$ patterning. One of the most used techniques for polymer or molecule patterning under mild conditions is the micro-contact printing. It is a method largely used because inexpensive, fast, simple and does not require clean room instrumentation. Micro-contact printing is based on using a stamp, normally made of polydimethylsiloxane (PDMS), which is used to deposit polymers or molecules onto a flat surface (positive stamping), or to remove material from a layer according to the structures presented at the

PDMS surface (negative stamping). When certain molecules need to be deposited on a surface, the PDMS is incubated with the molecule solution (ink) and the stamp is put in contact with the substrate applying a small pressure. Thus, patterned molecules are transferred onto the surface according to the original shape and structure of PDMS (Figure 3.9A).

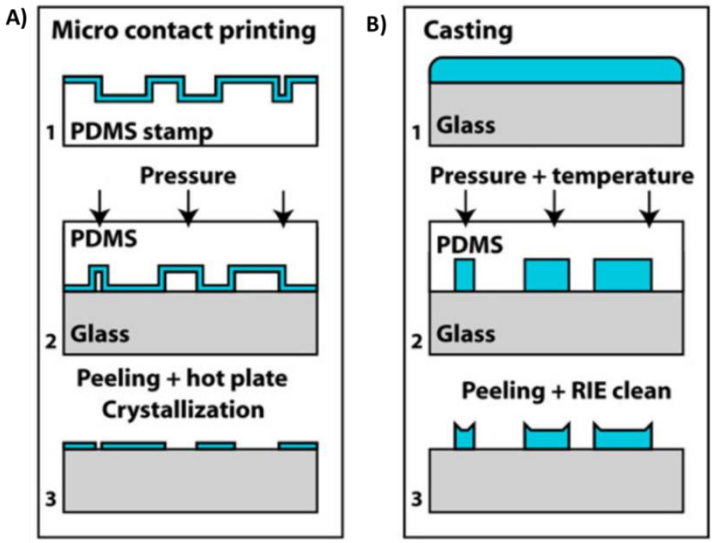


**Figure 3.9** Schematic of soft lithography processes normally used for the fabrication of micro-structures on different substrates. Reproduced from [183]. (**A**) The micro-contact printing consists on the use of a PDMS stamp that is incubated with an ink solution (1), and it is put in contact with the substrate by applying a small pressure (2); then the stamp is removed and desired structures remain deposited onto the substrate surface (3). (**B**) The PDMS mold can be also applied for the removal of desired layers after casting process (1); when the stamp is in contact with the substrate, the layer is removed according to the contact areas exposed to the PDMS mold (2). The resulting structures are then cleaned (3).

The stability of these printed molecules depends on the interactions involved between the molecules and the surface, hence on the chemical properties of the support. A different approach for the fabrication of micro-structures is the casting, where a molecule solution is deposited on a support and afterwards a PDMS stamp is pressed against the surface. A temperature increase can help to remove molecules or polymer in correspondence of the stamp-layer contact areas (Figure 3.9B). Both described techniques, micro-contact printing and casting, are widely used to create chemically micro-patterned surfaces: for example various structures on PEDOT:PSS layers are produced through PDMS casting, although large variations in thickness are found.[183]

The production of PEDOT-$N_3$ micro-electrodes can be achieved by using the printing approach and in particular, a method previously developed in our group, is applied. This technology, called *printed dissolution* is a versatile, simple, cheap and fast procedure adopted to fabricate patterns on PEDOT-based films. The main benefit on using such method is that it locally removes specific areas of conductive polymer from a support, and re-exposes the surface of the underlying support in an un-perturbed state. The principle of this process in based on the use of an agarose stamp which is

immersed in an oxidizing agent solution (sodium hypochlorite, NaOCl) and put it in contact with a PEDOT-$N_3$ film.


**Figure 3.10** Photos of the main components required for printed dissolution procedure. On the left, the pictures indicate the silicon mold used for fabricating the agarose stamp. It contains two sets of inter-digitated electrodes 100µm wide and 100µm spacing. On the right, the agarose stamp produced by melting an agarose solution onto the silicon mold. After cooling down a negative replica of electrodes is obtained on the stamp surface.

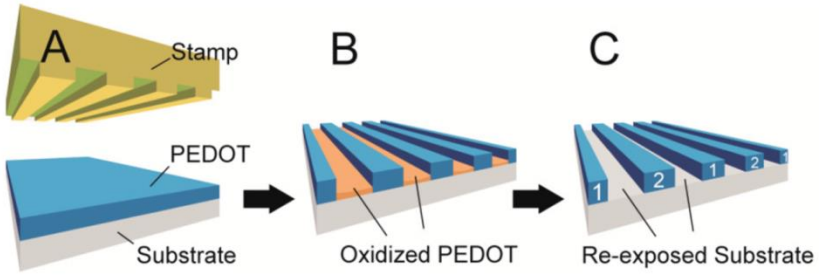


**Figure 3.11** Illustration of the steps involved on printed dissolution. (**A**) The agarose stamp is soaked into a solution of an oxidizing agent (sodium hypochlorite, NaOCl), and is put in contact with a PEDOT film. (**B**) After removal of the stamp, over-oxidized and non-conductive polymer residues remain in the gaps between the electrodes. (**C**) The leftover PEDOT is removed by introducing a non-ionic detergent inside the agarose stamp or washing the sample in a solution of detergent.[184] See the experimental section at the end of this chapter for more details.

The agarose stamp is formed by melting a polymer solution on top of a silicon mold (Figure 3.10, on the left) and cooling down the solution. On the silicon mold, two sets of inter-digitated electrodes 100µm wide are included; hence, when the agarose solution is cooled down onto the mold surface, a negative replica of the electrodes results on the agarose stamp surface (Figure 3.10, on the right).

In earlier reported works in our group, it was found that when the stamp is immersed in a solution of NaOCl (Figure 3.11A), then it can be used to locally remove the conductivity of PEDOT-based films due to an over-oxidation induced by the oxidizing agent; thus, it breaks the conjugated system of the polymer backbone and the conductivity is lost.[185] When the stamp is kept in contact for a while with the PEDOT film, a stable over-oxidized polymer layer remains in the gaps between the electrodes, as

shown in Figure 3.11B. Nevertheless, the application of a non-ionic detergent (Triton X-100) directly in the agarose stamp or during a subsequent washing step, removes these over-oxidized polymer residues from the support which is now available for following functionalization (Figure 3.11C). When PEDOT-$N_3$ films are exposed to printed dissolution using the described procedure, a patterned surface formed of two sets of inter-digitated electrodes is obtained (Figure 3.12). A detailed description of the process is found in the Experimental section of Chapter III.

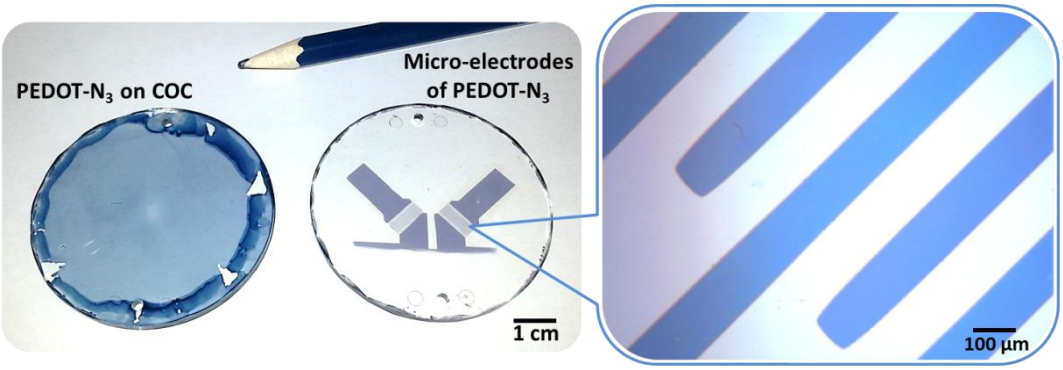


**Figure 3.12** Photo of a spin-coated PEDOT-$N_3$ film (thickness around 150nm) on COC support. The sample is put in contact with an agarose stamp and through printed dissolution, two sets of inter-digitated electrodes are obtained (on the left). In the enlargement, the optical micrograph of the fabricated electrodes. Light blue areas correspond to the polymer film and the transparent areas represent the underlying COC support obtained after agarose stamping. More details are found in the experimental section.

The use of printed dissolution for fabricating PEDOT-$N_3$ electrodes permits not only the local removal of conductive polymer but also generates a multiple surface chemistries. In fact, on the electrodes surface the azido groups are available for subsequent post-fabrication modifications; moreover, the underlying COC surface in the gaps between electrodes results accessible to any functionalization.

### 3.3.3 Coating and functionalization of COC support prior PEDOT-$N_3$ micro-fabrication

As anticipated just above, when polymer micro-electrodes are produced, in-register surface chemistries are presented at the surface (azido groups corresponding to electrode areas and COC between polymer structures). Although a post-fabrication functionalization of PEDOT-$N_3$ electrodes may be adopted to locally immobilize desired molecules or chemical moieties, the reactivity of COC for any functional groups or modification is poor. In other words, the modification of the support after

agarose stamping is unlikely achievable unless a physical adsorption is utilized. However, the adsorption of molecules onto the electrodes surface may not be selective meaning that the entire fabricated film will be modified by the same chemical moiety. Since one of the main advantages on using printed dissolution is that it guarantees the chemical reactivity of the polymer surface and also of the underlying support, it may be possible to coat prior fabrication, the COC support with functional groups or molecules that will be useful for a subsequent modification after electrodes fabrication. Many different methods may be applied to modify the COC chemistry including physical adsorption or chemical deposition. The way in which the support surface is changed depends on the final application and requirements for a certain purpose. Ideally, the platform to be produced for our drug screening application, should present functionalizable PEDOT-$N_3$ electrodes to locally immobilize drug-loaded liposomes, and eventually it should include a second chemical modification to enhance antibodies binding on the areas between the electrodes. As described in the introduction of this chapter, the use of EDOT-$N_3$ monomers allows to covalently functionalize the electrodes surface after fabrication through `click-chemistry reaction´, thus promoting a local nano-particles immobilization. On the other hand, a chemical modification of the support may allow a further functionalization of the electrodes surrounding regions.

In the light of these considerations, different approaches to modify COC surface are presented. In general, these procedures involve a physical adsorption of various molecules or polymers in order to obtain a surface able to prevent passive adsorption of compounds during post-fabrication functionalization, and that has a chemical reactivity toward subsequent modifications. Once the support is coated with desired molecules, a film of PEDOT-$N_3$ should be polymerized onto the modified-COC; therefore, the chemical reactivity of the underlying layer is evaluated before and after printed dissolution in order to compare a preserved functionality of the sample.

#### 3.3.3.1 PS-$N_3$ coating and functionalization of COC support

One of the approaches that could be adopted to obtain a chemical reactive COC surface is the physical deposition of poly(4-(azidomethyl)styrene) shortly PS-$N_3$, through spin-coating process (in Figure 3.13A, the chemical structure of PS-$N_3$ monomer and COC coating are reported). The azido-modified polystyrene creates transparent films when deposited at high spin speed and it can be easily patterned through UV-light exposure due to its sensitivity, thus when is illuminated in the UV-range light a crosslinking of film will occur. The process by which the azido-polystyrene is crosslinked when exposed to UV-light has been proposed by Akhrass *et al.*[186] Hence, a film of PS-$N_3$ is spin-coated on a COC support (see the experimental section for details) and the coating is characterized measuring the water contact angle and optical microscopy. In Figure 3.13B, an optical micrograph of a spin-coated layer of PS-$N_3$ dissolved in dioxane is produced on a COC support (magnification 20X). A homogeneous thin film is obtained and is characterized through water contact angle to evaluate how the

hydrophobicity/hydrophilicity of the support changes. As depicted in Figure 3.13C, when a film of PS-$N_3$ is polymerized onto the COC surface, an increase on hydrophilicity is reached. In fact, COC is typically really hydrophobic and the subsequent coating creates a more hydrophilic surface as indicated by the static, advancing and receding values. However, when spin-coated PS-$N_3$ films are kept under environment conditions for a while, many in-homogeneity and particles are generated onto the surface and the films fabrication is poorly reliable. Different structures are detected through optical microscope: comet, agglomerate and coffee-ring shapes are found. Apparently, the stability of PS-$N_3$ film is poor over time and it may be due to the solvent 1,4-dioxane which is hygroscopic and therefore water molecules up-taken from the environment humidity may affect the film appearance (Figure 3.14). As the exposure time to environment increases, a large number of defects are provoked into the film probably induced by water uptake onto the layer or solvent evaporation. The solution of PS-$N_3$ dissolved in dioxane is also filtered prior spin-coating (filter Ø=0.22µm) to discourage particles deposition.

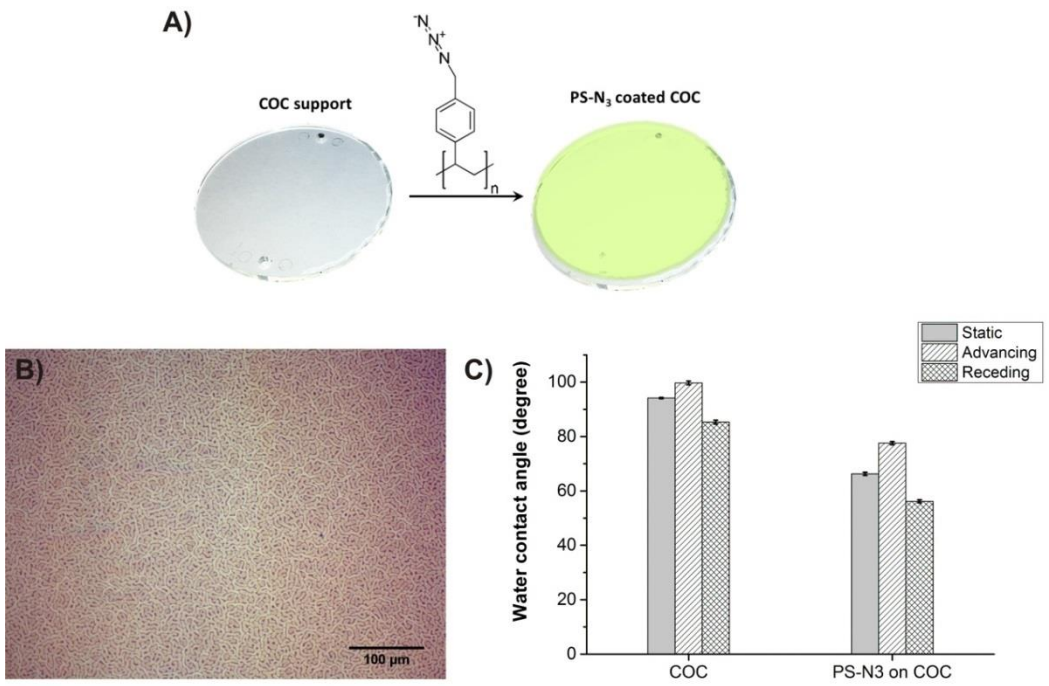


**Figure 3.13** Characterization of spin-coated PS-$N_3$ films on COC support. (**A**) Illustration of the process involved on the azido-polystyrene deposition and its chemical structure. The green layer indicates the polymeric coating on COC. (**B**) Optical micrograph of the obtained thin layer of PS-$N_3$ on COC (magnification 20X); a homogeneous film is produced. The picture is recorded just after spin-coating and washing. (**C**) Water contact angle measurement of a clean COC sample and PS-$N_3$ coated COC; the static, advancing and receding values are reported as average value of 10 processed samples (n=10). An increased hydrophilicity of the surface is achieved when PS-$N_3$ is deposited.

Therefore, an optimization process to obtain homogeneous and stable PS-$N_3$ films for a subsequent PEDOT-$N_3$ polymerization is necessary. Due to the solvent properties that are unsuitable for PS-$N_3$ film

deposition, a different solvent may be adopted to dissolve the polymer, for example PGMEA (propylene glycol monomethyl ether acetate). This solvent is generally used to dissolve photoresists because it inhibits fast evaporation and does not tend to form particles. Thus, PS-$N_3$ dissolved in PGMEA is spin-coated on COC support and, even if not perfectly homogeneous films are produced, the lack of consistent defects caused by solvent evaporation or water uptake, leads us to select PGMEA as solvent. Once the azido-polystyrene is deposited on the COC support, ideally a thin film of PEDOT-$N_3$can be formed on top of it and micro-electrodes fabrication may be conducted. Now, some questions may come out: first of all, does the PS-$N_3$ layer introduce a surface reactivity on the underlying PEDOT-$N_3$ film? Secondly, can the COC coating prevent physical adsorption of molecules for post-fabrication functionalization? And finally, do the azido groups of polystyrene permit a local functionalization on the gaps areas between electrodes?

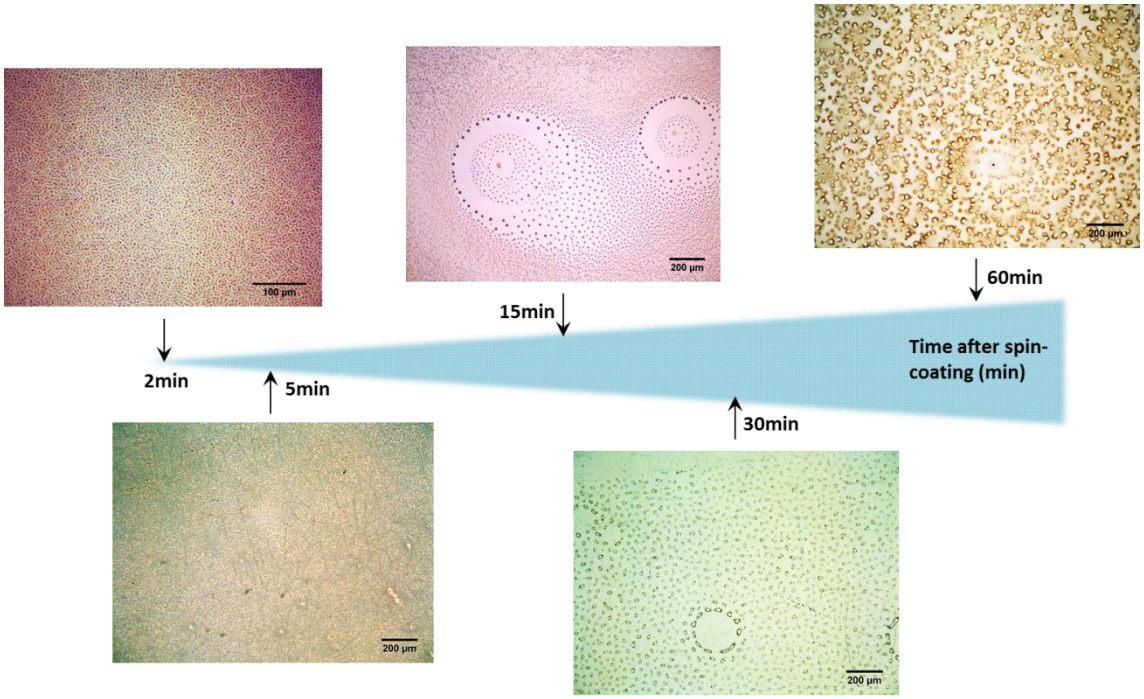


**Figure 3.14** Illustration of optical micrographs of spin-coated PS-$N_3$ films (dissolved in dioxane) on COC maintained under environment conditions. The quality of films is reported as function of time. After spin-coating (2min), a homogeneous surface is observed whereas already after 5min some imperfections are found. As the exposure time increases, larger structural defects are created: rings, particles and comets morphologies are detected until 1h after deposition process.

The presence of PS-$N_3$ film on COC support confers to the surface a reactivity that is higher than that of COC, especially toward alkene species whereas the bare support may be modified through molecule physical adsorption. This means that azido groups in presence of alkyne moieties can form stable covalent bonding of such compounds onto the PS-$N_3$ surface via ´click-chemistry reaction´. Regarding molecule adsorption of PS-$N_3$ layer, a preliminary evaluation of repellency properties of azido-

polystyrene is conducted by incubating a fluorescent protein (fluorescein isothiocyanate-avidin) onto the spin-coated PS-$N_3$ film (Figure 3.15). The results suggest that a high protein adsorption onto the surface is encouraged even after 1hour of surface washing (confocal micrograph in Figure 3.15). A possible approach that can be adopted to create protein repellent surfaces by taking advantage of azido reactivity on PS-$N_3$ film, it consists on covalent modification of the polymer through click-chemistry reaction. In particular, poly(ethylene glycol) (PEG) moieties can be covalently bound to polystyrene in order to discourage protein adsorption. In fact PEG is known to confer higher hydrophilicity to surfaces and to prevent molecule and cell adhesion. Different PEG-based molecules are selected to evaluate whether PEG assembled layers reduce molecules adhesion on PS-$N_3$; furthermore, since polystyrene is sensitive to UV-light, various patterns on PS-$N_3$ films are produced to better visualize the specificity of functionalization reaction through click-chemistry reaction with different PEG molecules. As depicted in Figure 3.16, a spin-coated PS-$N_3$ film is exposed to UV-light with a maximum emission peak at 365nm using a traditional UV-aligner; for the fabrication of defined patterns onto the film, a chrome mask presenting square grids with different sized structures, is applied. The sample is illuminated for 30min and washed with DMSO, isopropanol and ethanol to remove degraded polymer. The areas that are exposed to UV-light (in correspondence of transparent regions on the mask) are crosslinked in 3D structures. Ideally using this process, any type of 3D structures can be produced on the spin-coated film.

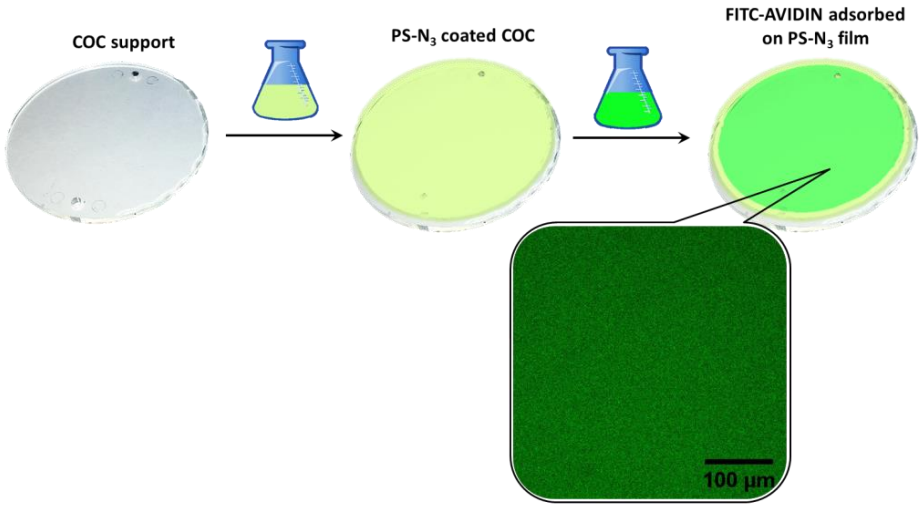


**Figure 3.15** Illustration of the procedure used to evaluate the molecule adsorption repellency of PS-$N_3$ films. A COC support is coated with a layer of PS-$N_3$ (light green), and after polymerization a solution 20µg/mL of FITC-avidin dissolved in PBS is incubated on the polymer surface for 30min (dark green). The sample is then washed with PBS for 30 and 60min and the FITC fluorescence is detected through confocal laser scanning microscopy (LSM 5, Carl Zeiss, Oberkochen, Germany) using exciting light at 488 nm and collecting emitted light of wavelength longer than 505 nm.

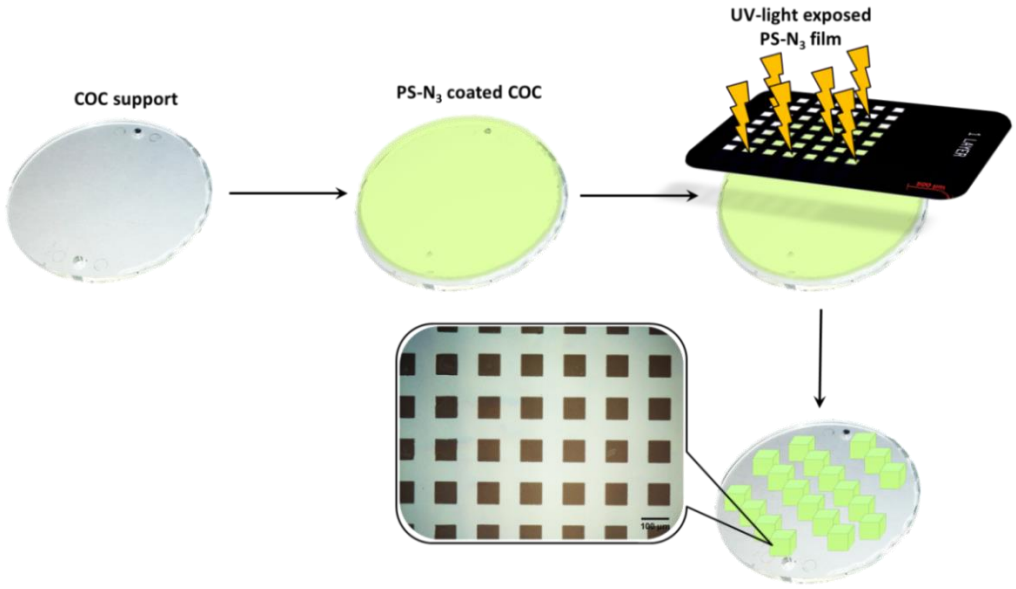


**Figure 3.16** Illustration of 3D patterning process used to create PS-$N_3$ structures. A coated PS-$N_3$ support is exposed to UV-light (with a maximum emitting light at 365nm) by applying a chrome mask composed of squared grids (7 x 7 squares with a dimension of 60µm). On the chrome mask, in correspondence of transparent areas the UV-light will pass through inducing a crosslinking of polymer film, while in correspondence to chrome regions, the light cannot pass and sample is un-exposed. After UV-light patterning the sample is washed with DMSO, isopropanol and ethanol to remove degraded film.

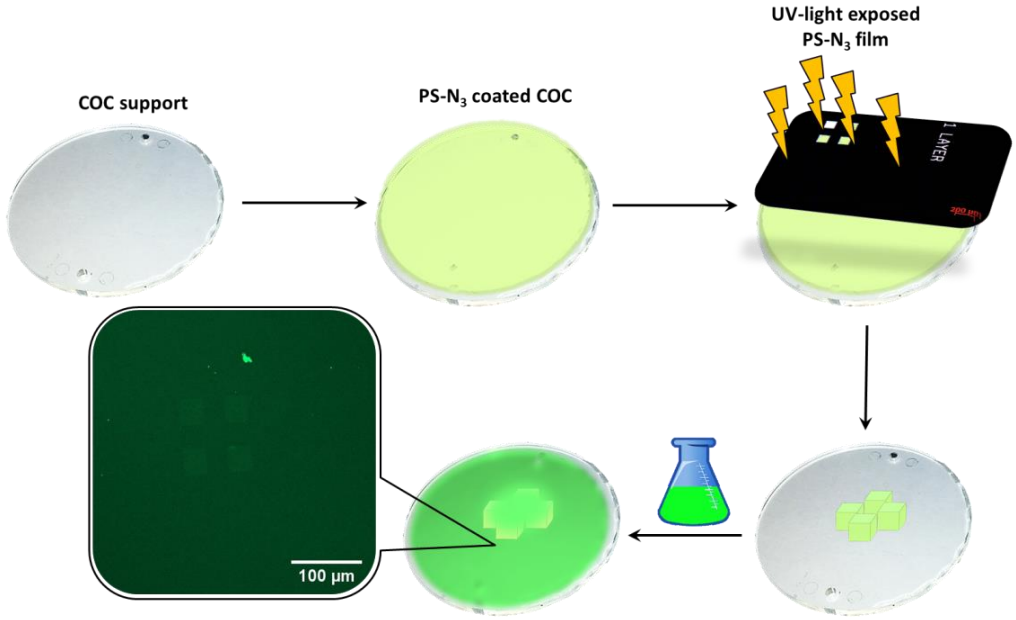


**Figure 3.17** Illustration of the process used to form 3D patterns on PS-$N_3$ film through UV-light exposure (365nm). A chrome mask formed by a grid of squares with a diameter of 66µm (4 x 4) is employed to create the corresponding pattern. After washing, the 3D structures are incubated with 20µg/mL of FITC-avidin for 30min in PBS. The un-adsorbed molecules are washed away and the FITC fluorescence is detected through confocal microscopy (excitation at 488nm and emission collected at wavelengths longer than 505nm). The confocal micrograph is reported: the signal of FITC is homogeneous all over the sample meaning that the surface is still prone to adsorb molecules.

Defined PS-$N_3$ structures are obtained and their further functionalization with PEG-based molecules may prevent protein adsorption. In fact, when FITC-avidin is incubated onto the patterned film and washed, the fluorescence is found all over the sample (on exposed COC and on 3D PS-$N_3$ patterns, as depicted in Figure 3.17). Thus, as also previously shown for un-patterned PS-$N_3$ surfaces, a high protein adsorption still occurs and a PEG-modification of film may overcome this limitation. Two main PEG molecules are tested: they differ on PEG chain length and chemical reactivity. PEG-alkyne (MW~800Da) and PEG-dialkyne (MW~1kDa) contains one and two alkyne groups, respectively. These molecules are particularly reactive against the azido groups which are coupled through click-chemistry reaction. The click-chemistry reaction, also known as copper catalyzed 1,3-dipolar cycloaddition of alkynes and azides (CuAAC), was originally developed by the groups of Meldal[187] and Sharpless[188]. The copper catalyzed reaction (Figure 3.18) is highly selective, tolerates a number of other functional groups and in general proceeds in high yields at ambient conditions or at moderate temperatures. Depending on the copper source it can be tolerant to oxygen and be performed in a number of solvents. The catalyst most often used is Cu(I), added as salt or generated *in situ* by the reduction of $CuSO_4$ with sodium ascorbate (NaAsc), where the latter is preferred due to a lower cost, high purity of the active catalyst and stability toward oxygen. CuAAC is largely applied for end group functionalization both by post and pre-polymerization strategies. This reaction between an azide and a primary alkyne can take place in water, in aqueous mixture and in organic solvents at inert reaction conditions. The mechanism of 1,4-triazole formation which is the product of reaction, involves Cu(I) that conjugates to the alkyne bond and subsequently coordinates to azide causing the formation of triazole. The scheme in Figure 3.18 represents the click-chemistry reaction mechanism that is used to functionalized patterned PS-azide surfaces with PEG-alkyne and -dialkyne species.

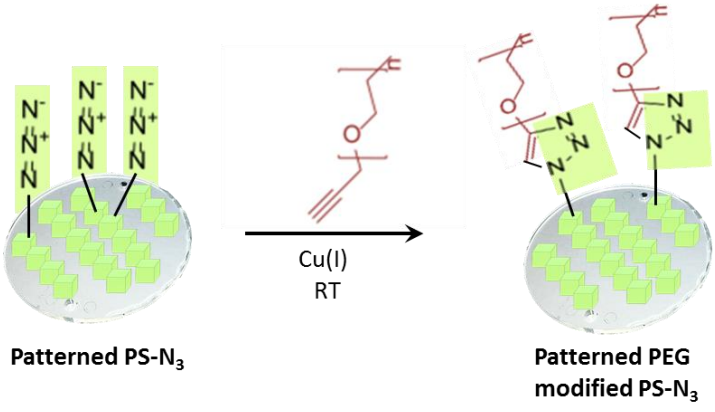


**Figure 3.18** Schematic of click-chemistry functionalization of patterned PS-$N_3$ films. The available azide groups onto the polymer surface (in green) react with the incubated PEG-based alkyne species (in red) to form new covalent bonds that result on the production of 1,4-triazole groups. The reaction is conducted in presence of a catalyst, Cu(I) which can be added as salt or is generated by *in situ* reduction together with sodium ascorbate. The mechanism takes place at room temperature and in different solvents including water or mixture of water and organic solvents. Different types of alkyne or dialkyne species may be used: for our purposes, PEG-alkyne (MW=800Da) and PEG-dialkyne (MW=1kDa) are employed.

The process is ensured by incubating a mixture of PEG-alkyne (or PEG-dialkyne), copper salt ($CuSO_4$), sodium ascorbate (NaAsc) dissolved in 30%v/v DMSO/water; the reaction takes place for circa 10hours at room temperature. After reaction the sample is extensively washed to remove un-reacted compounds; thus, the alkyne or dialkyne molecules that reacted with the available azide groups onto polystyrene surface, are covalently bound to the surface via triazole formation. The reaction of PEG-alkyne species with azide groups permits to cover the patterned polymer with a thin assembled layer of PEG. Nevertheless, introducing PEG-dialkyne molecules is possible to benefit of the PEG coating and in addition, insert a chemical reactive group (alkyne) onto the surface that may be useful for a later post-functionalization.

Therefore, both PEG-based molecules (alkyne and dialkyne) are tested on patterned PS-$N_3$ surfaces to evaluate the efficiency of click-chemistry functionalization and thus, the ability to generate protein repellent surfaces due to covalent PEG coating. From the water contact angle measurement (Figure 3.19) it seems that the functionalization of patterned PS-$N_3$ surface with PEG-alkyne molecules does not confer an increased hydrophilicity to the film as expected; the contact angle of PEG-alkyne coated surfaces is similar to the one measured for un-modified patterned PS-$N_3$. According to these findings, a concentration of FITC-avidin 20µg/mL is incubated in that surface and confocal microscopy detection is used collecting the fluorescent signal from the dye after an extensive washing. Conversely to what is observed when FITC-avidin is incubated with un-modified PS-$N_3$ (Figure 3.17) in which the molecules are found all over the surface, a different scenario is observed when these structures are functionalized with PEG-alkyne. In fact, the patterns are clearly visible meaning that a difference on fluorescence signal between modified polymer and underlying COC is detected. A larger fluorescence is recorded on the COC areas in which the protein is more likely adsorbed, whereas on the PEG-modified PS-$N_3$ square structures a lower FITC signal is found. However, it is also notable that the physical adsorption of FITC-avidin onto the squares is not completely prevented since a consistent fluorescent signal is still detected. There are many possible reasons for that behavior: the concentration of PEG-alkyne molecules used for click-chemistry functionalization may be too low; or the PEG chain length is too short to create a proper steric hindrance; or the functionalization efficiency is low and partially modified surfaces are achieved. Although, the reaction of PEG-alkyne species and azide groups is selective and no PEG adsorption is found on COC regions; this means that, due to the lack of azide groups on COC surface, the click-chemistry in these regions cannot take place and a consequent protein adsorption is detected. A different outcome is observed when PS-$N_3$ structures are functionalized with PEG-dialkyne moieties: from water contact angle measurement it comes out that an increase on hydrophilicity of these structures is found with a decrease in water contact angle. This result already suggests that the click-chemistry with PEG-dialkyne species was successful and a further incubation of FITC-avidin (20µg/mL) with the modified surface, results on protein repellent structures. The confocal micrograph of PEG-dialkyne modified PS-$N_3$ shows that no fluorescent signal is detected onto the surface of square structures while a strong signal of the dye is recorded on bare COC regions. These

combined results indicate that protein repellent surfaces can be obtained when a click-chemistry reaction is conducted with PEG-dialkyne molecules; the reaction takes place only where the azide groups are available and hydrophilic surfaces are generated. Further, PEG-alkyne compounds may be also used for this purpose but higher concentrations or PEG chain lengths should be used.

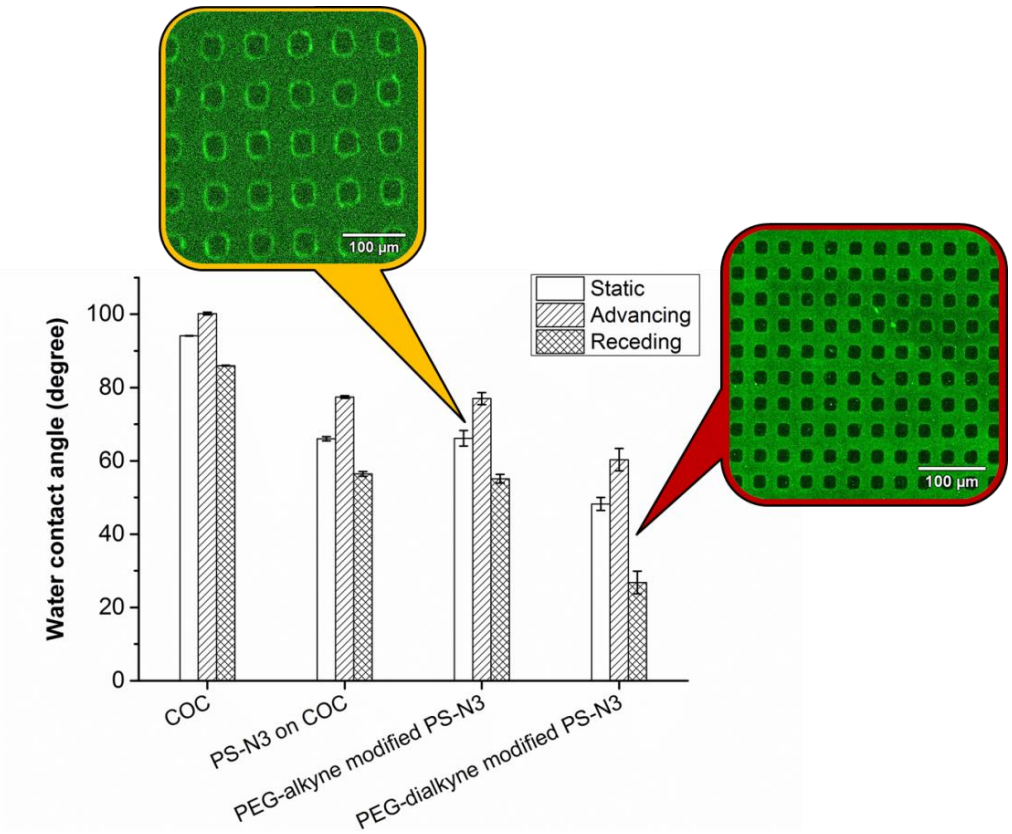


**Figure 3.19** Functionalization of patterned PS-$N_3$ surfaces (square structures with a diameter of 20µm) with PEG-alkyne and PEG-dialkyne molecules through click-chemistry reaction. The reactions are conducted by incubating a mixture of PEG-alkyne (800Da, 2mM) or PEG-dialkyne (1kDa, 2mM), $CuSO_4$ (1mM), NaAsc (15mM) in 30%v/v DMSO/water for 10h at room temperature. After washing, the samples are characterized through water contact angle measurement; then, 20µg/mL of FITC-avidin dissolved in PBS is incubated for 30min onto the surface and washed for 1h in PBS. The confocal micrographs show the fluorescence signal of FITC recorded by exciting at 488nm and collecting the emitted signal for wavelengths longer than 505nm.

In the light of these considerations, surfaces of PEG-coated COC can be produced in order to have a molecule repellent support; the fabrication of PEDOT-$N_3$ electrodes onto this surface will give the possibility to create conductive electrodes produced via printed dissolution and functionalize them after polymerization. Hence, the molecule repellent underlying layer will be presented in the gaps between electrodes. The surface reactivity corresponding to the areas between electrodes may be varied according to the final purpose of the platform; as shown, PEG-alkyne modification confers partial adsorption repellency to the COC support, and PEG-dialkyne functionalization induces a great

coverage of PS-$N_3$. Furthermore, the PS-$N_3$ modification with PEG-dialkyne molecules creates a chemical reactive surface due to alkyne groups available at the end of PEG chains. The chemical reactivity of these free terminal groups on PEG-dialkyne molecules is evaluated prior PEDOT-$N_3$ polymerization onto modified COC support. In specific, the reactivity of free alkyne groups on PEG-dialkyne functionalized PS-$N_3$ is tested by using multiple reaction steps: firstly, a click-chemistry reaction with biotin-$PEG_{(7)}$-$N_3$ is conducted in order to functionalize the available alkyne groups onto the surface; then, after a proper washing step, FITC-avidin is incubated. The second reaction will permit to visualize the biotin-PEG-$N_3$ modified surface thanks to the high binding constant between avidin and biotin. In Figure 3.20 is reported the schematic of reactions and compounds involved on the functionalization process. The sample is then analyzed through confocal microscopy to visualize whether fluorescence signal is localized onto PS-$N_3$ surface. The enlargement shows a confocal micrograph of FITC-avidin fluorescence on the sample, and on the right a 3D plot of the recorded picture is included. The fluorescence signal is highly concentrated onto the surface of PS-$N_3$ square structures, especially at the edges of the polymer. This result suggests that, even though a passive adsorption of FITC-avidin is still localized on COC support, the immobilization of fluorescent molecules onto the patterned polymer is augmented through click-chemistry reactions and biotin-avidin covalent interaction. However, the originally square shaped PS-$N_3$ pattern seems to be lost since circle-like structures are detected when chemical functionalization takes place. It should be also considered that three sequential functionalization processes are conducted on the same polymer area; thus, click-chemistry ensures a selective modification of azide-compounds and its utility may be applied for further functionalization.

In this study, it was presented an approach based on PS-$N_3$ coating of COC support and subsequent functionalization via click-chemistry reaction. Depending on the final purpose of a certain application, the polymer film can be modified with different molecules; in particular here it was proposed PS-$N_3$ functionalization with PEG-alkyne and –dialkyne moieties. As stated just above, according to the goal on building our platform, one of these two molecules may be preferred to the other. For example, the need of a stable repellent coating onto PS-$N_3$ surface may be achieved by covalently binding PEG-alkyne species; otherwise, when a certain functionality is required at the surface, PEG-dialkyne molecules should be chosen due to their steric hindrance and free available alkyne groups. These compounds are only examples of many existing functional groups that may be selected. Although this method for COC coating and modification can be adopted for other purposes, our goal is to produce a COC surface that is chemically reactive and discourages physical adsorption of compounds whether post-fabrication modifications will occur.

Moreover, the use of UV-light assisted patterning of PS-$N_3$ films permitted to locally functionalize the polymer according to the presented clicked molecules. For our application, a homogeneous, molecules repellent and chemical reactive PS-$N_3$ film is required. The polymerization of PEDOT-$N_3$ on modified COC support requires a flat surface in order to create spatially defined micro-electrodes. In fact, the

presence of patterned PS-$N_3$ will have a negative effect on the electrodes fabrication, thus no structures of PS-$N_3$ are produced rather a flat thin film of PS-$N_3$ is applied.

An alternative simple, cheap and fast method for COC coating in order to guarantee the needed characteristics is based on the direct coating of support with PEG-based molecules and the method is described in the following paragraph.

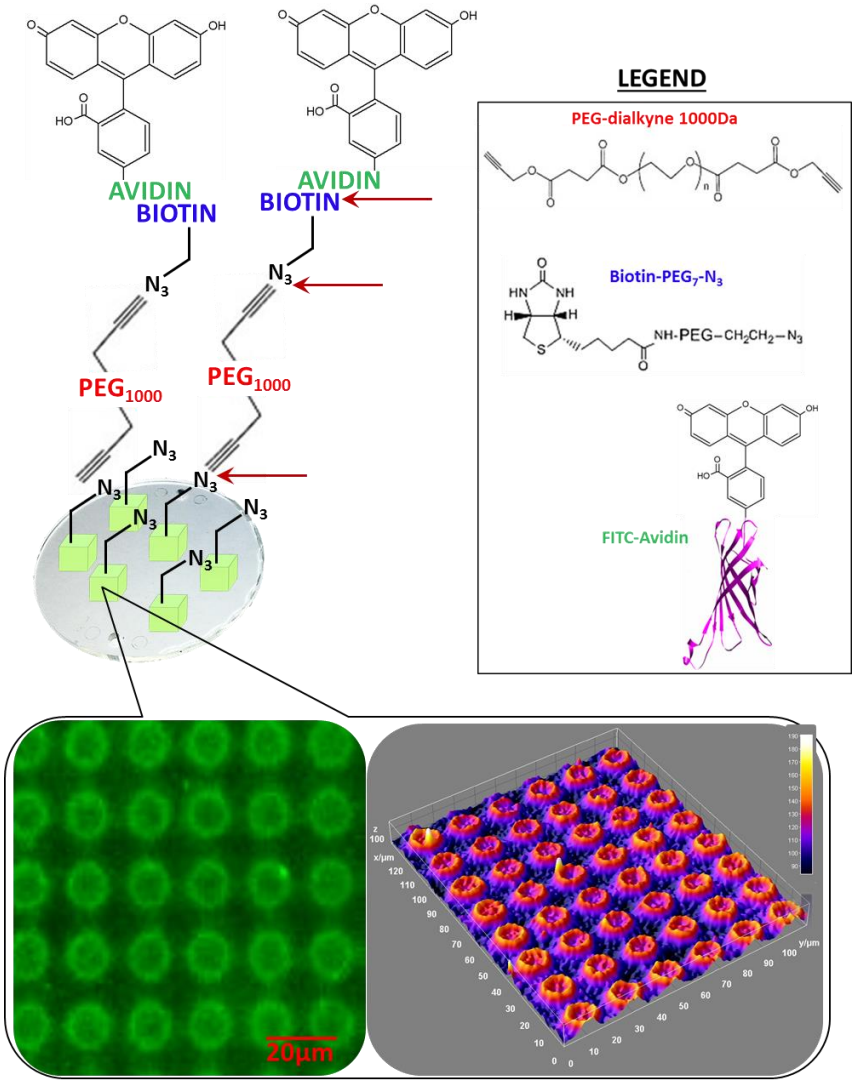


**Figure 3.20** Illustration of the reactions involved on the modification of PS-$N_3$ pattern (squares having a diameter of 10µm) through click-chemistry reactions and avidin-biotin covalent bonding. On top it is reported a schematic of the mechanism used to functionalize the patterned polymer (the red arrows indicate the chemical groups involved in each functionalization step). A first click-chemistry is conducted using PEG-dialkyne (1kDa, 2mM), $CuSO_4$ (1mM), NaAsc (15mM) in 30%v/v DMSO/water; then, a second click-chemistry is applied to modified the free alkyne groups of PEG with biotin-$PEG_{(7)}$-$N_3$ (2mM) using the same reaction conditions. The exposed biotin molecules at the surface are thus available for a further interaction with FITC-avidin (20µg/mL). The sample is washed with PBS and the fluorescence intensity of FITC is recorded using an excitation wavelength at 488nm and collecting the emission at wavelengths longer than 505nm. The confocal micrograph of the surface and the 3D fluorescence plot are reported on the bottom part of the figure. A small legend with the chemical structures of the used components is depicted on the right side.

#### 3.3.3.2 PEG-coating of COC for PEDOT-$N_3$ deposition

The production of modified COC supports for minimizing nonspecific molecules adsorption can be achieved utilizing an alternative process to the one based on PS-$N_3$ coating and functionalization. This method consists on the PEG coating of support surface through covalent immobilization. In general, the approaches used to create PEG coatings include `grafting to´ or `grafting from´ mechanisms.[189] With grafting from the surface, a PEG layer is formed via polymerization initiated at the surface which can result on a high yield of grafting but less defined coating thicknesses. Grafting to the surface covalently binds PEG molecules onto the substrate which can form a stable coating of defined thicknesses and homogeneity but a low grafting density may be induced due to steric hindrance surface during coupling.[190] In our group, a one-step `grafting to´ method was developed to produce low-binding PEG surface coatings on different surfaces.[190,191] This method is based on photo-chemically immobilizing PEG coatings onto a surface in an aqueous environment in presence of a water soluble photo-sensitizer, benzophenone amine. When PEG and benzophenone (Bz) molecules dissolved in aqueous environment are exposed to UV-light, which has a broad illumination maximum from 330-380nm, using a one-step process, a covalent immobilization of PEG molecules is achieved (Figure 3.21). The coupling of PEG molecules onto the surface is directed by UV-assisted formation of amide bonds between the activated NHS ester group on PEG molecules and the amine group of benzophenone. Under UV illumination, the benzophenone forms bi-radical species that can extract hydrogen from any carbon-hydrogen containing molecules at the surface or in solution, including benzophenone itself.[192] These activated radicals can then recombine with other radicals and form a new bond onto the surface. Benzophenone can be coupled to the surface via its methylene group. The formation of Bz-PEG conjugate is induced by radical species that are responsible for the amide bond arrangement without the need of coupling agents, such as ethyl(dimethylaminopropyl) carbodiimide (EDC), which are normally used to form amide bonds. The process of PEG coating of COC surfaces depends on many parameters, for instance the UV exposure time, the Bz (4-benzoyl benzylamine hydrochloride) and PEG-NHS (poly(ethylene glycol)N-hydroxysuccinimide) concentrations and the PEG chain length. Once the support is PEG coated, the propensity of surface to adsorb molecules is evaluated using a protein as model molecule. From a previous work in our group (Larsen *et al.*[190]), a concentration of 2.5mg/mL Bz and 7.5mg/mL PEG-NHS (MW= 700Da) were found to be the optimal amounts for coating of different supports. A solution of Bz and PEG-NHS is dissolved in PBS and a COC support is immersed on that mixture. The sample is exposed to UV-light (emission range between 330 and 380nm) for 30min and, after a washing step, the water contact angle is measured to estimate the hydrophilicity degree of the surface (Figure 3.22A). Furthermore, Larsen *et al.* incubated a concentration of BSA between 0-1mg/mL on treated and un-treated COC surfaces and the nitrogen content of different samples was measured by X-ray photoelectron spectroscopy (XPS), as shown in Figure 3.22B.[190]

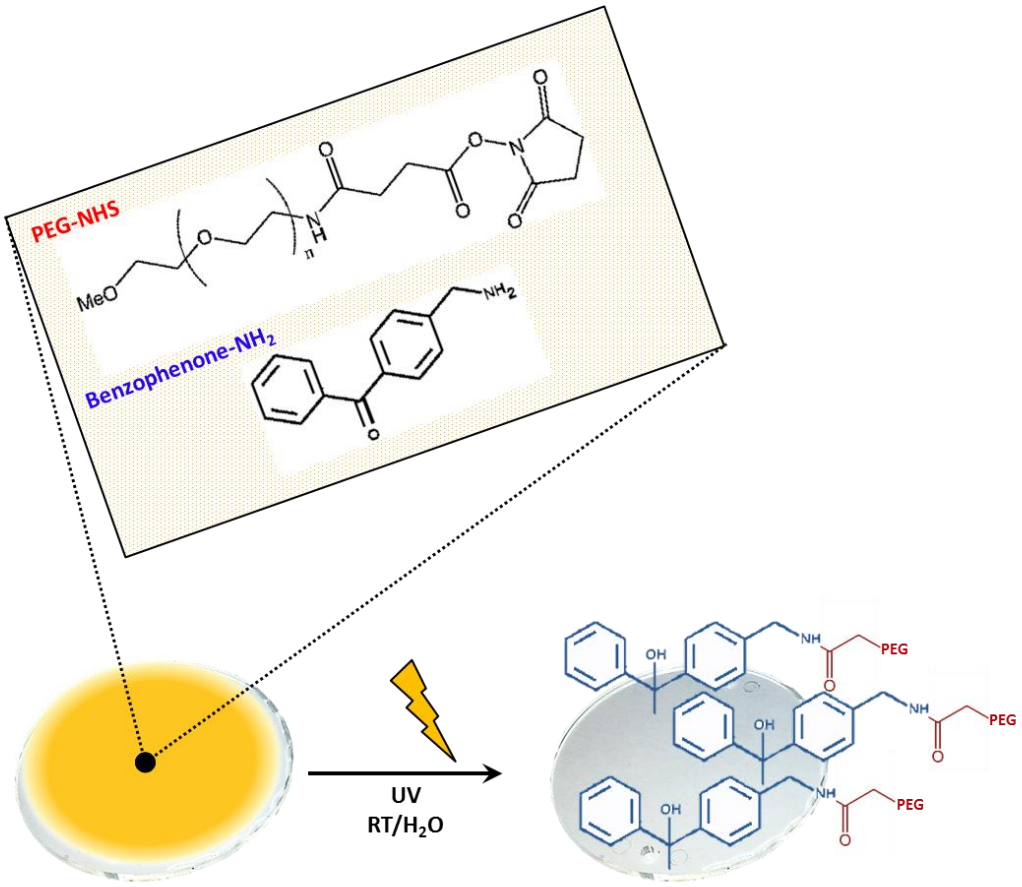


**Figure 3.21** Schematic of PEG-coating of cyclic olefin copolymer using UV-light assisted "grafting to" method. A solution of PEG-NHS and Bz is poured onto COC surface and the sample is illuminated to UV-light (emission range between 330-380nm) for 30min. After washing a PEG coating is covalently attached onto the support surface. The photochemical immobilization of PEG is conducted in aqueous environment at room temperature. When Bz is exposed to UV-light, bi-radical species are produced and they are responsible for the extraction of hydrogen atoms from any carbon-hydrogen containing molecules. These radicals can recombine with other radicals and induce the formation of new bonds at the surface or in solution. The Bz itself can be bound to the surface through its methylene group. PEG-NHS is indicated in red and Bz-amine in blue.

In Figure 3.22A it is reported the water contact angle of various modified COC surfaces. In order to compare the hydrophilicity of the surface obtained from the coating described in the previous paragraph, COC supports modified with PS-$N_3$ and PEG-dialkyne functionalized PS-$N_3$ surfaces are also reported. The covalent immobilization of PEG through photo-sensitizer and UV-light reaction results on a hydrophilic COC surface, more hydrophilic than that obtained through PS-$N_3$ deposition and consequent functionalization. It should be also considered that the process involving PEG-NHS and Bz requires a single-step reaction, whereas the previously described approach implies PS-$N_3$ deposition and further PEG functionalization through click-chemistry reaction.

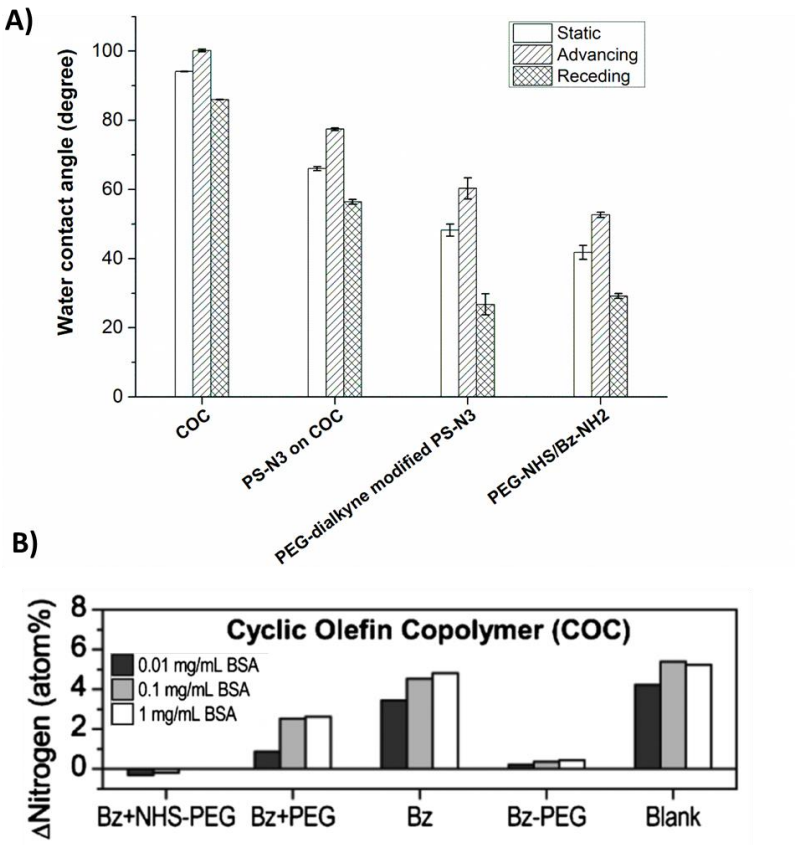


**Figure 3.22** Characterization of PEG-coated COC surfaces through water contact angle measurement and X-ray photoelectron spectroscopy (XPS). (**A**) Water contact angle measurement of the reference (bare COC), PS-$N_3$ film deposited onto COC, PEG-modified PS-$N_3$ layer and PEG-coated support via Bz+PEG-NHS photo-chemical immobilization. The contact angle measurements obtained from the method described in the previous paragraph are also reported in order to compare the surface hydrophilicity obtained with different strategies. (**B**) XPS analysis of increasing concentrations of BSA incubated on modified COC supports. Results show the difference in nitrogen surface concentration, measured by XPS, before and after incubation with nitrogen-containing BSA for 4 h on modified COC. This study was conducted by Larsen *et al.*[190]

In this study conducted by Larsen *et al.*,[190] the PEG-coated COC surfaces were incubated with increasing concentrations of protein (bovine serum albumin, BSA) for 4h. After washing, the surfaces were analyzed by XPS: the difference in nitrogen surface concentration before and after incubation with BSA was taken as a measure of the amount of adsorbed protein, with the caveat that polyimide contains nitrogen in its molecular structure. As reported in Figure 3.22B, the amount of protein adsorbed on bare COC increases as the incubated BSA concentration increased. Contrarily, a negligible amount of protein was found on PEG-coated COC surface when a Bz and PEG-NHS solution were UV-exposed to create a protein repellent layer. A similar result was observed when a pre-formed UV-light Bz-PEG conjugate was re-exposed onto the surface. In absence of PEG or NHS group, a high amount of adsorbed protein was detected suggesting the importance of reagent chemical reactivity and the need

of PEG molecules to create a steric hindrance at the surface. Therefore, the application of PEG molecules together with a photo-sensitive compound (Bz) permits to obtain protein repellent PEG-coated COC surfaces when exposed to UV-light using a one-step process in aqueous environment.

As previously pointed out, the presence of chemical reactive groups onto the modified support surface may be useful for further modifications. Although the use of PEG-NHS permits to obtain protein repellent and hydrophilic surfaces, the poor reactive groups at the chain end may be not useful for certain purposes. However, other PEG-based molecules may be applied for PEG immobilization on COC support via Bz-amine photo-chemistry. For this reason, the coating of COC supports is evaluated using a solution of benzophenone-amine and PEG-diacrylate (PEGDA) which contains an acrylate group at each end of the PEG chain; the solution is exposed to UV-light in order to induce radical species formation. As described above, the illumination of Bz-amine molecules enhances the production of Bz-PEGDA conjugates which are immobilized onto the surface. Once the support is PEG-coated, available free acrylate groups are presented at the surface and subsequent functionalization may be applied. A preliminary test of PEGDA coating with Bz-amine of COC support is conducted: different concentrations of PEGDA (2 – 5 – 10 mg/mL; MW=5kDa) and benzophenone-amine (1 – 2.5 – 5 mg/mL) are dissolved in PBS and UV-exposed for 30min onto the support surface. After washing, the water contact angle of surfaces is measured and 20μg/mL of FITC-BSA is incubated on each sample to determine the fluorescent signal coming from passively adsorbed protein (Figure 3.23). After 30min of exposure, a thin film of PEGDA is immobilized onto the surface, as confirmed by water contact angle measurements of samples. A hydrophilic surface is produced for all combinations of PEGDA and Bz amounts even though in the graph it is reported only the contact angle of COC discs prepared with a concentration of 5mg/mL PEGDA and various Bz amounts. Further, the values of contact angle achieved with PEGDA 5kDa are comparable to those obtained using PEG-NHS as grafted polymer. As shown in the plot, despite the increasing concentration of benzophenone, the water contact angle remains constant suggesting that the amount of Bz (1mg/mL) is enough to create a PEGDA-coated COC. When fluorescent BSA is incubated in each sample, a high signal is observed for bare COC disc while a lower fluorescence is recorded for modified surfaces. These results indicate the possibility to use PEGDA as coating polymer and a deeper study of the process may permit to produce surfaces with free available acrylate groups discouraging molecules adsorption. To further improve the PEGDA grafting density onto the surfaces, a multi-step process is adopted: a solution of 5mg/mL PEGDA and 1mg/mL Bz is exposed for 30min onto the disc; then it is washed and a fresh solution of PEGDA-Bz (5:1) is illuminated again for 30min onto the same sample. The process is repeated for a third time resulting on a three-layers coating achieved in multiple steps.

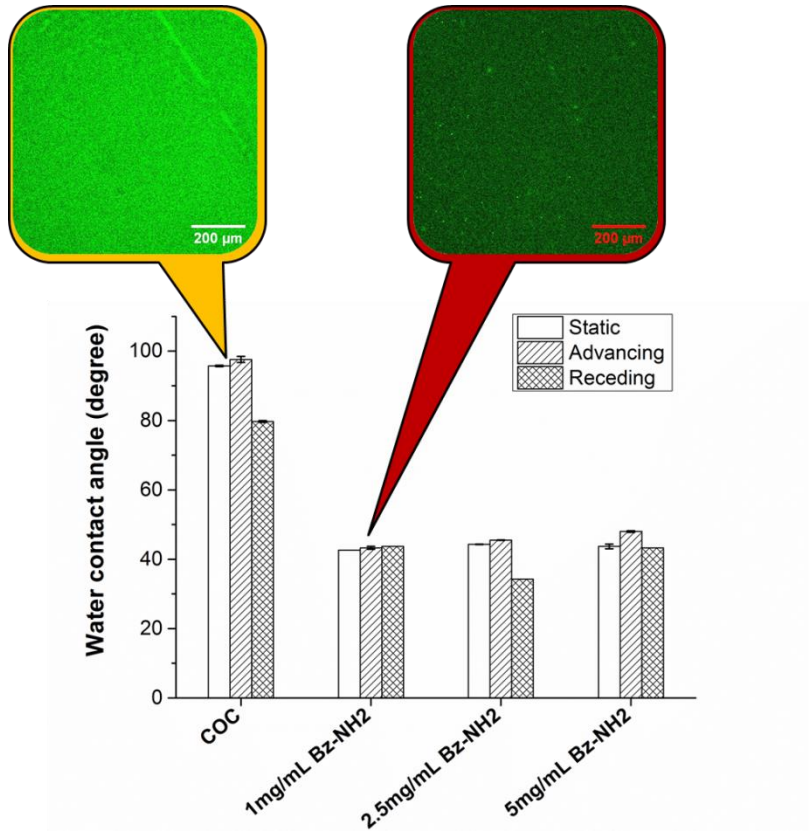


**Figure 3.23** Characterization of PEGDA-coated COC discs through water contact angle measurement. Different concentrations of PEGDA (2 – 5 – 10 mg/mL, MW=5kDa) and Benzophenone (1 – 2.5 – 5 mg/mL) are UV-exposed for 30min onto support surface. After washing, the contact angle is measured: in the plot are reported the values obtained when a concentration of 5mg/mL PEGDA and three different amounts of Bz are used (including the reference bare COC). These samples are then incubated with 20µg/mL FITC-bovine serum albumin (BSA) for 30min and after washing, the fluorescent signal coming from protein molecules physically adsorbed onto the surfaces is recorded. The confocal micrographs are obtained by using an excitation wavelength at 488nm and the signal is collected for wavelengths longer than 505nm.

In Figure 3.24, the water contact angles of PEGDA-coated COC discs formed respectively by a single, double and triple layers using fresh 5mg/mL PEGDA and 1mg/mL Bz solutions, are reported. As before, 20µg/mL FITC-BSA is then incubated for 30min onto each modified surface and the fluorescence of adsorbed protein molecules is detected by confocal microscopy. The production of multi-layers onto the COC disc does not affect the hydrophilicity of the surface since the water contact angle of double and triple layers is comparable to that composed of a single layer. However, a great improvement of PEGDA grafting coverage of discs results from the amount of FITC-BSA passively adsorbed onto the surfaces of double and triple layers. In fact, as the number of PEGDA coatings increases, a consistent reduction of BSA adsorption is observed until almost completely protein repellent surfaces are formed (triple PEGDA layers).

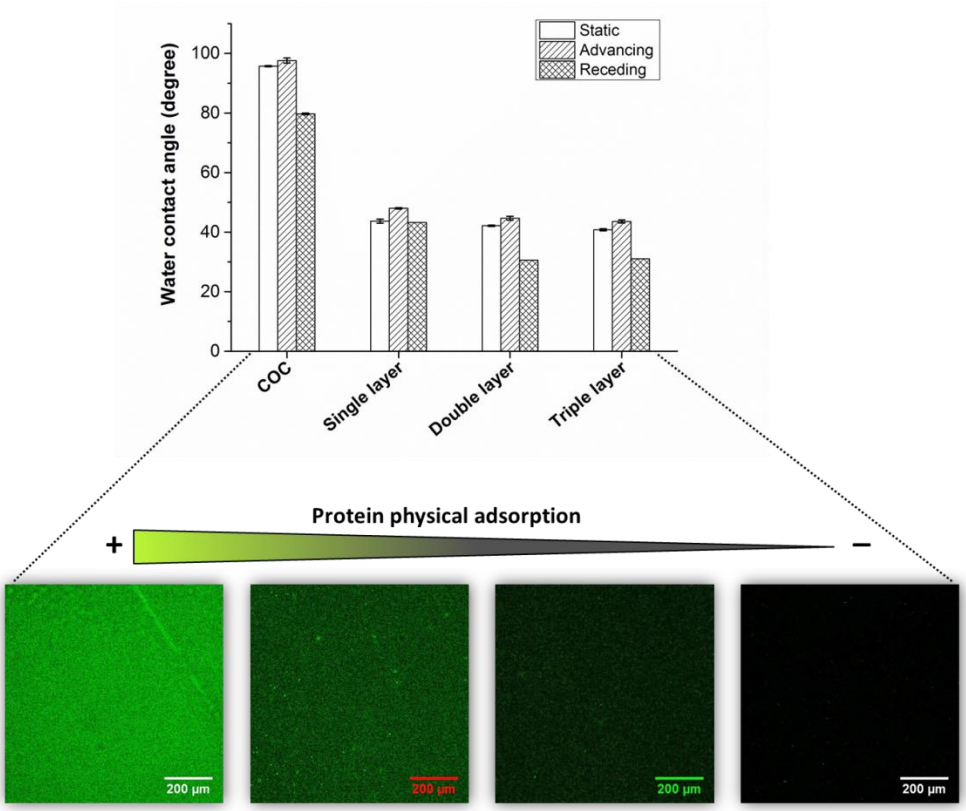


**Figure 3.24** Characterization through water contact angle and confocal microscopy of multi-layer PEGDA coating. PEGDA-coated COC discs are produced by a multi-step process in which fresh solutions of 5mg/mL PEGDA and 1mg/mL Bz are exposed for 30min to UV-light repeating the procedure for one, two and three times (a washing step is included between a coating process and the other). The water contact angle values of single, double and triple-layers are really similar since the hydrophilicity conferred to the surface is comparable due to equal PEGDA-Bz solutions used, in terms of chemical composition. Then 20µg/mL FITC-BSA is incubated on each sample and the fluorescent signal is detected by confocal microscopy. As shown from the confocal micrographs, as the number of PEGDA coatings increases, a consistent reduction of adsorbed molecules is found.

In the light of the promising results obtained from COC coating with multiple PEGDA layers, triple PEGDA-coated surfaces are used to evaluate the chemical reactivity of free available acrylates onto their surface. Therefore, samples composed of three PEGDA layers are produced and incubated with a concentration 1%v/v of bromine dissolved in water ($Br_2$) for 30min and after reaction, they are washed with water. The incubation of bromine with free acrylate groups onto the surface results on a bromination of acrylate moieties through classical halogenation, based on the electrophilic addition of bromine atoms to alkene groups (Figure 3.25A). Once the bromine molecules are bound to the available acrylates, the modified COC discs are analyzed by X-ray photoelectron spectroscopy (XPS) measuring the atomic composition at the surface. The content of oxygen, carbon, nitrogen and bromine is thus evaluated (Figure 3.25B). As reported in the plot, an increase of oxygen content is detected when COC is coated with PEGDA compare to bare COC (in which oxygen should not be detected since

Topas is composed of only carbon atoms). Furthermore, really small percentages of nitrogen are found on modified discs, suggesting that low amount of benzophenone may remain entrapped within the coating layers and a prolonged washing step may be needed. Particularly interesting it is the content of bromine on each sample: as the number of PEGDA layers composing the coating increases, a proportional amount of bromine is detected onto the surface. This behavior could be due to a higher PEGDA grafting density compare to a single layer, thus a larger number of free available acrylate groups is detected.

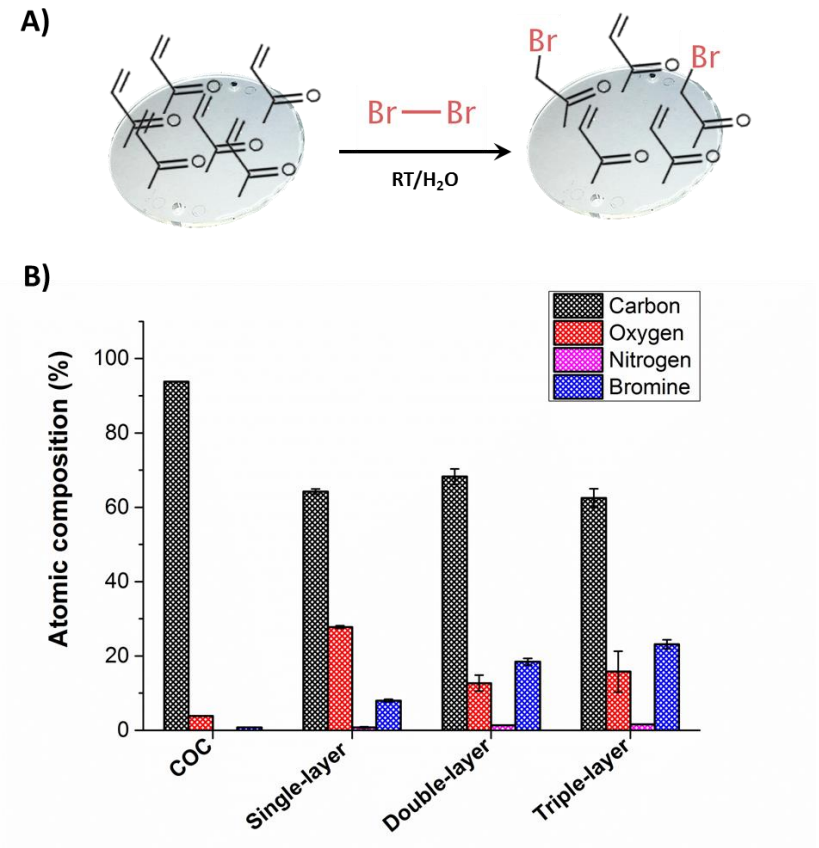


**Figure 3.25** Multi-layer PEGDA coatings are characterized by bromination and consequent X-ray photoelectron spectroscopy measurement in order to evaluate whether acrylate groups onto surfaces are chemically reactive. (**A**) Schematic of bromination reaction: this process involves bromine atoms incubated at a concentration of 1%v/v in water and free alkyne moieties. Through electrophilic addition of bromine atoms to acrylate groups, bromines are bound to the surface in an aqueous environment and at room temperature. (**B**) After washing, the samples are analyzed by XPS and their content of oxygen, nitrogen, carbon and bromine is measured.

The photochemical immobilization of PEGDA molecules onto COC discs aided by photosensitizer and UV-light exposure is a one-step process that is conducted in aqueous environment at room temperature. Hence, the easiness, low-cost and high efficiency of PEG molecules grafting render this process extremely useful for fabricating protein repellent coating and chemical reactive surfaces. For

these reasons, this surface modification is adopted to produce functionalized COC discs which are subsequently utilized for PEDOT-$N_3$ electrodes micro-fabrication. After PEDOT-$N_3$ *in situ* polymerization onto a modified support and printed dissolution of the thin film to produce micro-electrodes, the underlying PEG-coating should ensure a poor chemicals adsorption and post-fabrication functionalization. In the next paragraph the process involved on electrodes production and spatially-controlled chemical modification of the surface is described in more detail.

## 3.4 PEDOT-$N_3$ micro-electrodes fabrication on PEG-modified COC support

In the previous paragraphs, a detailed characterization of two main methods for COC coating and PEDOT-$N_3$ micro-electrodes fabrication on bare COC was described. The integration of these processes will ensure the realization of a platform in which conductive polymer micro-electrodes are generated on a low-binding PEG-coated surface. In addition, such system will present in-register surface chemical reactivity; this means that corresponding to electrodes areas, azide groups will be presented at the surface while in the gaps between electrodes reactive acrylate moieties will be found after printed dissolution. The choice of use agarose printed dissolution instead of other micro-fabrication techniques is mainly due to the possibility of producing structures on a pre-formed coating without damaging its chemical functionality. Therefore, inter-digitated PEDOT-$N_3$ micro-electrodes with a dimension of 100μm in width are fabricated through printed dissolution on three-layer PEG-coated COC support and the resulting platform is characterized through water contact angle, X-ray photoelectron spectroscopy and microscopy. PEGDA-based coating, rather than modified PS-$N_3$ technology, is chosen because fast, cheap and with sequential steps, low-binding PEGDA-coatings are achieved. In Figure 3.26 it is shown a schematic of the process used for the fabrication of PEDOT-$N_3$ electrodes onto PEG-coated support. By using a multi-step process, COC support is modified with a triple layer of PEGDA (5kDa) and Bz upon UV-exposure; after washing, a thin film of PEDOT-$N_3$ is *in situ* polymerized onto the surface through spin-coating deposition. The pre-polymer solution is composed of EDOT-$N_3$ monomer, Fe(III)TsO and butanol which form a homogeneous thin polymer layer (circa 150nm). The film is then exposed to agarose stamping: 10% w/w agarose stamp is pre-formed by melting the solution onto the surface of silicon mold. Once the system is cooled down, a negative replica of the mold design is found onto the agarose stamp surface. The pattern consists of two sets of inter-digitated electrodes 100μm wide, 0.5cm long and with 100μm spacing. The formed stamp is soaked in an aqueous solution containing the oxidizing agent (sodium hypochlorite, NaOCl) and after 15min in the stamping solution, the stamp is pressed gently onto the PEDOT-$N_3$ surface to establish a contact and left there for 1min. After printing the sample is washed with a proper post-stamping washing procedure which is made of an aqueous solution containing a non-ionic detergent,

Triton X-100, and a solution 10%v/v Fe(III)TsO in MQ water. The detailed description of printed dissolution procedure is reported in the Experimental section of this chapter. Once the sample is washed, the film areas that were in contact with the stamp are removed during the washing, whereas the regions of PEDOT-$N_3$ un-exposed to the stamp remain onto the surface to form two sets of inter-digitated electrodes.

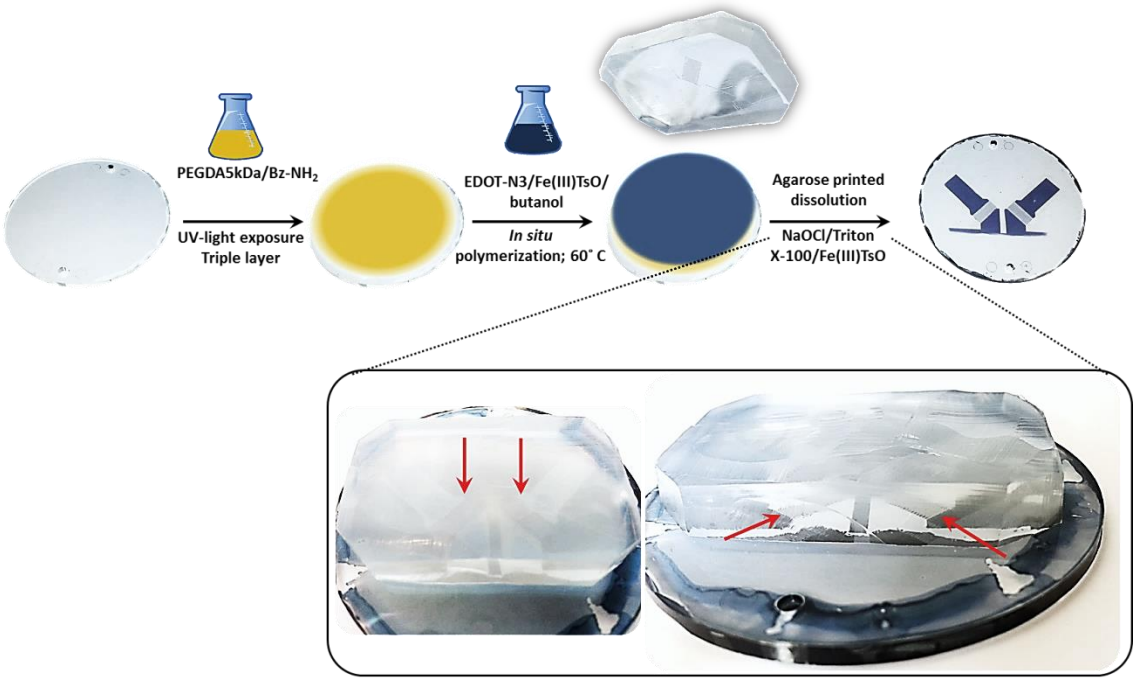


**Figure 3.26** Schematic of the process involved on the fabrication of micro-electrodes from a thin layer of PEDOT-$N_3$ polymerized on a modified COC support. The Topas disc is functionalized through multi-step process with PEGDA (5kDa) and Bz via UV-assisted exposure. A thin film of PEDOT-$N_3$ is *in situ* polymerized onto the functionalized support by spin-coating deposition. An agarose stamp is molded according to the pattern design of a silicon mold: two sets of inter-digitated electrodes (100µm wide, 0.5cm long and 100µm spacing) are formed onto the surface of the stamp. Then, it is immersed into a stamping solution composed of aqueous sodium hypochlorite (NaOCl) for 15min. The stamp is quickly dried in a stream of nitrogen and put it in contact with PEDOT-$N_3$ surface. After 1min the stamp is detached and soaked again into stamping solution for re-use. The printed sample is washed with Triton X-100, Fe(III)TsO and water to remove the degraded polymer regions that were in contact with the stamp. The photos show the surfaces contact between the agarose stamp and the sample: from the top side of stamp is possible to see when the degradation process starts and completes. The red arrows indicate inter-digitated electrodes onto the agarose stamp.

Agarose has been chosen as stamping material because of its great mechanical stability and fast internal diffusion due to the high water content (85-98%); thus, when it is immersed on the stamping solution within few minutes an impregnation of the stamp with NaOCl is achieved. The chemical dissolution through sodium hypochlorite is known to over-oxidize and degrade the conductive

polymer poly(3,4-ethylenedioxythiophene) (PEDOT) leading also to a consistent loss of conductivity corresponding to the areas in contact with the stamp.[185,193] The mechanism by which PEDOT degrades when exposed to NaOCl is based on the oxidation of the thiophene ring to thiophene-1,1-dioxide followed by ring-opening and loss of $SO_4^{2-}$ (Figure 3.27).[194] Hypochlorite is also known to degrade conductive polymer polypyrrole[195] and in general it attacks double bonds of organic compounds. As also reported by Hansen *et al*., the deactivation of PEDOT films when in contact with the stamp ranges from few seconds to minutes depending on the film thickness and polymer support.[185] Furthermore, it has been proved that the agarose stamp may be re-used several times by immersing it onto aqueous sodium hypochlorite solution between a printing cycle and other one.

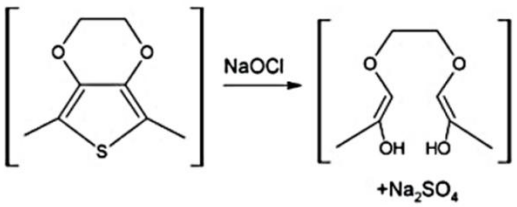


**Figure 3.27** Chemical structures of 3,4-ethylenedioxythiophene, the building block of PEDOT (in the left), and the thiophene ring-opening and splitting off of $SO_4^{2-}$ (in the right). This process is caused by the contact of sodium hypochlorite (NaOCl) during printed dissolution, and it results on a chemical over-oxidation of PEDOT in the areas in contact with the stamp. A degradation and loss of conductivity at these points is observed. Reproduced from [185].

From a previous work in our group, an optimized stamping solution and post-printing washing procedure have been established, and these methods were utilized for the removal of PEDOT films from COC support.[196] Here, the same conditions are adapted for printed dissolution of PEDOT-$N_3$ films on modified COC support and bare COC. Hence, Topas discs are coated with a triple layer of PEGDA (5kDa) and a thin film of PEDOT-$N_3$ is formed onto the support surface; then the samples are printed through agarose stamping. The same procedure is followed for the fabrication of micro-electrodes on an un-coated COC support. In Figure 3.28 it is reported the water contact angle of samples after their PEGDA-grafting, PEDOT-$N_3$ spin-coating, and printed dissolution by measuring the contact angle of fabricated electrodes and of the underlying modified and un-modified support. As previously discussed, the hydrophilicity of COC surface increases when PEGDA molecules are immobilized onto it. The contact angle of PEDOT-$N_3$ film on bare and modified support is comparable suggesting that the presence of a PEGDA coating does not affect the upper polymer layer. After printed dissolution the areas in contact with the stamp are removed and the underlying COC and modified-COC are exhibited. The contact angle value of exposed COC indicates a more hydrophobic surface than the native PEDOT-$N_3$ film; however, the contact angle is lower than that of bare COC. The same outcome is observed for the underlying PEGDA-modified support: it is expected a hydrophilic surface while the contact angle is really close to the PEDOT-$N_3$ electrodes value. The interpretation of these findings is quite difficult

since it may be that the agarose stamping process affects the chemical and physical properties of the layers, or it may be that PEDOT-$N_3$ is partially removed in correspondence of the contact areas with the stamp. Further, it could happen that the chemicals used for printed dissolution or those that are degraded during stamping, remain entrapped on the PEGDA coating and a prolonged washing step may be needed.

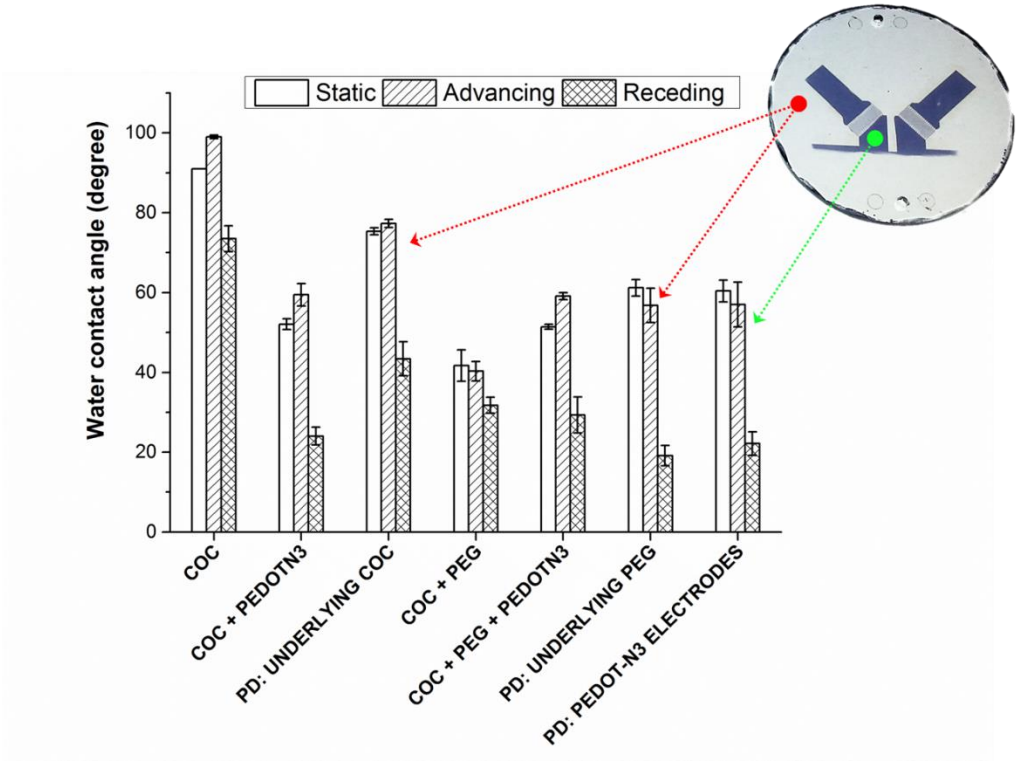


**Figure 3.28** Water contact angle measurement of various samples after PEGDA-coating, PEDOT-$N_3$ polymerization, and printed dissolution. Inter-digitated electrodes are fabricated both on modified and un-modified COC supports. After stamping, the contact angle of corresponding underlying film is measured (PD: UNDERLYING COC or PEG, where PD = printed dissolution), including also that of electrodes surface. In the graph, the red arrows indicate the regions of underlying layer in which the contact angle is acquired, and the green arrow corresponds to the area of electrode that is considered for the measurement.

In order to understand which of these hypotheses is plausible, X-ray photoelectron spectroscopy (XPS) measurement is conducted across the fabricated electrodes. For the analysis of surface atomic composition, a line scan mode is applied (spot size 50µm) and it is based on drawing a line of a certain length across the electrodes; at defined intervals (30µm) along the line, the atomic composition is recorded within the spot size. Thus, it is expected to see a profile of the atomic percentage across micro-electrodes since the spots selected along the line are partially overlapped (20µm) and a continuous signal is detected. In Figure 3.29, the optical micrograph of printed PEDOT-$N_3$ on bare COC and the corresponding XPS analysis are reported (A); in Figure 3.29B, the optical and spectroscopic characterization of electrodes on PEG-coated COC is included. The optical micrographs show an

electrode width and spacing that are circa 100µm; nevertheless, the structures formed onto PEG coating present some residues on PEDOT-$N_3$ surface and their coloration is not exactly the same of the original film. A clear difference between the two samples on the local atomic composition comes out from the two XPS plots: even though the optical picture of electrodes on COC suggests that defined structures and complete degradation of polymer in the gaps may be occurred, the XPS profile contradicts this observation. Corresponding to the electrodes areas, carbon, oxygen, nitrogen and sulfur are detected, while where the polymer is removed, an increase of carbon amount and a substantial decrease of the other atoms is observed. However, on the underlying COC, which is composed of 100% carbon, circa 10% of the total atomic composition is represented by oxygen and even if a smaller amount, also 2% sulfur. The XPS plot of electrodes formed onto PEG-modified surface is even worse than the previous one.

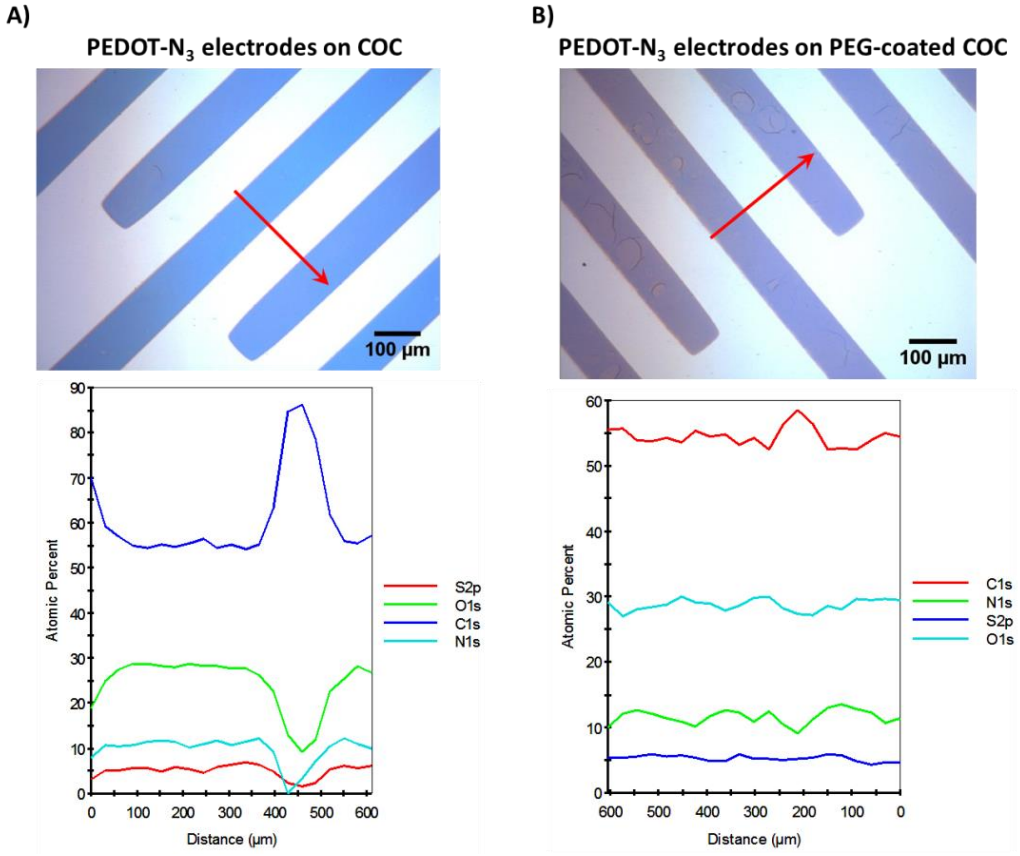


**Figure 3.29** Characterization of printed PEDOT-$N_3$ electrodes on bare COC (**A**) and on PEGDA-modified COC support (**B**). In the optical micrographs, inter-digitated electrodes have a width and spacing of 100µm and colored residues are observed on the electrodes surface (B). The red lines indicate the Line scan mode that is used to evaluate the local atomic surface composition of both samples through X-ray photoelectron spectroscopy (XPS). The measurement is conducted by drawing a line of a certain length across the electrodes. The samples are analyzed at defined positions along the line with an interval of 30µm and a spot size of 50µm; thus, for each spot there is a signal overlapping of 20µm. In such way, an atomic composition profile of surfaces will be recorded. In the XPS graphs, the atomic composition (oxygen, carbon, nitrogen and sulfur) is plotted against the position of the spot along the line.

The lack of an atomic composition profile suggests that the polymer is partially removed between electrodes. In fact, a constant amount of sulfur is detected across the entire length of the line scan and in correspondence of PEG underlying coating it is expected at least a reduction of nitrogen and sulfur content. Unfortunately, from these preliminary results it seems that the procedure of agarose stamping adopted for PEDOT-$N_3$ removal needs to be optimized. Moreover, as shown by XPS, the printed dissolution works better on bare support than those PEGDA-coated; the presence of immobilized PEGDA molecules may hinder the degradation process, or the adhesion of PEDOT-$N_3$ on such modified support may be stronger than the film adhesion on hydrophobic support, thus it results more difficult to remove. Various parameters affecting the printed dissolution method may be tuned: for instance, the oxidizing agent concentration on the stamping solution, or the non-ionic detergent concentration during the washing step, or the temperature at which the process takes place, or the stamping exposure time and many other factors. For example, as also reported from the experimental study of PEDOT stamping,[196] the substrate stamped without detergent in the stamping solution and/or during washing procedure, were found to contain a significant amount of oxygen and sulfur between the electrodes indicating the presence of a coherent film. When detergent was added either in the stamp and/or in subsequent wash, the printed film was dissolved and washed off exposing the underlying COC. It was observed that the presence of Triton X-100 in the stamp helped the removal of over-oxidized PEDOT from COC accelerating also the process. Contrarily, when detergent was included on the stamping solution for PEDOT-$N_3$ printing on COC, a deceleration of stamping was observed; thus, the role of detergent was found to be related to the oxidation of PEDOT at the interphase with the support. A relevant factor that was tested previously in our group, was the selection of a proper solvent for the removal of over-oxidized PEDOT from COC.[196] The PEDOT or PEDOT-$N_3$ films were observed to be resistant to a number of polar solvents such as water, ethanol, iso-propanol, n-butanol, acetone, acetonitrile and 1,4-dioxane. When PEDOT-$N_3$ films were patterned with an agarose stamp soaked in NaOCl, an orange-brown film was produced; by washing them after stamping with DMF or DMSO solvent, a transparent film was obtained. However, DMF and DMSO are quite effective solvents for dissolving a large number of polymers, therefore their applicability for removal of stamped PEDOT materials is limited. It was observed that DMSO/water mixtures up to 90%v/v DMSO were able to prevent the dissolution of some supports such as polystyrenes. Although many parameters were previously tested in our group, few successful results were obtained on the agarose stamping process of PEDOT-$N_3$ films. Here, different factors influencing the printed dissolution are considered in order to create defined micro-electrodes and also understand the mechanisms involved on the removal of PEDOT-$N_3$ films from COC. PEDOT-$N_3$ films on PEGDA-coated COC supports are produced and printed by varying some experimental conditions during the stamping and/or the washing processes. Different Triton X-100 concentrations, in the stamp and in the washing solution, and various temperatures at which the washing step occurs, are evaluated (Figure 3.30). After micro-electrodes fabrication the samples are characterized through XPS by measuring the atomic composition of the underlying

support. In Figure 3.30, the experimental conditions and the resulting XPS atomic compositions are reported. As described in the table, the stamping solution is composed of constant concentration of the oxidizing agent (NaOCl) and variable Triton X-100 amount (0.1 or 1%v/v). The washing solution is formed of an aqueous solution containing the detergent and Fe(III)TsO. After 5min of stamping, the samples are washed for 10min at variable temperatures through direct immersion of discs into the washing solution (which is heated up when required).

| Experimental factors | | | | | XPS atomic composition | | | | | |
|---|---|---|---|---|---|---|---|---|---|---|
| Stamping process | | Washing process | | | | | | | | |
| Triton %v/v | NaOCl %v/v | Triton %v/v | Fe(III)TsO %v/v | Temperature ° C | C | O | N | S | Fe | Cl |
| 1 | 2 | 1 | 4 | 22 | 54.35 | 26.25 | 11.34 | 6.66 | 0.92 | 0.48 |
| 1 | 2 | 0.1 | 4 | 22 | 51.69 | 32.65 | 9.11 | 5.22 | 0.79 | 0.54 |
| 1 | 2 | 1 | 4 | 50 | 51.98 | 31.49 | 10.00 | 5.81 | 0.33 | 0.39 |
| 1 | 2 | 0.1 | 4 | 50 | 55.48 | 27.42 | 10.79 | 5.51 | 0.36 | 0.44 |
| 0.1 | 2 | 1 | 4 | 22 | 68.56 | 15.09 | 9.80 | 5.12 | 0.85 | 0.58 |
| 0.1 | 2 | 0.1 | 4 | 22 | 51.8 | 29.91 | 11.26 | 5.55 | 0.81 | 0.67 |
| 0.1 | 2 | 1 | 4 | 50 | 54.62 | 31.41 | 8.28 | 4.96 | 0.27 | 0.46 |
| 0.1 | 2 | 0.1 | 4 | 50 | 57.73 | 25.41 | 10.58 | 5.15 | 0.31 | 0.82 |
| 1 | 2 | 1 | 4 | 55 | 69.02 | 19.01 | 8.08 | 3.43 | 0.15 | 0.31 |
| 1 | 2 | 1 | 4 | 65 | 75.45 | 11.95 | 10.25 | 1.76 | 0.09 | 0.15 |
| 1 | 2 | 5 | 4 | 55 | 82.71 | 10.41 | 4.53 | 2.05 | 0.19 | 0.11 |
| 1 | 2 | 5 | 4 | 65 | 81.53 | 11.70 | 5.09 | 1.49 | 0.11 | 0.08 |
| PEG- COC | | | | | 70.15 | 28.86 | 0.99 | | | |

**Figure 3.30** Study of the effect of different experimental conditions on the fabrication of PEDOT-$N_3$ electrodes on PEGDA-coated COC surfaces. When high Triton concentrations and elevated temperatures are applied, an increased efficiency on PEDOT-$N_3$ removal is observed. In the table it is reported also the atomic composition of the reference, PEGDA-coated COC and of the underlying modified supports after printed dissolution.

From the XPS results and the appearance of fabricated micro-electrodes (the samples are also analyzed through optical microscopy), some considerations about the effect of different experimental conditions can be drawn. In general, when the samples are washed at increasing temperatures, a lower amount of iron, sulfur, chlorine and nitrogen are detected. The presence of iron on the underlying support may be due to its adsorption onto the PEG coating and a prolonged washing step with water may be needed. Regarding chlorine atoms, they derived from the contact of the stamp with the sample and a small amount is found in all samples. The heating at increasing temperatures may enhance the evaporation of chlorine molecules resulting therefore on a lower amount of chlorine between electrodes. The presence of nitrogen and sulfur are clearly due to a partial removal of PEDOT-$N_3$ between the electrodes and, as the temperature and detergent concentration on the washing solution increase a lower amounts are observed. More interesting is the percentage of carbon detected in the underlying PEG coating: when a combination of high Triton concentration in the washing solution and elevated temperatures are applied, an increased carbon signal is found. Moreover, the use of 0.1%v/v Triton in

the stamping solution results in a decelerated removal process since the discoloration of polymer in the contact areas starts after 3min; on the other hand, a concentration 1%v/v of Triton in the stamp enhances the speed of dissolution and already after 1min from the contact, the film starts to be removed. However, even if the best results are obtained when high temperature and Triton concentration are applied, the fabricated PEDOT-$N_3$ electrodes still present some imperfections such as orange residues, and the size of polymer structures, especially the width and spacing, are smaller than the expected sizes (between 50 and 80µm rather than 100µm each). As shown in Figure 3.31, a colored polymer film is found in the gaps between electrodes when samples are washed at room temperature independently from the Triton concentration used in the stamping solution and during the washing (Figure 3.31A). More clear and clean surfaces are obtained when samples are heated at 55 or 65° C (Figure 3.31B).

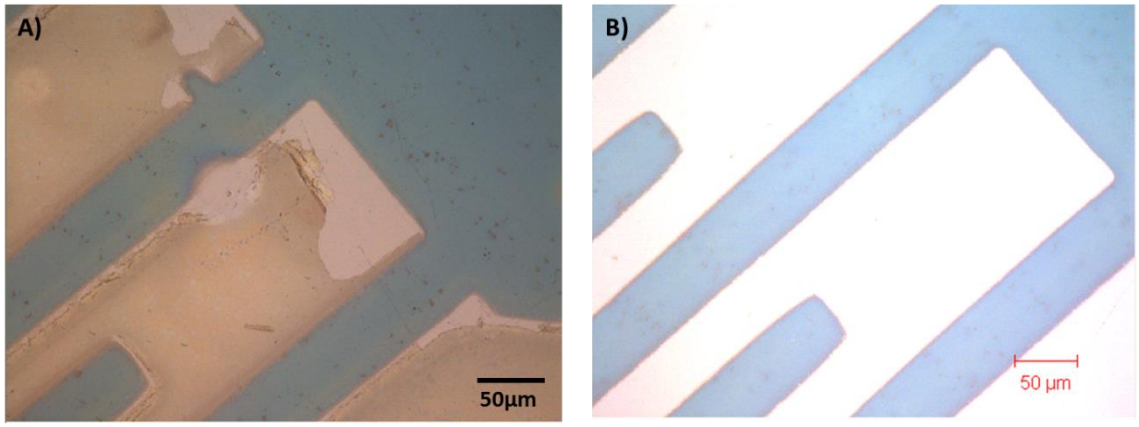


**Figure 3.31** Optical micrographs of printed PEDOT-$N_3$ electrodes on PEGDA-coated COC using a stamping solution containing 1%v/v Triton and 2% NaOCl and a washing solution made of 1%v/v Triton, 4%v/v Fe(III)TsO kept at room temperature (**A**); stamping solution made of 1%v/v Triton and 2%v/v NaOCl and a washing solution containing 5%v/v Triton, 4%v/v Fe(III)TsO heated at 65° C (**B**).

The fabrication of electrodes using the experimental conditions adopted in Figure 3.31B (stamping solution made of 1%v/v Triton and 2%v/v NaOCl and a washing solution containing 5%v/v Triton, 4%v/v Fe(III)TsO heated at 65° C) is repeated multiple times in order to evaluate the reliability of the process. A further washing step of samples is introduced after heating in the washing solution; in fact, a concentration of 60%v/v DMSO/water is used to remove the residues found onto the surfaces. Unfortunately, a degradation of the PEGDA coating and reduction of electrodes sizes is observed.

Potential improvements of the printed dissolution process may be achieved for instance, studying the interaction of PEGDA-coated COC with the upper film of PEDOT-$N_3$; a strong interaction of the support with the polymer may be make the removal process quite difficult. Furthermore, some limitations of the proposed stamping method should be considered; a relevant issue may be the risk of partial integration of the PEDOT-$N_3$ in the substrate, leading to a more complicated removal of polymer during

printed dissolution. For a better understanding of the reasons that lead to a un-complete PEDOT-$N_3$ removal, many samples consisting of PEDOT-$N_3$ film deposited onto bare COC supports are prepared according to the stamping procedure described above. Briefly, a thin layer of polymer is *in situ* polymerized on COC discs and after washing, it is subjected to agarose stamping utilizing the same inter-digitated electrodes design. A stamping solution composed of 1%v/v Triton and 2%v/v NaOCl is prepared; the agarose stamp is soaked into this solution and employed for electrodes fabrication. Then the samples are washed in an aqueous solution made of 5%v/v Triton and 4%v/v Fe(III)TsO at a temperature of 65° C. In Figure 3.32, the XPS atomic composition of underlying COC presented after printed dissolution is reported. Ten samples are stamped using the same agarose stamp and the atomic compositions of the areas in which PEDOT-$N_3$ is removed are analyzed.

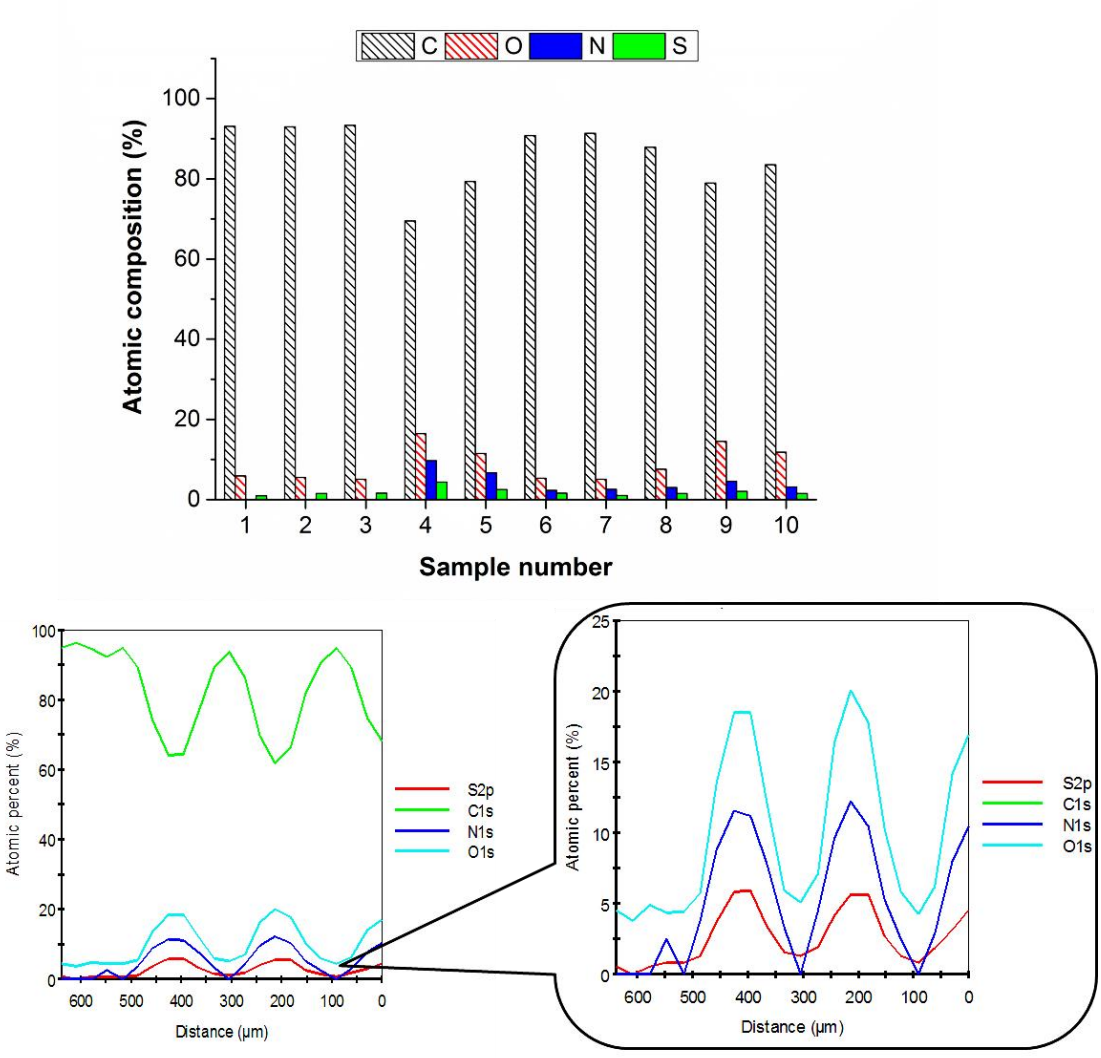


**Figure 3.32** XPS analysis of ten samples composed of PEDOT-$N_3$ film on bare COC which are stamped with the same re-usable agarose stamp. The amounts of chlorine and iron are not reported since their values are null. On the bottom of the figure, it is shown the atomic composition profile of one of these ten sample (number 4) obtained by drawing a line across the electrodes (spot size 50μm; interval spot 30μm). From the enlargement is possible to better visualize the content of sulfur, nitrogen and oxygen.

The resulting data from this experiment are quite promising even though the process is poorly reliable due to the high variability of results. However, in many samples the nitrogen composition is negligible meaning that PEDOT-$N_3$ film has been removed in the gaps; perhaps, this observation is not completely correct since a high amount of sulfur between electrodes is still found (less than 5% of the total atomic composition). According to the chemical interaction of NaOCl with PEDOT materials, in addition to the thiophene oxidation, the byproduct $SO_4^{2-}$ is also produced. It may be that $SO_4^{2-}$ is difficult to remove from the polymer electrodes and COC surface, but anyway it is difficult to predict the reason why after printing the sulfur is still present between the electrodes. Despite these considerations, from Figure 3.32 it is notable a clear atomic composition profile across the structures, whereas PEDOT-$N_3$ films printed on PEG-coated COC were characterized by a constant atomic composition profile across the surfaces. Therefore with these results we may conclude that the presence of PEG-coating below PEDOT-$N_3$ film affects somehow the ability of printed dissolution to remove desired PEDOT-$N_3$ areas. On the other hand, a low-binding PEG-coating is necessary for further selective molecules and nanoparticles immobilization onto electrodes surface. The physical adsorption of molecules onto a printed PEDOT-$N_3$ film on PEG-coated COC should be discouraged on the regions between electrodes. Thus, a concentration of 20µg/mL FITC-avidin is incubated on patterned PEDOT-$N_3$ electrodes to evaluate the localization of molecules across the surface.

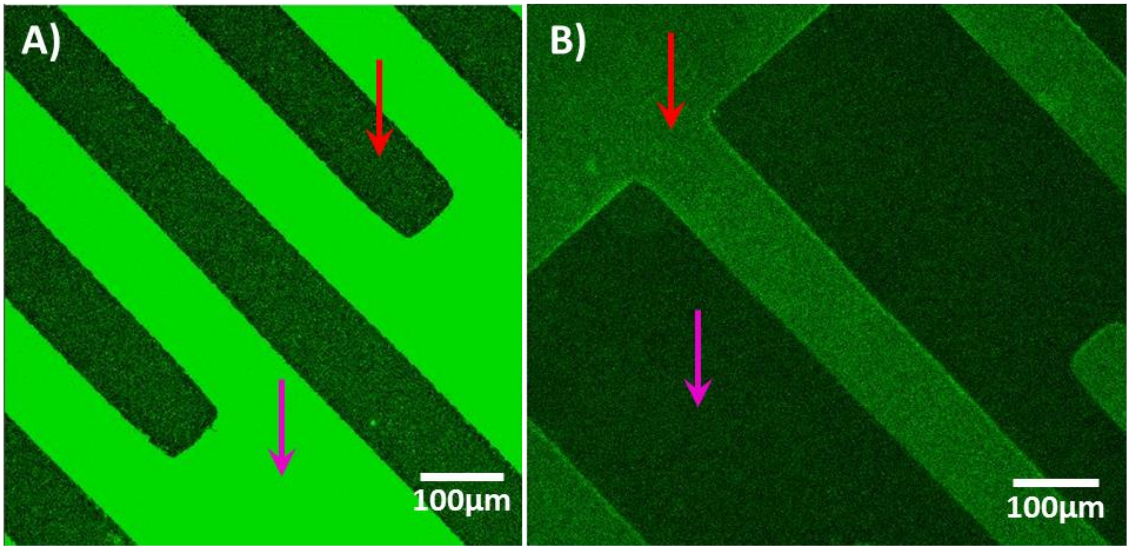


**Figure 3.33** Incubation of 20µg/mL FITC-avidin onto printed PEDOT-$N_3$ electrodes on bare COC (**A**) and on PEG-coated COC (**B**). The red arrows indicate the polymer micro-electrodes while the magenta arrows represent the underlying COC or PEG-coated COC.

As reported in Figure 3.33, when FITC-avidin is incubated onto printed PEDOT-$N_3$ on bare COC, a high amount of passively adsorbed molecules are found on the underlying COC (A), while a low fluorescent signal is detected when the PEGDA-coating is the underlying support (B). Hence, it seems that after

printed dissolution the PEGDA coating below PEDOT-$N_3$ electrodes is maintained functional and consistent protein repellency is achieved.

Although the printed dissolution of PEDOT-$N_3$ films on PEG-coated COC support is not fully optimized because of high variability of fabricated micro-electrodes and poor reliability, the data also suggest that the PEG-coating underlying electrodes is still functional after polymer removal. Thus, the overall study of support modification and electrodes fabrication encouraged us to explore drug-loaded liposomes immobilization onto PEDOT-$N_3$ electrodes through chemical functionalization of PEDOT-$N_3$ via click-chemistry reaction, despite a deeper optimization of electrodes fabrication is still needed.

## 3.5 Chemical immobilization of nanoparticles onto PEDOT-$N_3$ micro-electrodes

Liposomes are excellent drug carrier because of high loading concentration, stability and under proper conditions they can release the loaded compounds. As previously described in Chapter 2, the nanoparticles in which we are interested consist of nano-vesicles (diameter around 100nm) which are thermo-sensitive. It means that when they are exposed to heat treatment at a specific temperature, their cargo is released on the surrounding compartment due to an increased mobility of lipid bilayer. More details about liposomes and the mechanism involved on molecule release from their aqueous compartment are found in Chapter 2. Since the lipid bilayer of liposomes can be functionalized with desired chemical groups or molecules, a suspension of nanoparticles presenting biotin molecules grafted onto bilayer are synthesized. Further, the liposomes are composed of stabilizing component such as cholesterol and PEG-modified lipids; for a preliminary test, fluorescent vesicles are produced by including Rhodamine-labeled lipid (Rho-DSPE) into bilayer. The functionalization of PEDOT-$N_3$ electrodes to enhance liposomes immobilization is realized by multiple steps based on chemical coupling via click-chemistry reaction. The presence of free azide groups onto the electrodes surface is utilized to introduce PEG molecules onto the PEDOT-$N_3$ surface. In such way, a chemical spacer between the surface and nanoparticles is formed; in particular PEG-dialkyne molecules are reacted with available azide groups through click-chemistry. A second step of functionalization is employed to add biotin molecules at one of the terminal alkyne group of pre-bound PEG-dialkyne; the incubation of fluorescent avidin (FITC-avidin) results on a modified PEDOT-$N_3$ surface with protein molecules. Rhodamine-labeled liposomes are derived introducing Biotin-PEG-lipid molecules into the vesicles bilayer; a strong binding of such nanoparticles should occur when avidin molecules are presented at the surface of the polymer platform. These reactions have been already discussed in the Chapter 3 (Figure 3.20) where is reported the multi-step chemical functionalization. In Figure 3.34, it is visualized the schematic of liposomes immobilization onto printed PEDOT-$N_3$ fabricated on PEG-coated COC supports. During these multiple reactions, the overall platform surface is exposed to chemicals

and solvents. The presence of a PEG-coating onto COC should ensure a low-binding of these components.

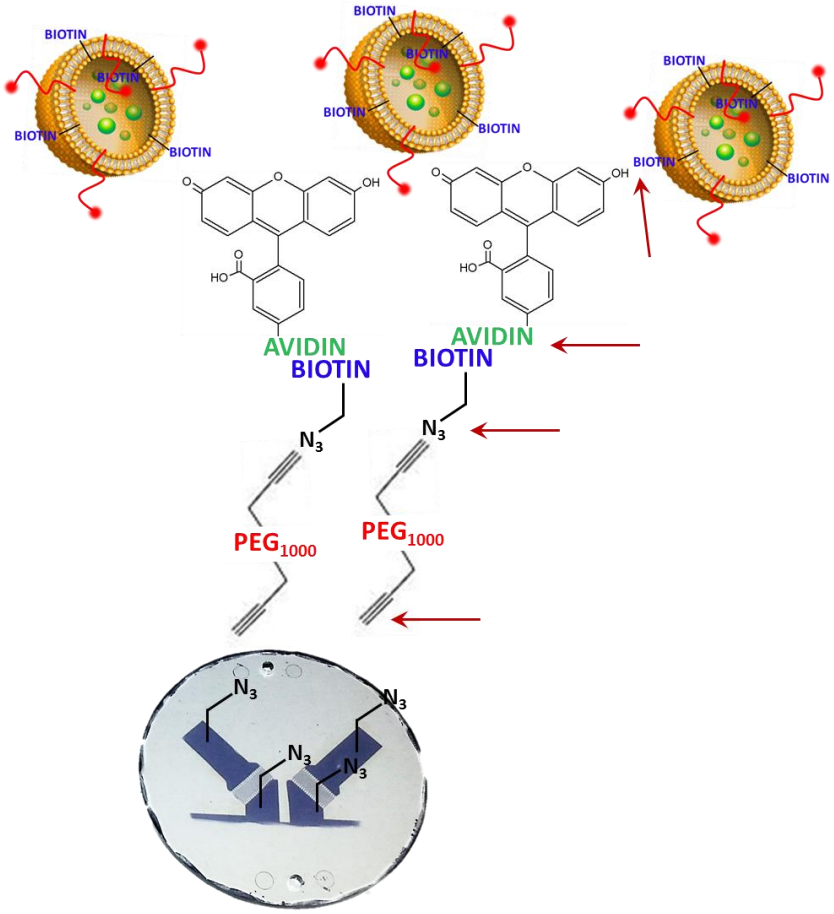


**Figure 3.34** Schematic of the reactions and compounds involved on the functionalization of printed PEDOT-$N_3$ electrodes on PEG-coated COC to stably immobilize nanoparticles onto polymer surface. The red arrows indicate where and which are the chemical groups participating to the functionalization. A first click-chemistry is conducted using PEG-dialkyne molecules (MW=1kDa), $CuSO_4$, NaAsc in DMSO/water; after washing, a second click-chemistry is involved to modify the free alkyne groups with biotin molecules. Then, FITC-avidin is incubated onto the surface and extensively washed; when Rho-labeled liposomes are added to the platform, the vesicles should be covalently bound to the free avidin sites.

Since avidin and liposomes are labeled with FITC (green emission) and Rhodamine (red emission) respectively, the co-localization of dyes is detected through confocal laser scanning microscopy by exciting FITC at 488nm and collecting the fluorescence at wavelengths longer than 505nm, and exciting Rho at 543nm and the fluorescent signal is collected for wavelengths longer than 560nm. Both dyes are immobilized on PEDOT-$N_3$ electrodes surface (light blue arrows), as indicated in Figure 3.35A and B, and lower fluorescence intensities are found on the underlying regions, PEG-coated COC (magenta arrows). In panel B some dots on the PEDOT-$N_3$ surface are also observed; these small

particles may be residues coming from polymer dissolution or they might be liposome aggregates. An inadequate electrode fabrication results from the morphology and size of the structures which are bigger than the expected size (100µm).

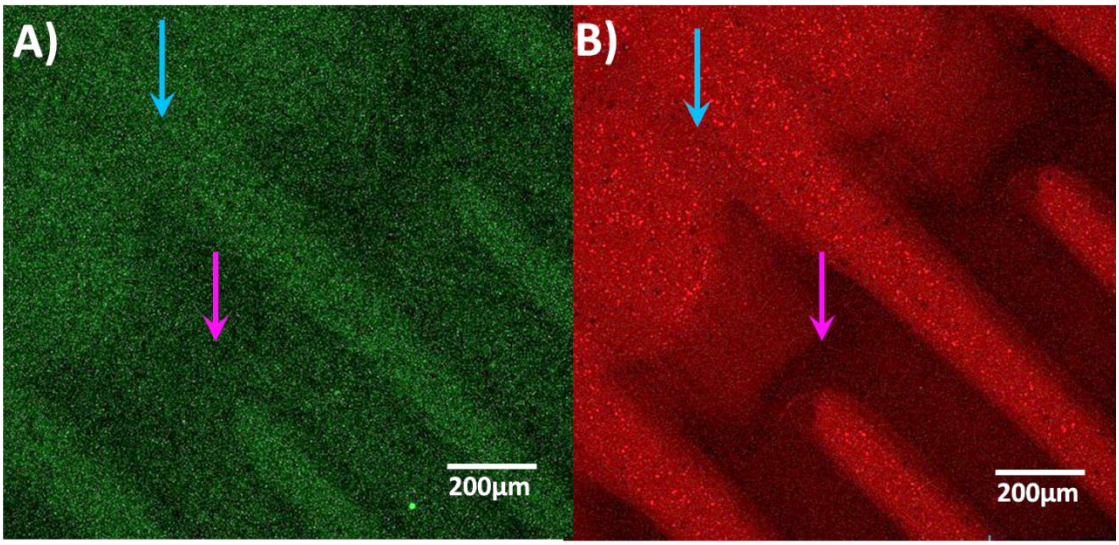


**Figure 3.35** Confocal characterization of PEDOT-$N_3$ electrode surface modification. The polymer is deposited on a PEG-coated COC support. The electrodes are then functionalized through click-chemistry reactions with PEG-dialkyne molecules, and with a subsequent step involving biotin-PEG-azide molecules. FITC-avidin is incubated and after washing, the immobilization of Rhodamine-labeled liposomes is ensured via avidin-biotin covalent binding. The FITC is excited at 488nm and its fluorescence is collected at wavelengths longer than 505nm, while Rho is excited at 543nm and its fluorescent signal is acquired for wavelengths longer than 560nm. The light blue arrows indicate the PEDOT-$N_3$ micro-electrode surface while the magenta arrows correspond to the underlying PEG-coated COC support.

Although the poor definition of polymer electrodes and the presence of residues onto the surface, the avidin and liposomes seem to be co-localized on the same areas corresponding to the PEDOT-$N_3$ electrodes. The steric hindrance of PEG molecules onto the underlying coating again, demonstrates to be effective against protein physical adsorption. However these results are not reproducible meaning that many issues are encountered when trying to immobilize liposomes. For instance, liposomes aggregation onto the overall surface is often observed and co-localization of avidin and biotin-liposomes rarely happens due to defects on stamped electrodes or a complete coverage of the platform surface with liposomes. These considerations suggest that a further optimization of printed dissolution and reaction conditions needs to be done; the platform should be stable and reliable and defined polymer regions must be fabricated, to direct the immobilization of liposomes within precise and confined structures. Other improvements may be done changing the surface chemistry, or the electrode design, or the stability of liposomes suspension. Printed dissolution is an in-expensive process because avoids clean-room processes. The novelty of the method lies in the use of non-ionic

detergents to remove polymer films, even though it is not clear if the detergent aids the general oxidation of the film in the bulk. In general, a locally over-oxidation and dissolution of a conducting polymer thin film induces the exposure of an underlying chemical reactive support; thus, this technology might be suitable for other types of polymers. A deeper investigation of PEDOT-$N_3$ fabrication should be conducted in order to have a clear consciousness of how the previously described experimental factors affect the proposed methodology.

## 3.6 Conclusions

Originally, the development of such micro- and nano-platform was intended for co-localization of drug-loaded liposomes and cancer cells (CRC cells). In-register surface chemistries for liposomes immobilization and cells capture on the platform surface could be applied ideally for any kind of particles or cell lines. During the fabrication of this system, different approaches for support coating have been proposed. Depending on the intended application of the platform, a PEG-coating onto the support surface can be introduced to discourage molecules physical adsorption. The coating may be achieved using various types of PEG-based compounds: for instance, PEG-NHS has been demonstrated to be grafted onto a surface when exposed to UV-light in presence of a proper photo-sensitizer (Bz). Otherwise, PS-$N_3$ may be deposited onto a surface and subsequently functionalized with PEG mono- or di-alkyne species; or PEGDA molecules can be directly grafted onto a support through photochemical activation. All these methods are suitable for surface coating and, depending on the intended application, one is preferred to the other; for example, the photo-induced PEG grafting is advantageous when rapid processes are involved, since it is conducted through a single step reaction in aqueous environment. In our case, a stable and high PEG density grafting is necessary because many post-fabrication processes need to be consecutively applied on the same surface. Moreover the coating should remain un-damaged when a printed dissolution process is used for removal of thin PEDOT materials. Post-functionalization of micro-structures can be achieved through click-chemistry reaction that represents a stable covalent modification of a surface copper-catalyzed in DMSO/water solution.
In conclusion, the use of printed dissolution for creating polymer structures needs to be optimized for our final purposes even though it showed important advantages compare to traditional nano-fabrication technology. Once the fabricated micro-electrodes are defined in morphology, size and composition, a post-functionalization of their surface will permit to immobilize ideally, any type of molecules. In future, the possible application of a specific current to conductive electrodes may permit to locally induce the release of drugs from thermo-sensitive liposomes due to their sensitivity towards temperature changes.

## 3.7 Experimental section

*Fabrication of Cyclic Olefin Copolymer (COC) supports*

Cyclic Olefin Copolymer (COC) supports, also known as TOPAS from the brand, were made using injection molding. We applied in-house fabricated circular supports with a diameter of 5cm and 2mm in thickness using a commercial injection molding machinery (ENGEL VC 80/45, Schwertberg, Austria). TOPAS 5013 supports were made at 130˚ C using a 4min cooling process.

*PEDOT-$N_3$ deposition and in situ polymerization*

The monomer EDOT-$N_3$ was synthesized in accordance with an earlier reported procedure.[175] PEDOT and PEDOT-$N_3$ thin films were fabricated by spin-coating and *in situ* polymerization on injection molded cyclic olefin copolymer supports (TOPAS 5013, TOPAS® Advanced Polymers, Frankfurt, Germany). The COC were washed before with acetone, iso-propanol, ethanol and water prior to spin-coating. EDOT-$N_3$ (20mg, 0.15mmol), CLEVIOS C-B40 (0.48mL, 40 wt% Fe(III)tosylate (TsO) in 1-butanol, H. C. Starck, Goslar, Germany), and 1-butanol (0.48mL) were mixed and spin-coated onto the COC surface at 1000rpm for 30s. EDOT (220µL), CLEVIOS C-B40 (6.5mL, 40wt% Fe(III)tosylate (TsO) in 1-butanol), pyridine (150µL) and 1-butanol (2.0mL) were mixed and spin-coated at 1000rpm for 30s. The samples were placed in a hotplate at 70˚ C for 3min and subsequently washed with water and ethanol and blown dry in a nitrogen flow, yielding a film thickness of approximately 150nm.

*Agarose stamp preparation*

For the printed dissolution technique, an agarose stamp presenting the negative replica of a silicon mold pattern was prepared. The silicon mold was fabricated using conventional photolithography and deep reactive ion etching. Prior the use of silicon mold for agarose stamp fabrication, the mold was washed in ethanol and rinsed in air plasm to remove residues of organic material. The silicon mold was placed in a hotplate at 65˚ C. A solution 10%w/v of agarose (Sigma Aldrich) in MQ water was mixed thoroughly and it was heated up in a microwave oven until air bubbles disappeared from the solution. To prevent boiling of agarose solution, this was done by using multiple short heating steps. The melted agarose was poured directly onto the silicon mold surface aided by a polystyrene Petri dish (Ø 5cm) where the bottom was removed in order to contain the solution when melted onto the mold. The container was covered with its lid and kept for 10min on the hotplate. The mold was transferred to the fridge for 20min to cool down. After fabrication of the stamp, it was usually cut to have a final thickness around 1-1.5cm for improved handling.

*Agarose stamping procedure*

After fabrication, the agarose stamp was soaked into a stamping solution for at least 15min and before contact with the sample, it was blown off using air gun. The stamp was gently pressed onto the surface of the sample to establish a contact, and left for 5min (1min for PEDOT removal). The stamp was then removed and immersed again on the stamping solution for subsequent re-use. The stamping solution was composed of NaOCl (stock solution 10-15%w/v, Sigma Aldrich) at a final concentration of 2%w/v, and Triton X-100 (Sigma Aldrich) at various concentrations (we tested 0.1 and 1%v/v) in aqueous solution.

*Post-stamping washing procedure*

Normally, after stamping the samples were washed for 10min in an aqueous solution of 0.1%v/v Triton X-100; then they were washed twice for 10min with MQ water at 50° C and 10min in 80%v/v DMSO/MQ at room temperature, before rinsing in ethanol and MQ. Some of the samples were washed also with various concentrations of Triton X-100 (0.1 – 1 – 5%v/v) and with CLEVIOS C-B40/MQ (4%v/v). In some cases the temperature at which the samples were heated up was 55 or 65° C.

*Synthesis of 4-(azidomethyl)styrene (PS-$N_3$)*

PS-$N_3$ was synthesized and characterized by Dr. A.E. Daugaard.

2,2'-Azobisisobutyrylnitrile (AIBN, 71.2 mg, 0.4 mmol), 4-(chloromethyl)styrene (10 mL, 71.0 mmol and xylene were mixed in a Schlenk tube and the solution was bubbled through with nitrogen for 30 min. The polymerization was run under a positive nitrogen pressure at 65°C for 18 h. The polymer was precipitated in methanol, filtered and dried in vacuo. The isolated intermediate (poly(4-(chloromethyl)styrene)) was a white powder and was used for the following step without further purification (6.4 g, Mn= 30000 g/mol, PDI= 1.7). FT-ATR-IR (cm-1): 3100-2800 (C-H stretch); 1612+1510 (aromatic ring stretch); 672 (C-Cl stretch). 1H-NMR(CDCl3, 300 MHz, dH, ppm): 1.39 (m, 2H, CH2-CH); 1.70 (m, 1H, CH-CH2); 4.52 (s, 2H, CH2-N3); 6.49, 7.05 (2xm, 4H, aromatic H). HSQC confirmed the following proton/carbon correlations (dH/dC (ppm)): 1.39/41.6 (CHCH2); 1.70/38.7 (CH-CH2-ph); 4.52/44.9 (CH2-N3); 6.49/126.4 (aromatic CH); 7.05/127.0 (aromatic CH). Poly(4-(chloromethyl)styrene) (5.18 g, 34.0 mmol functional group) was dissolved in DMF (100 mL) and NaN3 (2.75 g, 42.4 mmol) was added to the solution. The reaction mixture was stirred at 40°C for 18 h under nitrogen. After reaction the excess of reagent was removed by precipitation into H2O. The precipitate was isolated by filtration and rinsed with copious amounts of H2O and methanol. The solid was dissolved in THF and precipitated in methanol to afford poly(4-(azidomethyl)styrene) as a white powder (4.62 g, 86%). FT-ATR-IR(cm-1): 3100-2800 (C-H stretch); 2090 (C-N3 stretch); 1612+1510 (aromatic ring stretch). 1H-NMR(CDCl3, 300 MHz, dH, ppm): 1.39 (m, 2H, CH2-CH); 1.69 (m, 1H, CH-CH2); 4.24 (s, 2H, CH2-N3); 6.48, 6.97 (2xm, 4H, aromatic H). HSQC confirmed the following

proton/carbon correlations (dH/dC (ppm)): 1.39/44.9 (CHCH2); 1.69/40.4 (CH-CH2-ph); 4.24/54.0 (CH2-N3); 6.48/127.7 (aromatic CH); 6.97/127.7 (aromatic CH). NMR spectroscopy was performed on a 300 MHz Cryomagnet from Spectrospin & Bruker (1H-NMR at 300 MHz, 13C-NMR at 75 MHz), at room temperature. IR was performed on a PerkinElmer Spectrum One model 2000 Fourier transform infrared system with a universal attenuated total reflection sampling accessory on a ZnSe/diamond composite.

*PS-$N_3$ film deposition on COC support*

Solutions of PS-$N_3$ were prepared by dissolving 5mg/mL of polymer in 4-dioxane (Sigma Aldrich) or PGMEA and they were filtered through Ø =0.22μm pores. The solutions were spin-coated on COC supports at 1000rpm for 30s, and they were heated up on a hotplate at 60˚ C to remove residual solvent. The films were characterized measuring the water contact angle of surfaces (Data Physics OCA20 contact angle system). Prior each measurement, the samples were blow with inert gas to remove dust.

*Protein physical adsorption onto different surfaces*

To evaluate the propensity of molecules to passively adsorb onto various surfaces, the samples were incubated with a concentration of 20μg/mL of FITC-avidin or FITC-BSA (both dissolved in PBS buffer) for 30 minutes using a 10mm x 10mm *in situ* Gene frame (Thermo Scientific). FITC-BSA and FITC-avidin were obtained from Life Technologies. 100μL of solution was incubated onto desired surfaces. After incubation, the samples were washed three times with PBS and rinsed with PBS. For visualization of fluorescence signal, a cover slip (10mm x 10mm) was placed onto the gene frame and confocal laser scanning microscopy was used to evaluate fluorescence (LSM 5, Carl Zeiss, Oberkochen, Germany).

*Fabrication of patterns on PS-$N_3$ films*

PS-$N_3$ films were deposited on COC discs and they were exposed to UV-light at 365nm in a MA4 mask aligner (Suss Microtec) by using a chrome mask presenting square grids with different sized structures. A grid of 7 x 7 squares with diameter of 60μm was used to form the pattern. The samples were exposed for 30min and washed with DMSO, iso-propanol and ethanol to remove degraded polymer.

*Functionalization of patterned PS-$N_3$ via post-polymerization CuAAC*

In correspondence of fabricated patterns, a Gene frame (10mm x 10mm) was placed onto the PS-$N_3$. The functionalization of polymer was conducted using two different molecules: PEG-alkyne (MW=800Da) and PEG-dialkyne (MW=1kDa). These molecules were purchased by Creative PEGWorks. A mixture of 2mM PEG-alkyne, 1mM $CuSO_4$, 15mM NaAsc and 70mM NaCl dissolved in 30%v/v DMSO/water, and a mixture of 2mM PEG-dialkyne, 1mM $CuSO_4$, 15mM NaAsc and 70mM NaCl

dissolved in 30%v/v DMSO/water were incubated on the printed PS-$N_3$ surface (100µL total volume). The solution was incubated for 10h at room temperature and the samples were washed with water and rinsed with MQ water for confocal characterization. The samples that were functionalized with PEG-dialkyne were subjected to a subsequent click-chemistry reaction by incubation 2mM azide-$PEG_{(7)}$-biotin (Creative PEGWorks), 1mM $CuSO_4$, 15mM NaAsc and 70mM NaCl dissolved in 30%v/v DMSO/water. The reaction was stopped after 10h by extensively washing the samples with MQ water. Then, 20µg/mL of FITC-avidin was incubated on the sample for 30min. After washing with PBS, the surface was rinsed with PBS and a cover slip was placed on top of the gene frame. The fluorescence signal of protein was detected through confocal microscopy.

*PEG-NHS and Bz-$NH_2$ coating of COC supports*

Small pieces of COC support were cut and attached with a tape on the bottom of a 24 well-microtiter plate (Nunc, Thermo Scientific). The samples were immersed in a solution of 7.5mg/mL PEG-NHS (MW=700Da, Iris Biotech) and 2.5mg/mL Benzophenone-amine (FluoroChem, Hadfield, UK) dissolved in 80%v/v PBS/MQ water. The plate was illuminated for 30 min in a photo-reactor (Philips Cleo S-R fluorescent tubes) at an emission maximum between 330-380nm. The samples were washed with water three times and with ethanol. The water contact angle and the X-ray photoelectron spectroscopy (XPS) were used to characterize the surfaces atomic composition. Data analyses of the XPS spectra were performed using Avantage software package supplied by the manufacturer. For the line-scan measurements, the elemental composition of each spot was determined from the high resolution spectra, using the build-in add-peak function with a linear background. In the following atomic content determination a standard of 0.9 signal to noise threshold was used for all samples. For line-scan investigations a 50µm spot size and an interval size of 30µm were utilized. This means that in each single 100µm electrode, as well as in each gap area, there will be at least one measurement point where the atomic composition will originate entirely from that electrode/spacing area. For all samples, flood-gun charge compensation was used.

*PEGDA and Bz-$NH_2$ coating of COC supports*

In a 24 well-microtiter plate, small pieces of COC support were attached to the bottom of each well using a tape and different concentrations of PEGDA (MW=5kDa, Iris Biotech) and Benzophenone were added to each sample. 2 – 5 – 10 mg/mL of PEGDA and 1 – 2.5 – 5 mg/mL of Bz were the selected amounts to be tested; these mixtures were dissolved in 80%v/v PBS/MQ and poured in various wells. The entire plate was exposed to UV-light in a photo-reactor for 30min; after washing with water, the samples were analyzed through water contact angle. Further, 20µg/mL of FITC-BSA dissolved in PBS was incubated in all samples using a gene frame (10mm x 10mm) for 30min. The un-adsorbed molecules were washed off with PBS and samples were rinsed in PBS, and a cover slip was placed onto the frame. The fluorescent intensity of all surfaces was recorded by LSM confocal microscopy.

From the obtained results, the optimal concentrations of PEGDA and benzophenone were found to be 5mg/mL of PEGDA and 1mg/mL Bz. Multiple layer of PEGDA/Bz were also produced on the same support using a layer-by-layer photochemical grafting. As before, small pieces of COC were attached on the bottom of 24 well-microtiter plate with a tape. A mixture of PEGDA/Bz (5:1) was poured in each well and they were exposed to UV-light in the photo-reactor for 30min. After washing with MQ water and blown dry, they were re-immersed in a fresh solution of PEGDA/Bz (5:1). Again, the samples were exposed for others 30min and after illumination the pieces were washed with water. A third step using the same conditions and concentrations of reagents was conducted. 20µg/mL of FITC-BSA was incubated in each surface as previously described and the fluorescence was evaluated.

*Bromination of free available acrylate groups*

The chemical reactivity of PEGDA-coated COC supports was evaluated incubating a concentration of 1%v/v Bromine (Sigma Aldrich) dissolved in water onto the modified surface of COC. After 30min of incubation with $Br_2$, the supports were washed with water and analyzed by XPS, since bromine is a good XPS marker. The nitrogen, oxygen, carbon and bromine atomic composition was recorded using point-mode (point size=20µm).

*Fabrication of printed PEDOT-$N_3$ micro-electrodes on un-coated and three-layer PEGDA-coated COC support*

A three-layer PEGDA coating on COC support was produced by using the procedure described just above; thus, PEDOT-$N_3$ films were produced on bare COC and PEGDA-modified support. After polymerization, the agarose stamp was prepared according to the desired pattern: it consisted of two sets of inter-digitated micro-electrodes (100µm in width and spacing and 0.5cm long). The negative replica was fabricated onto the stamp surface, which was immersed in a solution of 1%v/v Triton and 2%w/v NaOCl. After 15min of impregnation, the stamp was put in contact with samples. The discs were washed using a solution of 1%v/v Triton and 4%w/v CLEVIOS in aqueous solution at room temperature. The samples were then rinsed with MQ water and blown off. The XPS was used to investigate the elemental composition applying a line-scan measurement (spot size= 50µm; interval size= 30µm). Moreover, the water contact angle of the underlying COC or PEGDA coating was analyzed.

*Optimization of printed dissolution*

In order to evaluate at which conditions was observed a complete removal of PEDOT-$N_3$ from PEGDA-coated surfaces in the gap regions, different parameters were tested: the concentration of Triton in the stamping solution and in the washing procedure, and the temperature at which the washing step took place. The Triton concentration tested in the stamping solution was 0.1 – 1 %v/v whereas in the washing procedure a detergent amount of 0.1 – 1 – 5 %v/v was tested. Further, a constant amount of

NaOCl (2%v/v) and CLEVIOS (4%v/v) respectively in the stamping and washing solutions were utilized. Various temperatures of washing were also explored: room temperature, 50, 55, 65° C. A glass Petri dish containing Triton and CLEVIOS in aqueous solution was used to immerse the sample into the washing solution keeping the dish in a hotplate at a certain temperature without lid in order to favorite evaporation. The stamp was left on the sample for 5min and placed in the stamping solution for 15min. The fabricated micro-electrodes were analyzed through water contact angle and XPS (line-scan mode).

*PEDOT-$N_3$ micro-electrodes fabrication on bare COC support*

Ten samples of PEDOT-$N_3$ film deposited onto bare COC supports were produced according to the protocol previously described. Then an agarose stamp with inter-digitated electrodes was fabricated and kept in a stamping solution composed of 1%v/v Triton and 2%v/v NaOCl for 15min. The samples were stamped for 5min each using the same agarose mold; they were washed in a washing solution made of 5%v/v Triton and 4%v/v CLEVIOS for 15min at 65° C. Then they were washed with water and blown off with air flow. Their atomic composition was analyzed by XPS (point size= 20μm).

*Covalent immobilization of Rhodamine-labeled liposomes on PEDOT-$N_3$ micro-electrodes deposited on PEGDA-coated COC support*

A liposomes suspension having an average diameter of 117.7nm (polydispersity= 0.118) and a zeta-potential of -7.09mV (± 0.41mV), were synthesized according to the protocol reported on the manuscript (Appendix 1). The lipid composition was formed by: 94.5% DSPC, 4% DSPE-$PEG_{2000Da}$, 1% DSPE-$PEG_{2000Da}$-biotin and 0.5% DOPE-rhodamine. All lipids were purchased from Avanti Polar Lipids. The liposomes were prepared to have a functional group into the bilayer, biotin, and a dye to track their fluorescence (Rhodamine).
PEDOT-$N_3$ electrodes were produced on a three-layer PEGDA-coated COC support and they were functionalized according to the protocol previously described ("*Functionalization of patterned PS-$N_3$ via post-polymerization CuAAC*"). Therefore, the electrodes were functionalized through a double click-chemistry to present at their surface, FITC-avidin molecules. The stock suspension of liposomes (25mM) was diluted in HEPES buffer 1000-times to have a final concentration of 25μM. Using a Gene frame (10mm x 10mm), 100μL of 25μM Rhodamine-labeled liposomes were incubated for 1h onto the functionalized surface. Then, the samples were washed with PBS buffer and rinse with PBS. A cover slip was placed onto the Gene frame and the FITC-avidin and Rhodamine-liposomes fluorescent intensities were analyzed by LSM confocal microscopy.

# 4 Perspectives & Conclusions

In this thesis two main polymer platforms have been developed for drug screening purposes. One of these technologies consists on using PEGDA hydrogels for controlled embedding of single drugs and combinations of chemotherapeutics commonly used for the treatment of colorectal cancer (CRC). Eventually, drug-loaded nanoparticles (liposomes) can be entrapped within the polymer matrix to protect and temporally control the release of loaded molecules. The cytotoxicity of such system has been tested on human colorectal adenocarcinoma cell line (HT29) comparing the anti-proliferative effect of small doses of free drugs (dispersed in the cell medium) with those of compounds embedded within PEGDA hydrogel. Furthermore, the application of a home-made technology based on the use of visible-light printing has permitted to fabricate spatially defined hydrogel matrices. The production of hydrogels having certain architectures and sizes was accomplished through *in situ* visible-light photo-polymerization in a rapid, low cost and reliable process. Moreover, the overall procedure has been conducted in an aqueous environment limiting the exposure of the cell line to organic or toxic solvents. The great outcomes and reproducibility obtained with such platform demonstrate the possibility to extend the use of PEGDA hydrogels for other molecules screening. By tuning the chemical and physical properties of PEGDA networks and by including drug-loaded liposomes within the gel, was possible to temporally control the release of certain molecules. Hence, the use of PEGDA hydrogels may be extended towards the screening of various compounds or in different fields. For instance, the hydrogels might be fabricated in even smaller scale, and integrated in microfluidic devices for perfused rather than static release. In future, PEGDA gels might be used for tissue engineering purposes by releasing necessary molecules such as growth factors for the enhancement of cell differentiation. In addition, it has been demonstrated that large molecules can be released when hydrogel composition is adjusted; thus, a possible future application could be the release study of interesting molecules such as antibodies which are largely used in cancer therapy. Although the major focus of this study has been to tailor the properties of PEGDA hydrogel for drug screening purposes and cell handling systems, we believe that our findings should be of general understanding of PEG-based hydrogels, and that this polymer will also be useful for adapting hydrogels to other applications such as tissue engineering.

The second platform that has been studied is based on the fabrication of conductive polymer micro-electrodes for drug-loaded liposomes immobilization and cell capture purposes. PEDOT-type conductive polymer has been selected as candidate for the realization of such system. In particular, PEDOT-$N_3$ thin film has been used to create micro-patterns on a support. The presence of reactive groups at the polymer surface has permitted to post-fabrication functionalize the micro-structures to covalently immobilize drug-loaded nanoparticles onto such surfaces. One of the important requirements for succeeding nanoparticle immobilization and cells capture when tuning the surface

chemistry of advanced materials for bio-medical devices, is the specificity. The need of a support that is repellent meaning that it should discourage molecules physical adsorption is crucial. In fact, the unspecific adsorption of molecules, particularly proteins, can change the biochemical properties of a substrate. This problem is mostly prominent when the support is being subjected to long-time exposure to solutions containing such bio-molecules. Our approach to solve this issue was to engineer the support surface by introducing highly hydrophilic molecules in order to prevent unspecific adsorption and at the same time presenting functional moieties. We fabricated a support that was coated with PEG-molecules containing chemical reactive groups. Photo-chemical immobilization of PEG-NHS or PEGDA molecules on COC supports was produced with a fast and reliable process involving the use of a specific photo-sensitizer. The support was alternatively coated with PS-$N_3$ polymer that was functionalized after deposition with PEG molecules. The use of PEG-NHS or PEGDA coatings was preferred to the modified PS-$N_3$ because their use was more rapid, reproducible and the coating process was entirely conducted in an aqueous environment. To ensure specificity on immobilizing nanoparticles, the synthesis of vesicles was optimized to have functional groups into the lipid bilayer. Biotin-functionalized liposomes were used to favorite their binding onto PEDOT-$N_3$ electrodes through specific modification of conductive polymer surface. The click-chemistry reaction (CuAAC) has been applied for micro-electrodes modification and liposomes binding was evaluated. Another requirement for the development of that micro- and nano-platform was the fabrication technique to be applied for integrating bio-components on the polymeric device. In our group, an innovative and fast method for PEDOT materials micro-fabrication (printed dissolution) was developed and successfully utilized for the production of PEDOT micro-electrodes. Despite the great suitability of printed dissolution to pattern conductive polymers and the un-necessary clean room facilities, agarose stamping has been proved to be inefficient for patterning of PEDOT-$N_3$ films when polymerized onto PEG-modified cyclic olefin copolymers. Inhomogeneous polymeric electrodes have been obtained due to a partial dissolution of thin film between the electrode areas, and leftover residues were observed at the polymer surface. An extensive optimization of the methodology is required: different PEG-modified supports should be tested and the experimental conditions should be explored more deeply to understand how and with which importance they affect the stamping process. In our efforts to create a platform presenting in-register chemistries for liposomes immobilization and cell capture, there are many important issues and approaches that we did not investigate. For example, even though liposomes were found to be chemically bound to the polymer electrode surface, nanoparticles precipitation and agglomeration was observed. We did not attempt to control the surface roughness of our electrodes after conjugation with liposomes. In the light of that, when nanoparticles are immobilized onto the polymer, ideally it could be possible to temporally control the release of their cargo (for example a drug). We have demonstrated that thermo-sensitive liposomes can release loaded molecules by applying a thermal trigger reaching a temperature that corresponds to the phospholipids phase transition temperature. Therefore, for future studies should be interesting to

monitor the molecule release from liposomes induced by the application of current on the polymer electrodes. Despite the charge transfer along electrodes, a local resistive heating might be induced. Preliminary studies should be conducted to determine the voltage required to induce a phase transition temperature of liposomes; a fluorescent ruthenium complex sensitive to small temperature changes may be used to track the local increase of temperature at the electrodes surface when various voltages are applied.[197,198] Other improvements of our platform can be studied in future by immobilizing cell-capturing molecules on the modified support corresponding to the areas between polymer electrodes. For example, specific antibodies for cell capture can be immobilized through Protein G or A adsorption onto the support.[199] The conjugation of immobilized antibody molecules to antigen moieties presented at the cell membrane may be exploited to capture specific cell lines onto the platform. In addition, an important progress of our micro- and nano-platform may be achieved in future integrating the support with fabricated electrodes with a microfluidic system. In such a way, the two components can be bonded together to have a final micro-fluidic chip in which the presence of a channel might be useful for post-fabrication polymerization. With this approach some of the issues previously described may be overcome: liposomes aggregation during their immobilization can be avoided through a perfused functionalization step and a close system can guarantee the sterility required for cells capturing.

# References


[1] IndiTreat, "IndiTreat Project," can be found under http://www.inditreat.dk/

[2] A. Dasari, W. a Messersmith, *Clin. Cancer Res.* **2010**, *16*, 3811.

[3] S. Leong, W. a Messersmith, A. C. Tan, S. G. Eckhardt, *Cancer J.* **2010**, *16*, 273.

[4] B. A. Justice, N. A. Badr, R. A. Felder, *Drug Discov. Today* **2009**, *14*, 102.

[5] J. Bin Kim, *Semin. Cancer Biol.* **2005**, *15*, 365.

[6] S. Ugurel, D. Schadendorf, C. Pföhler, K. Neuber, A. Thoelke, J. Ulrich, A. Hauschild, K. Spieth, M. Kaatz, W. Rittgen, S. Delorme, W. Tilgen, U. Reinhold, *Clin. Cancer Res.* **2006**, *12*, 5454.

[7] R. D. Blumenthal, D. M. Goldenberg, *Mol. Biotechnol.* **2007**, *35*, 185.

[8] J. Friedrich, R. Ebner, L. A. Kunz-Schughart, *Int. J. Radiat. Biol. 83*, 849.

[9] H. Gallion, W. A. Christopherson, R. L. Coleman, L. DeMars, T. Herzog, S. Hosford, H. Schellhas, A. Wells, B.-U. Sevin, *Int. J. Gynecol. Cancer 16*, 194.

[10] J. Trojan, S.-Z. Kim, K. Engels, S. Kriener, P. S. Mitrou, K. U. Chow, *Anticancer. Drugs* **2005**, *16*, 87.

[11] K. U. Chow, D. Nowak, S.-Z. Kim, B. Schneider, M. Komor, S. Boehrer, P. S. Mitrou, D. Hoelzer, E. Weidmann, W.-K. Hofmann, *Pharmacol. Res.* **2006**, *53*, 49.

[12] D. D. Von Hoff, G. M. Clark, B. J. Stogdill, M. F. Sarosdy, M. T. O'Brien, J. T. Casper, D. E. Mattox, C. P. Page, A. B. Cruz, J. F. Sandbach, *Cancer Res.* **1983**, *43*, 1926.

[13] P. Engblom, V. Rantanen, J. Kulmala, S. Grènman, *Anticancer Res. 16*, 1743.

[14] L. M. Weisenthal, J. A. Marsden, P. L. Dill, C. K. Macaluso, *Cancer Res.* **1983**, *43*, 749.

[15] D. H. Kern, C. R. Drogemuller, M. C. Kennedy, S. U. Hildebrand-Zanki, N. Tanigawa, V. K. Sondak, *Cancer Res.* **1985**, *45*, 5436.

[16] H. Kobayashi, M. Higashiyama, K. Minamigawa, K. Tanisaka, T. Takano, H. Yokouchi, K. Kodama, T. Hata, *Jpn. J. Cancer Res.* **2001**, *92*, 203.

[17] L. Kangas, M. Grönroos, A. L. Nieminen, *Med. Biol.* **1984**, *62*, 338.

[18] K. Csoka, R. Larsson, B. Tholander, E. Gerdin, M. de la Torre, P. Nygren, *Gynecol. Oncol.* **1994**, *54*, 163.

[19] L. V Rubinstein, R. H. Shoemaker, K. D. Paull, R. M. Simon, S. Tosini, P. Skehan, D. A. Scudiero, A. Monks, M. R. Boyd, *J. Natl. Cancer Inst.* **1990**, *82*, 1113.

[20] D. S. Waldenmaier, A. Babarina, F. C. Kischkel, *Toxicol. Appl. Pharmacol.* **2003**, *192*, 237.

[21] M. Fenech, *Mutat. Res.* **2000**, *455*, 81.

[22] J. R. Huddy, *World J. Gastroenterol.* **2015**, *21*, 4111.

[23] "National Cancer Institute," can be found under http://www.cancer.gov/cancertopics/pdq/treatment/colon/Patient

[24] G. Binefa, F. Rodríguez-Moranta, A. Teule, M. Medina-Hayas, *World J. Gastroenterol.* **2014**, *20*, 6786.

[25] A. Z. Wilczewska, K. Niemirowicz, K. H. Markiewicz, H. Car, *Pharmacol. Reports* **2012**, *64*, 1020.

[26] A. Kura, S. Fakurazi, M. Hussein, P. Arulselvan, *Chem. Cent. J.* **2014**, *8*, 46.

[27] K. Kasemets, A. Ivask, H.-C. Dubourguier, A. Kahru, *Toxicol. Vitr.* **2009**, *23*, 1116.

[28] K. Luyts, D. Napierska, B. Nemery, P. H. M. Hoet, *Environ. Sci. Process. Impacts* **2013**, *15*, 23.

[29] S. Nie, Y. Xing, G. J. Kim, J. W. Simons, *Annu. Rev. Biomed. Eng.* **2007**, *9*, 257.

[30] B. J. Blaauboer, *Toxicol. Lett.* **2008**, *180*, 81.

[31] D. Castro, P. Ingram, R. Kodzius, D. Conchouso, E. Yoon, I. G. Foulds, *2013 IEEE 26th Int. Conf. Micro Electro Mech. Syst.* **2013**, 457.

[32] S. J. Bryant, C. R. Nuttelman, K. S. Anseth, *J. Biomater. Sci. Polym. Ed.* **2000**, *11*, 439.

[33] M. BIKRAM, C. FOULETIERDILLING, A. GOBIN, A. DAVIS, E. OLMSTEDDAVIS, J. WEST, *Mol. Ther.* **2005**, *11*, 263.

[34] K. Ghosh, X.-D. Ren, X. Z. Shu, G. D. Prestwich, R. A. F. Clark, *Tissue Eng.* **2006**, *12*, 601.

[35] Y. Ji, K. Ghosh, X. Z. Shu, B. Li, J. C. Sokolov, G. D. Prestwich, R. A. F. Clark, M. H. Rafailovich, *Biomaterials* **2006**, *27*, 3782.

[36] S. Kwon, K. Yu, K. Kweon, G. Kim, J. Kim, H. Kim, Y.-R. Jo, B.-J. Kim, J. Kim, S. H. Lee, K. Lee, *Nat. Commun.* **2014**, *5*, DOI 10.1038/ncomms5183.

[37] P. M. George, D. a. Lavan, J. a. Burdick, C. Y. Chen, E. Liang, R. Langer, *Adv. Mater.* **2006**, *18*, 577.

[38] *CA. Cancer J. Clin.* **2004**, *54*, 362.

[39] P. C. Nowell, *Cancer Res.* **1986**, *46*, 2203.

[40] G. M. Cooper, *The Cell: A Molecular Approach. 2nd Edition*, National Center For Biotechnology Informations Bookshelf, **2000**.

[41] A. I. Baba, C. Catoi, *Comparative Oncology*, The Publishing House Of The Romanian Academy, **2007**.

[42] A. B. Ballinger, C. Anggiansah, *BMJ* **2007**, *335*, 715.

[43] "Staging of Colorectal Cancer," can be found under http://www.webmd.com/colorectal-cancer/ss/slideshow-colorectal-cancer-overview

[44] S. M. Farrington, A. Tenesa, R. Barnetson, A. Wiltshire, J. Prendergast, M. Porteous, H. Campbell, M. G. Dunlop, *Am. J. Hum. Genet.* **2005**, *77*, 112.

[45] R.-D. Hofheinz, F. Wenz, S. Post, A. Matzdorff, S. Laechelt, J. T. Hartmann, L. Müller, H. Link, M. Moehler, E. Kettner, E. Fritz, U. Hieber, H. W. Lindemann, M. Grunewald, S. Kremers, C. Constantin, M. Hipp, G. Hartung, D. Gencer, P. Kienle, I. Burkholder, A. Hochhaus, *Lancet. Oncol.* **2012**, *13*, 579.

[46] A. de Gramont, C. Boni, M. Navarro, J. Tabernero, T. Hickish, C. Topham, A. Bonetti, P. Clingan, C. Lorenzato, T. Andre, *ASCO Meet. Abstr.* **2007**, *25*, 4007.

[47] S. L. Wong, P. B. Mangu, M. A. Choti, T. S. Crocenzi, G. D. Dodd, G. S. Dorfman, C. Eng, Y. Fong, A. F. Giusti, D. Lu, T. A. Marsland, R. Michelson, G. J. Poston, D. Schrag, J. Seidenfeld, A. B. Benson, *J. Clin. Oncol.* **2010**, *28*, 493.

[48] G. Fiorentini, C. Aliberti, M. Tilli, L. Mulazzani, F. Graziano, P. Giordani, A. Mambrini, F. Montagnani, P. Alessandroni, V. Catalano, P. Coschiera, *Anticancer Res.* **2012**, *32*, 1387.

[49] R. Seidensticker, T. Denecke, P. Kraus, M. Seidensticker, K. Mohnike, J. Fahlke, E. Kettner, B. Hildebrandt, O. Dudeck, M. Pech, H. Amthauer, J. Ricke, *Cardiovasc. Intervent. Radiol.* **2012**, *35*, 1066.

[50] G. Colucci, V. Gebbia, G. Paoletti, F. Giuliani, M. Caruso, N. Gebbia, G. Cartenì, B. Agostara, G. Pezzella, L. Manzione, N. Borsellino, A. Misino, S. Romito, E. Durini, S. Cordio, M. Di Seri, M. Lopez, E. Maiello, S. Montemurro, A. Cramarossa, V. Lorusso, M. Di Bisceglie, M. Chiarenza, M. R. Valerio, T. Guida, V. Leonardi, S. Pisconti, G. Rosati, F. Carrozza, G. Nettis, M. Valdesi, G. Filippelli, S. Fortunato, S. Mancarella, C. Brunetti, *J. Clin. Oncol.* **2005**, *23*, 4866.

[51] A. Falcone, S. Ricci, I. Brunetti, E. Pfanner, G. Allegrini, C. Barbara, L. Crinò, G. Benedetti, W. Evangelista, L. Fanchini, E. Cortesi, V. Picone, S. Vitello, S. Chiara, C. Granetto, G. Porcile, L. Fioretto, C. Orlandini, M. Andreuccetti, G. Masi, *J. Clin. Oncol.* **2007**, *25*, 1670.

[52] "Drugs Approved for Colon and Rectal Cancer - National Cancer Institute," can be found under http://www.cancer.gov/cancertopics/treatment/drugs/colorectal#dal1

[53] M. E. Wall, M. C. Wani, C. E. Cook, K. H. Palmer, A. T. McPhail, G. A. Sim, *J. Am. Chem. Soc.* **1966**, *88*, 3888.

[54] T. R. Govindachari, N. Viswanathan, *Phytochemistry* **1972**, *11*, 3529.

[55] J. A. Gottlieb, A. M. Guarino, J. B. Call, V. T. Oliverio, J. B. Block, *Cancer Chemother. Rep.* **1970**, *54*, 461.

[56] F. M. Muggia, P. J. Creaven, H. H. Hansen, M. H. Cohen, O. S. Selawry, *Cancer Chemother. Rep.* **1972**, *56*, 515.

[57] Y. H. Hsiang, R. Hertzberg, S. Hecht, L. F. Liu, *J. Biol. Chem.* **1985**, *260*, 14873.

[58] M. Méndez, A. Salut, C. García-Girón, M. Navalon, P. Diz, M. J. García López, P. España, A. de la Torre, P. Martínez del Prado, I. Duarte, E. Pujol, A. Arizcun, J. J. Cruz, *Clin. Colorectal Cancer* **2003**, *3*, 174.

[59] M. L. Rothenberg, *Semin. Oncol.* **1998**, *25*, 39.

[60] C. Jaxel, K. W. Kohn, M. C. Wani, M. E. Wall, Y. Pommier, *Cancer Res.* **1989**, *49*, 1465.

[61] R. P. Hertzberg, M. J. Caranfa, K. G. Holden, D. R. Jakas, G. Gallagher, M. R. Mattern, S. M. Mong, J. O. Bartus, R. K. Johnson, W. D. Kingsbury, *J. Med. Chem.* **1989**, *32*, 715.

[62] V. M. Herben, W. W. Ten Bokkel Huinink, J. H. Schellens, J. H. Beijnen, *Pharm. World Sci.* **1998**, *20*, 161.

[63] C. H. Takimoto, S. G. Arbuck, *Oncology (Williston Park).* **1997**, *11*, 1635.

[64] Y. H. Hsiang, M. G. Lihou, L. F. Liu, *Cancer Res.* **1989**, *49*, 5077.

[65] W. J. Jansen, B. Zwart, S. T. Hulscher, G. Giaccone, H. M. Pinedo, E. Boven, *Int. J. Cancer* **1997**, *70*, 335.

[66] H. A. Burris, A. R. Hanauske, R. K. Johnson, M. H. Marshall, J. G. Kuhn, S. G. Hilsenbeck, D. D. Von Hoff, *J. Natl. Cancer Inst.* **1992**, *84*, 1816.

[67] A. Tanizawa, A. Fujimori, Y. Fujimori, Y. Pommier, *J. Natl. Cancer Inst.* **1994**, *86*, 836.

[68] J. Fassberg, V. J. Stella, *J. Pharm. Sci.* **1992**, *81*, 676.

[69] Y. Pommier, *Nat. Rev. Cancer* **2006**, *6*, 789.

[70] E. Rudolf, S. John, M. Cervinka, *Toxicol. Lett.* **2012**, *214*, 1.

[71] R. H. te Poele, S. P. Joel, *Br. J. Cancer* **1999**, *81*, 1285.

[72] J. T. Hartmann, H.-P. Lipp, *Drug Saf.* **2006**, *29*, 209.

[73] D. B. Longley, D. P. Harkin, P. G. Johnston, *Nat. Rev. Cancer* **2003**, *3*, 330.

[74] R. M. Wohlhueter, R. S. McIvor, P. G. Plagemann, *J. Cell. Physiol.* **1980**, *104*, 309.

[75] H. Sommer, D. V. Santi, *Biochem. Biophys. Res. Commun.* **1974**, *57*, 689.

[76] D. V. Santi, C. S. McHenry, H. Sommer, *Biochemistry* **1974**, *13*, 471.

[77] *Lancet* **1995**, *345*, 939.

[78] P. G. Johnston, S. Kaye, *Anticancer. Drugs* **2001**, *12*, 639.

[79] S. Giacchetti, B. Perpoint, R. Zidani, N. Le Bail, R. Faggiuolo, C. Focan, P. Chollet, J. F. Llory, Y. Letourneau, B. Coudert, F. Bertheaut-Cvitkovic, D. Larregain-Fournier, A. Le Rol, S. Walter, R. Adam, J. L. Misset, F. Lévi, *J. Clin. Oncol.* **2000**, *18*, 136.

[80] J. Douillard, D. Cunningham, A. Roth, M. Navarro, R. James, P. Karasek, P. Jandik, T. Iveson, J. Carmichael, M. Alakl, G. Gruia, L. Awad, P. Rougier, *Lancet* **2000**, *355*, 1041.

[81] A. Carrato, J. Gallego, E. Díaz-Rubio, *Crit. Rev. Oncol. Hematol.* **2002**, *44*, 29.

[82] S. R. McWhinney, R. M. Goldberg, H. L. McLeod, *Mol. Cancer Ther.* **2009**, *8*, 10.

[83] R. M. Goldberg, D. J. Sargent, R. F. Morton, C. S. Fuchs, R. K. Ramanathan, S. K. Williamson, B. P. Findlay, H. C. Pitot, S. R. Alberts, *J. Clin. Oncol.* **2004**, *22*, 23.

[84] M. J. McKeage, *Drug Saf.* **1995**, *13*, 228.

[85] L. Kelland, *Nat. Rev. Cancer* **2007**, *7*, 573.

[86] I. Ali, W. a Wani, K. Saleem, A. Haque, *Anticancer. Agents Med. Chem.* **2013**, *13*, 296.

[87] C. P. Saris, P. J. M. Van de Vaart, R. C. Rietbroek, F. a. Blommaert, *Carcinogenesis* **1996**, *17*, 2763.

[88] E. Raymond, S. G. Chaney, a Taamma, E. Cvitkovic, **2008**, 1053.

[89] K. Chválová, V. Brabec, J. Kaspárková, *Nucleic Acids Res.* **2007**, *35*, 1812.

[90] U. S. Food, **2004**, 8.

[91] C. Keshava, N. Keshava, W.-Z. Whong, J. Nath, T. Ong, *Mutat. Res. Mol. Mech. Mutagen.* **1998**, *397*, 221.

[92] T. André, C. Boni, M. Navarro, J. Tabernero, T. Hickish, C. Topham, A. Bonetti, P. Clingan, J. Bridgewater, F. Rivera, A. De Gramont, *J. Clin. Oncol.* **2009**, *27*, 3109.

[93] M. L. Rothenberg, *Ann. Oncol.* **1997**, *8*, 837.

[94] K. Murono, N. H. Tsuno, K. Kawai, K. Sasaki, K. Hongo, M. Kaneko, M. Hiyoshi, N. Tada, T. Nirei, E. Sunami, K. Takahashi, J. Kitayama, **2012**, *872*, 865.

[95] J. a. Houghton, P. J. Cheshire, J. D. Hallman, L. Lutz, X. Luo, Y. Li, P. J. Houghton, *Clin. Cancer Res.* **1996**, *2*, 107.

[96] S. Mullany, S. H. Kaufmann, **1998**, 391.

[97] J. A. Bertout, S. A. Patel, M. C. Simon, *Nat. Rev. Cancer* **2008**, *8*, 967.

[98] N. Peppas, *Eur. J. Pharm. Biopharm.* **2000**, *50*, 27.

[99] S. Van Vlierberghe, P. Dubruel, E. Schacht, *Biomacromolecules* **2011**, *12*, 1387.

[100] A. S. Hoffman, *Adv. Drug Deliv. Rev.* **2002**, *54*, 3.

[101] M. F. Butler, A. H. Clark, S. Adams, *Biomacromolecules* **2006**, *7*, 2961.

[102] P. Gupta, K. Vermani, S. Garg, *Drug Discov. Today* **2002**, *7*, 569.

[103] N. A. Peppas, *Adv. Drug Deliv. Rev.* **2004**, *56*, 1529.

[104] C.-C. Lin, K. S. Anseth, *Pharm. Res.* **2009**, *26*, 631.

[105] N. A. Peppas, J. Z. Hilt, A. Khademhosseini, R. Langer, *Adv. Mater.* **2006**, *18*, 1345.

[106] J. L. Drury, D. J. Mooney, *Biomaterials* **2003**, *24*, 4337.

[107] M. B. Mellott, K. Searcy, M. V. Pishko, *Biomaterials* **2001**, *22*, 929.

[108] N. A. Peppas, K. B. Keys, M. Torres-Lugo, A. M. Lowman, *J. Control. Release* **1999**, *62*, 81.

[109] C. R. Nuttelman, M. A. Rice, A. E. Rydholm, C. N. Salinas, D. N. Shah, K. S. Anseth, *Prog. Polym. Sci.* **2008**, *33*, 167.

[110] J. A. Burdick, K. S. Anseth, *Biomaterials* **2002**, *23*, 4315.

[111] R. G. Schoenmakers, P. van de Wetering, D. L. Elbert, J. A. Hubbell, *J. Control. Release* **2004**, *95*, 291.

[112] J. W. DuBose, C. Cutshall, A. T. Metters, *J. Biomed. Mater. Res. A* **2005**, *74*, 104.

[113] H. Soyez, E. Schacht, M. Jelinkova, B. Rihova, *J. Control. Release* **1997**, *47*, 71.

[114] J. B. Rothbard, M. L. Gefter, *Annu. Rev. Immunol.* **1991**, *9*, 527.

[115] D. D. Lasic, *Trends Biotechnol.* **1998**, *16*, 307.

[116] M. a. Khan, S. T, *J. Sci. Res.* **2009**, *1*, DOI 10.3329

[117] N. A. Peppas, B. Narasimhan, *J. Control. Release* **2014**, *190*, 75.

[118] P. L. Ritger, N. a. Peppas, *J. Control. Release* **1987**, *5*, 23.

[119] R. Pjanović, N. Bo.sković-Vragolović, J. Veljković-Giga, R. Garić-Grulović, S. Pejanović, B. Bugarski, *J. Chem. Technol. Biotechnol.* **2010**, *85*, 693.

[120] T. Lian, R. J. Ho, *J. Pharm. Sci.* **2001**, *90*, 667.

[121] R. Banerjee, *J. Biomater. Appl.* **2001**, *16*, 3.

[122] a. Laouini, C. Jaafar-Maalej, I. Limayem-Blouza, S. Sfar, C. Charcosset, H. Fessi, *J. Colloid Sci. Biotechnol.* **2012**, *1*, 147.

[123] A. Jesorka, O. Orwar, *Annu. Rev. Anal. Chem. (Palo Alto. Calif).* **2008**, *1*, 801.

[124] G. M. Whitesides, B. Grzybowski, *Science* **2002**, *295*, 2418.

[125] A. D. Bangham, J. De Gier, G. D. Greville, *Chem. Phys. Lipids* **1967**, *1*, 225.

[126] S. Sala, E. Elizondo, E. Moreno, T. Calvet, M. A. Cuevas-Diarte, N. Ventosa, J. Veciana, *Cryst. Growth Des.* **2010**, *10*, 1226.

[127] E. Elizondo, J. Larsen, N. S. Hatzakis, I. Cabrera, T. Bjørnholm, J. Veciana, D. Stamou, N. Ventosa, *J. Am. Chem. Soc.* **2012**, *134*, 1918.

[128] M. Eeman, M. Deleu, *Focus (Madison).* **2010**, *14*, 719.

[129] P. R. Cullis, D. B. Fenske, M. J. Hope, *Biochem. Lipids, Lipoproteins Membr.* **1996**, DOI 10.1016/S0167-7306(08)60508-6.

[130] T. Y. Tsong, *Proc. Natl. Acad. Sci. U. S. A.* **1974**, *71*, 2684.

[131] J.-P. Fouassier, *Photoinitiation, Photopolymerization, and Photocuring: Fundamentals and Applications*, **1995**.

[132] H. Ikehata, T. Ono, *J. Radiat. Res.* **2011**, *52*, 115.

[133] G. M. Cruise, O. D. Hegre, D. S. Scharp, J. A. Hubbell, *Biotechnol. Bioeng.* **1998**, *57*, 655.

[134] C. G. Williams, A. N. Malik, T. K. Kim, P. N. Manson, J. H. Elisseeff, *Biomaterials* **2005**, *26*, 1211.

[135] T. Majima, W. Schnabel, W. Weber, *Die Makromol. Chemie* **1991**, *192*, 2307.

[136] B. D. Fairbanks, M. P. Schwartz, C. N. Bowman, K. S. Anseth, *Biomaterials* **2009**, *30*, 6702.

[137] G. Odian, *Principles of Polymerization*, John Wiley & Sons, Inc., New York

[138] L. M. Weber, C. G. Lopez, K. S. Anseth, *J. Biomed. Mater. Res. A* **2009**, *90*, 720.

[139] M. H. Gaber, K. Hong, S. Kun Huang, D. Papahadjopoulos, *Pharm. Res.* **1995**, *12*, 1407.

[140] N. Yellin, I. W. Levin, *Biochemistry* **1977**, *16*, 642.

[141] G. Zhao, E. S. Ford, C. Li, K. J. Greenlund, J. B. Croft, L. S. Balluz, *Nutr. J.* **2011**, *10*, 102.

[142] U. Lange, N. V Roznyatovskaya, V. M. Mirsky, *Anal. Chim. Acta* **2008**, *614*, 1.

[143] A. Goetzberger, C. Hebling, H.-W. Schock, *Mater. Sci. Eng. R Reports* **2003**, *40*, 1.

[144] L. . Hung, C. . Chen, *Mater. Sci. Eng. R Reports* **2002**, *39*, 143.

[145] J. R. Fried, *Polymer Science and Technology*, **1995**.

[146] A. Heeger, A. G. MacDiarmid, H. Shirakawa, *Stock. Sweden R. Swedish Acad. Sci.* **2000**, 1.

[147] R. Qian, Q. Pei, Y. Li, *Synth. Met.* **1993**, *61*, 275.

[148] R. Prakash, R. Srivastava, P. Pandey, *J. Solid State Electrochem.* **2014**, *6*, 203.

[149] G. Milczarek, T. Rebis, *Int. J. Electrochem.* **2012**, *2012*, 1.

[150] N. Izaoumen, D. Bouchta, H. Zwjli, M. Kaoutit, A. Stalcup, K. Temsamani, *Talanta* **2005**, *66*, 111.

[151] E. Pringsheim, E. Terpetschnig, S. A. Piletsky, O. S. Wolfbeis, *Adv. Mater.* **1999**, *11*, 865.

[152] C. Li, M. Numata, M. Takeuchi, S. Shinkai, *Angew. Chemie* **2005**, *117*, 6529.

[153] B. Adhikari, S. Majumdar, *Prog. Polym. Sci.* **2004**, *29*, 699.

[154] M. S.-P. López, E. López-Cabarcos, B. López-Ruiz, *Biomol. Eng.* **2006**, *23*, 135.

[155] P. T. Hammond, *Curr. Opin. Colloid Interface Sci.* **1999**, *4*, 430.

[156] B. Piro, L. A. Dang, M. C. Pham, S. Fabiano, C. Tran-Minh, *J. Electroanal. Chem.* **2001**, *512*, 101.

[157] C. H. Chang, P. S. Son, J. Yang, S. Choi, *J. Korean Chem. Soc.* **2009**, *53*, 111.

[158] J. M. Goddard, J. H. Hotchkiss, *Prog. Polym. Sci.* **2007**, *32*, 698.

[159] A. P. O'Mullane, S. E. Dale, J. V Macpherson, P. R. Unwin, *Chem. Commun. (Camb).* **2004**, *2*, 1606.

[160] O. A. Raitman, E. Katz, A. F. Bückmann, I. Willner, *J. Am. Chem. Soc.* **2002**, *124*, 6487.

[161] S. Da Silva, L. Grosjean, N. Ternan, P. Mailley, T. Livache, S. Cosnier, *Bioelectrochemistry* **2004**, *63*, 297.

[162] C. M. Halliwell, E. Simon, C.-S. Toh, P. N. Bartlett, A. E. . Cass, *Anal. Chim. Acta* **2002**, *453*, 191.

[163] A. Guiseppi-Elie, A. M. Wilson, J. M. Tour, T. W. Brockmann, P. Zhang, D. L. Allara, *Langmuir* **1995**, *11*, 1768.

[164] Q. Hao, M. Rahm, D. Weiss, V. M. Mirsky, *Microchim. Acta* **2003**, *143*, 147.

[165] S. Kirchmeyer, K. Reuter, *J. Mater. Chem.* **2005**, *15*, 2077.

[166] W. Lövenich, *Polym. Sci. Ser. C* **2014**, *56*, 135.

[167] L. Groenendaal, F. Jonas, D. Freitag, H. Pielartzik, J. R. Reynolds, *Adv. Mater.* **2000**, *12*, 481.

[168] A. Elschner, S. Kirchmeyer, W. Lovenich, U. Merker, K. Reuter, *PEDOT: Principles and Applications of an Intrinsically Conductive Polymer*, CRC Press, **2010**.

[169] M. Nishizawa, K. Nagamine, in *DIRECT ELECTROPORATION Adher. CELLS BY HYDROGEL-BASED MICROELECTRODES*, Freiburg, Germany, **2013**, pp. 1734–1736.

[170] K. Ø. Andresen, M. Hansen, M. Matschuk, S. T. Jepsen, H. S. Sørensen, P. Utko, D. Selmeczi, T. S. Hansen, N. B. Larsen, N. Rozlosnik, R. Taboryski, *J. Micromechanics Microengineering* **2010**, *20*, 055010.

[171] F. Jonas, R. Dhein, K. Lerch, *Scratch-Resistant Conductive Coatings*, EP0825219 A2.

[172] K. Z. Xing, M. Fahlman, X. W. Chen, O. Inganäs, W. R. Salaneck, *Synth. Met.* **1997**, *89*, 161.

[173] M. E. Alf, A. Asatekin, M. C. Barr, S. H. Baxamusa, H. Chelawat, G. Ozaydin-Ince, C. D. Petruczok, R. Sreenivasan, W. E. Tenhaeff, N. J. Trujillo, S. Vaddiraju, J. Xu, K. K. Gleason, *Adv. Mater.* **2010**, *22*, 1993.

[174] F. Jonas, W. Krafft, B. Muys, *Macromol. Symp.* **1995**, *100*, 169.

[175] A. E. Daugaard, S. Hvilsted, T. S. Hansen, N. B. Larsen, *Macromolecules* **2008**, *41*, 4321.

[176] D. L. Smith, D. W. Hoffman, *Phys. Today* **1996**, *49*, 60.

[177] M. Ohring, J. L., *Materials Science of Thin Films*, Elsevier, **2002**.

[178] B. R. Lawn, *J. Mater. Res.* **2011**, *19*, 22.

[179] Ossila, "Spin coating: a guide to theory and techniques," can be found under http://www.ossila.com/pages/spin-coating

[180] T. A. P. GmbH, "TOPAS cyclic olefin copolymers," can be found under http://www.topas.com/

[181] M. Matteucci, T. L. Christiansen, S. Tanzi, P. F. Østergaard, S. T. Larsen, R. Taboryski, *Microelectron. Eng.* **2013**, *111*, 294.

[182] S. Tanzi, P. F. Østergaard, M. Matteucci, T. L. Christiansen, J. Cech, R. Marie, R. Taboryski, *J. Micromechanics Microengineering* **2012**, *22*, 115008.

[183] B. Charlot, G. Sassine, A. Garraud, B. Sorli, A. Giani, P. Combette, *Microsyst. Technol.* **2012**, *19*, 895.

[184] J. U. Lind, C. Acikgo, A. E. Daugaard, T. L. Andresen, S. Hvilsted, M. Textor, N. B. Larsen, **2012**.

[185] T. S. Hansen, K. West, O. Hassager, N. B. Larsen, *Adv. Mater.* **2007**, *19*, 3261.

[186] S. Al Akhrass, R.-V. Ostaci, Y. Grohens, E. Drockenmuller, G. Reiter, *Langmuir* **2008**, *24*, 1884.

[187] C. W. Tornøe, C. Christensen, M. Meldal, *J. Org. Chem.* **2002**, *67*, 3057.

[188] V. V Rostovtsev, L. G. Green, V. V Fokin, K. B. Sharpless, *Angew. Chem. Int. Ed. Engl.* **2002**, *41*, 2596.

[189] K. Emoto, J. M. Harris, J. M. Van Alstine, *Anal. Chem.* **1996**, *68*, 3751.

[190] E. K. U. Larsen, N. B. Larsen, *Lab Chip* **2013**, *13*, 669.

[191] E. K. U. Larsen, M. B. L. Mikkelsen, N. B. Larsen, *Biomacromolecules* **2014**, *15*, 894.

[192] Y. Chen, D. Chen, Y. Ma, W. Yang, *J. Polym. Sci. Part A Polym. Chem.* **2014**, *52*, 1059.

[193] Y. Yoshioka, P. D. Calvert, G. E. Jabbour, *Macromol. Rapid Commun.* **2005**, *26*, 238.

[194] B. Winther-Jensen, K. Fraser, C. Ong, M. Forsyth, D. R. MacFarlane, *Adv. Mater.* **2010**, *22*, 1727.

[195] C. C. Chen, *J. Electrochem. Soc.* **1994**, *141*, 2942.

[196] J. U. Lind, Smart Surface Chemistries of Conducting Polymers, PhD Thesis, **2012**.

[197] O. Filevich, R. Etchenique, *Anal. Chem.* **2006**, *78*, 7499.

[198] L. H. Thamdrup, N. B. Larsen, A. Kristensen, *Nano Lett.* **2010**, *10*, 826.

[199] J. M. Lee, H. K. Park, Y. Jung, J. K. Kim, S. O. Jung, B. H. Chung, *Anal. Chem.* **2007**, *79*, 2680.

[200] C. Helwick, *Asco Post* **2013**, *4*.

# Acknowledgements

This thesis is the result of my PhD project, IndiTreat, carried out at the Technical University of Denmark (DTU) at Department of Micro- and Nanotechnology from 2012 to 2015. The project was financed in part by DTU and by the Danish Council for Strategic Research.

Foremost I would like to thank my supervisor Professor Niels Bent Larsen for giving me the opportunity of working on this interesting and challenging project. I have always appreciated your support and your guidance with the project. During these years you have been a great mentor for me since I have learn many things at a scientific level but also at an organization and communication level. My expectations on this project and in general on working in a scientifically high-level field were many and today I am really glade to say that all of them have been reached and also because of your help and the passion that you put into your daily work. I would like to thank you also for pushing me into my "dark matter": teaching.

I would like to thank all people of our former and previous group, PolyCell at Nanotech: firstly, Johan that helped me a lot during the first months of my work, Thor to be an entertaining and good friend, Esben for his help with surface photo-chemical modification, Mark, Morten, Lee for his humor, Gertrud, Rujing and Rodrigo. A huge thank to all the technicians that helped me every day with their great work and company and all the people working in administration; so, thank to Ina, Ole, Lotte, Lene, Jannik, Louise, Dorthe, Jette and Michael. Further, I want to thank all the people with which I have collaborated during these years: Fredrik, Sergey, Paolo, Stephan and all the collaborators that have worked with us in the IndiTreat project.

During these three years I had a great time and I met many interesting and exciting people: thank Claudia and Chiara! You are the loveliest (ma tantissimo!!) persons that I have never met in my life. Apart the fact that you are two ninja-girls on your work and I really proud to have met two responsible ladies like you, I needed and still need you as friend and I will be here for you! Pavel, thanks to be the craziest guy that you are! All time that I meet you there is always something new and cool, and please leave some girls to the other Italians! Anyway, you are a really good friend for me and Ricca and we always know that we can account on you and the same for you. Even if new to Nanotech environment, thanks Rofri to be the person that you are! We had the pleasure to know each other for a short period but it was enough to appreciate our pros and cons. I personally like your honesty, generosity and positivity!! I had a really good time with you and Gina in Hawaii!!!!....and honestly, I hope to stay around with you as much as I can! A huge thank to Marco to be always diplomatic and to stop our fiery Italian personality when necessary!! I hope on my future to have just half of your patience and courage!

I want to thank also all the people that I met in DTU Nanotech and in other contexts: François, Peter, Jose, Alberto, Andrea "il Crovetto", Ada, Solene, David, Filo "Il Cavalca", Filly, Fabione, Bjarke, Tim, Thor,

Anne, Petra, Giova, Gosia, Mette, Solene, Nicò, Sarah, Kinga, Arto, Davide, Diego, Ken, Chris, Andrea “La ragazza”, Simone, Filo, all the bartenders of the Friday Bar and all the others that I forgot!
I want to thank all the guys that participated with me to the ESONN summer school: Esben, Peter, Mikkel, Solene, Chiara, Nis, Kasper, Anders thanks a lot for the amazing time together!!!
Last but not least, a huge thank to my formidable family to have supported me all time even though I was far from you! Grazie mamma per essere sempre amorosa e presente per i tuoi ancora “bambini”, e grazie babbo per essere continuamente il mio punto di riferimento e sei un esempio per tutti noi. Grazie Franci per avermi dato sempre il tuo affetto, sei il fratello migliore che si possa volere ed un ottimo babbo! Grazie anche alla mia piccola Buby che è bellissima e ti adoro già, anche se non parli! Un grazie infinito anche a Grace: you are the mom more brave that I know and your two princesses are exactly like you: lovely, intelligent and beautiful!
A huge THANK to my boyfriend Riccardo, to have been always present for me especially during the last period of my thesis. Your support was and is still crucial for me! Ti amo tesoro e spero che un giorno potremo goderci ogni momento della nostra vita senza, o quasi, ostacoli! Grazie mille ai tuoi genitori che sono sempre tanto premurosi ed ormai mi sento proprio in una grande famiglia! My thesis was also possible because of you and your help!

# External Communication Activities

## Peer-reviewed journal papers included in this thesis

### MULTIPLEXED DOSING ASSAYS BY DIGITALLY DEFINABLE HYDROGEL VOLUMES

Adele Faralli, Fredrik Melander, Esben Kjær Unmack Larsen, Sergey Chernyy, Thomas Lars Andresen, and Niels Bent Larsen

Manuscript submitted to *Advanced Healthcare Materials*

## Peer-reviewed journal papers not included in this thesis

### GOLD NANOPARTICLE-BASED SENSORS ACTIVATED BY EXTERNAL RADIO FREQUENCY FIELDS

Della Vedova, Paolo; Ilieva, Mirolyuba; Zhurbenko, Vitaliy; Mateiu, Ramona Valentina; Faralli, Adele; Dufva, Martin; Hansen, Ole

*Small*, 11, (2), pp. 248-256, **2015**

### AVIDIN FUNCTIONALIZED MAGNEMITE NANOPARTICLES AND THEIR APPLICATION FOR RECOMBINANT HUMAN BIOTINYL-SERCA PURIFICATION

Magro, Massimiliano; Faralli, Adele; Baratella, Davide; Bertipaglia, Ilenia; Giannetti, Sara; Salviulo, Gabriella; Zboril, Radek; Vianello, Fabio

*Langmuir*, 28, pp. 15392-15401, **2012**

## Conference contributions (presenter underlined)

Abstract and oral presentation:

**DIGITAL DRUG DOSING: DOSING IN DRUG ASSAYS BY LIGHT-DEFINEDVOLUMES OF HYDROGELS WITH EMBEDDED DRUG-LOADED NANOPARTICLES**

Faralli, Adele; Melander, Fredrik; Larsen, Esben Kjær Unmack; Chernyy, Sergey; Andresen, Thomas Lars; Larsen, Niels Bent

52th Nordic Polymer Days, IDA Polymer,
Copenhagen, Denmark, **2015**

Abstract and poster:

**DIGITAL DRUG DOSING: DOSING IN DRUG ASSAYS BY LIGHT-DEFINEDVOLUMES OF HYDROGELS WITH EMBEDDED DRUG-LOADED NANOPARTICLES**

Faralli, Adele; Melander, Fredrik; Larsen, Esben Kjær Unmack; Andresen, Thomas Lars; Larsen, Niels Bent

2nd IEEE EMBS Micro and Nanotechnology in Medicine Conference,
Oahu, Hawaii, **2014**

Abstract book and poster:

**SUSTAINABLE MEDICATION: MICROTECHNOLOGY FOR PERSONALIZING DRUG TREATMENT**

Faralli, Adele; Melander, Fredrik; Andresen, Thomas Lars; Larsen, Niels Bent

DTU Sustain Conference, 2014

Technical University of Denmark, Kgs. Lyngby, Denmark, **2014**

Abstract and poster:

**DIGITAL DRUG DOSING FOR CELL SCREENING ASSAYS**

Faralli, Adele; Melander, Fredrik; Larsen, Esben Kjær Unmack; Chernyy, Sergey; Andresen, Thomas Lars; Larsen, Niels Bent

Stem Cell and Tissue Engineering Conference 2015

Vejle, Denmark **2015**

Abstract and poster:

**FABRICATION OF DRUG-LADEN POLY(VINYLPYRROLIDONE) (PVP) MICROGELS BY UV-PHOTOLITHOGRAPHY AND SUPERCRITICAL IMPREGNATION**

Marizza, Paolo; Keller, Stephan Sylvest; Faralli, Adele; Mateiu, Ramona Valentina; Müllertz, Anette; Larsen, Niels Bent; Boisen, Anja

40th International Conference on Micro and Nano Engineering,

Lausanne, **2014**

# Appendix 1:

## MULTIPLEXED DOSING ASSAYS BY DIGITALLY DEFINABLE HYDROGEL VOLUMES

*Adele Faralli, Fredrik Melander, Esben Kjær Unmack Larsen, Sergey Chernyy, Thomas Lars Andresen, and Niels Bent Larsen*[*]

Manuscript submitted to Advanced Healthcare Materials

# Multiplexed Dosing Assays by Digitally Definable Hydrogel Volumes

*Adele Faralli, Fredrik Melander, Esben Kjær Unmack Larsen, Sergey Chernyy, Thomas L. Andresen, and Niels B. Larsen*[*]

A. Faralli, Dr. F. Melander, Dr. E. K. U. Larsen, Dr. S. Chernyy, Dr. T. L. Andresen, Dr. N. B. Larsen

Department of Micro- and Nanotechnology, DTU Nanotech, Technical University of Denmark

Ørsteds Plads 345B, 2800 Kgs. Lyngby, Denmark

E-mail: niels.b.larsen@nanotech.dtu.dk

**Keywords**: hydrogels, photopolymerization, projection lithography, poly(ethylene glycol), multiplexed compound screening, liposomes, cancer

**Abstract**

Spatially defined projected light photopolymerization of hydrogels with embedded active compounds is introduced as a flexible and cost-efficient method for producing multiplexed dosing assays. Stable and cost-efficient multiplexed drug sensitivity assays using small cell or tissue volumes are in demand for personalized medicine, including cancer patient specific combination chemotherapy considered here. Here, the high spatial resolution of light projector technology defines multiple compound doses by the volume of individual compound-embedded hydrogel segments. Quantitative dosing of multiple proteins are demonstrated using fluorescent-

labeled albumins with a dynamic range of 1-2 orders of magnitude. The hydrogel matrix results from photopolymerization of low cost poly(ethylene glycol)diacrylates (PEGDA), and tuning of the PEGDA composition enables fast complete dosing of all tested compounds. Dosing of hydrophilic and hydrophobic compounds is demonstrated using two first-line chemotherapy regimens combining oxaliplatin, SN-38, 5-fluorouracil, and folinic acid, with each compound being dosed from a separate light-defined hydrogel segment. Cytotoxicity studies using a colorectal cancer cell line show equivalent effects of dissolved and released compounds. Further control of the dosing process is demonstrated by liposomal encapsulation of oxaplatin, stable embedding of the liposomes in hydrogels for >3 months, and heat-triggered complete release of the loaded oxaplatin.

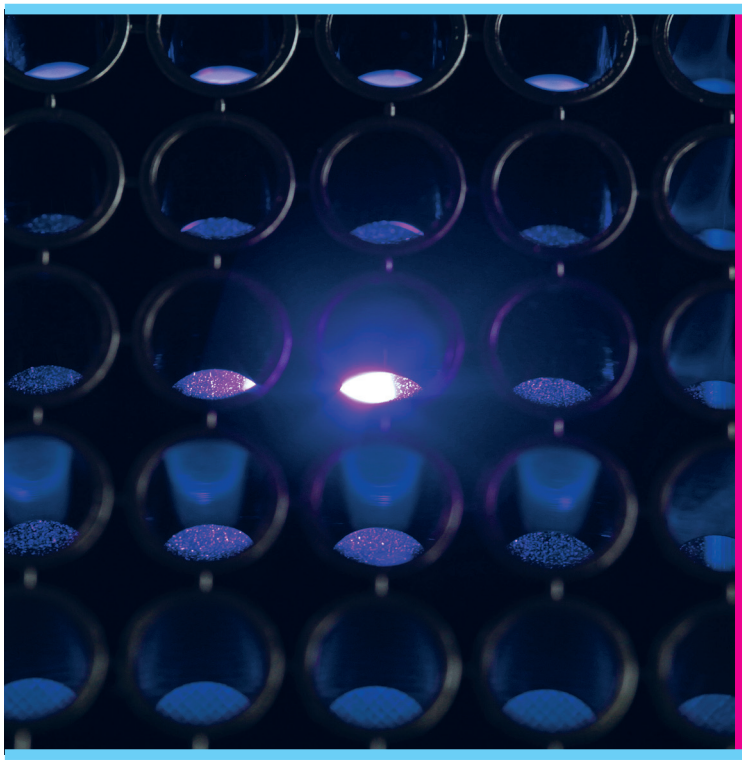



Published by:
DTU Nanotech
Department of Micro- and Nanotechnology
Technical University of Denmark
Ørsteds Plads, building 345B
DK-2800 Kgs. Lyngby